

Sheffield Hallam University

Investigation of nutrient solutions for the hydroponic growth of plants

SEAMAN, Callie

Available from the Sheffield Hallam University Research Archive (SHURA) at:

<http://shura.shu.ac.uk/18141/>

A Sheffield Hallam University thesis

This thesis is protected by copyright which belongs to the author.

The content must not be changed in any way or sold commercially in any format or medium without the formal permission of the author.

When referring to this work, full bibliographic details including the author, title, awarding institution and date of the thesis must be given.

Please visit <http://shura.shu.ac.uk/18141/> and <http://shura.shu.ac.uk/information.html> for further details about copyright and re-use permissions.

Investigation of Nutrient Solutions for the Hydroponic Growth of Plants

Callie Seaman

A thesis submitted in fulfilment of the requirement of Sheffield Hallam University for
the degree of Doctor of Philosophy

October 2017

Acknowledgments

I would first like to thank the EPSRC for funding my PhD and Prof Neil Bricklebank for being an understanding and patient supervisor. I would like to give special thanks to my and dear friend Ian Stansfield, for spending many hours' proof reading my thesis and correcting my work. I would like to thank Michael Cox of the Technical staff at Sheffield Hallam University, who spent many hours helping me with many instruments of various ages and capabilities. Without him I would not have half the data I do. I would also like to thank Gareth Hopcroft for his help during the Afterlife project.

Thank you to Bence Paul and Dany Savard of Iolite 3.32 who gave me so much support with the data processing of the LA-ICP-MS.

Bob Burton and Deeba Zahoor of MERI, Sheffield Hallam university, for performing analysis with XRD, XRF and Raman Spectroscopy. Also, I would like to thank Dr Antonio Feteira of MERI for allowing me to use their ball mill.

I would like to thank Bryn Flinders of the FOM Institute AMOLF, Science Park 104, 1098 XG Amsterdam, The Netherlands for performing the Meta-SIMS imaging of the radish.

I would like to thank all my friends and family for believing in me and keeping me focused during some very difficult times, particularly, Ian Dickinson Emma Pearson and Lucy Sweeny. I would like to thank my husband David Seaman and son Baden Fixter-Seaman for supporting me through this difficult journey and listening to me moan about everything.

I would like to thank the following people within the BMRC for helping me with various instrumentation and methodology: Prof Malcom Clench, Jenni Chen, Laura Cole, Jeffrey Deakin, Jillian Longsdale and Jamie Young.

Abstract

Hydroponics is used extensively in food production and plant research, allowing optimal control over the supply of elements to the plant. In hydroponics, nutrient can be delivered via a solution that is supplied to the growing plant or as a seed coat or treatment that is applied to the seed before sowing and germination. The form in which the nutrients are supplied to the plant influences their bioavailability, up-take, and distribution within the plant.

Commercially produced hydroponic nutrients are typically supplied as two separate concentrated solutions. If these are mixed before being diluted then precipitates are formed which limit the bioavailability of certain elements in the nutrient solution. The chemical nature of the precipitate has been investigated by XRD, XRF, ion-chromatography and IR and Raman spectroscopies, with the aim of understanding its composition.

Mass spectrometry is a highly sensitive analytical technique which has been applied to the monitoring of uptake and distribution of elements and compounds in plant tissue. Techniques including MALDI-MS, LA-ICP-MS and HPLC-ICP-MS have been utilized in the work presented here to demonstrate the distribution and accumulation of elements and compounds within plant material that has been grown hydroponically.

The use of a zinc based seed coating as a nutrient source for barley seeds in a hydroponic fodder production system has been investigated. The effect of the zinc on the yield and dry mass of the fodder was determined. The total zinc content in the fodder has been determined using ICP mass spectrometry. A method to map the location and distribution of zinc and other metallic elements in seeds and the fodder plants using Laser-Ablation ICP Mass Spectrometry LA-ICP-MS has been developed.

Selenium is an essential element for human health. Broccoli is known to be a hyper-accumulator of selenium and the use of selenium-containing hydroponic nutrients for the biofortification of broccoli with selenium is presented. Laser-Ablation ICP Mass Spectrometry LA-ICP-MS has been used to monitor the accumulation and distribution of selenium in the broccoli plants.

Imaging MALDI-MS has allowed the demonstration of the nitrogen cycle in plants and to show pictorially that atoms and molecules from dead plants are incorporated into new life. Radish plants were grown hydroponically using a nutrient solution system containing isotopically-enriched nitrogen-15 KNO_3 (98% labelled) as the only source of nitrogen. Plants were cropped and left to ferment in water for 2 weeks to create a radish "tea", which was used as a source of nitrogen for radish grown in a second hydroponics experiment. After 5 weeks of growth, the radish plants were harvested and cryosectioned, and sections were imaged by positive-ion MALDI imaging. The presence of labelled species in the plants grown using ^{15}N KNO_3 as nutrient and those grown from the radish "tea" was readily discernible. The uptake of ^{15}N into several identifiable metabolites has been studied by MALDI-MS imaging.

Contents

Acknowledgments.....	2
Abstract.....	3
Abbreviations.....	10
1. Introduction.....	17
1.1 Plant nutrition.....	18
1.2 How are elements taken up by plants?.....	19
1.3 Biofortification.....	22
1.4 Sources of nutrients.....	24
1.4.1 Fertilizers.....	24
1.4.2 Seed coats.....	25
1.4.3 Seed priming.....	26
1.4.4 Foliar sprays.....	26
1.5 Hydroponics.....	27
1.5.1 Hydroponic techniques.....	32
1.5.2 Hydroponic nutrient solutions.....	34
1.5.3 Fodder production.....	38
1.6 Urban farming and Z-farming.....	42
1.7 Aims of this study.....	45
1.8 References.....	47
2. Methods and materials.....	53
2.1 Materials.....	54
2.2 Preparation of standard solution for calibration of instrumentation.....	55
2.3 Glassware preparation.....	55
2.4 Sample preparation.....	56
2.4.1 Microwave digestion.....	56
2.4.2 Freeze drying.....	56
2.4.3 Cryosectioning.....	56
2.4.4 Application of matrix to plant material for analysis using MALDI-MS ..	57
2.4.5 Laser ablation reference material preparation.....	57
2.4.6 Acid extraction of selenium species in broccoli sprouts.....	58
2.5 Analytical techniques.....	59
2.5.1 Inductively coupled plasma optical emission spectroscopy (ICP-OES)...	59
2.5.2 Ion chromatography.....	60
2.5.2.1 Preparation of Ion chromatography eluent and regenerant.....	61

2.5.3	X-ray diffraction (XRD)	61
2.5.4	X-ray fluorescence (XRF) spectrometry	61
2.5.5	Fourier transform infrared (FT-IR) spectroscopy	61
2.5.6	Raman spectroscopy.....	62
2.5.7	Inductively coupled plasma mass spectrometry (ICP-MS).....	62
2.5.7.1	Hewlett Packard (HP) 4500 series ICP-MS	62
2.5.7.2	PerkinElmer NexIon 350X.....	63
2.5.8	Reverse phase high performance liquid chromatography Inductively coupled plasma mass spectrometry (RP-HPLC-ICP-MS).....	63
2.5.8.1	Preparation of HPLC mobile phase for seleno-amino acid detection	65
2.5.9	Matrix assisted laser desorption/ionisation time of flight mass spectrometry (MALDI-TOF-MS)	65
2.5.10	Laser ablation inductively coupled mass spectrometry (LA-ICP-MS)...	66
2.5.10.1	Calculation of spatial resolution of laser ablation images.....	68
2.5.11	Carbon-13 isotope analysis	70
2.6	Data Processing	71
2.6.1	Production of images and processing of matrix assisted laser desorption ionisation mass spectrometry data	71
2.6.2	Production of images and processing of laser ablation inductively coupled mass spectrometry data	71
2.7	References	72
3.	Identification of precipitate formed in a single component hydroponic nutrient solution	73
3.1	Introduction	74
3.2	Material and methods	76
3.2.1	Reagents	76
3.2.2	Precipitate formation.....	78
3.2.3	Microwave digestion methods	78
3.2.3.1	Method 1	79
3.2.3.2	Method 2	80
3.3	Results and discussion.....	82
3.3.1	Composition of the nutrient	82
3.3.2	Precipitate quantification	86
3.3.2.1	Elemental analysis of the precipitate.....	88
3.3.2.2	Ion chromatography	89
3.3.2.3	X-ray diffraction	93
3.3.2.4	Vibrational spectroscopy.....	95

3.3.2.5	Bioavailability reduction of ions by precipitate formation	100
3.4	Conclusion.....	104
3.5	References	106
4.	The use of zinc based seed coating in barley fodder production	108
4.1	Introduction	109
4.2	Material and methods	111
4.2.1	Cultivation - Barley for fodder production	111
4.2.2	Experimental design – Treatments.....	113
4.2.3	Fodder yield	114
4.2.3.1	Total fresh mass	114
4.2.3.2	Percentage dry mass of sample shoots	114
4.2.4	Sample preparation.....	116
4.2.4.1	Time dependent analysis sample preparation of seeds.....	116
4.2.4.2	Seed cryosections.....	117
4.2.4.3	Matrix assisted laser desorption/ionisation matrix application (deposition).	117
4.2.4.4	Reference material preparation for calibration of laser ablation ICP-MS.....	118
4.2.4.5	Digestion method	119
4.2.5	Analytical method (instrumentation)	121
4.2.5.1	Matrix assisted laser desorption/ionisation mass spectrometry	122
4.2.5.2	Characterization of Teprosyn Zn/P	122
4.2.5.3	Inductively coupled plasma optical emission spectroscopy (ICP-OES).....	122
4.2.5.4	Inductively coupled plasma mass spectrometry (ICP-MS).....	123
4.2.5.5	Laser ablation inductively coupled plasma mass spectrometry	124
4.2.6	Calculations - Elemental content	127
4.2.7	Germination rate.....	127
4.2.8	Statistical analysis	128
4.2.9	Data processing	128
4.3	Results and discussion.....	129
4.3.1	Characterization of Teprosyn Zn/P	129
4.3.2	Germination rate.....	130
4.3.3	The effects on yield as dry and fresh mass.	133
4.3.4	Elemental content of plant material	138
4.3.4.1	Quantitative analysis of ground leaf material after treatment with Teprosyn Zn/P using ICP-OES	138
4.3.4.2	Quantitative analysis of ground leaf material after treatment with Teprosyn Zn/P using LA-ICP-MS.	143

4.3.4.3	The use of vanillic acid to improve of laser ablation inductively coupled plasma mass spectrometry analysis.....	147
4.3.5	Quantitative analysis of laser ablation inductively coupled plasma mass spectrometry reference leaf tissue.....	151
4.3.5.1	Limit of Detection (LOD) for laser ablation inductively coupled plasma mass spectrometry.....	153
4.3.6	Monitoring the distribution in leaf material using laser coupled mass spectrometry imaging.....	154
4.3.6.1	Matrix assisted laser desorption/ionisation mass spectrometry imaging of leaf material	154
4.3.6.2	Semi-quantitative laser ablation inductively coupled plasma mass spectrometry imaging of barley leaves.	155
4.3.6.3	Quantitative laser ablation inductively coupled plasma mass spectrometry imaging of barley leaves.....	164
4.3.7	Monitoring the uptake of seed coat over time by pre-germinated seeds using laser coupled mass spectrometry imaging.....	176
4.3.7.1	Matrix assisted laser desorption/ionisation mass spectrometry imaging of seeds	176
4.3.7.2	Quantitative analysis of laser ablation inductively coupled plasma mass spectrometry reference seed material.....	177
4.3.7.3	Quantitative laser ablation inductively coupled plasma mass spectrometry imaging of barley seeds.....	179
4.3.8	Distribution of zinc in broccoli sprouts.....	188
4.4	Conclusion.....	190
4.5	References.....	193
5.	Selenium biofortification of broccoli sprouts.....	199
5.1	Introduction.....	200
5.1.1	Selenium and human health.....	200
5.1.2	Selenium biofortification.....	200
5.1.3	Selenium uptake and metabolism by plants.....	202
5.1.4	Selenium and the production of medically beneficial compounds.	206
5.2	Material and methods.....	207
5.2.1	Cultivation method.....	207
5.2.2	Sample preparation.....	208
5.2.2.1	Seedlings for imaging.....	209
5.2.2.2	Reference material preparation for calibration of LA-ICP-MS.....	209
5.2.2.3	Microwave digestion for total Se content.....	210
5.2.2.4	Seleno-amino acid Extraction.....	211
5.2.3	Inductively coupled plasma mass spectrometry for total Se content.	211

5.2.4	Inductively coupled plasma mass spectrometry analysis of the laser ablation reference material.....	213
5.2.5	Reversed phase high performance liquid chromatography inductively coupled plasma mass spectrometry.....	214
5.2.6	Matrix assisted laser desorption/ionisation time of flight mass spectrometry.....	214
5.2.7	Laser ablation inductively coupled plasma mass spectrometry.....	215
5.2.8	Statistical analysis.....	217
5.2.9	Data processing.....	217
5.3	Results and discussion.....	217
5.3.1	Total selenium content by inductively coupled plasma mass spectrometry 218	
5.3.2	Quantitative analysis of laser ablation inductively coupled plasma mass spectrometry reference material.....	220
5.3.3	Total selenium content by laser ablation inductively coupled plasma mass spectrometry.....	221
5.3.4	Limit of detection for laser ablation method.....	222
5.3.5	Selenium speciation.....	222
5.3.6	Accumulation of Se species over time.....	225
5.3.7	The effect of sodium selenate on plant yield and germination rate.	227
5.3.8	Monitoring the distribution within plant using Matrix assisted laser desorption/ionisation mass spectrometry imaging.....	229
5.3.9	Distribution within plant using laser ablation inductively coupled plasma mass spectrometry.....	230
5.3.9.1	Limit of detection.....	238
5.4	Conclusion.....	239
5.5	References.....	241
6.	The “Afterlife Experiment”: Use of MALDI-MS imaging for the study of the nitrogen cycle within plants.....	250
6.1	Introduction.....	251
6.2	Materials and Methods.....	256
6.2.1	Materials.....	256
6.2.2	Cultivation.....	256
6.2.3	Sample preparation.....	257
6.2.4	Matrix assisted laser desorption/ionisation mass spectrometry matrix deposition.....	258
6.2.5	Secondary ion mass spectrometry (SIMS) sample gold coating.....	258
6.3	Instrumentation.....	259

6.3.1	Applied Biosystems Q-Star Pulsar I	259
6.3.2	Waters Synapt G2 HDMS	259
6.3.3	Metallization secondary ion mass spectrometry (MetA-SIMS) imaging	260
6.4	Data processing	260
6.5	Results and discussion.....	261
6.6	Conclusion.....	272
6.7	References	273
7.	Conclusion and suggestions for future work.....	277
	Appendices.....	281

Table of Figures

Figure 1.2-1: Cation exchange between roots and soil.	19
Figure 1.2-2: The movement of water through a plant during transpiration.....	20
Figure 1.2-3: A comparison of the different types of nutrient uptake via root.	21
Figure 1.5-1: Commercially hydroponically grown tomatoes	29
Figure 1.5-2: Hydroponic drip system growing tomatoes	32
Figure 1.5-3: Diagrammatic representation of deep water culture system.	33
Figure 1.5-4: Aeroponic propagator.....	33
Figure 1.5-5: The availability of elements to plants at different pH levels. (Resh, 2002)	37
Figure 1.5-6: Hydroponic fodder production system.....	38
Figure 1.5-7: Fodder solutions hydroponic fodder system.	39
Figure 1.5-8: The "Biscuit" produced by the sprouted barley in the fodder system after 6 days.	40
Figure 1.6-1: Vertical growing systems.	43
Figure 2.5-1: Schematic diagram of ICP-OES.....	59
Figure 2.5-2: Ion chromatography process	60
Figure 2.5-3: Mobile phase gradient parameter used for the detection of seleno-amino acids using RP-HPLC	65
Figure 2.5-4: A) UP213 Laster Ablation system. B) Front view of laser and sample chamber. C) Sample stage. D) Laser ablating tissue.....	68
Figure 2.5-5: Spatial resolution directions of tissues ablated differently.	68
Figure 3.3-1: The amount of precipitate, as a percentage of the total mass, formed when Vita link Max part A and part B are mixed together in equal quantities	87
Figure 3.3-2: Comparison of the effect of different digestion methods on the results achieved from ion chromatography A) Microwave digestion method 1 (Aqua Regia) spiked with standard solution. B) Standard solution. C) Digestion blank Aqua Regia. D) Digestion blank – H ₂ O ₂ and HCl. Note: Standard solution containing fluoride, chloride, phosphate, nitrate and sulphate.	91
Figure 3.3-3: The chromatograms of the precipitates formed when equal volumes of the various matching Vita Link part A & B are mixed.....	92
Figure 3.3-4: XRD diffractogram of the various precipitates of the different 4 different Vita Link formulations.....	94
Figure 3.3-5: Raman spectra of the precipitate from Vita Link Hard Water Part A and Part B mixed.....	97
Figure 3.3-6: Raman spectra of the precipitates from Vita Link Max Soft Water Part A and Part B mixed.....	98
Figure 3.3-7: FT-IR spectra of the precipitates produced from the various formulation of Vita Link solutions.....	99
Figure 3.3-8: Dissociation of phosphoric acid.	103
Figure 4.2-1: The spray head of the irrigation system delivering a fine mist of solution to the sprouted seeds.	112
Figure 4.2-2: Trays used in the fodder system, showing 3 sections filled with seeds to produce 3 individual "biscuits". The growth after 6 days can be seen in the second image.....	112

Figure 4.2-3: a) Three fully grown biscuits with the location of the sample. b) 10cm cut sample.	115
Figure 4.2-4: Schematic diagram of seed preparation for LA-ICP-MS imaging.....	117
Figure 4.2-5: Suncollect automated pneumatic sprayer, coating plant tissue with matrix.	118
Figure 4.2-6: MARS6 microwave digestion parameters for the digestion of barley seeds.	120
Figure 4.2-7: MARS6 microwave digestion run parameters for laser ablation reference barley leaf material.....	121
Figure 4.2-8: Germination rate grid	127
Figure 4.3-1: Comparison of the effect of Teprosyn Zn/P seed treatment on the germination rate over a 144-hour period, taken every 24hr.....	130
Figure 4.3-2: The effects of Teprosyn Zn/P seed treatment at various concentrations on germination rate (%) of barley in fodder production.	131
Figure 4.3-3: Comparison of root mat formation with the use of Teprosyn Zn/P at 3.6ml per 1.2kg of seed.	133
Figure 4.3-4: A cross sectional comparison of the barley development with varying concentration of Teprosyn.....	134
Figure 4.3-5: The effect of varying concentration of Teprosyn Zn/P on the dry mass (%) of barley grown for 6 days.	136
Figure 4.3-6: The effect of varying concentrations of Teprosyn Zn/P on fresh mass of barley grown for 6 days (kg).	137
Figure 4.3-7: The effect of increasing concentration of Teprosyn Zn/P seed coat on Zn content of barley shoots.	140
Figure 4.3-8: The phosphorus content of barley leaves after treatment with various concentrations of Teprosyn Zn/P.	140
Figure 4.3-9: LA-ICP-MS mean Zn concentration of pelleted barley leaf treated with varying concentrations of Teprosyn Zn/P seed treatment.....	146
Figure 4.3-10:LA-ICP-MS mean P concentration of pelleted barley leaf treated with varying concentrations of Teprosyn Zn/P seed treatment.....	146
Figure 4.3-11: A comparison of the stat summaries of the effects of vanillic acid on the sensitivity of LA-ICP-MS. *VA = Vanillic acid	150
Figure 4.3-12: LA-ICP-MS calibration curves of barley leaf reference material.	152
Figure 4.3-13: MALDI-MS images of barley leaf of 756.82 m/z, believed to be phytic acid Zn adduct.	155
Figure 4.3-14: Semi-quantitative LA-ICP-MS image of control barley leaf.	157
Figure 4.3-15: Semi-quantitative LA-ICP-MS image of barley leaf treated with 3.6ml Teprosyn Zn/P.....	158
Figure 4.3-16: Semi-quantitative 3D LA-ICP-MS image of ⁶⁶ Zn distribution in the barley leaves in the control group.	159
Figure 4.3-17: 3D LA-ICP-MS image of ⁶⁶ Zn distribution in the barley leaves treated with 3.6ml Teprosyn.	160
Figure 4.3-18: A comparison of the summary statistical plot of ⁶⁶ Zn for the control group and treated group of barley leaf.	161
Figure 4.3-19: Comparison of ⁶⁶ Zn stack plots of control group and treated.	163
Figure 4.3-20: Quantitative LA-ICP-MS elemental distribution images of control group barley leaf (mg/Kg).	165

Figure 4.3-21:Quantitative LA-ICP-MS elemental distribution images of barley leaf 0.5ml Teprosyn treatment group (mg/Kg).	166
Figure 4.3-22: LA-ICP-MS elemental distribution images of 1.0ml Teprosyn treatment group.	167
Figure 4.3-23:LA-ICP-MS elemental distribution images of 3.6ml Teprosyn treatment group.	168
Figure 4.3-24: Comparison of the Zn content of barley leave with increasing concentration treatment of Teprosyn. Elemental distribution images produced using LA-ICP-MS.	169
Figure 4.3-25: LA-ICP-MS 3D image of the distribution of Zn in.....	170
Figure 4.3-26: Graphical representation of the average elemental content of barley leaves treated with various concentrations of Teprosyn, using LA-ICP-MS imaging.	172
Figure 4.3-27: Graphical representation of the average elemental content of barley leaves treated with various concentrations of Teprosyn Zn/P, using LA-ICP-MS imaging.....	172
Figure 4.3-28:Graphical representation of the average elemental content of barley leaves treated with various concentrations of Teprosyn Zn/P, using LA-ICP-MS imaging....	173
Figure 4.3-29: Comparison of the statistical summary plots of ⁶⁶ Zn for all the treatments of Teprosyn Zn/P on barley seedlings.....	174
Figure 4.3-30: Histograms to compare the frequency of ⁶⁶ Zn in barley leaves treated with Teprosyn.	175
Figure 4.3-31: Structure of a monocot and dicot seed.	176
Figure 4.3-32: LA-ICP-MS calibration curve of seed material spiked with standard solutions.	178
Figure 4.3-33: ⁶⁶ Zn LA-ICP-MS distribution map of barley seeds treated with varying concentrations of Teprosyn Zn/P.	180
Figure 4.3-34: ³¹ P LA-ICP-MS distribution map of barley seeds treated with varying concentrations of Teprosyn Zn/P.	181
Figure 4.3-35: ⁵⁶ Fe LA-ICP-MS distribution map of barley seeds treated with varying concentrations of Teprosyn Zn/P.	182
Figure 4.3-36: ⁴⁴ Ca LA-ICP-MS distribution map of barley seeds treated with varying concentrations of Teprosyn Zn/P.	184
Figure 4.3-37: ³⁹ K LA-ICP-MS distribution map of barley seeds treated with varying concentrations of Teprosyn Zn/P.	185
Figure 4.3-38: ²⁴ Mg LA-ICP-MS distribution map of barley seeds treated with varying concentrations of Teprosyn Zn/P.	186
Figure 4.3-39: ⁶³ Cu LA-ICP-MS distribution map of barley seeds treated with varying concentrations of Teprosyn Zn/P.	187
Figure 4.3-40: ⁶⁶ Zn distribution in broccoli seedling over a 10-day period using LA-ICP-MS imaging technique. NB. The white dotted marks the separate imagers boarder	188
Figure 4.3-41:Distribution of ⁶⁶ Zn in 10-day old broccoli seedling using LA-ICP-MS imaging technique. NB. The white dotted marks the separate imagers boarder.....	189
Figure 4.3-42: A 3D distribution map of ⁶⁶ Zn in a 10-day old broccoli seedling using LA-ICP-MS imaging technique.	189
Figure 5.1-1: Schematic representation of the main steps in Se metabolism within plants (Germ, Stibilj and Kreft 2007).	203

Figure 5.1-2: Se metabolism within plant cells (Pilon-Smits and Quinn 2010).	205
Figure 5.2-1: Hydroponic growing system.	207
Figure 5.3-1: Comparison of the total selenium content of broccoli sprouts irrigated with either water or sodium selenate.	218
Figure 5.3-2: LA-ICP-MS quantitative data of broccoli shoots.	221
Figure 5.3-3: HPLC chromatograms for the detection of various seleno-amino acids .A) Standard solution of inorganic Se and Se-amino acids	224
Figure 5.3-4: Comparison of various Se-amino acids in broccoli sprout irrigated with sodium selenate or water over a 10-day period; A) Methyl-SeCys; B) Se-Met;	226
Figure 5.3-5: Comparison of broccoli sprouts irrigated with 20µg/L sodium selenate or water on productivity parameters A) Fresh Mass; B) % Dry mass; C) Germination rate (%); D) Fresh to Dry mass ratio	228
Figure 5.3-6: MALDI-MS image of broccoli sprouts treated with Se at day 10 after sowing.	229
Figure 5.3-7: LA-ICP-MS images of broccoli irrigated with water or sodium selenate.	232
Figure 5.3-8: 3D distribution map of ⁷⁸ Se in broccoli sprout irrigated with sodium selenate for 10 days using LA-ICP-MS.	233
Figure 5.3-9: Iolite 3.32 software Statistical comparison of the Se content and distribution within broccoli sprouts, 3 days after germination within the control and selenium treated A) histograms B) stats summary from LA-ICP-MS analysis.	234
Figure 5.3-10: Iolite 3.32 software Statistical comparison of the Se content and distribution within broccoli sprouts, 7 days after germination within the control and selenium treated A) histograms B) stats summary from LA-ICP-MS analysis.	235
Figure 5.3-11: Iolite 3.32 software statistical comparison of the Se content and distribution within broccoli sprouts, 10 days after germination within the control and selenium treated A) histograms B) stats summary from LA-ICP-MS analysis.	236
Figure 5.3-12: Iolite 3.32 software statistical comparison of the Se content and distribution within broccoli roots, 10 days after germination in the selenium treat group A) histograms B) stats summary from LA-ICP-MS analysis.	237
Figure 6.1-1: A model of absorption and metabolism of ammonium and nitrate in plant root cell. (Image taken from : http://www.intechopen.com/books/a-comprehensive-survey-of-international-soybean-research-genetics-physiology-agronomy-and-nitrogen-relationships/soybean-seed-production-and-nitrogen-nutrition).....	252
Figure 6.1-2: A diagrammatic representation of the nitrogen cycle.	254
Figure 6.2-1: Experimental workflow used in this study.	256
Figure 6.5-1: MALDI-MSI images showing the distribution of choline at m/z 104.1 and 105.1 with the leaf and the bulb of the radish (normalized against the TIC).....	262
Figure 6.5-2: MALDI-MS spectra obtained from the leaves of the a) control, b) ¹⁵ N radish and c) second generation ¹⁵ N plant.	263
Figure 6.5-3: MALDI-MS/MS spectrum of a) m/z 104.1 and b) m/z 105.1 and the fragments taken from the N15 leaf.....	264
Figure 6.5-4: MALDI-MSI images showing the distribution of a) a species identified as anthocyanidin pelargonidin at m/z 271, b) choline at m/z 104.1, c) ¹⁵ N labelled choline at m/z 105.1, d) phosphocholine at m/z 184, e) ¹⁵ N labelled phosphocholine at m/z 185, f) ¹⁵ N labelled choline at m/z 105.1 overlaid onto the unknown species at 271 and g) ¹⁵ N labelled phosphocholine at m/z 185 overlaid onto pelargonidin species at m/z 271....	265

Figure 6.5-5: MALDI-MS/MS spectrum of Pelargonidin and fragments.....	266
Figure 6.5-6: a) Optical image of the control radish bulb section and MetA-SIMS images showing b) the total ion current, the distribution of c) choline at m/z 104.1 and d) ¹³ C isotope of choline at m/z 105, and e) MetA-SIMS spectrum obtained from the radish bulb.....	268
Figure 6.5-7: a) Optical image of the first-generation radish bulb section and MetA-SIMS images show (b) the total ion current, the distribution of (c) choline at 104.1 and (d) ¹⁵ N-labelled choline at m/z 105.1, and (e) MetA-SIMS spectrum obtained from the radish bulb.....	269
Figure 6.5-8: a) Optical image of the second-generation radish bulb section and MetA-SIMS images show (b) the total ion current, the distribution of (c) choline at 104.1 and (d) ¹⁵ N-labelled choline at m/z 105.1, and (e) MetA-SIMS spectrum obtained from the radish bulb.....	270

Abbreviations

CHCA = α -cyano-4-hydroxycinnamic acid

CPS = Counts per second

DHB = 2, 5-dihydroxybenzoic acid

DM = Dry matter.

DTPA = Diethylenetriamine pentaacetate

EDTA = Ethylenediaminetetraacetic acid.

FT-IR = Fourier transform infrared

HFBA = Heptafluorobutyric acid

HW = Hard water

ICP-OES = Inductively coupled plasma optical emission spectrometer

LA-ICP-MS = Laser ablation inductively coupled plasma mass spectrometer

LOD = Limit of detection

MALDI-MS = Matrix assisted laser desorption/ionisation mass spectrometry.

MALDI-TOF-MS = Matrix assisted laser desorption/ionisation time of flight mass spectrometry.

MeOH = Methanol

MERI = Materials & Engineering Research Institute.

Meta-SIMS = Metallization secondary ion mass spectrometry

Methyl-SeCys = Seleno-methylselenocysteine

NFT = nutrient film technique.

RP-HPLC-ICP-MS = Reverse phase high performance liquid chromatography

Inductively coupled plasma mass spectrometer

rpm = Revolutions per minute

RSD = Relative standard deviation

SD = Standard deviation

Se-Met = Seleno-L-methionine

SIMS = Secondary ion mass spectrometry

SW = Soft water

TFA = Trifluoroacetic acid

VA = Vanillic acid

XRD = X-ray Diffraction

XRF = X-ray fluorescence spectrometry

Chapter 1

1. Introduction

1.1 Plant nutrition

Plant nutrition has been studied for centuries, with the first recorded scientific discovery in 1600 by the Belgian scientist Jan van Helmont. Plant nutrition is defined as the study of externally supplied chemical elements and compounds that are necessary for plant metabolism and growth. In accordance with Justus von Liebig's law of the minimum, for an element to be classified as essential for plant growth, it should either form part of an essential metabolite or plant component or in its absence the plant is unable to complete a normal life cycle (Epstein 1972).

To date, there are 17 elements known to be essential for plant growth and can be split into two categories. The first of these are required in relatively high concentrations, ranging from 10-400 ppm, making up between 0.2% - 0.4% dry plant matter concentration and are referred to as macrolelements (Marschner 2012). These include carbon (C), oxygen (O) and hydrogen (H), which can be obtained from the air. The other six macronutrients are obtained from the growing media and can be split into primary macronutrients (nitrogen(N), potassium (K) and phosphorus (P)) and secondary macronutrients (calcium (Ca), magnesium (Mg) and sulphur(S)). The other eight elements are referred to as micronutrients and are required in much lower concentrations ranging from 0.001-10 ppm and are found to be less than 0.02% in the dry plant material (Barker, Pilbeam 2015) . These are iron (Fe), boron (B), copper (Cu), zinc (Zn), molybdenum (Mo), nickel (Ni), chlorine (Cl) and manganese (Mn). Other elements that are beneficial to plant growth, but are not essential include selenium (Se), vanadium (V), aluminium (Al), cobalt (Co), silicon (Si) and sodium (Na) (Barker, Pilbeam 2015).

1.2 How are elements taken up by plants?

There are two routes in which nutrients can enter the plant, either via the leaves or via the roots. The nutrient is then transported around the plant to where it is required. Most of the elements are up taken via the roots from the surrounding growing media via a process known as cation exchange, where hydrogen ions are pumped into the surrounding media from the roots (Sonneveld, Voogt, 2009). This, in turn, releases the cations, such as calcium and potassium from the soil particles, allowing them to be taken up into the roots (Figure 1.2-1). The plant also secretes carbon dioxide from the roots, which in turn reacts with water to form carbonic acid (H_2CO_3). The carbonic acid further dissociates, releasing more hydrogen ions in to the media and increasing the availability of the ions to the plant.

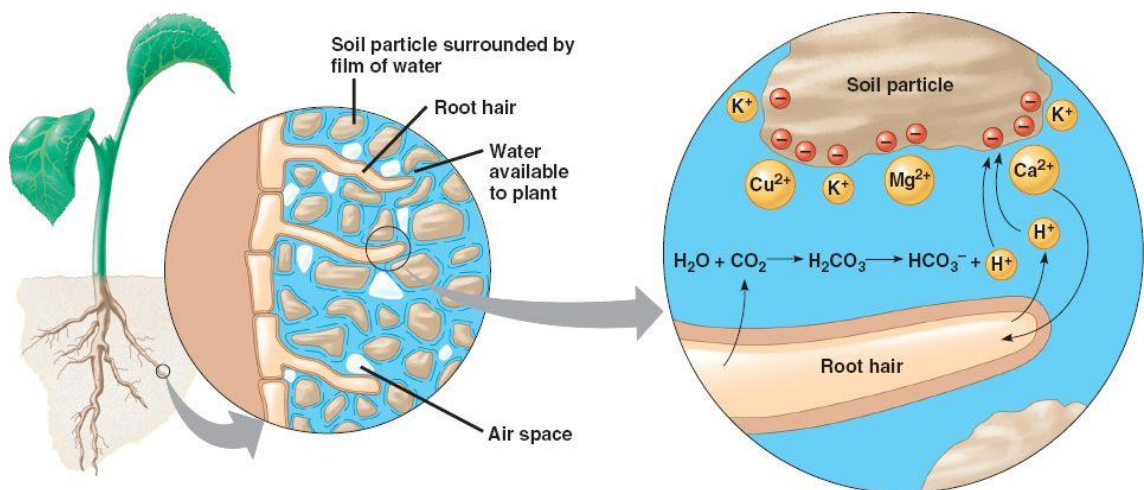


Figure 1.2-1: Cation exchange between roots and soil.

(image from http://bio1152.nicerweb.com/Locked/media/ch37/soil_availability.html)

Elements are taken up as ions and are only bioavailable to the plant in this form. One of the major factors in the uptake of any nutrient via the roots is the water potential of the soil and the air surrounding the plant. Plants undergo a process known as transpiration, in which there is a loss of water via pores on the leaves known as stomata. Transpiration rate increases with high temperature and low humidity around the leaves; this is

designed to cool the plant. A syphoning effect happens within the plant as transpiration occurs, creating a negative water potential within the roots, pulling water and nutrient into the plant via the roots (Figure 1.2-2).

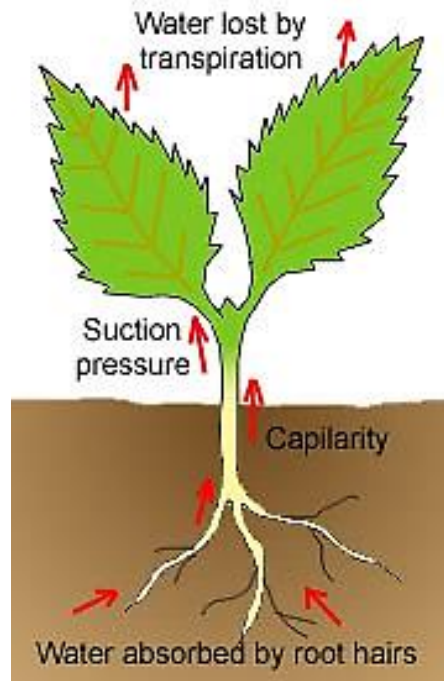


Figure 1.2-2: The movement of water through a plant during transpiration.

There are three methods in which nutrients can be taken up into the roots, these include simple diffusion, facilitated diffusion, and active transport (Figure 1.2-3). As the name suggests, simple diffusion involves nonpolar molecules passing across the epidermis with the concentration gradient. This includes the transport of small, hydrophobic, uncharged molecules, including nitrogen, oxygen, water, and carbon dioxide. The other two methods involve additional molecules to help the transportation into the root and are usually for large molecules and ions. Facilitated diffusion involves the element

binding to a transport molecule, such as humic acid or a protein, and moving into the plant via a concentration gradient through channel proteins embedded in the membrane.

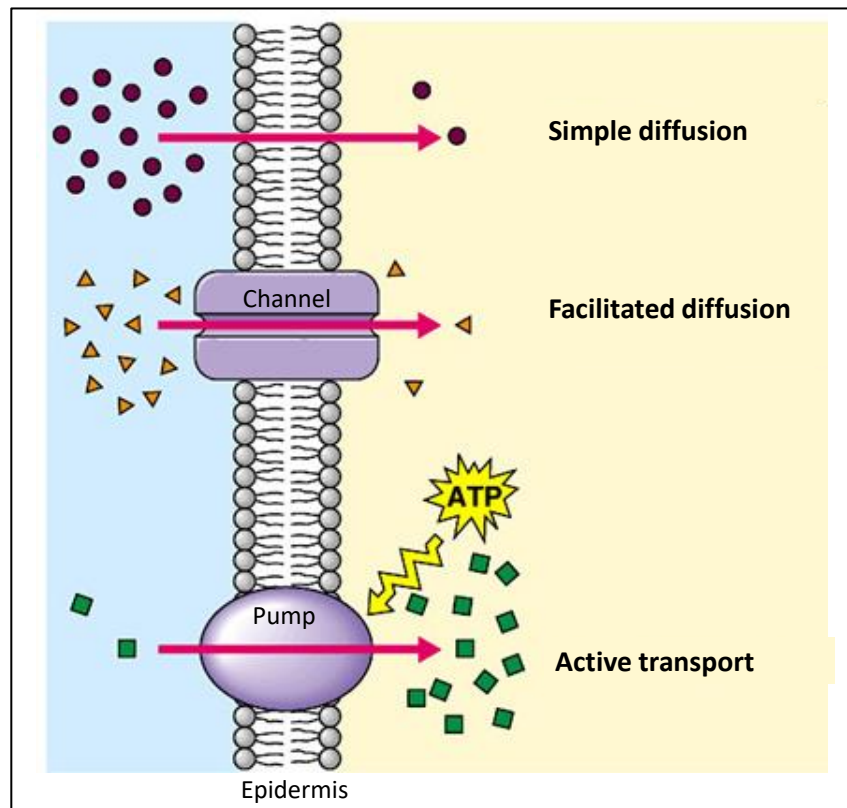


Figure 1.2-3: A comparison of the different types of nutrient uptake via root.

Image adapted from <http://biology4ibdp.weebly.com/14-membrane-transport.html>

Active transport involves the use of pumps in the root membrane, which use energy in the form of adenosine triphosphate (ATP) to actively transport the element into the plant.

Once the nutrient has passed through the cortex of the root it can then be transported to the aerial parts of the plant via the xylem or the phloem. Bulk movement of dissolved ions and water occurs via the xylem, along the transpiration stream and the flow through the xylem is dictated to by the rate of transpiration. Areas in the plant that suffer from low transpiration rate, such as fruit, use the phloem to redistribute ions and other molecules to these areas and prevent deficiencies.

Other means of making nutrient bioavailable to the plant is with the assistance of microorganisms such as mycorrhizal fungus, rhizobacteria and Trichoderma fungus, which form symbiotic relationships with the plant. These include nitrifying bacteria which convert nitrates to nitrates (Tikhonovich, Provorov 2011, Lapeyrie, Ranger *et al.* 1991, Kurth, Feldhahn *et al.* 2015, Wallander, Wickman *et al.* 1997).

Fertilizers can be applied by spraying directly on to the leaves of the plant and is most commonly used to agriculture to correct for deficiencies and to apply pesticides. Foliar absorption involves penetration of the cuticular membrane on the leaf, however, absorption can also occur via the stomata (Bukovac, Wittwer 1957, Kannan, Charnel 1986). Once the nutrient has entered the leaf, it is then transported to other parts of the plant via the phloem (Kannan, Charnel 1986). As much as five times as much nutrient can be absorbed via the leaf, when compare to the same concentration applied to the roots. This is due to transpiration dictating to the rate of uptake of nutrients, when root fed.

1.3 Biofortification

Biofortification are the methods used to increase the nutritional content of a plant, which may be in the form of elemental content or for the encouragement of beneficial metabolite production. Such metabolites include chemotherapeutic compounds like sulforaphane, phenolic acid and seleno-amino acids (Abdulah, Faried *et al.* 2009).

Biofortification is an effective way to combat deficiencies in areas of the world where the soil is low in particular elements. This, in turn, can help to reduce the incidents of preventable diseases in both humans and livestock, such as myopathy and anaemia.

Developing countries tend to have a diet which is monotonous and made up mainly of grain and milled cereal, which have low bioavailable mineral content (Christou,

Twyman 2004). In these areas the most common mineral deficiencies include calcium, zinc, selenium and iron and result in a number of diseases and stunted development in children (Gómez-Galera, Rojas *et al.* 2010).

Plants such as rice, beans, wheat, barley, and sweet potatoes have been targeted for iron and zinc biofortification, whilst plants such as wheat and broccoli have been targeted for selenium biofortification. This is not for the correction of deficiencies, but for the production of chemotherapeutic compounds that selenium forms (Robbins, Keck *et al.* 2005, Hauder, Winker *et al.* 2011, Matusheski, Wallig *et al.* 2001, Fahey, Zhang *et al.* 1997, Li, Wu *et al.* 2008, Zhang, Svehlikova *et al.* 2003, Li, Wang *et al.* 2012, Finley, Ip *et al.* 2001, Finley, Sigrid-Keck *et al.* 2005).

Methods of biofortification include genetic engineering, fertilization, plant breeding and soil management. Each of the methods have their advantages and disadvantages, environmentally, economically, and ethically. The method adopted needs to be sustainable, be beneficial to health and carry a minimal risk. The more traditional methods such as plant breeding and soil management, are perceived as being more environmentally friendly and are more comfortable with these methods, however they tend to be more labour intensive and have a longer time scale for effect. Genetic engineering offers the most precise method, though it does have ethical issues with the long-term effects difficult to predict and the cost for development can be high. Fertilization offers the quickest and most effective results, however leaching into rivers and the poisoning of wildlife, along with sustainability of the resources all remain as challenging issues. The delivery method of the fertilizer is key in the reduction of the pollution created and the availability to the plant.

1.4 Sources of nutrients

1.4.1 Fertilizers

A fertilizer is defined as a material which is applied to a plant, and supplies one or more essential elements for plant growth. There are many different types of fertilizers which are commercially available today and are classified in many different ways. They can be split into either; inorganic/synthetic fertilizers which have come from mineral extraction and which have undergone numerous chemical treatments and refinement, or organic fertilizers, which have generally come from animal or plant material e.g. compost or manure. Further classification is based on the number of primary macronutrients (N, P, K) they supply. A single nutrient (straight) only supplies one of the primary macronutrients. For example, ammonium nitrate (NH_4NO_3) or calcium nitrate ($\text{Ca}(\text{NO}_3)_2$). Multi-nutrient or complex fertilizers contain two or more of the primary macronutrients, such as potassium phosphate (KH_2PO_4).

Fertilizers can be delivered in several different ways: in powder form (applied directly to the growing media) or dissolved into a solution and fed directly to the roots or sprayed onto the leaves.

In recent years, the use of nanoparticles for delivery of nutrients to plants has become more popular, with particles such as silver, iron, copper, and zinc all being investigated (Nair, Varghese *et al.* 2010, Kumar, Yadav 2009). Elements are bound to carrier molecules such as amino acids via electrostatic forces, making them much more bioavailable to the plant. Nano materials offer the advantages of increased uptake of elements, more efficient use of nutrients, increased yields, improved food security and a more economical fertilizer (Chaudhry, Scotter *et al.* 2008, Khot, Sankaran *et al.* 2012,

Nair, Varghese *et al.* 2010, Coles, Frewer 2013, Sastry, Rashmi *et al.* 2011, Dietz, Herth 2011).

Bio-fertilizers and organic farming has grown in popularity over the last decade, with more of the general public becoming concerned about the intensification and methods of commercial farming. There is an increasing trend towards people wanting to know what has been applied to their food before consuming it. Bio-fertilizers are defined as organic based substances derived from animal or plant and have not undergone extensive purification processes. These include compost tea, compost, and manure (Mehilal, Dhabbe *et al.* 2012, Tikhonovich, Provorov 2011, Sonneveld, Voogt 2009).

1.4.2 Seed coats

A seed coat is a thick chemical solution that is designed to cover and be retained by a seed before planting. It is usually made up of a polymer coating and inert carriers, such as pumice, for fertilizers, growth promoters, antimicrobial, antifungal and, less often, insecticidal chemicals to bind to. Micronutrients tend to be the most commonly used fertilizers for this method, due to the lower concentration requirements and it being a more economical method of delivery. Previous work using seed coats has proven it to be a successful method of fertilization and biofortification of crops (Scott, Mitchell *et al.* 1985, Scott, Jessop *et al.* 1987, Karaguzel, Cakmakci *et al.* 2004, Masauskas, Masauskiene *et al.* 2008, Peltonen-Sainio, Kontturi *et al.* 2006, Rebafka, Bationo *et al.* 1993, Sekiya, Yano 2010).

1.4.3 Seed priming

Seed priming is the use of a solution to pre-treat the seed. The seed is usually soaked in a solution and subsequently dehydrated until required. The solution can include nutrients, hormones, or other plant beneficial additives, such as seaweed, fulvic acid or mycorrhizal fungus, but more often than not, just water is used. The hydration of the seed begins the germination process, kick-starting important metabolic pathways. Once dehydrated the seed is placed in a kind of stasis, which remains until rehydration occurs. This method offers many advantages for the farmer including ease of use, preparation of seed can be performed anytime, more efficient use of nutrient and reduction in waste (as excess nutrient which is not absorbed is not flushed down the drain).

It has been well documented that seed priming increases germination rate, produces more uniform germination, increases seed vigour and plant productivity (Masauskas, Masauskiene *et al.* 2008, Ajouri, Asgedom *et al.* 2004, Khaliq, Aslam *et al.* 2015).

1.4.4 Foliar sprays

Application of a nutrient can also be delivered via the leaves as a spray. The most popular nutrient to be applied by this method is calcium, due to its lack of mobility around the plant. Issues with leaf damage are often reported with foliar application of nutrients. This can be attributed to many factors such as the time of day applied, temperature, humidity, and chemical burns. Most field agriculture applies fertilizer via sprayers attached to tractors, therefore delivery is via the leaves. It can be a much more efficient means of delivery, as the plant does not need to use energy in active transport of certain elements from the roots.

1.5 Hydroponics

Hydroponics is the growth of plants without soil. The term encompasses a number of related technologies, many of which require some form of inert media, such as mineral wool, clay pebbles or perlite, to support the growing plant. Other systems, such as the Nutrient Film Technique (NFT), which is widely used commercially in the UK, only use supporting media during propagation, and the plants are grown in a solution permanently and so are truly hydroponic (Seaman and Bricklebank 2011). See section 1.5.1 for more details on the different techniques. The common feature of all hydroponic systems is the requirement for a solution containing all of the key elements for growth and development which are delivered to the plants via an irrigation system. These are in the form of inorganic ions and minerals essential for healthy plant growth and development.

Hydroponics is not 'new' technology and can trace its history back thousands of years to the legendary gardens of the Babylonians and Aztecs. However, its commercial usage has increased massively in the latter part of the twentieth century. More recently, NASA has investigated hydroponics as a means of producing the crops required to meet the life support needs of astronauts in long-term space exploration missions through their 'Biomass Production Facility', and scientists have even exploited hydroponics in nanotechnology by 'growing' metal nanoparticles in living plants (Wheeler *et al.* 2008).

Systems have also been designed for the production of livestock fodder, over a 6-day period. Seeds such as barley, lupin or sunflower are allowed to sprout within a controlled environment. The sprouted grain is then fed to the livestock. In arid and semi-arid areas such as Jordan, one of the major constraints on livestock production is the high cost of imported feed and the low quality of forage produced (Al-Karaki 2011).

Hydroponics is used for the large scale commercial production of salad crops sold in supermarkets. The most popular crops grown hydroponically are tomatoes (Figure 1.5-1), cucumbers and sweet peppers; other crops include melons, lettuce, strawberries, herbs, aubergine, chillies, and ornamental plants and flowers. The most common crops grown hydroponically in the UK are tomatoes and cucumbers. In 2012, the UK produced 84,000 tonnes of tomatoes, mostly using the NFT technique in greenhouses covering c. 200 ha of land and employing almost 2500 people (<http://www.britishtomatoes.co.uk/facts/marketinfo.html>). Approximately 3520 ha of land would be required to cultivate the equivalent quantity in soil (Sonneveld and Voogt 2009).

There are many advantages to hydroponic production, especially faster growing times, which enables multiple crops per season, higher yields, and year-round production with reduced risk of crop failure due to adverse weather, pests, or disease. Furthermore, the plants are grown much more closely together than in soil, often by vertical-training or in columns, leading to greater space efficiency and higher yields per unit of land and it has been estimated that productivity through hydroponic cultivation is increased 4-fold for cucumber, 10-fold for tomatoes and 3-fold for lettuce. These controlled environments lead to a more consistent quality of produce and the earlier detection and correction of nutritional deficiencies than in conventional soil-based horticulture (Seaman, 2011).

These advantages can be attributed to the optimization of crop nutrition, and, in turn, an improvement in water and nutrient efficiency (Gorbe, Calatayud 2010). Soilless culture can offer productivity within areas of the world where soil conditions are unfavourable for cultivation due to poor soil texture, erosion, or high salinity. However, in many countries such as Spain, Egypt and other developing countries, production with this method is still limited due to their lower technological development in horticulture

(Gorbe and Calatayud 2010). Economic factors can also play a role in the limitation of hydroponics in these countries, as the initial capital expenditure is often very high.



Figure 1.5-1: Commercially hydroponically grown tomatoes
(Image from <http://www.insideurbangreen.org/2010/03/index.html>)

There are a number of factors which influence the productivity of a soilless system, therefore making good management of the system essential. The lower buffering capacity of hydroponic systems in comparison to soil systems is the reason for this (Gorbe and Calatayud 2010). These factors include: water supply, nutrient solution composition and concentration, electrical conductivity (EC) and pH of the nutrient solution, dissolved oxygen concentration and temperature of the nutrient solution (Sonneveld and Voogt 2009, Kläring 2001). A summary of these effects can be found in Table 1.5-1.

Mismanagement of any of these factors will lead to stress within the plant and result in a loss in both the quality and quantity of the produce. The plant will respond to these stresses in the short term by activating defence mechanisms, directing its energy away from fruit production. An accumulation of mild stress in the long term will lead to a

reduction in productivity and may even seriously damage the plant if the stress becomes too severe.

Factor	Effect of mismanagement
Water supply	Over supply: reduced uptake of ions, reduction in oxygen uptake, loss of ions from the roots, drowning. Under supply: increase in salinity in the surrounding media and, therefore, toxicity.
Nutrient solution composition.	Nutrient deficiencies or toxicity.
pH	Reduction in elemental availability, elemental lock out (resulting in deficiencies).
Nutrient solution concentration	Stress, toxicity, or deficiencies.
Temperature of the nutrient solution.	Too hot: reduction in dissolved oxygen content, increased risk of pathogenic infection Too cold: root cell damage, reduced solubility, and elemental availability.
Dissolved oxygen concentration	Reduction in anion exchange between root and external media.

Table 1.5-1: The effects of mismanagement of key factors of nutrient solutions on plants

Environmental factors such as air temperature, light intensity, photoperiod, relative humidity, and CO₂ concentration also play a vital role in the productivity of the plant (Resh 2002, Sonneveld, 2009, Gorbe 2010). These factors influence nutrient uptake through the transpiration rate of the plant. The movement of water and ions into a plant is driven by the evaporation of water from the stomata on the leaf surface, and is known as transpiration. This loss of water at the leaf surface, in turn, draws up water and nutrient through the roots. The concentration of the nutrient at the root surface is what affects nutrient uptake, not the average solution concentration. A high transpiration rate results in a higher concentration of ions at the root surface as they are drawn to the root by mass flow, which, in turn, allows a higher nutrient uptake (Gorbe and Calatayud 2010). High environmental temperatures and low humidity increase the transpiration

rate, thus increasing the water and nutrient uptake. If the nutrient solution is not reduced during these conditions, the concentration of the ions could become toxic to the plant as an excess of water is lost through transpiration. In order to provide a plant with the optimal nutrition these factors must be managed.

Global issues such as environmental pollution, water shortage and instability of ecological systems could all be mitigated with the use of hydroponics according to Ghazi N, 2011. By optimising the conditions in which the plants grow, a more efficient use of fertilizers and water can be achieved, which, in turn, addresses some of the environmental and resource problems this planet will face in the future (Tekin, Kapur 2010). However, there are still issues facing the hydroponic industry worldwide, including the need for sustainable pest control, a reduction in the need for mined mineral resources, a reduction in non-renewable energies and the adoption of more recycling technologies (Carruthers 2005). These issues are being addressed with the development of hydroponic systems which do not use electricity (Ikeda, Hamamoto *et al.* 2005), the move towards organic hydroponics in the United States (Brentlinger 2005) and the use of waste water in the systems ((Mehilal, Dhabbe *et al.* 2012, Al-Karaki 2011).

Hydroponic technologies have helped to reduce global poverty and hunger and also improve food security in regions including Latin America, the Caribbean, India, Korea and Malaysia (Kamaruddin 2005, Singh, Mehto *et al.* 2005, Bradley, Marulanda 2005, Izquierdo 2005, Kwon, Jang *et al.* 2005).

1.5.1 Hydroponic techniques

There is not a single 'hydroponic' method and the term actually incorporates a number of related techniques which can be split into two broad categories; media and non-media based hydroponics. Media based systems utilise materials such as mineral wool, coir fibre, perlite, or clay pebbles to support the growing plants (Figure 1.5-2). The nutrient solutions are delivered by drip-feeding or by ebb-and-flow, in which, the plants are flooded with a nutrient solution at pre-determined intervals, pulling oxygen from the atmosphere to the root zone (Seaman and Bricklebank 2011, Resh 2002). The solution can be drained back into a header tank and re-circulated (in what is known as a closed system) or discarded (Bugbee 2004).



Figure 1.5-2: Hydroponic drip system growing tomatoes

Non-media techniques include NFT, in which the plants are grown in an 'open root system' with re-circulating nutrient solutions. In so-called deep-water culture, the roots of the plant are permanently submerged in a nutrient solution which is aerated to maintain adequate levels of dissolved oxygen and prevent stagnation (Figure 1.5-3).

In aeroponics the roots are suspended in an environmental chamber and sprayed with nutrient solution (Figure 1.5-4).

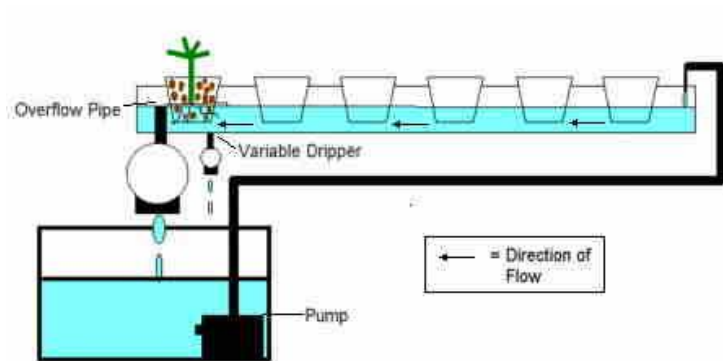


Figure 1.5-3: Diagrammatic representation of deep water culture system.



Figure 1.5-4: Aeroponic propagator

1.5.2 Hydroponic nutrient solutions

Nutrient solutions are made up of inorganic salts which supply all the elements required for healthy growth (Table 1.5-2 and Table 1.5-3). The elements can be separated into two groups: the macroelements (N, P, K, Ca, S, and Mg) and microelements (Zn, Fe, Mn, B, Cu, and Mo). Macroelements are essential for growth and are required at higher concentration, usually between 10 and 400 ppm, depending on the element (Table 1.5-3).

Element	Range (ppm)	Function in plant	Inorganic salts used in nutrients	Available form of element
Nitrogen	70-250	Forms part of amino acids, proteins, co-enzymes, nucleic acid, and chlorophyll.	KNO ₃ Ca(NO ₃) ₂ Mg(NO ₃) ₂ NH ₄ NO ₃ (NH ₄) ₂ SO ₄ (NH ₄) ₂ HPO ₄ NH ₄ H ₂ PO ₄	NO ₃ ⁻ , NH ₄ ⁺
Potassium	150-400	Essential for protein synthesis and functions as a co-enzyme.	K ₂ SO ₄ KNO ₃ KH ₂ PO ₄ KH ₂ PO ₃ KCl	K ⁺
Phosphorus	15-80	Important in hydrolysis of starch to simple sugars. Important in fruit production.	KH ₂ PO ₄ KH ₂ PO ₃ (NH ₄) ₂ HPO ₄ NH ₄ H ₂ PO ₄ H ₃ PO ₄	H ₂ PO ₄ ⁻ HPO ₄ ²⁻
Magnesium	15-80	Necessary in the formation of chlorophyll and as carrier of P.	MgNO ₃ MgSO ₄ .7H ₂ O	Mg ²⁺
Calcium	70-200	Maintains cell integrity, helps reduce the toxic effect of other salts by precipitating as calcium oxalate in vacuoles.	Ca(NO ₃) ₂ CaCl ₂ .6H ₂ O	Ca ²⁺
Sulphur	20-200	Building material in the formation of protein and amino acids.	MgSO ₄ .7H ₂ O K ₂ SO ₄ (NH ₄) ₂ SO ₄	SO ₄ ²⁻

Table 1.5-2: Macroelements required for healthy plant growth, their function and source (Adapted from Resh, 2002 and Barry, 1996).

Other elements essential for plant growth are needed at much lower concentrations, <5ppm, dependent on the element. These are referred to as microelements (Table 1.5-3), and are often supplied in a chelated form, most commonly with EDTA.

As early as 1933, Hoagland and Snyder developed the first solution that contained all the elements required for plant growth. Today, this is still widely used and has been adapted to meet the needs of specific plants.

Element	Range (ppm)	Function in plant	Compound	Available form
Iron	0.8-6	Required for the formation of chlorophyll, but does not form part of it. Essential for the activation of other enzymes.	FeEDTA FeDTPA FeSO ₄ ·7H ₂ O	Fe ³⁺ , Fe ²⁺
Zinc	0.1-0.5	Required for the formation of the auxin indole acetic acid and activates a number of other enzymes.	ZnEDTA ZnCl ₂ ZnSO ₄ ·7H ₂ O	Zn ²⁺
Manganese	0.5-2	Activates enzymes in fatty acid synthesis.	MnEDTA	Mn ²⁺
Copper	0.05-0.3	May be involved in nitrogen fixation. Activates a number of enzymes involved in DNA and RNA formation.	CuEDTA CuSO ₄ ·5H ₂ O	Cu ²⁺ , Cu ⁺
Molybdenum	0.05-0.15	Acts as an electron carrier in conversion of nitrate to ammonium, also essential for N ₂ fixation.	(NH ₄) ₆ Mo ₇ O ₂₄	MoO ₄ ²⁻
Boron	0.1-0.6	Assists in plant use of calcium, essential part in carbohydrates and nitrogen metabolism.	H ₃ BO ₃	BO ₃ ³⁻ , B ₄ O ₇ ²⁻

Table 1.5-3: Microelements required for healthy plant growth, their function and source (EDTA = Ethylenediaminetetraacetic acid, DTPA = Diethylenetriamine pentaacetate).

A concentrate is usually produced by manufacturers and is then diluted by the consumer to the desired strength. Hydroponic nutrient solutions differ from common garden centre fertilizers as they are more concentrated and contain a broader range of elements.

There are two types of solutions available on the market today. The most commonly used are the two-part solutions (part A and B), the other is a single component solution. As the name suggests, the two-part solution comes as two distinct liquids, usually referred to as part A and part B. In one solution, all the calcium containing compounds can be found. The other solution contains all the sulphate and phosphate compounds. These elements are kept separate to prevent them reacting and forming insoluble precipitates that are unavailable to plants. Single part nutrients involve one solution containing all of the elements required for healthy plant growth. Some form of chelating agent is required to prevent precipitation of calcium salts. Unfortunately, there can be problems associated with the production and scaling up of a single part nutrient solution, such as precipitation, blockages, compaction of precipitate, lack of homogeneity and lack of stability. Other factors dictating the type of nutrient used include: media type, plant variety, water quality and growth stage. The media type is important due to the differing cation exchange capacity (CEC) of the different media (Sonneveld, Voogt 2009). The CEC is the total quantity of cations that a growth medium is capable of holding. For example, coir fibre has a high CEC (350-600 mmol kg⁻¹ dry matter) and will sequester metal ions from the nutrient solution, whilst displacing potassium into the system. Coir fibre, therefore, requires lower levels of potassium in the nutrient solution as it is naturally released over time; over supply of this element will result in toxicity. A media with a high CEC will hold on to more nutrients, which, consequently, can result in a build-up of particular elements around the root zone, leading to an imbalance and toxicity if ignored.

Plant variety and growth stage are also factors that must be considered when formulating a nutrient solution. Leafy crops, such as lettuce, require more nitrogen and

less phosphorus than, say, tomatoes as phosphorus plays a vital role in the production of fruit (Morgan 1999).

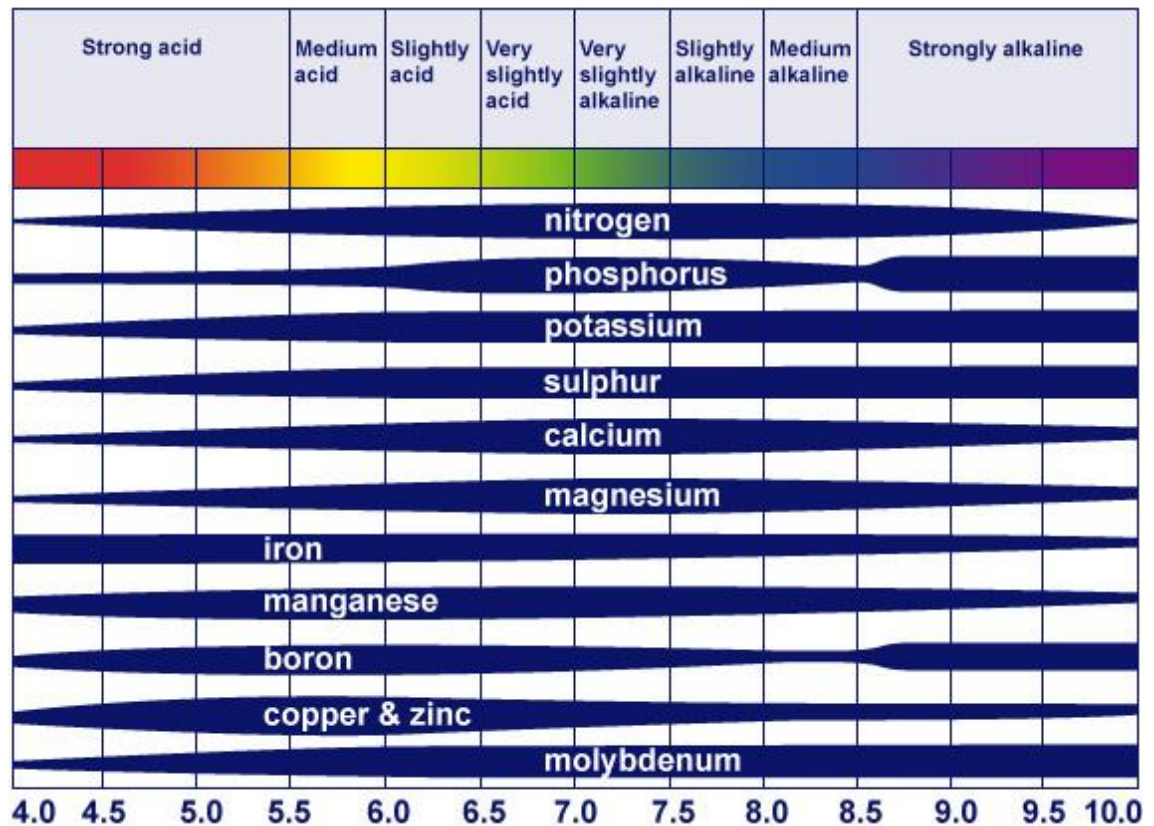


Figure 1.5-5: The availability of elements to plants at different pH levels. (Resh, 2002)

It has been well documented that increasing the available phosphorus to fruiting plants increases yields and quality (Sonneveld, Voogt 2009, Xue, Xia *et al.* 2016, Schachtman, Reid *et al.* 1998, Resh 2002, Barker, Pilbeam 2015, De Jesus Juarez Hernandez, Baca Castillo *et al.* 2006). Therefore, a nutrient solution which has the correct balance is important in order to meet the nutritional requirements of the plant variety and stage of growth. Water quality is the last of these factors that must be considered. Soft water areas, such as Sheffield, contain lower levels of carbonates and calcium in the water supply and, therefore, require nutrient solutions with higher levels of calcium. Hard water contains higher levels of carbonates and calcium and, therefore, a nutrient

solution will require less calcium but higher levels of acid to alter the pH to the desired level of 5.2 to 6.5, within which range all elements are available for the plant to uptake via the roots (Figure 1.5-5).

1.5.3 Fodder production

Other applications for hydroponics include the production of fodder, which is important in the diet of domesticated livestock (Morales, Fuente *et al.* 2009, Lopez-Aguilar, Murillo-Amador *et al.* 2009, Chatterjee, *et al.* 2010, Al-Karaki, Al-Hashmi 2010, Dung, Godwin *et al.* 2010, Fazal, Golmohammadi *et al.* 2011). Semi-automated fodder production systems allow the rapid growth of fodder in the form of sprouted grains of barley, sunflower and lupin within a controlled environment (Figure 1.5-6).



Figure 1.5-6: Hydroponic fodder production system.

Another potential application for semi-automated hydroponic systems such as these is the production of crops for use as biofuels. As competition for land between crops for food and fuel increases, (and with the assistance of genetic engineering) these systems could be used to produce lignocellulosic biomass which, in turn, can be digested and then fermented to produce ethanol, thus easing the burden on farmland (Seaman 2011).

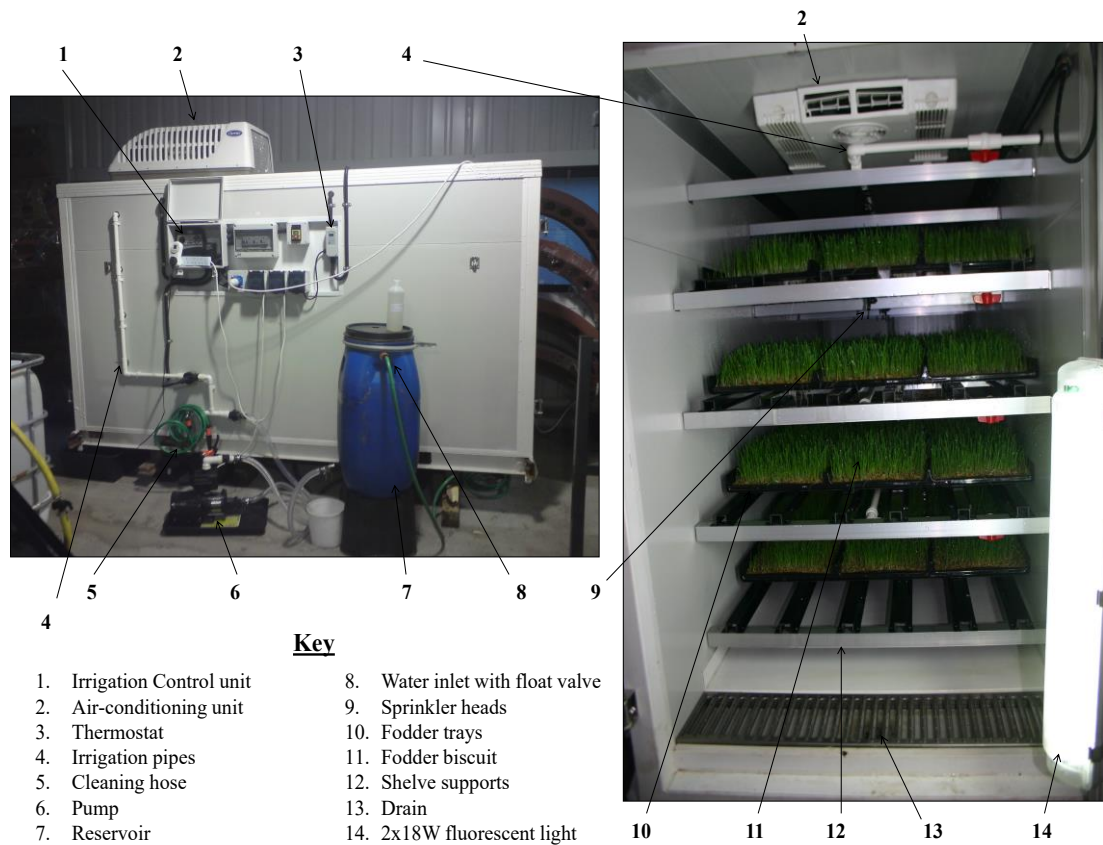


Figure 1.5-7: Fodder solutions hydroponic fodder system.

Over the next 50 years, major changes in the way in which we produce crops will be required if the supply of food is to meet the anticipated demand. One issue is the production of food for livestock. Conventional feeds include dry pellets made from crushed barley seeds, hay, vitamin supplements and molasses. Haylage, a specialist grass seed mix which is cut, dried, and wrapped by a farmer, is another important source of animal feed, which requires large areas for production. Hydroponic systems

have been developed by a number of manufacturers for the rapid production of fodder, including Fodder Solution (Figure 1.5-7), FodderTech, CropKing, H2O Farm and Hydro Fodder Farm.

These hydroponic systems all work in a similar way and spray a fine mist of water onto trays of seeds within a controlled environment. A temperature of 18-23°C is maintained with an average relative humidity of 60-70%. As the seeds germinate, a mat of sprouting grains forms, which is known as a “biscuit” (Figure 1.5-8). The biscuits are harvested during the 3rd phase of germination just 6 days after sowing.

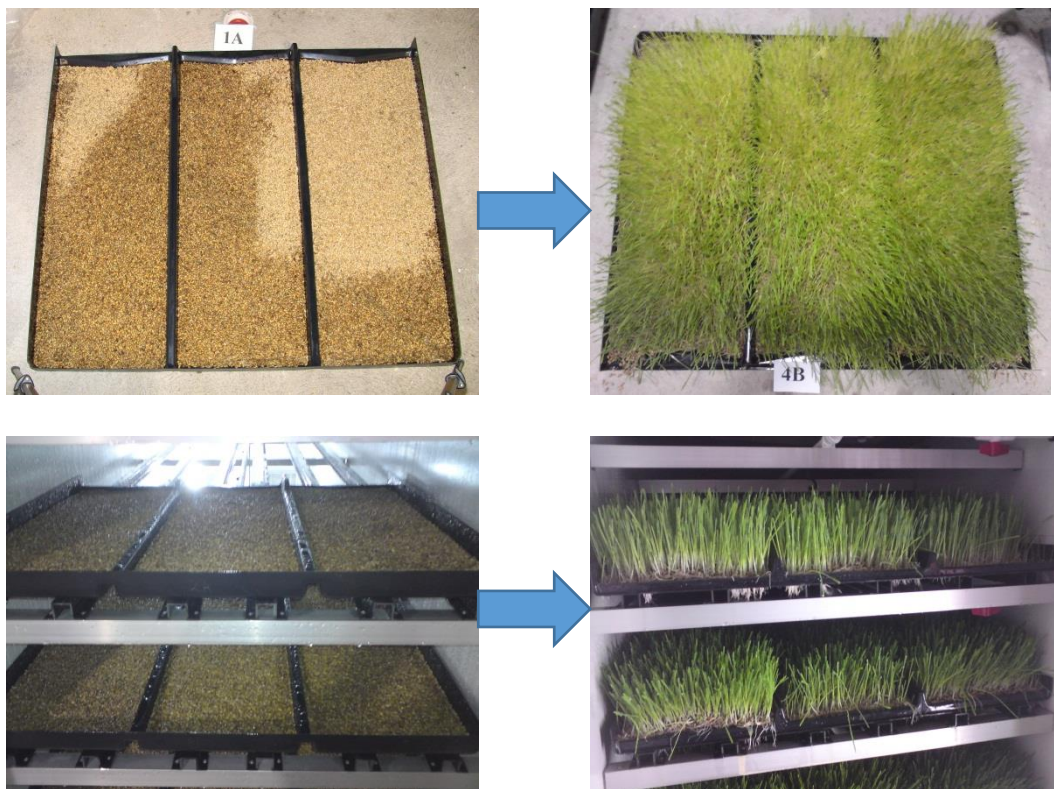


Figure 1.5-8: The "Biscuit" produced by the sprouted barley in the fodder system after 6 days.

As early as the late 1930's, investigations into the use of sprouted grain as a food source for livestock have been reported (Peer, Leeson 1985a, Peer, Leeson 1985b, Mansbridge, Gooch 1985, Chatterjee, Singh 1983, Herrera-Torres, Andrea Cerrillo-Soto *et al.* 2010, Al-Karaki, Al-Hashmi 2010, Scott, Mitchell *et al.* 1985, Steveni, Norringtondavies *et*

al. 1992, Lopez-Aguilar, Murillo-Amador *et al.* 2009, Dung, Godwin *et al.* 2010, Fazaeli, Golmohammadi *et al.* 2011). Today's systems have been significantly modernized, regulating irrigation frequencies and volumes, utilizing thermostatically controlled environments allowing optimal growing conditions to be created. Other advantages of these systems include water and space efficiency, constant production, reduced risk of crop failure, consistent feed, reduction in the effect on biodiversity as a single crop is kept within the system, reduction in long term adverse effect on the environment by the prevention of leaching of fertilizers into the watercourse from fields (Al-Karaki and Al-Hashmi 2010, Lopez-Aguilar, Murillo-Amador and Rodriguez-Quezada 2009, Dung, Godwin and Nolan 2010a, Dung, Godwin and Nolan 2010b, Al-Karaki and Othman 2009).

Previously, studies into hydroponically grown fodder have been used to feed a variety of animals, including rabbits (Morales *et al.* 2009), goats (Marsico *et al.* 2009), sheep, pigs, and poultry (Peer and Leeson 1985, Oduguwa, Pirgozliev and Acamovic 2007) but predominately dairy and beef cattle (McKenzie *et al.* 2004, Greene 2000, Nocek, Socha and Tomlinson 2006, Fazaeli *et al.* 2011, Lopez-Aguilar, Murillo-Amador, and Rodriguez-Quezada 2009). These studies of this type of production have focused on the digestibility of dry matter content and nutrient profile of the fodder with the use of nutrient solution and tap water (Dung, Godwin, and Nolan 2010b, Dung, Godwin, and Nolan 2010a). In both studies, Dung *et al.* 2010 concluded that there was no significant impact on the dry mass, or digestibility of the fodder produced, when a nutrient solution was applied. It was suggested that this was probably due to the short growth period of six days, as this was not long enough to allow the nutrient to have the desired effect.

Many micro-minerals are important in the development and productivity of livestock. Two of the most common minerals cattle will be deficient in are phosphorous and zinc,

particularly with lactating cows (Greene 2000, Greene 1999, Fazaeli, Golmohammadi *et al.* 2011, Sneath, McIntosh 2003). Studies in the US have found only 2.5% of forage have adequate levels of Zn in them (Suttle 2010). Zn is important for cell growth, maintaining the immune system and is involved in a number of enzymes that are concerned with carbohydrate and protein metabolism.

In recent years, fodder production in this manner has been adapted to recycle water and purify manure (Ghazi, N 2011). These types of systems can have disadvantages if the methodology is not optimised correctly, including high energy use for climate control and high-water consumption.

1.6 Urban farming and Z-farming

In recent years, there has been an increase in the popularity of urban farming, as more people become aware of farming practices and the need for food security. This is frequently labelled “Z-farming” and is defined as "zero acreage farming" due to the multi-functional use of the land (Homier, Specht *et al.* 2015, Specht, Siebert *et al.* 2015, Specht, Siebert *et al.* 2014). Areas such as rooftops, high-rise buildings, abandoned warehouses, sides of buildings, balconies and patios within densely populated urban regions are converted into spaces for growing plants, for both produce that is food and non-food (Thomaier, Specht *et al.* 2015, Baudoin 2005). Hydroponics is often used within these spaces to grow the plants on a commercial scale; however, soil based systems have also been adopted (Baudoin 2005). Hydroponics is most frequently used due to its space efficiency and high output. Vertical growing systems have been developed to be used for Z-farming, and involve multiple layers of plants being grown soilless (Mok, Williamson *et al.* 2014) (Figure 1.6-1).



Figure 1.6-1: Vertical growing systems.

Within developing countries, micro garden technologies have been developed to help reduce poverty and hunger by allowing families to obtain their own food security on a small scale and is, essentially, Z-farming (Bradley, Marulanda 2005). Production of a broad range of plants including lettuce, potatoes, celery, mint, sweet pepper, tomatoes, coriander, and beans, to name a few, have diversified and improved the diet of resource-poor families in developing countries (Baudoin 2005).

Z-farming could be a solution to the growing problem of increased population and demand for food as space and resources decline. It offers environmental advantages such as reduction in environmental impact of food transportation, improving resource and energy efficiency, helping increase the bee population, helping to reduce pollution in cities, recycling of waste from the city and reducing the carbon footprint of our food (Specht, Siebert *et al.* 2014, Specht, Siebert *et al.* 2015). This type of farming also offers economic and social benefits such as creating jobs, educational resources, improving local food security and helping to build communities (Thomaier, Specht *et al.* 2015, Specht, Siebert *et al.* 2014).

One of the biggest limiting factors for this type of farming is the acceptance of the soilless techniques, which are often seen as “unnatural” by many consumers, who worry over the health implications attached to consuming products grown in this manner (Mok, Williamson *et al.* 2014, Specht, Siebert *et al.* 2015). Addressing the concerns through education and research is the key to its success. Close monitoring and proper management is required with this system in order to prevent some of the issues with pollution and energy consumption, particularly of the indoor facilities where artificial light and air-conditioning is used. However, this can be tackled with the use of renewable energy such as solar panels.

It is clear from many of the reviews that more research needs to be done on the economic and environmental implications to get a clearer understanding of Z-farming and its place in modern agriculture and horticulture. Currently there are 96 existing projects in North America, Europe, and Asia, which are helping to achieve this (Siebert 2015).

1.7 Aims of this study

Nutrients and fertilizers are key to the productivity of plants. The movement and bioavailability of these have been studied using many different methods. Within this thesis, we aim to track the movement of essential and non-essential elements through plants using different forms of fertilizers. Each chapter looks at a different type of fertilizer and application method of a variety of elements, using a variety of analytical methods.

Within chapter 3 the problems faced with liquid fertilizer production will be addressed and we aim to:

- Identify the precipitates formed in hydroponic liquid fertilizers.
- Investigate how the precipitation effects the bioavailability of the nutrients.
- Develop strategies to prevent the precipitate forming with the aim of producing a hydroponic nutrient solution free from precipitate that is chemically stable, commercial viable and improves the productivity of the plants it is applied to.

Chapter 4 focuses on the use of a zinc and phosphorus based seed coat in the production of barley fodder for livestock feed and the aim is to:

- Monitor the effect of increasing concentration of seed coat applied on:
 - Germination rate
 - Fresh mass
 - Dry mass
 - Elemental content

- Establish if the seed coat is absorbed in to the seed pre-germination.
- Monitor the distribution of elements within the plant.

The effect of selenium fertigation of broccoli sprouts is under investigation in Chapter 5, looking at the production of seleno-amino acid and developing techniques to monitor the distribution. The aim of the study is to:

- Monitor the effect of selenium fertilization on:
 - Germination rate
 - Dry mass
 - Fresh mass
 - Selenium content and distribution
 - Production of different seleno-amino acids
- Optimise the time period from planting to harvest

Finally, in Chapter 6, we planned to track the movement of nitrogen within plant, from one generation to the next. We aim to:

- Grow a first generation of mustard with ^{15}N as the only source of nitrogen.
- Establish the incorporation of the ^{15}N into the first generation.
- Produce a tea with the first generation and feed to a second generation of radish.
- Prove the movement of the ^{15}N into the second generation of radish.

1.8 References

ABDULAH, R., FARIED, A., KOBAYASHI, K., YAMAZAKI, C., SURADJI, E.W., ITO, K., SUZUKI, K., MURAKAMI, M., KUWANO, H. and KOYAMA, H., 2009. Selenium enrichment of broccoli sprout extract increases chemosensitivity and apoptosis of LNCaP prostate cancer cells. *Bmc Cancer*, **9**, pp. 414.

AJOURI, A., ASGEDOM, H. and BECKER, M., 2004. Seed priming enhances germination and seedling growth of barley under conditions of P and Zn deficiency. *Journal of Plant Nutrition and Soil Science-Zeitschrift Fur Pflanzenernahrung Und Bodenkunde*, **167**(5), pp. 630-636.

AL-KARAKI, G.N. and AL-HASHMI, M., 2010. Effect of mineral fertilization and seeding rate on barley green fodder production and quality under hydroponic conditions. *International Conference & Exhibition on Soilless Culture*, 8-13 March 2010 2010.

AL-KARAKI, G.N., 2011. Utilization of treated sewage wastewater for green forage production in a hydroponic system. *Emirates Journal of Food and Agriculture*, **23**(1), pp. 80-94.

BARKER, A.V. and PILBEAM, D.J., 2015. *Handbook of Plant Nutrition*. CRC press.

BAUDOIN, W., 2005. Micro Garden Technologies, *International Conference and Exhibition on Soilless Culture: ICESC 2005 742 2005*, pp. 21-22.

BRADLEY, P. and MARULANDA, C., 2005. A Study on Microgardens that Help Reduce Global Poverty and Hunger, *International Conference and Exhibition on Soilless Culture: ICESC 2005 742 2005*, pp. 115-123.

BRENTLINGER, D., 2005. New trends in hydroponic crop production in the US, *International Conference and Exhibition on Soilless Culture: ICESC 2005 742 2005*, pp. 31-33.

BUKOVAC, M.J. and WITTEWER, S.H., 1957. Absorption and Mobility of Foliar Applied Nutrients. *Plant Physiology*, **32**(5), pp. 428-435.

CARRUTHERS, S., 2005. Challenges faced by the hydroponics industry worldwide, *International Conference and Exhibition on Soilless Culture: ICESC 2005 742 2005*, pp. 23-27.

CHATTERJEE, B.N. and SINGH, A.I., 1983. Barley Production from Seeds Treated before Sowing. *Journal of Agricultural Science*, **100**(FEB), pp. 235-239.

CHAUDHRY, Q., SCOTTER, M., BLACKBURN, J., ROSS, B., BOXALL, A., CASTLE, L., AITKEN, R. and WATKINS, R., 2008. Applications and implications of nanotechnologies for the food sector. *Food Additives and Contaminants*, **25**(3), pp. 241-258.

CHRISTOU, P. and TWYMAN, R.M., 2004. The potential of genetically enhanced plants to address food insecurity. *Nutrition Research Reviews*, **17**(01), pp. 23-42.

COLES, D. and FREWER, L., 2013. Nanotechnology applied to European food production—A review of ethical and regulatory issues. *Trends in Food Science & Technology*, **34**(1), pp. 32-43.

DE JESUS JUAREZ HERNANDEZ, M., BACA CASTILLO, G.A., ACEVES NAVARRO, L.A., SANCHEZ GARCIA, P., TIRADO TORRES, J.L., SAHAGUN CASTELLANOS, J. and COLINAS DE LEON, M.T., 2006. Formulation of nutrient solutions for plant nutrition studies. A proposal. *Interciencia*, **31**(4), pp. 246-253.

DIETZ, K. and HERTH, S., 2011. Plant nanotoxicology. *Trends in Plant Science*, **16**(11), pp. 582-589.

DUNG, D.D., GODWIN, I.R. and NOLAN, J.V., 2010. Nutrient Content and In sacco Degradation of Hydroponic Barley Sprouts Grown Using Nutrient Solution or Tap Water. *Journal of Animal and Veterinary Advances*, **9**(18), pp. 2432-2436.

EPSTEIN, E., 1972. *Mineral nutrition of plants: principles and perspectives*.

FAHEY, J.W., ZHANG, Y.S. and TALALAY, P., 1997. Broccoli sprouts: An exceptionally rich source of inducers of enzymes that protect against chemical carcinogens. *Proceedings of the National Academy of Sciences of the United States of America*, **94**(19), pp. 10367-10372.

FINLEY, J.W., IP, C., LISK, D.J., DAVIS, C.D., HINTZE, K.J. and WHANGER, P.D., 2001. Cancer-protective properties of high-selenium broccoli. *Journal of Agricultural and Food Chemistry*, **49**(5), pp. 2679-2683.

FINLEY, J.W., SIGRID-KECK, A., ROBBINS, R.J. and HINTZE, K.J., 2005. Selenium enrichment of broccoli: Interactions between selenium and secondary plant compounds. *Journal of Nutrition*, **135**(5), pp. 1236-1238.

FAZAELI, H., GOLMOHAMMADI, H.A., SHOAYEE, A.A., MONTAJEBI, N. and MOSHARRAF, S., 2011. Performance of Feedlot Calves Fed Hydroponics Fodder Barley. *Journal of Agricultural Science and Technology*, **13**(3), pp. 367-375.

GÓMEZ-GALERA, S., ROJAS, E., SUDHAKAR, D., ZHU, C., PELACHO, A.M., CAPELL, T. and CHRISTOU, P., 2010. Critical evaluation of strategies for mineral fortification of staple food crops. *Transgenic Research*, **19**(2), pp. 165-180.

GORBE, E. and CALATAYUD, A., 2010. Optimization of Nutrition in Soilless Systems: A Review. *Advances in Botanical Research*, Vol 53, **53**, pp. 193-245.

GREENE, L.W., 2000. Designing mineral supplementation of forage programs for beef cattle. **77**(E-Suppl),.

GREENE, L.W., 1999. Designing mineral supplements for beef cattle. *Journal of Animal science*, **77**(SUPPL. 1), pp. 125-125.

HERRERA-TORRES, E., ANDREA CERRILLO-SOTO, M., SAUL JUAREZ-REYES, A., MURILLO-ORTIZ, M., GERARDO RIOS-RINCON, F., REYES-ESTRADA, O. and BERNAL-BARRAGAN, H., 2010. Effect of Harvest Time on the Protein and Energy Value of Wheat Hydroponic Green Fodder. *Interciencia*, **35**(4), pp. 284-289.

HAUDER, J., WINKER, S., BUB, A., RUEIFER, C.E., PIGNITTER, M. and SOMOZA, V., 2011. LC-MS/MS Quantification of Sulforaphane and Indole-3-carbinol Metabolites in Human Plasma and Urine after Dietary Intake of Selenium-Fortified Broccoli. *Journal of Agricultural and Food Chemistry*, **59**(15), pp. 8047-8057.

IKEDA, T., HAMAMOTO, H., YAMAZAKI, K. and TANAKA, K., 2005. A No-Electricity Hydroponic Culture System for Fruit Vegetables, *International Conference and Exhibition on Soilless Culture: ICESC 2005 742 2005*, pp. 95-97.

IZQUIERDO, J., 2005. Simplified hydroponics: A tool for food security in Latin America and the Caribbean, *International Conference and Exhibition on Soilless Culture: ICESC 2005 742 2005*, pp. 67-74.

KAMARUDDIN, R., 2005. Design and Development of Naturally Ventilated Tropical Crop Protection Structures and Hydroponics Systems, *International Conference and Exhibition on Soilless Culture: ICESC 2005 742 2005*, pp. 139-154.

KANNAN, S. and CHARNEL, A., 1986. Foliar absorption and transport of inorganic nutrients. *Critical Reviews in Plant Sciences*, **4**(4), pp. 341-375.

KARAGUZEL, O., CAKMAKCI, S., ORTACESME, V. and AYDINOGLU, B., 2004. Influence of seed coat treatments on germination and early seedling growth of *Lupinus varius* L. *Pakistan Journal of Botany*, **36**(1), pp. 65-74.

KHALIQ, A., ASLAM, F., MATLOOB, A., HUSSAIN, S., GENG, M., WAHID, A. and REHMAN, H.U., 2015. Seed Priming with Selenium: Consequences for Emergence, Seedling Growth, and Biochemical Attributes of Rice. *Biological Trace Element Research*, **166**(2), pp. 236-244.

KHOT, L.R., SANKARAN, S., MAJA, J.M., EHSANI, R. and SCHUSTER, E.W., 2012. Applications of nanomaterials in agricultural production and crop protection: a review. *Crop protection*, **35**, pp. 64-70.

KUMAR, V. and YADAV, S.K., 2009. Plant-mediated synthesis of silver and gold nanoparticles and their applications. *Journal of Chemical Technology and Biotechnology*, **84**(2), pp. 151-157.

KURTH, F., FELDHAHN, L., BOENN, M., HERRMANN, S., BUSCOT, F. and TARKKA, M.T., 2015. Large scale transcriptome analysis reveals interplay between development of forest trees and a beneficial mycorrhiza helper bacterium. *Bmc Genomics*, **16**, pp. 658.

KWON, Y., JANG, S., IM, J., KIM, W., RYU, S., LEE, E. and LEE, J., 2005. Stable Production of Summer Spinach (*Spinacia oleracea* L.) in Soilless Culture in the

Highlands, *International Conference and Exhibition on Soilless Culture: ICESC 2005* 742 2005, pp. 89-94.

LAPEYRIE, F., RANGER, J. and VAIRELLES, D., 1991. Phosphate-Solubilizing Activity of Ectomycorrhizal Fungi In vitro. *Canadian Journal of Botany-Revue Canadienne De Botanique*, **69**(2), pp. 342-346.

LI, D., WANG, W., SHAN, Y., BARRERA, L.N., HOWIE, A.F., BECKETT, G.J., WU, K. and BAO, Y., 2012. Synergy between sulforaphane and selenium in the up-regulation of thioredoxin reductase and protection against hydrogen peroxide-induced cell death in human hepatocytes. *Food Chemistry*, **133**(2), pp. 300-307.

LI, D., WU, K., HOWIE, A.F., BECKETT, G.J., WANG, W. and BAO, Y., 2008. Synergy between broccoli sprout extract and selenium in the upregulation of thioredoxin reductase in human hepatocytes. *Food Chemistry*, **110**(1), pp. 193-198.

LOPEZ-AGUILAR, R., MURILLO-AMADOR, B. and RODRIGUEZ-QUEZADA, G., 2009. Hydroponic Green Fodder (Hgf): an Alternative for Cattle Food Production in Arid Zones. *Interciencia*, **34**(2), pp. 121-126.

MANSBRIDGE, R.J. and GOOCH, B.J., 1985. A Nutritional Assessment of Hydroponically Grown Barley for Ruminants. *Animal Production*, **40**(JUN), pp. 569-570.

MARSCHNER, H., 2012. Marschner's mineral nutrition of higher plants. *Experimental Agriculture*, **48** (2), pp 305

MATUSHESKI, N.V., WALLIG, M.A., JUVIK, J.A., KLEIN, B.P., KUSHAD, M.M. and JEFFERY, E.H., 2001. Preparative HPLC method for the purification of sulforaphane and sulforaphane nitrile from Brassica oleracea. *Journal of Agricultural and Food Chemistry*, **49**(4), pp. 1867-1872.

MASAUSKAS, V., MASAUSKIENE, A., REPSIENE, R., SKUODIENE, R., BRAZIENE, Z. and PELTONEN, J., 2008. Phosphorus seed coating as starter fertilization for spring malting barley. *Acta Agriculturae Scandinavica Section B-Soil and Plant Science*, **58**(2), pp. 124-131.

MEHILAL, DHABBE, K.I., KUMARI, A., MANOJ, V., SINGH, P.P. and BHATTACHARYA, B., 2012. Development of an eco-friendly method to convert life expired composite propellant into liquid fertilizer. *Journal of Hazardous Materials*, **205**, pp. 89-93.

MOK, H., WILLIAMSON, V.G., GROVE, J.R., BURRY, K., BARKER, S.F. and HAMILTON, A.J., 2014. Strawberry fields forever? Urban agriculture in developed countries: a review. *Agronomy for Sustainable Development*, **34**(1), pp. 21-43.

MORALES, M.A., FUENTE, B., JUAREZ, M. and AVILA, E., 2009. Short Communication: Effect of Substituting Hydroponic Green Barley Forage for a Commercial Feed on Performance of Growing Rabbits. *World Rabbit Science*, **17**(1), pp. 35-38.

- MORGAN, L., 1999. Hydroponic lettuce production. *Casper Productions, Narrabeen, NSW Australia*, .
- NAIR, R., VARGHESE, S.H., NAIR, B.G., MAEKAWA, T., YOSHIDA, Y. and KUMAR, D.S., 2010. Nanoparticulate material delivery to plants. *Plant Science*, **179**(3), pp. 154-163.
- PEER, D.J. and LEESON, S., 1985a. Feeding Value of Hydroponically Sprouted Barley for Poultry and Pigs. *Animal Feed Science and Technology*, **13**(3-4), pp. 183-190.
- PEER, D.J. and LEESON, S., 1985b. Nutrient Content of Hydroponically Sprouted Barley. *Animal Feed Science and Technology*, **13**(3-4), pp. 191-202.
- PELTONEN-SAINIO, P., KONTTURI, M. and PELTONEN, J., 2006. Phosphorus seed coating enhancement on early growth and yield components in oat. *Agronomy Journal*, **98**(1), pp. 206-211.
- REBAFKA, F.P., BATIONO, A. and MARSCHNER, H., 1993. Phosphorus Seed Coating Increases Phosphorus Uptake, Early Growth and Yield of Pearl-Millet (Pennisetum-Glaucum (L) R Br) Grown on an Acid Sandy Soil in Niger, West-Africa. *Fertilizer Research*, **35**(3), pp. 151-160.
- RESH, H.M., 2002. *Hydroponic Food Production 6th Ed.* 6 edn. CRC Press.
- ROBBINS, R.J., KECK, A.S., BANUELOS, G. and FINLEY, J.W., 2005. Cultivation conditions and selenium fertilization alter the phenolic profile, glucosinolate, and sulforaphane content of broccoli. *Journal of Medicinal Food*, **8**(2), pp. 204-214.
- SASTRY, R.K., RASHMI, H. and RAO, N., 2011. Nanotechnology for enhancing food security in India. *Food Policy*, **36**(3), pp. 391-400.
- SEAMAN, C. and BRICKLEBANK, N., 2011. Soil-free farming. *Chemistry & Industry*, (6), pp. 19-21.
- SCHACHTMAN, D.P., REID, R.J. and AYLING, S.M., 1998. Phosphorus Uptake by Plants: From Soil to Cell. *Plant Physiology*, **116**(2), pp. 447-453.
- SCOTT, J.M., JESSOP, R.S., STEER, R.J. and MCLACHLAN, G.D., 1987. Effect of Nutrient Seed Coating on the Emergence of Wheat and Oats. *Fertilizer Research*, **14**(3), pp. 205-217.
- SCOTT, J.M., MITCHELL, C.J. and BLAIR, G.J., 1985. Effect of Nutrient Seed Coating on the Emergence and Early Growth of Perennial Ryegrass. *Australian Journal of Agricultural Research*, **36**(2), pp. 221-231.
- SEKIYA, N. and YANO, K., 2010. Seed P-enrichment as an effective P supply to wheat. *Plant and Soil*, **327**(1-2), pp. 347-354.
- SIEBERT, R., 06 March 2015, 2015-last update, ZFarm. Available: <http://www.zalf.de/htmlsites/zfarm/Seiten/zfarmenglish/index.html>.

- SINGH, V., MEHTO, S., SINGH, B. and KUMAR, M., 2005. Plug-Tray Nursery Raising of Cucurbits in Soilless Media: a Sustainable Technology for Off-Season Crop Production under Northern Plains of India, *International Conference and Exhibition on Soilless Culture: ICESC 2005 742* 2005, pp. 85-87.
- SNEATH, R. and MCINTOSH, F., 2003. Review of hydroponic fodder production for beef cattle. *Meat & Livestock Australia Limited*, .
- SONNEVELD, C. and VOOGT, W., 2009. *Plant Nutrition of Greenhouse Crops*. 1st edition. Springer.
- SPECHT, K., SIEBERT, R., HARTMANN, I., FREISINGER, U.B., SAWICKA, M., WERNER, A., THOMAIER, S., HENCKEL, D., WALK, H. and DIERICH, A., 2014. Urban agriculture of the future: an overview of sustainability aspects of food production in and on buildings. *Agriculture and Human Values*, **31**(1), pp. 33-51.
- SPECHT, K., SIEBERT, R. and THOMAIER, S., 2015. Perception and acceptance of agricultural production in and on urban buildings (ZFarming): a qualitative study from Berlin, Germany. *Agriculture and Human Values*, pp. 1-17.
- STEVENI, C.M., NORRINGTONDAVIES, J. and HANKINS, S.D., 1992. Effect of Seaweed Concentrate on Hydroponically Grown Spring Barley. *Journal of Applied Phycology*, **4**(2), pp. 173-180.
- SUTTLE, N.F., 2010. *Mineral nutrition of livestock*. 4th Edition. Cabi.
- TEKIN, S. and KAPUR, B., 2010. Effect of irrigation management on yield and quality of tomatoes grown in different soilless media in a glasshouse.
- THOMAIER, S., SPECHT, K., HENCKEL, D., DIERICH, A., SIEBERT, R., FREISINGER, U.B. and SAWICKA, M., 2015. Farming in and on urban buildings: Present practice and specific novelties of Zero-Acreage Farming (ZFarming). *Renewable Agriculture and Food Systems*, **30**(01), pp. 43-54.
- TIKHONOVICH, I.A. and PROVOROV, N.A., 2011. Microbiology is the basis of sustainable agriculture: an opinion. *Annals of Applied Biology*, **159**(2), pp. 155-168.
- WALLANDER, H., WICKMAN, T. and JACKS, G., 1997. Apatite as a P source in mycorrhizal and non-mycorrhizal *Pinus sylvestris* seedlings. *Plant and Soil*, **196**(1), pp. 123-131.
- XUE, Y., XIA, H., CHRISTIE, P., ZHANG, Z., LI, L. and TANG, C., 2016. Crop acquisition of phosphorus, iron and zinc from soil in cereal/legume intercropping systems: a critical review. *Annals of Botany*, **117**(3), pp. 363-77.

Chapter 2

2. Methods and materials

2.1 Materials

The TraceSELECT[®] for trace analysis reagents hydrochloric acid (30%) (HCl), nitric acid $\geq 69\%$ (HNO₃), hydrogen peroxide $\geq 30\%$ (H₂O₂), trifluoroacetic acid (TFA), zinc phosphate $\geq 99.9\%$ (Zn₃(PO₄)₂), 2, 5-dihydroxybenzoic acid (DHB), potassium nitrate-¹⁵N 98 atom % ¹⁵N (¹⁵N- KNO₃), potassium nitrate ReagentPlus[®] $\geq 99.0\%$, α -cyano-4-hydroxycinnamic acid (CHCA), vanillic acid (VA), seleno-L-methionine (Se-Met), sodium selenite (Na₂SeO₃), seleno-methylselenocysteine (Methyl-SeCys), ammonium acetate, heptafluorobutyric acid (HFBA) $\geq 99.5\%$, sulphuric acid $\geq 95\%$ (H₂SO₄) and ALUGRAM1 SIL G/UV254 pre-coated aluminium sheets. were purchased from Sigma Aldrich (Gillingham, Dorset, UK)

The solvents methanol, acetonitrile, acetone and reagents formic acid, sodium carbonate anhydrous $\geq 99.9\%$ (Na₂CO₃), sodium hydrogen carbonate $\geq 99.9\%$ (NaHCO₃), sodium selenate (Na₂SeO₄), choline chloride 99%, 4-aminobutyric acid 99+% were purchased from Fisher Scientific (Loughborough, UK).

The following fertilizer ingredients were kindly donated by Aquaculture Ltd (Sheffield, UK), potassium phosphate, potassium phosphite, magnesium nitrate, potassium sulphate, magnesium sulphate, potassium nitrate, trace element mix (Hortifeeds), boric acid (SLS), ammonium nitrate (Yara), calcium nitrate, nickel sulphate (Sigma), cobalt sulphate (Sigma), the preservative (Rocima[™] 553) and thiamine hydrochloride, calcium chloride, calcium sulphate, magnesium sulphate, potassium phosphate and a trace element mix were all purchased from Hortifeeds (Lincoln, UK).

Carbon adhesive disc 12 mm diameter and carbon adhesive tape were purchased from TAAB Laboratories Equipment Ltd (Aldermaston, UK).

2.2 Preparation of standard solution for calibration of instrumentation

For ICP-MS and ICP-OES, multi-element standard solution, (EPA method 200.7 LPC solution), single element standard for ICP – S (1000 µg/ml), Au (1000 µg/ml), Rh (1000 µg/ml) and Sb (1000 µg/ml) were purchased from LGC Ltd (Teddington, UK) and diluted with deionised water (18Ω).

Ion pairing chromatography utilized a five-anion standard solution, purchased from Dionex UK Ltd. This was serially diluted to produce calibrations curves.

Stock solutions of sodium selenite (5 g/L), sodium selenate (5 g/L), seleno-L-methionine (100 mg/L) and seleno-methylselenocysteine (100 mg/L) were made using 0.1M HCl solution and stored at 4°C before serial dilutions were performed.

2.3 Glassware preparation

All spatulas, glass and plastic ware were treated in the following manner before use:

1. Soaked in detergent solution.
2. Rinsed in water.
3. Rinsed with 100% methanol.
4. Rinsed with acetone and air dried.
5. Soaked in 10% nitric acid for a minimum of 1 hour.
6. Rinsed with deionised water and air dried.

2.4 Sample preparation

2.4.1 Microwave digestion

A CEM MDS2000 microwave digestion system with 12 lined digestion vessels was used for the experiments in Chapter 3, Section 3.2.3 and Chapter 4, Section 4.2.4.5.

Digestion performed in Chapter 4 and Chapter 5 of broccoli and barley that had been previously freeze dried for the analysis of reference material used in LA-ICP-MS utilized the CEM MARS 6 microwave digestion system.

Before operation all tubes and lids were cleaned in the following manner. The digestion vessels were placed in an ultrasonic bath for 40 minutes. The tubes were then placed in 1% micro-cleaning solution (glassware cleaner) for 18 hours. The tubes were then rinsed with deionised water and dried in an oven at 60-70°C for a minimum of 1 hour. Finally, the tubes were rinsed in 5-10% nitric acid solution. All glassware was rinsed in 10% nitric acid and dried before use.

2.4.2 Freeze drying

Pre-frozen samples were freeze dried using a Thermo Fisher Scientific Modulyo Freeze Drying system running at a temperature of -52 °C, under vacuum at a pressure of 0.120 mBar.

2.4.3 Cryosectioning

Tissue was sectioned at a temperature of -20 °C using a Leica Cryostat (Leica, Wetzlar, Germany) to obtain between 12- 40 µm sections, which were then mounted onto glass slides or pre-cut aluminium sheets using carbon tape as an adhesive.

2.4.4 Application of matrix to plant material for analysis using MALDI-MS

A 5 mg/ml solution of α -cyano-4-hydroxycinnamic acid (CHCA) in 70:30 methanol: deionised water, with 0.2% trifluoroacetic acid was prepared and stored at 4°C. Samples for MALDI-MS imaging were coated with a 5 mg/ml solution of CHCA in 70:30 methanol: water with 0.2% TFA using the SuncollectTM automated pneumatic sprayer (Sunchrom GmbH, Friedrichsdorf, Germany) in a series of 10 layers. The initial seeding layer was performed at 2 μ l/minute and subsequent layers were performed at 3 μ l/minute.

2.4.5 Laser ablation reference material preparation

After washing with deionised water to remove any residual nutrients or particles, the plant material was freeze dried (Section 2.4.2) to a constant mass. The plant material was then ground in an electric coffee grinder and passed through a 40-micron sieve to ensure homogeneity. The ground plant material was then split into 5 groups, weighed into glass pots and saturated with increasing concentration of standard elemental solution. Each pot was then vortexed to ensure all powder was dispersed into the solution. All the pots were capped and placed onto an oscillating table for 30 minutes at 200 RPM. All standards were then instantly frozen in liquid nitrogen (Jurowski *et al.* 2014) and placed into the freezer at -20 °C overnight. Samples were then freeze dried at -52 °C and 0.120 mBar until a constant mass was achieved.

Powdered vanillic acid was added to each of the dried standards at a rate of 25% w/w. The vanillic acid was used as a binder and absorbs strongly at the laser wavelength of 213 nm. It has previously been documented to improve the sensitivity of LA-ICP-MS

analysis and standardises the absorptivity of the matrix, which in turn improves the quality of the data. (O'Connor, Landon *et al.* 2007)

The resulting mixture was placed into plastic pots with 5 mm ceramic zirconia milling material and placed on to a rotary mill for 66 hrs at 44.6 rpm. This was to improve the homogeneity of the samples. The milled material was passed through a sieve to remove the zirconia and compressed either into 3 mm pellets or 13 mm pellets, using a bench press under vacuum, applying 2 tonnes of pressure for the 13 mm discs and 0.5 tonne of pressure for the 3-mm disc for 1-2 mins.

The reference materials were then digested, using a microwave method (Section 2.4.1) and analysed using the PerkinElmer NexIon 350X ICP-MS.

2.4.6 Acid extraction of selenium species in broccoli sprouts.

For the speciation of the Se compound Se-Met and Methyl-SeCys, a gentler method of extraction was performed based on work performed by Montes-Bayon *et al.* 2006. 0.2 g \pm 0.005 of dried plant material was weighed directly into a 10-ml falcon tube and 2.5 ml of 0.1M HCl was added. The mixture was vortexed to ensure all powder was wet before the samples were then placed into a rotary incubator at 37 °C for 20 hours and continuously shaken at a speed of 230 rpm. The samples were then centrifuged at 2000 rpm for 20 minutes at room temperature. The supernatant was then removed and filtered through at 0.45 μ m syringe filter and diluted with 0.1M HCl. All samples were spiked before analysis by RP-HPLC-ICP-MS with 10 ppm Se-Met, 10 ppm Methyl-SeCys, 10 ppm Na₂SeO₃, 10 ppm Na₂SeO₄ and 10 ppm Sb standard as internal standards and were run in triplicate.

2.5 Analytical techniques

2.5.1 Inductively coupled plasma optical emission spectroscopy (ICP-OES)

After samples had been digested using methods stated in Section 2.4.1, they were run on an ICP-OES "Activa" Horiba Jobin Yvon, with a power of 1000 W, slit width 10 mm, pump speed 15 s, nebulizer flow 0.87 ml/min, nebulizer pressure 2.85 psi. The nebulizer was a glass concentric and the spray chamber a glass cyclonic. The analysis mode was run on mean, with an integration time of 5 seconds, with 3 replicates performed each sample. Argon was used as the carrier gas, with a plasma flow of 12.3 L/min. Data were collected by ACTIVAnalyst 5.4 software. The process of analysis of the digested and filtered samples, using this technique can be seen in Figure 2.5-1.

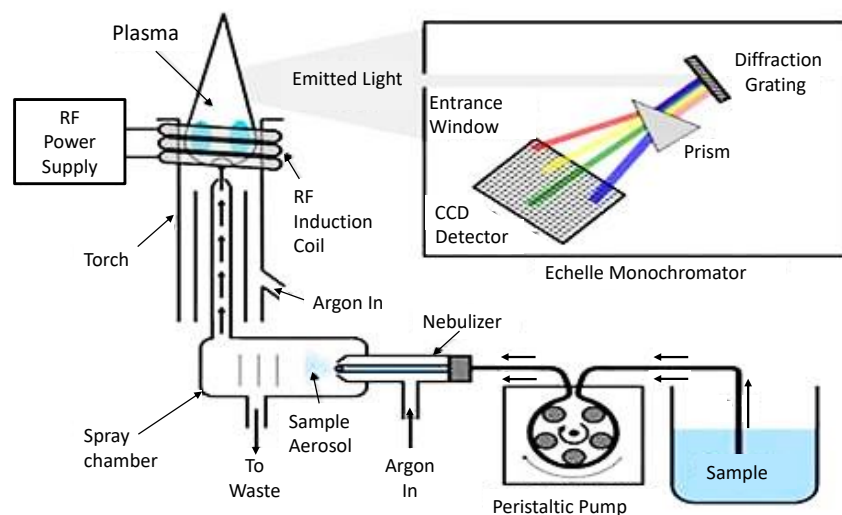


Figure 2.5-1: Schematic diagram of ICP-OES

(image adapted from <http://www.rohs-cmet.in/content/icp-oes>)

The specific wavenumber chosen for each element are summarized in Table 2.5-1.

Element	Wavenumber (nm)	Interferences
Calcium	393.366	U, Ce
Magnesium	279.553	Th
Phosphorus	213.618	Cu, Mo
Iron	259.940	Hf, Nb
Zinc	213.856	Ni, Cu, V

Table 2.5-1: Wavenumbers used in the ICP-OES methods for each element.

2.5.2 Ion chromatography

The Dionex ICS-90 Ion Chromatography system was used for ionic analysis. It was equipped with an isocratic pump, a MicroMembrane suppressor 300 and conductivity detector cell. Analytical separation was achieved with a IONPAC® AS14A analytical column (4 x 250 mm, P/N 056904) and IONPAC® AG14A guard column (4 x 50 mm, P/N 056897).

The eluent and regenerant were prepared as stated in Section 2.5.2.1 . An Eluent flow rate of 0.5 ml/min was maintained at a pressure of 1931 psi with an injection volume of 20 μ l. Data were acquired by using Chromeleon software. A general over view of the system can be found Figure 2.5-2.

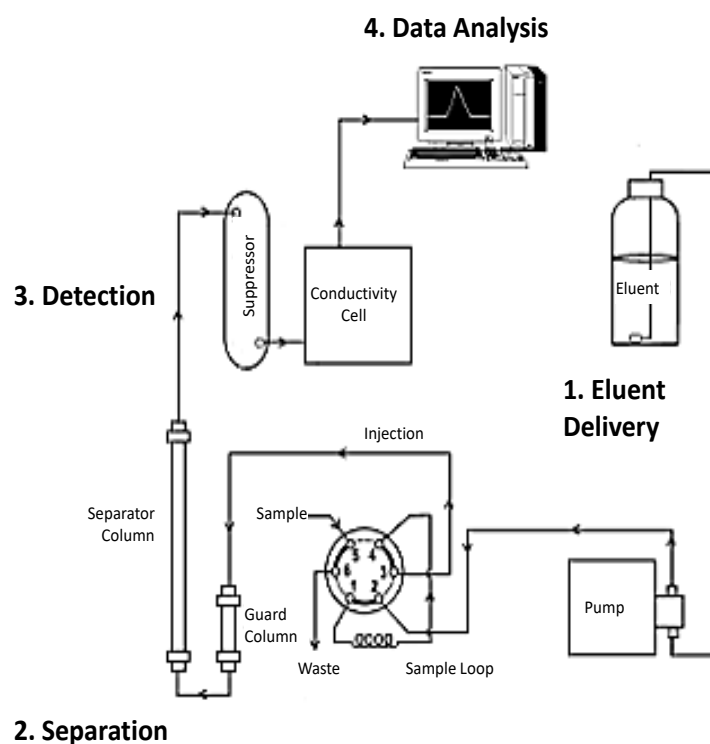


Figure 2.5-2: Ion chromatography process
(Adapted from https://tue.iitm.ac.in/Infrastructure/Analytical_Facility/ion_chromatography.php)

2.5.2.1 Preparation of Ion chromatography eluent and regenerant

An 88 mM Na₂CO₃/100 mM NaHCO₃ concentrate of the eluent was initially made and diluted (1:100) with degassed deionised water with a specific resistance of 17.8 mega ohms cm⁻¹, resulting in a final concentration of 8 mM Na₂CO₃/100 mM NaHCO₃. A 50 mM H₂SO₄ regenerate was made and degassed in a sonicator before use.

2.5.3 X-ray diffraction (XRD)

XRD analysis was performed at the Material & Engineering Research Institute (MERI), at Sheffield Hallam University, UK, with the PANalytical X'Pert Pro MPD diffractometer using Ni-filtered, CuK α radiation, a voltage of 45 kV, and a current of 40 mA with a scintillation counter. The instrument was operated in the continuous scanning speed of 4°/min over a range of 5°C to 40°C.

2.5.4 X-ray fluorescence (XRF) spectrometry

XRF analysis was performed at the Material & Engineering Research Institute (MERI), at Sheffield Hallam University, UK, with the Philips PW2440 Magix Pro sequential spectrometer using the oxide program.

2.5.5 Fourier transform infrared (FT-IR) spectroscopy

FT-IR analysis was performed using attenuated total reflection (ATR) technique with a Perkin Elmer Spectrum 100 FT-IR spectrophotometer. The scanning range was 650 to 4000 cm⁻¹ and the resolution was 2 cm⁻¹.

2.5.6 Raman spectroscopy

Solid powder samples were analysed using a Reinshaw system 200 system fitted with 785 nm He-Cd Laser and a Leica DMLM optical microscope equipped with 50 x objective lenses. The laser beam was focused on to the sample using 20 x objective and the laser power of 100% was employed for 20. This was performed in replicate. The Raman spectra of the samples were taken in the range of 100-2000 cm^{-1} .

2.5.7 Inductively coupled plasma mass spectrometry (ICP-MS)

There were two instruments used in the studies performed.

2.5.7.1 Hewlett Packard (HP) 4500 series ICP-MS

Hewlett Packard (HP) 4500 series ICP-MS was used for the analysis of Se in broccoli and connected to the HPLC for the speciation work (Section 2.5.8). The ICP-MS utilized the Chemstation 4500 series software to produce data and Microsoft Excel was used to process the data. Table 2.5-2 displays the operating parameters.

Parameter	Value
Nebulizer	Glass concentric
Spray Chamber	Glass cyclonic
Cones	Nickel
Sample uptake rate	0.5 ml/min
Plasma gas flow	14.8 L/min
Auxiliary gas flow rate	1.0 L/min
Carrier gas	Argon
Nebulizer flow rate	0.83 L/min
Carrier gas flow	1.36 L/min
RF power	1250 W
Mode	Standard
Scan mode	Peak hopping
Detector	Dual

Table 2.5-2: HP4500 ICP-MS standard parameters.

2.5.7.2 PerkinElmer NexIon 350X

Liquid samples were analysed using an auto sampler on a PerkinElmer NexIon 350X ICP-MS under normal operating conditions (Table 2.5-3)

Parameter	Value
Nebulizer	Glass concentric
Spray Chamber	Glass cyclonic
Cones	Nickel
Sample uptake rate	0.3 ml/min
Plasma gas flow	18.0 L/min
Auxiliary gas flow	1.2 L/min
Carrier gas	Argon
Nebulizer flow rate	0.95 L/min for liquid analysis 1.41 L/min for laser analysis
Carrier gas flow	1.4 L/min
Collision gas	Helium
RF power	1600 W
Mode	Collision
Scan mode	Peak hopping
Detector	Dual

Table 2.5-3: NexIon 350X ICP-MS operating condition

2.5.8 Reverse phase high performance liquid chromatography Inductively coupled plasma mass spectrometry (RP-HPLC-ICP-MS).

Reverse phase high performance liquid chromatography (RP-HPLC) was performed using the Hewlett Packard (HP) 4500 series ICP-MS system and was connected with PEEK tubing to a LDC Analytical Constametric 4100 (Quaternary) delivery system. A zorbax C8 – 25 cm x 4.6 mm (5µm) (part no: ZC8-250A) column, coupled with a guard column, was used. The ICP-MS utilized the Chemstation 4500 series software to produce data and Microsoft Excel was used to process the data. The parameters stated in Table 2.5-4 and Figure 2.5-3 were used.

All samples were spiked before analysis with 10 ppm Se-Met, 10 ppm, Methyl-SeCys, 10 ppm Na₂SeO₃, 10 ppm Na₂SeO₄ and 10 ppm Sb standard as internal standards and were run in triplicate.

Parameter	Value
ICP-MS	
Nebulizer	Glass concentric
Spray Chamber	Glass cyclonic
Sample uptake rate	0.5 ml/min
Cones	Nickel
Carrier gas	Argon
Plasma gas flow	14.8 L/min
Auxiliary gas flow rate	1.0 L/min
Nebulizer flow rate	0.83 L/min
Carrier gas flow	1.36 L/min
RF power	1250 W
Mode	Standard
Scan mode	Peak hopping
Detector	Dual
Dwell time	1s
Isotopes	⁷⁷ Se, ⁷⁸ Se, ⁸² Se, ¹²¹ Sb (Internal standard)
HPLC	
Injector Loop	20 µl
Acquisition time	26 mins (1560 sec)
Mobile phase flow rate	1.4 ml/min
Mobile phase	Gradient (Error! Reference source not found.)
Solvent A	5.0% (v/v) MeOH + 0.1% (v/v) HFBA
Solvent B	0.1% (v/v) HFBA + Deionized water

Table 2.5-4: RP-HPLC-ICP-MS parameters.

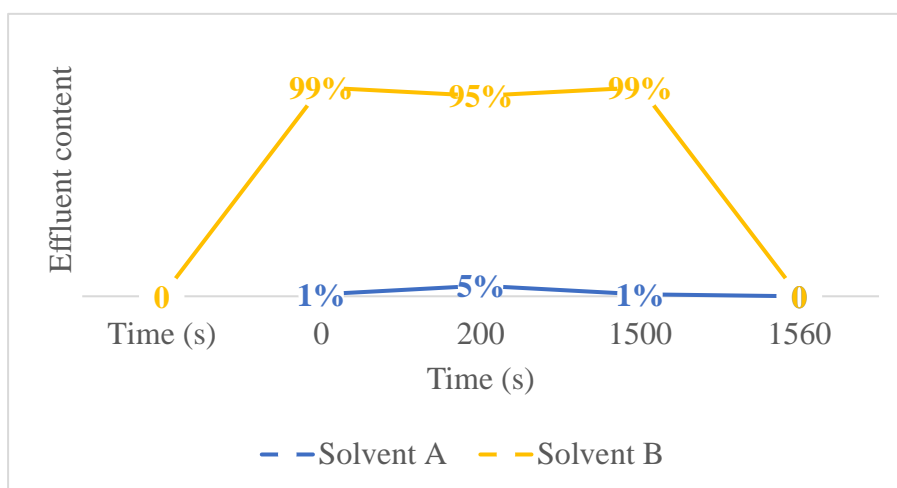


Figure 2.5-3: Mobile phase gradient parameter used for the detection of seleno-amino acids using RP-HPLC

2.5.8.1 Preparation of HPLC mobile phase for seleno-amino acid detection

A gradient was used for the speciation of the seleno-amino acids and therefore two solutions were prepared:

1. 5% (v/v) methanol with 0.1% (v/v) heptafluorobutyric acid (HFBA) solution was prepared with deionised water.
2. 0.1% (v/v) HFBA and deionised water solutions.

Both solutions were filtered through a 0.45-micron filter before use.

2.5.9 Matrix assisted laser desorption/ionisation time of flight mass spectrometry (MALDI-TOF-MS)

Initial mass spectrometric analyses were performed using an Applied Biosystems API Q-Star Pulsar i hybrid quadrupole time-of-flight (QTOF) instrument (Concord, Ontario, Canada) fitted with an orthogonal MALDI ion source and a 1 kHz Nd:YAG solid-state laser. Images were acquired at a spatial resolution of 150 μm x 150 μm in “raster

image” mode, (Trim *et al.* 2010) using ‘oMALDI Server 5.1’ software supplied by MDS Sciex (Concord, Ontario, Canada) and generated using the freely available Biomap 3.7.5.5 software (Novartis, Basel, Switzerland). Mass spectra were processed either in Analyst MDS Sciex (Concord, Ontario, Canada) or using the open source multifunctional mass spectrometry software mMass (Strohalm *et al.* 2010).

2.5.10 Laser ablation inductively coupled mass spectrometry (LA-ICP-MS)

Laser ablation (LA) ICP-MS analysis was performed using a UP213 Universal Platform Laser Ablation System (New Wave, Fremont, CA) utilizing a frequency quintupled NdYAG deep UV laser with the resulting wavelength of 213 nm. This was interfaced with the NexIon 350X via 5mm tubing and a trigger switch. Parameters for the ICP-MS can be found in Table 2.5-5 and the LA parameters for each chapter in Table 2.5-6. Prior to sample analysis, the LA-ICP-MS was optimized for x-y torch position, Lens voltage and nebulizer gas flow by ablating a 0.1mm² raster using NIST 612 glass as a standard and monitoring the multi-element signal.

Parameter	Value
Cones	Nickel
Plasma gas flow	18.0L/min
Auxiliary gas flow	1.2 L/min
Nebulizer/carrier gas flow	1.44 L/min
RF power	1600 W
Replicates per sample	1
Reading/Replicate	Variable
Mode	Collision (KED)
Nebulizer	Glass concentric
Carrier gas	Argon
Collision gas	Helium
Mode	Collision
Scan mode	Peak hopping
Detector	Dual

Table 2.5-5: ICP-MS parameters when coupled with LA system.

LA Parameter	Semi -quantitative (Chapter 4, Section 4.2.5.5)	Full quantitation (Chapter 4, Section 4.2.5.5)	Full quantitation (Chapter 5, Section 5.2.7)
Laser power	28%	28%	28%
Spot size	55 μm	55 μm	100 μm
Repetition rate	20 Hz	20 Hz	20 Hz
Laser energy/Fluence	0.06 J/cm ² (0.001 mJ)	0.06 J/cm ² (0.001mJ)	0.06 J/cm ² (0.001mJ)
Scan speed	95.4 $\mu\text{m/s}$	269.6 $\mu\text{m/s}$	490 $\mu\text{m/s}$
Raster spacing	55 μm	55 μm	100 μm
Laser warm up time	20s	40s	40s
Washout time	25s	40s	40s
Isotopes	⁶⁶ Zn, ³¹ P, ³⁹ K, ²⁴ Mg, ²³ Na, ⁶³ Cu, ⁵⁶ Fe, ⁴⁴ Ca, ³² S	⁶⁶ Zn, ³¹ P, ⁷⁸ Se, ³⁹ K, ²⁴ Mg, ²³ Na, ⁶³ Cu, ⁵⁶ Fe, ⁴⁴ Ca, ¹³ C	⁶⁶ Zn, ⁷⁷ Se, ⁷⁸ Se, ⁸² Se, ¹³ C

Table 2.5-6: Comparison of the laser ablation parameters used for analysis.

Data was initially acquired by Syngistix™ software for ICP-MS, Version 1.0 supplied by PerkinElmer, Inc. The data was then processed using Iolite 3.32 software, (Melbourne, Australia) (Paton *et al.* 2011). Two-dimensional distribution images were produced by running equally spaced, identical consecutive ablations parallel to one another to produce a raster image (Figure 2.5-4D).

Due to the restricted area on the stage within the sample chamber that the laser will ablate in (shown by the red circle in Figure 2.5-4C), some of the tissues were therefore cut into two sections and analysed separately. The two resulting images were then joined together. This is clearly shown in the data with a white dotted line.

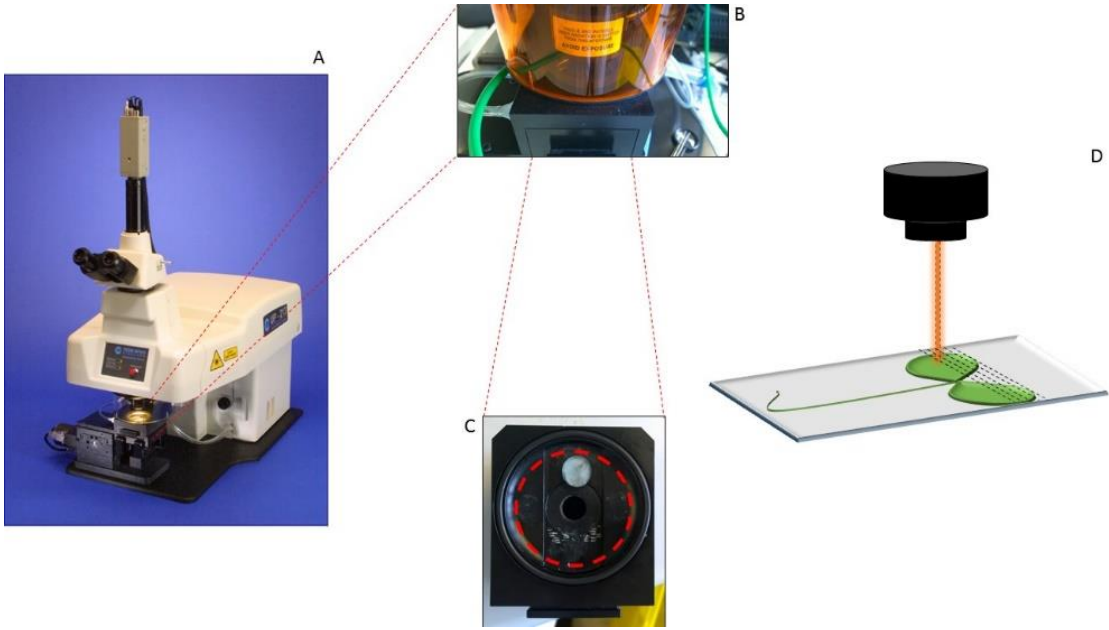


Figure 2.5-4: A) UP213 Laser Ablation system. B) Front view of laser and sample chamber. C) Sample stage. D) Laser ablating tissue.

2.5.10.1 Calculation of spatial resolution of laser ablation images

The spatial resolution of the images was calculated for both the x-direction (the direction the laser passed) and y-direction (the directions the raster followed).

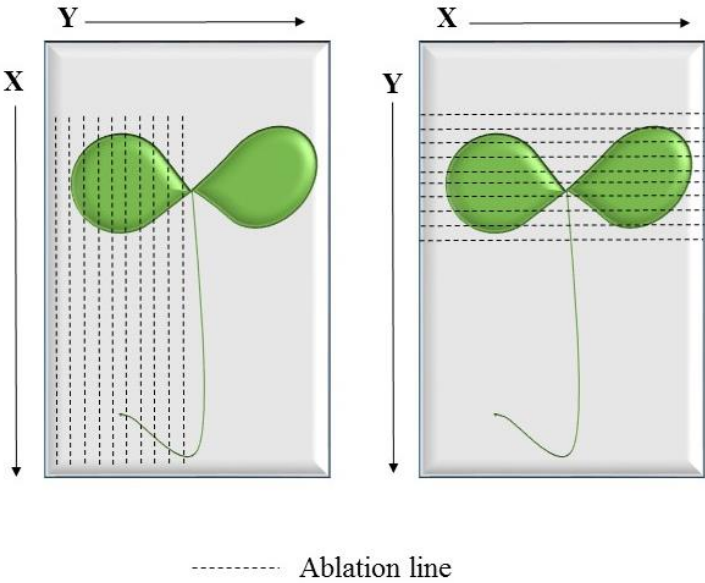


Figure 2.5-5: Spatial resolution directions of tissues ablated differently.

Figure 2.5-5 demonstrates that the spatial resolution is dependent on the direction in which the laser travels. Each plane should be calculated separately and can be calculated. The x-direction is calculated as follows (Equation 2.5-1):

Equation: 2.5-1

$$\text{Spatial resolution} = \varnothing_{\text{spot}} + (T_{\text{mass}} \times V_{\text{scan}}) + D_{\text{washout}}$$

- $\varnothing_{\text{spot}}$ = Laser beam diameter/spot size of the laser that is applied to the tissue)
- T_{mass} = Dwell time of a particular isotope. This is the amount of time (ms) that the instrument spends monitoring that particular element.
- V_{scan} = Scan Speed. The speed ($\mu\text{m/s}$) the laser moves across the tissue.
- D_{washout} = sample chamber washout time x V_{scan} .

The sample chamber washout time is the time taken for the signal to go from 100% to 1% signal once the laser has stopped firing. With the UP213 chamber this is approximately 20 seconds.

The spatial resolution in the y-direction = is the raster/scan line spacing.

This is usually the laser spot size, as the parallel raster lines are offset by the spot size in the y-direction. Larger spacing has been recommended to prevent contamination of adjacent tissue with debris from previous runs (Hutchinson *et al.* 2005).

2.5.11 Carbon-13 isotope analysis

To quantify the data obtained via LA-ICP-MS, an internal standard method was adopted. Carbon-13 was the isotope chosen and an independent analysis was required for the reference material to confirm the concentration. The methodology is outlined in this section.

Samples (0.5 g) of the three-reference material were sent to ISO Analytical, (Crewe, UK) for carbon-13 analysis using Elemental Analysis – Isotope Ratio mass spectrometry (EA-IRMS). In this technique, samples and reference materials are weighed into tin capsules, sealed, and then loaded into an automatic sampler on a Europa Scientific Roboprep-CN sample preparation module. From there they were dropped into a furnace held at 1000 °C and combusted in the presence of oxygen. The tin capsules flash combust, raising their temperature in the region of the sample to ~1700 °C. The combusted gases are swept in a helium stream over a combustion catalyst (Cr₂O₃), copper oxide wires (to oxidize hydrocarbons) and silver wool to remove sulphur and halides. The resultant gases (N₂, NO_x, H₂O, O₂, and CO₂) are swept through a reduction stage of pure copper wires held at 600 °C. This removes any oxygen and converts NO_x species to N₂. A magnesium perchlorate chemical trap removes water. Carbon dioxide is separated from nitrogen by a packed column gas chromatograph held at an isothermal temperature of 100 °C. The resultant CO₂ chromatographic peak enters the ion source of the Europa Scientific 20-20 IRMS where it is ionised and accelerated. Gas species of different mass are separated in a magnetic field then simultaneously measured using a Faraday cup collector array to measure the isotopomers of CO₂ at *m/z* 44, 45, and 46. Analysis was performed in triplicate and was reported as % carbon-13.

2.6 Data Processing

2.6.1 Production of images and processing of matrix assisted laser desorption ionisation mass spectrometry data

Images from the Q-Star instrument were processed using Biomap 3.7.5.5 software. All images were normalised against the total ion count (TIC). For presentation purposes, the mass spectra from the Analyst QS 1.1 software was exported in the form of a text file and then imported into the mMass software for processing.

MALDI-MSI data from the Waters Synapt instrument was converted into Analyze 7.5 format using MALDI imaging converter software (Waters Corporation) and visualised using the BioMap 3.7.5.5 software (Novartis, Basel, Switzerland). SIMS data was analysed and visualized using WinCadence software version 4.4.0.17 (Physical Electronics).

2.6.2 Production of images and processing of laser ablation inductively coupled mass spectrometry data

Images from the LA-ICP-MS were processed using Iolite 3.32 software (Paton, Hellstrom *et al.* 2011). The trace element (Paton, Hellstrom *et al.* 2011) data reduction scheme (DRS) was applied to all quantitative data and the semi- quantitative images used the baseline subtraction DRS. To further quantify and compare the image data, Iolite 3.32 was used to produce stack plot histograms and summary statistics, which included the mean concentration and the standard deviation as a percentage.

2.7 References

HUTCHINSON, R.W., COX, A.G., MCLEOD, C.W., MARSHALL, P.S., HARPER, A., DAWSON, E.L. and HOWLETT, D.R., 2005. Imaging and spatial distribution of β -amyloid peptide and metal ions in Alzheimer's plaques by laser ablation-inductively coupled plasma-mass spectrometry. *Analytical Biochemistry*, **346**(2), pp. 225-233.

JUROWSKI, K., SZEWCZYK, M., PIEKOSZEWSKI, W., HERMAN, M., SZEWCZYK, B., NOWAK, G., WALAS, S., MILISZKIEWICZ, N., TOBIASZ, A. and DOBROWOLSKA-IWANEK, J., 2014. A standard sample preparation and calibration procedure for imaging zinc and magnesium in rats' brain tissue by laser ablation-inductively coupled plasma-time of flight-mass spectrometry. *Journal of Analytical Atomic Spectrometry*, **29**(8), pp. 1425-1431.

MILISZKIEWICZ, N, WALAS, S. AND TOBIASZ, A., 2015. Current approaches to calibration of LA-ICP-MS analysis. *Journal of Analytical Atomic Spectrometry*, **30**, 327-338.

MONTES-BAYON, M., MOLET, M.J.D., GONZALEZ, E.B. and SANZ-MEDEL, A., 2006. Evaluation of different sample extraction strategies for selenium determination in selenium-enriched plants (*Allium sativum* and *Brassica juncea*) and Se speciation by HPLC-ICP-MS. *Talanta*, **68**(4), pp. 1287-1293.

O'CONNOR, C., LANDON, M.R. and SHARP, B.L., 2007. Absorption coefficient modified pressed powders for calibration of laser ablation inductively coupled plasma mass spectrometry. *Journal of Analytical Atomic Spectrometry*, **22**(3), pp. 273-282.

PATON, C., HELLSTROM, J., - PAUL, B., - WOODHEAD, J. and -HERGT, J., 2011. Iolite: Freeware for the visualisation and processing of mass spectrometric data. *Journal of Analytical Atomic Spectrometry*, **26**(12), pp. 2508.

STROHALM, M., KAVAN, D., NOVAK, P., VOLNY, M. and HAVLICEK, V., 2010. mMass 3: A Cross-Platform Software Environment for Precise Analysis of Mass Spectrometric Data. *Analytical Chemistry*, **82**(11), pp. 4648-4651.

TRIM, P.J., DJIDJA, M., ATKINSON, S.J., OAKES, K., COLE, L.M., ANDERSON, D.M.G., HART, P.J., FRANCESE, S. and CLENCH, M.R., 2010. Introduction of a 20 kHz Nd:YVO₄ laser into a hybrid quadrupole time-of-flight mass spectrometer for MALDI-MS imaging. *Analytical and Bioanalytical Chemistry*, **397**(8), pp. 3409-3419.

Chapter 3

3. Identification of precipitate formed in a single component hydroponic nutrient solution

3.1 Introduction

Hydroponic nutrient solutions can be considered as aqueous solutions of inorganic ions (De Rijck, Schrevens 1998a). They contain six essential macroelements, which are classified into cations, potassium (K^+), calcium (Ca^{2+}) and magnesium (Mg^{2+}), and anions, nitrate (NO_3^-), dihydrogen phosphate ($H_2PO_4^-$) and sulphate (SO_4^{2-}), together with the essential microelements. These essential elements can be supplied from many different compounds. Each of these compounds differs in the free ion availability to the plant. Solubility is one of the key factors that dictates the compound of choice, along with its economic viability. For example, monopotassium phosphate (KH_2PO_4) is highly soluble, but is also very expensive to purchase, therefore a mixture of other less expensive compounds, such as potassium sulphate, are used in combination with monopotassium phosphate.

In hydroponics, the inorganic elements, and ions essential for the successful growth and development of healthy crops are provided by nutrient solutions, usually by irrigation through continuous flow or drip-feed systems. The composition of nutrient solutions is essential for successful soilless horticulture and the optimisation of hydroponic nutrient solutions has been reviewed (Gorbe, Calatayud 2010). Nutrients are often formulated empirically for specific crops and/or local conditions. Most nutrients are based on a formulation developed by Hoagland (Hoagland, Arnon 1950, Hoagland, D. R., Arnon, D.I., 1938) . Variations in the composition of the nutrient solution are determined by the variety of plant, growth stage and chemical nature of the water used to dilute the concentrated nutrient solutions. Water which displays hard water characteristics ($CaCO_3 >120$ mg/L) requires less calcium and magnesium in the formulation and increased acidity to neutralise bicarbonates.

Despite the importance of nutrient solutions to the success of hydroponic growing, comparatively little research has been conducted into nutrient solutions, especially the characterisation and prevention of precipitate formation. Most of studies into nutrient solutions have focused on the effects of different nutrients, elements, or compositions on the growth of specific plants. The most comprehensive study of the nutrients themselves has been undertaken by De Rijck and Schrevens, who applied mixture theory to investigate the effects of variables including macro- and microelement content, pH, dissociation, complexation, and precipitate reactions, on the composition of nutrient solutions (De Rijck, Schrevens 1998a, 1998b, 1998c, 1998d, 1998e, 1998f, 1999a, 1998b). These papers examined the solubility product constants (K_{sp}), the common ion effect and the ion product (Q_c) to predict the formation of precipitates within the differing formulation. With the almost endless number of combinations of compounds, the use of these calculation and constants can save time and money when formulating a new nutrient solution.

Precipitate formation is harmful to plants because elements essential for their healthy growth and development are removed from the nutrient solution and the mineral composition changes. Furthermore, the formation of precipitates results in blockages in the irrigation systems that can result in heterogeneous production, diminishing the quality of the produce.

Commercially available nutrient solutions frequently come as a concentrated two-part set, known as part A and part B. Part A contains the calcium, magnesium, and nitrogen compounds, whereas part B contains the phosphorus, sulphur, and trace element compounds. The combination of the concentrated part A and part B quickly results in the formation of a precipitate believed to be predominantly calcium phosphate, which can cause many issues within irrigation systems. These include pipe work blockages

and scale build-up, resulting in pump failure. Furthermore, the precipitate reduces the quantities of certain elements that are available to the plants.

The work presented in this chapter includes the isolation, quantification and the identification of the precipitate found in two-part solution, utilizing a variety of analytical techniques. If we understand the composition of the precipitate, we can investigate methods of preventing its formation by altering the nutrient formulation.

The initial aim of this study was to create a commercially viable single solution for the hydroponic market that does not contain any solid content. To fore fill this we first aimed to quantify, identify, and characterise the precipitates that form in these solutions using a variety of analytical techniques.

3.2 Material and methods

3.2.1 Reagents

All Vita Link nutrient solutions were purchased from Aquaculture Ltd, the composition of which can be seen in Table 3.2-1 and Table 3.2-2. Hydrochloric acid (30%) Fluka, nitric acid (69%) Fluka, hydrogen peroxide (30%) and formic acid were utilized for the digestion of materials. The sodium carbonate, anhydrous 99.9% dried, and sodium hydrogen carbonate were all used for eluent and regenerant for ion selective chromatography, as stated in Section 2.5.2.1.

For the calibration of instruments and production of calibration curves, refer to Chapter 2, Section 2.1 and 2.2 for further details on these chemicals.

	Unit	Soft Water Grow	Soft Water Bloom	Hard Water Grow	Hard Water Bloom
pH		1.75	1.92	0.28	0.48
Total solid content	%	48.89	49.13	45.26	45.25
NO₃-N⁻	g/L	49.75	47.50	50.00	40.70
	mol/L	0.83	0.79	0.83	0.68
	%	4.98	4.75	5.00	4.07
NH₄-N⁺	g/L	4.75	3.75	3.75	1.16
	mol/L	0.15	0.12	0.12	0.04
	%	0.48	0.38	0.38	0.12
K⁺	g/L	62.50	77.50	77.50	77.74
	mol/L	1.60	1.99	1.99	1.99
	%	6.25	7.75	7.75	7.77
PO₄³⁻	g/L	11.25	17.50	11.25	17.50
	mol/L	0.12	0.18	0.12	0.18
	%	1.13	1.75	1.13	1.75
Ca²⁺	g/L	35.00	27.50	26.25	20.00
	mol/L	0.88	0.69	0.66	0.50
	%	3.50	2.75	2.63	2.00
Mg²⁺	g/L	10.00	10.00	7.50	7.78
	mol/L	0.42	0.42	0.31	0.32
	%	1.00	1.00	0.75	0.78
SO₄²⁻	g/L	7.67	8.08	6.33	4.08
	mol/L	0.08	0.08	0.07	0.04
	%	0.67	0.81	0.53	0.42

Table 3.2-1: The combined elemental composition of the different Vita Link Max nutrient solutions, according to the labels ($\pm 5\%$).

	Unit	Concentration
Fe	mg/L	680
Mo	mg/L	12.5
Cu	mg/L	20
B	mg/L	87.5
Mn	mg/L	145
Co	mg/L	12.5
Zn	mg/L	97.5
Ni	mg/L	12.5

Table 3.2-2: The trace element composition of the Vita Link Max nutrient solutions, according to the labels ($\pm 5\%$).

3.2.2 Precipitate formation

Each sample was weighed with a calibrated balance and recorded. After 14 days, a substantial amount of precipitate had formed in all the tubes, all the samples were centrifuged at 3500 rpm at 21 °C for 10 minutes. The pH was measured and recorded using a freshly calibrated (Jenway 350) pH meter. Samples were then filtered using a Büchner filter and Fisher brand 150 mm, QL100 qualitative filter paper. The filter paper and precipitate were then dried at 60 °C in an oven until a constant mass was obtained. The precipitates were recorded as a percentage of the total mass of the solution.

Microwave digestion methods stated in Section 3.2.3.1 and 3.2.3.2 were used for the preparation of the precipitate for ICP OES and ion chromatography analysis respectively. For methodology and instrument parameters refer to Chapter 2, Section 2.5.1 for ICP-OES and Section 2.5.2 for Ion selective chromatography.

The following analytical methods were also applied to the pre-digested material: x-ray powder diffraction (XRD) (Section 2.5.3), x-ray fluorescence (XRF) (Section 2.5.4), FT-IR (Section 2.5.5) and FT-Raman spectroscopy (Section 2.5.6), which were performed by the Materials & Engineering Research Institute (MERI) at Sheffield Hallam University.

3.2.3 Microwave digestion methods

Refer to Section 2.3 and 2.4.1 for instrument specification and preparation of digestion tubes. 0.1 g \pm 0.001 precipitate was weighed directly into each digestion tube using a calibrated balance. Deionised water (5 ml) was then added to each tube, including a blank.

All methods were adapted from previously published methods (Yash Kalra (Editor) 1997, Wang, Song *et al.* 2010, Colina, Gardiner 1999, Buldini, Tonelli *et al.* 2009, Gupta 1999).

3.2.3.1 Method 1

Concentrated (69%) nitric acid (5 ml) was added to each tube. The lids were replaced and the tubes were placed into the microwave turntable and connected to the vent tube.

The microwave was programmed as follows (Table 3.2-3):

Stage	1	2	3
Power	315 W (50%)	315 W (50%)	315 W (50%)
Pressure (PSI)	40	80	120
Time (mins)	8:00	8:00	20:00
Fan speed	100	100	100

Table 3.2-3: Microwave parameters

On completion, the samples were allowed to cool for five minutes in the microwave.

The turntable was removed from the system, placed in the fume hood and the digestion tubes were manually vented. 2 ml hydrochloric acid (37%) was then added to each tube and allowed to stand for five minutes. The lids were replaced and the turntable placed back in the microwave unit and the following program run (Table 3.2-4).

Once the program was completed the tubes were removed from the microwave and allowed to cool for five minutes by manually venting. The contents of each tube were then rinsed out with deionised water into a 100-ml volumetric flask (1:200 dilution).

The rinsing with deionised water was repeated three times, including the lid. The volumetric flask was then made up with deionised water and transferred to an ultrasonic

bath for 20 minutes. The resulting solution was then filtered (using 30 mm, 0.2 μm syringe filters), diluted and analysed by ICP-OES (Refer to Section 2.5.1)

Stage	1	2	3	4
Power	189 W (30%)	-	189 W (30%)	-
Pressure (PSI)	20	00	40	40
Time (mins)	5:00	5:00	5:00	5:00
Fan speed	100	100	100	100

Table 3.2-4: Microwave parameters

3.2.3.2 Method 2

All tubes were washed using the method stated in Section 2.3 and Section 2.4.1.

Approximately 0.2 g of sample was weighed into a glass sample vial and the mass recorded. The sample was transferred to the digestion tube and the vial rinsed with hydrogen peroxide (10 ml, 22%). 50 μl of formic acid was added to each tube and the lids secured. The vessels were then placed into the microwave digestion unit and the following program was run (Table 3.2-5):

Stage	1	2	3	4
% Power	250 W (40%)	-	600 W (95%)	-
Pressure (PSI)	20	20	20	-
Time (mins)	5:00	15:00	10:00	10:00
Fan speed	100	100	100	100

Table 3.2-5: Microwave parameters

The turntable, with samples, was removed from the microwave and cooled to room temperature in the fume hood. Once cooled, 1 ml of 37% hydrochloric acid was added

to each tube and placed back into the microwave unit and the following program was run (Table 3.2-6):

Stage	1	2	3	4
% Power	250 W (40%)	-	500 W (79%)	-
Pressure (PSI)	20	20	20	-
Time (mins)	5:00	2:00	5:00	5:00
Fan speed	100	100	100	100

Table 3.2-6: Microwave parameters

The samples were then removed from the microwave and cooled to room temperature in the fume hood. The contents of each tube were then rinsed into 50 ml volumetric flasks, with deionised water. Rinsing with deionised water was repeated three times, including the lid. The volumetric flask was then made up with deionised water and transferred to an ultrasonic bath for 20 minutes. The resulting solution was further diluted (1:20) then filtered using 30 mm, 0.2 µm syringe filters. Digested samples were analysed using the Dionex Ion Chromatography instrument (See Section 2.5.2).

3.3 Results and discussion

3.3.1 Composition of the nutrient

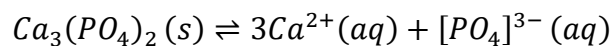
The composition of the Vita Link Max nutrient solutions, as specified on the labels is shown in Table 3.2-1 and Table 3.2-2. In accordance to industry standards, there is a $\pm 5\%$ tolerance with the elemental content stated on the label. Table 3.2-1 shows the macroelements as g/L and as a percentage of the total solution and Table 3.2-2 lists the microelement content as mg/L.

Commercially available nutrients are split and formulated for particular time points in the growth cycle to promote better yields. By convention they are split into “Grow” and “Bloom” formulations. The formulations are also found to be specific to a hardness, that is the calcium carbonate content of water to be used. The most noticeable differences include the lower proportion of phosphorus in the grow formulations and higher levels of calcium, magnesium, and sulphur in the soft water (SW) formulations. During a plant’s growth cycle the demand for particular elements changes over time. During the early season, when a plant is producing more vegetative growth, there is a greater demand for nitrogen, and a lower demand for phosphorus. To produce optimum yields, the fertilization program should be altered accordingly to match the plants’ nutritional needs. The reason for the lower levels of calcium and magnesium in the hard water (HW) nutrient is due to hard water already containing substantial amounts of both calcium and magnesium. Therefore, the nutrients do not require as much. Table 3.2-1 demonstrates a clear difference between the hard and soft water nutrients, with a lower pH in the hard water nutrients. It can also be seen from Table 3.2-1 that the grow formulations tend to be at a lower pH than the corresponding bloom formulation.

The only ion which will suffer from the common ion effect when mixing the A and B components is nitrate-N and is therefore making the common ion effect negligible (data not shown). However, when preparing the individual part A and part B, the common ion effect should be considered.

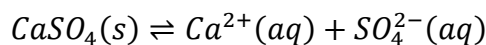
Table 3.2-1 demonstrates the presences of 7 ions, 3 anions (PO_4^{3-} , SO_4^{2-} & NO_3^-) and 4 cations (K^+ , Ca^{2+} , Mg^{2+} & NH_4^+) in the Vita Link nutrient solutions. Based on the solubility chart found in Linde, 2004, there are three compounds which may form which are sparingly soluble in water and acid, they are calcium phosphate, calcium sulphate and magnesium phosphate. The solubility product constant (K_{sp}), is the equilibrium constant for the solubility equilibrium of a slightly soluble ionic compound. It can be expressed as an equation and a value calculate as a constant, which is directly affected by temperature. Equation 3.1, 3.2 and 3.3 are examples of the solubility products for calcium phosphate, calcium sulphate and magnesium phosphate that could be found in the resulting solution after mixing of part A and part B.

Equation 3.1

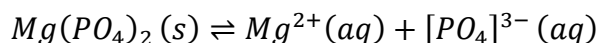


$$K_{sp} = [\text{Ca}^{2+}]^3 [\text{PO}_4^{3-}]^2$$

Equation 3.2



$$K_{sp} = [\text{Ca}^{2+}][\text{SO}_4^{2-}]$$

Equation 3.3

$$K_{sp} = [Mg^{2+}]^3 [PO_4^{3-}]^2$$

At 25° C the K_{sp} of the following compounds are (Linde 2004):

$$\text{Calcium phosphate (Ca}_3\text{(PO}_4\text{)}_2\text{)} = 2.07 \times 10^{-33} \text{ mol.dm}^{-3}$$

$$\text{Calcium sulphate (CaSO}_4\text{)} = 4.93 \times 10^{-5} \text{ mol.dm}^{-3}$$

$$\text{Magnesium phosphate (Mg(PO}_4\text{)}_2\text{)} = 1.04 \times 10^{-24} \text{ mol.dm}^{-3}$$

This can be used to calculate the solubility of a compound and predict if precipitation will occur from the mixing of ions of different concentrations. At the same time the solubility of a product can be used to calculate the K_{sp} of a compound. The smaller the K_{sp} value the lower the solubility of the compound. The work presented here does not involve the dissolving of solid material and the reaction between ions within a solution is of more interest. Therefore, the next step in calculating if a precipitate will form when two ion solutions are mixed together is to calculate what is known as the ion product (Q_c). This is the same as the solubility constant expression, however the concentrations of the substances are not in equilibrium. The Q_c is calculated from the concentration of the ions in the solution. By comparing the K_{sp} with the ion product (Q_c), the direction of the reaction can be predicted and therefore the formation of precipitate. If the Q_c is greater than the K_{sp} , precipitation is expected to occur and vice versa.

The ion product (Q_c) of the Vita Link solutions from Table 3.2-1 for $CaSO_4$ are as follows:

$$Q_c = [Ca^{2+}][SO_4^{2-}]$$

Equation 3.4 Soft water Grow: $(0.88) \times (0.08) = 0.0704$

Equation 3.5 Soft water Bloom: $(0.69) \times (0.08) = 0.0552$

Equation 3.6 Hard water Grow: $(0.66) \times (0.07) = 0.0462$

Equation 3.7 Hard water Bloom: $(0.50) \times (0.04) = 0.02$

The ion product (Q_c) of the Vita Link solutions from Table 3.2-1 for $\text{Ca}_3(\text{PO}_4)_2$ are as follows:

$$Q_c = [\text{Ca}^{2+}]^3 [\text{PO}_4^{3-}]^2$$

Equation 3.8 Soft water Grow: $(0.88) \times (0.12) = 0.1056$

Equation 3.9 Soft water Bloom: $(0.69) \times (0.18) = 0.1242$

Equation 3.10 Hard water Grow: $(0.66) \times (0.12) = 0.0792$

Equation 3.11 Hard water Bloom: $(0.50) \times (0.18) = 0.09$

The ion product (Q_c) of the Vita Link solutions from Table 3.2-1 for $\text{Mg}(\text{PO}_4)_2$ are as follows:

$$Q_c = [\text{Mg}^{2+}] [\text{PO}_4^{3-}]^2$$

Equation 3.12 Soft water Grow: $(0.42) \times (0.12) = 0.0504$

Equation 3.13 Soft water Bloom: $(0.42) \times (0.18) = 0.0756$

Equation 3.14 Hard water Grow: $(0.31) \times (0.12) = 0.0372$

Equation 3.15 Hard water Bloom: $(0.32) \times (0.18) = 0.0576$

Table 3.3-1 summarises these all the K_{sp} and Q_c calculated for the 3 sparingly soluble compounds which could form in the Vita Link solutions. All of the Q_c calculated for the Vita Link nutrients are larger than the K_{sp} constants of the precipitates and therefore the reaction favours the formation of a precipitate.

Compound	Soft Water Grow		Soft Water Bloom	Hard Water Grow	Hard Water Bloom
	K_{sp}	Q_c	Q_c	Q_c	Q_c
CaSO₄	4.95×10^{-5}	0.0704	0.0552	0.0462	0.0200
Ca₃(PO₄)₂	2.07×10^{-33}	0.1056	0.1242	0.0792	0.0900
Mg(PO₄)₂	1.04×10^{-24}	0.0504	0.0756	0.0372	0.0576

Table 3.3-1: Comparison of the solubility product constant (K_{sp}) and ion product (Q_c) of the possible precipitates that will form from each of the Vita Link recipes.

3.3.2 Precipitate quantification

Once the precipitate from each of the solutions had reached a constant mass after separation from the solution, a comparison between the groups was made, which can be seen in Figure 3.3-1. There is a clear difference between the hard and the soft water nutrients, with both the soft water formulations producing a larger amount of precipitate. This could be attributed to the lower pH of the hard water formulation.

Other possible reasons for the increased amount of precipitate in the soft water nutrients include the increased levels of calcium, magnesium and sulphur in these formulations and the overall amount of solid material that is used in the making of the soft water nutrients is also greater (Table 3.2-1). Further support can be seen in Table 3.3-1, with the ion product (Q_c) calculated for the soft water formulation being greater than the hard water formulation.

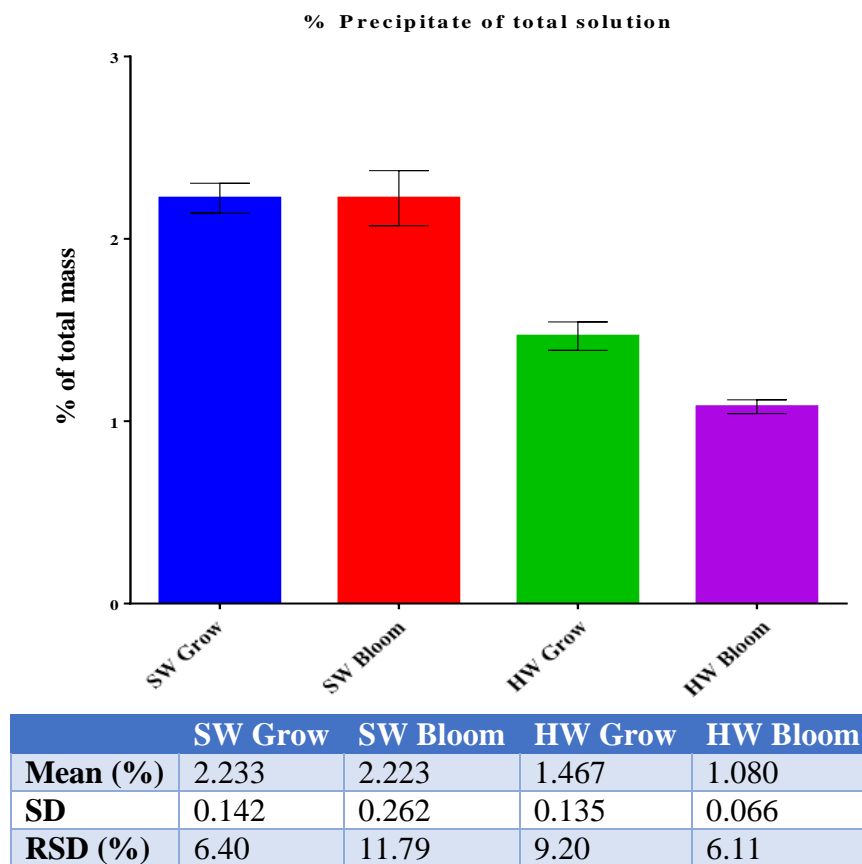


Figure 3.3-1: The amount of precipitate, as a percentage of the total mass, formed when Vita link Max part A and part B are mixed together in equal quantities (n = 3).

The formation of a precipitate will result in a reduction of the free ions within the solution being supplied to the plant, thus a reduction in bioavailability of particular elements to the plant. This, in turn, can cause deficiencies within the plant, leading to stunted growth, increased susceptibility to disease and an overall reduction in yield.

3.3.2.1 Elemental analysis of the precipitate

The results from the semi-quantitative ICP-OES analysis revealed that the precipitate contained calcium and sulphur, with a lower proportion of phosphorus. This suggests that the precipitate is predominantly some form of calcium sulphate mixed with calcium phosphate. As there are many different forms of calcium sulphate and calcium phosphate, with varying properties, it is important to identify which phase is forming.

	Unit	SW Grow	SW Bloom	HW Grow	HW Bloom
Na	%	0.10	0.09	0.11	0.08
Mg	%	0.03	0.03	0.03	0.02
P	%	3.45	4.44	0.50	0.80
S	%	32.89	33.68	42.39	33.82
K	%	0.20	0.21	0.16	0.18
Ca	%	34.92	34.56	34.93	33.72

Table 3.3-2: XRF data of the precipitates formed when Vita Link Max two-part nutrient solutions are mixed. This is reported as a percentage of the precipitate.

The XRF results are shown in Table 3.3-2. XRF is a non-destructive elemental analytical technique ideally suited to the characterisation of solid samples such as the precipitate described in this chapter. The data presented in Table 3.3-2 supports the ICP-OES data, demonstrating that the precipitate is predominantly made up of calcium and sulphur with small amounts of phosphorus present. A point to note is that in Table 3.3-2 both the soft water grow and bloom formulation precipitates have higher levels of phosphorus than the hard water formulation precipitates, suggesting that the precipitates which form within hard water nutrients have a different composition to the soft water nutrients. This again supports the suggestion that the pH of the solution influences the composition of the precipitate formed. Both Calcium sulphate and calcium phosphate

are both more soluble at lower pH and a reduction in precipitate formation occurs. This is due to the increased amounts of H^+ ion in the more acidic solution reacting with the anions, which in this case is the SO_4^{2-} and PO_4^{3-} , preventing them from reacting with the calcium and forming the precipitate.

The results in Table 3.3-2 further supports the data in Table 3.3-1. $CaSO_4$ has the greatest K_{sp} of all the compounds and therefore be expected to be the predominate precipitate formed. The ion product (Q_c) in Table 3.3-1, further support the composition of the different precipitates formed from the different formulations. The Q_c for $Ca_3(PO_4)_2$ in the hard water formulation are much lower than that of the soft water formulation, suggesting that that the formation of $Ca_3(PO_4)_2$ will be less in the hard water formulation. This is confirmed by the results in Table 3.3-2.

3.3.2.2 Ion chromatography

The anion content of the precipitate was determined using ion chromatography. Initial studies used nitric acid to digest the precipitate: however, the concentration of nitrates from the nitric acid caused interference, overlapping with the phosphate peak, as can be seen in Figure 3.3-2. Therefore, alternative microwave digestion methods were investigated. Initially, hydrogen peroxide was employed as the oxidizing agent with the rationale that since the main product from the reaction is water there would be no anions to interfere with the ion chromatography (Buldini, Tonelli *et al.* 2009). Formic acid was added to the samples to prevent the hydrolysis of the compounds. However, this method did not completely digest all of the solid material. Consequently, a mixture of hydrochloric acid and hydrogen peroxide were used instead (Buldini, Tonelli *et al.*

2009). Not only did this method successfully dissolve all of the precipitate, but the retention time of the chloride is very different to those of PO_4^{3-} , NO_3^- and SO_4^{2-} , as shown in Figure 3.3-2. Figure 3.3-3 displays the chromatograms of the digested precipitates. The quantitative results are summarised in Table 3.3-3 and shows that the predominant anion is sulphate with the soft water formulations containing much smaller amounts of phosphate.

Table 3.3-3 clearly demonstrates that the precipitate is predominately sulphate based and supports the other data produced by other techniques. The soft water formulations both contain significantly higher levels of phosphates than the respective hard water formulas. The most obvious reason would be the pH of the hard water solutions being much lower and therefore solubilising the precipitate.

These results further support the data in section 3.3.1 and section 3.3.2.1.

	Unit	SW Grow	SW Bloom	HW Grow	HW Bloom
Cl⁻	g/L	0.04	0.45	0.00	0.02
	%	0.97	11.16	0.00	0.49
NO₃-N	g/L	0.00	0.04	0.10	0.00
	%	0.00	1.01	2.48	0.00
PO₄³⁻	g/L	0.13	0.18	0.01	0.02
	%	3.25	4.40	0.36	0.45
SO₄²⁻	g/L	2.11	2.07	2.13	2.25
	%	32.59	31.11	33.12	35.92

Table 3.3-3: The anion composition of the precipitate formed from the addition of the various matching Vita Link Max part A and Part B formulation using ion chromatography.

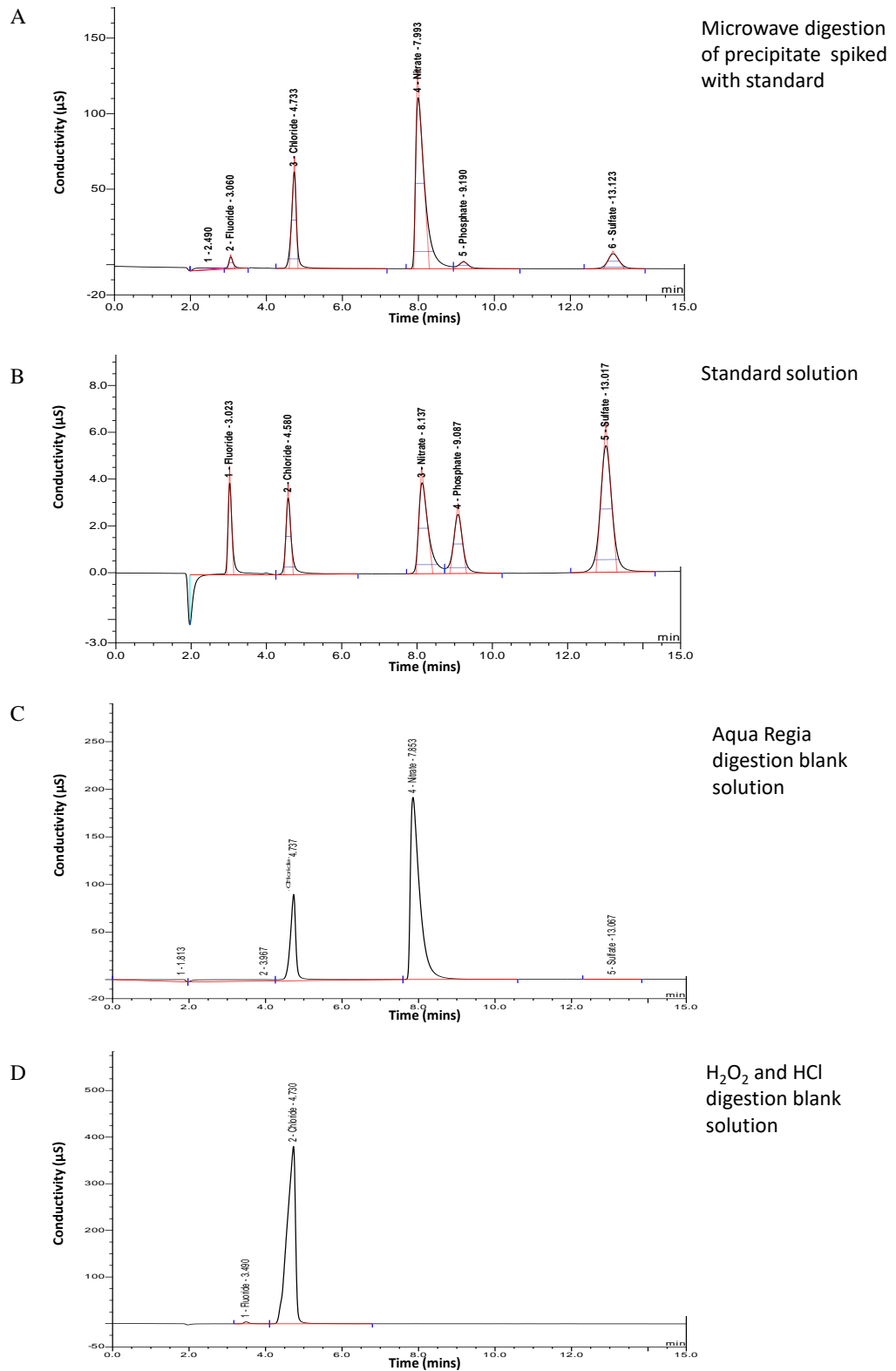


Figure 3.3-2: Comparison of the effect of different digestion methods on the results achieved from ion chromatography A) Microwave digestion method 1 (Aqua Regia) spiked with standard solution. B) Standard solution. C) Digestion blank Aqua Regia. D) Digestion blank – H₂O₂ and HCl. Note: Standard solution containing fluoride, chloride, phosphate, nitrate and sulphate.

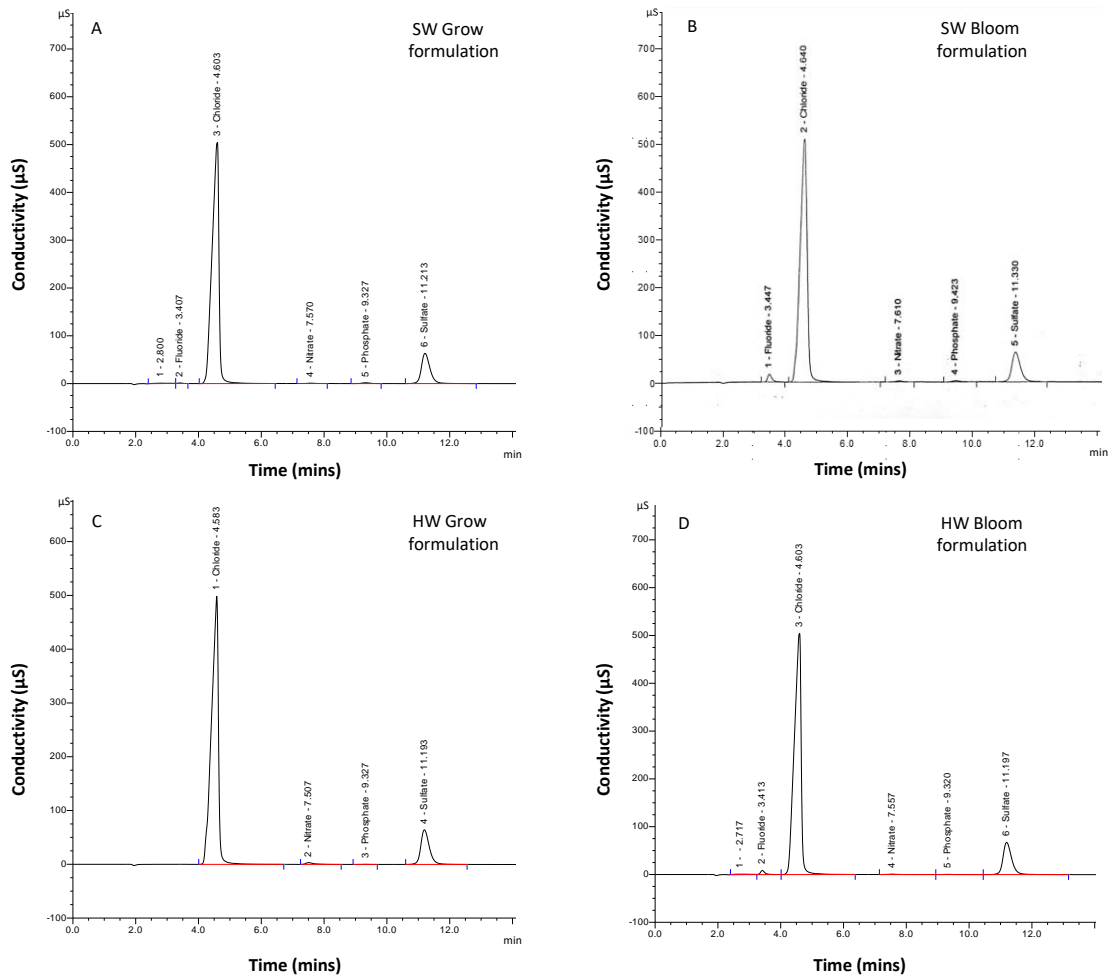


Figure 3.3-3: The chromatograms of the precipitates formed when equal volumes of the various matching Vita Link part A & B are mixed.

3.3.2.3 X-ray diffraction

All of the diffractograms in Figure 3.3-4 are very similar with the only difference being in peak intensity. Comparisons with data from the American Mineralogist Crystal Structure Database (<http://rruff.geo.arizona.edu/AMS/amcsd.php>) and the instrument database revealed that the peak patterns match those of gypsum ($\text{CaSO}_4 \cdot 2\text{H}_2\text{O}$), a form of calcium sulphate and Brushite ($\text{CaPO}_3(\text{OH})2\text{H}_2\text{O}$) a form of calcium phosphate.

The results obtained from the XRD provided addition information and further evidence of the composition of the precipitates found in the solutions. The results further support and confirm that the precipitate is predominately made of calcium sulphate, with small amounts of calcium phosphate present in the soft water formulations. Unfortunately, the peak patterns are very similar for these two compounds, making it more difficult to identify any significant difference between the formulations.

These results further support the data in section 3.3.1, section 3.3.2.1, and section 3.3.2.2.

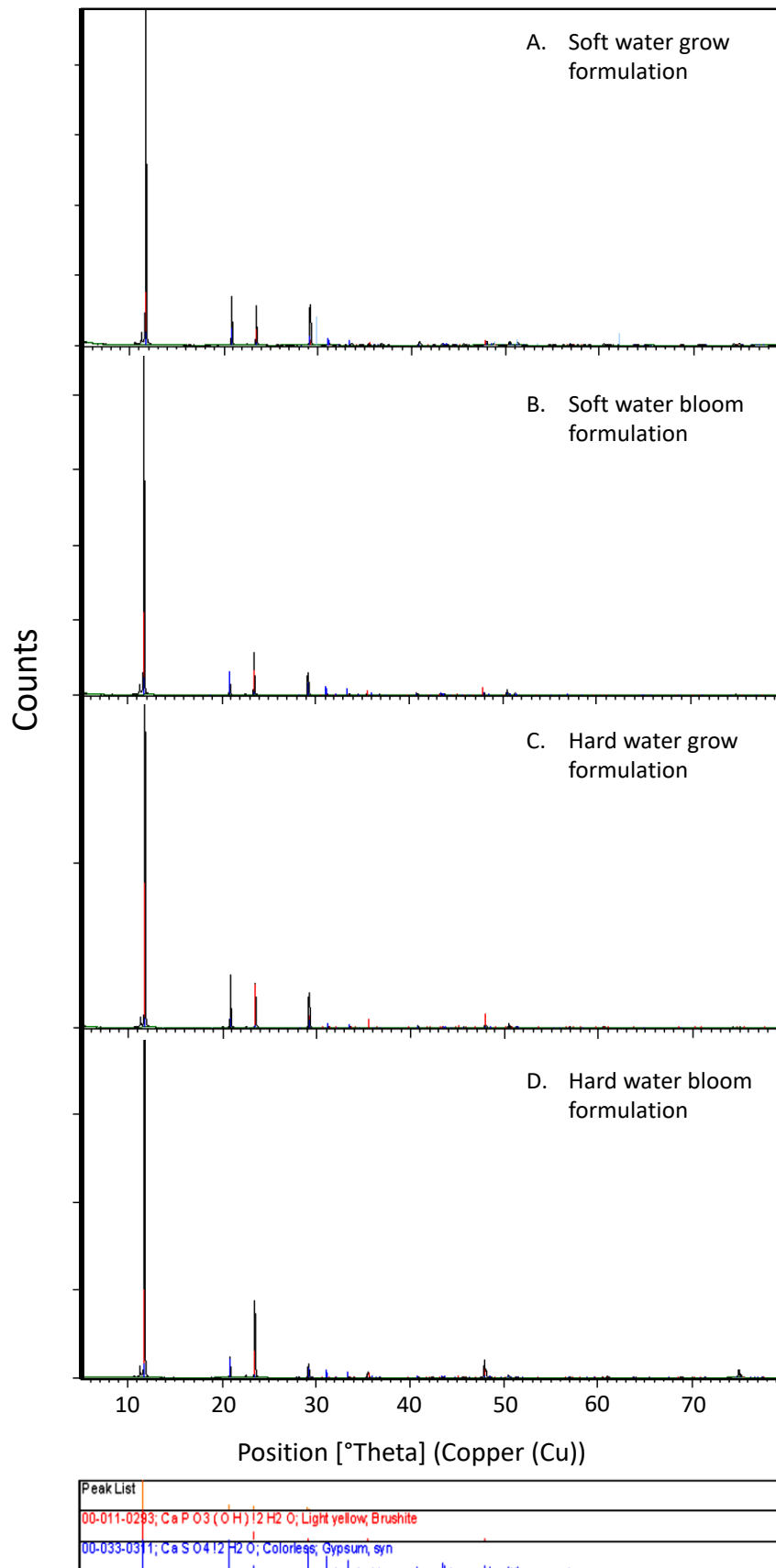


Figure 3.3-4: XRD diffractogram of the various precipitates of the different 4 different Vita Link formulations.

3.3.2.4 Vibrational spectroscopy

IR and Raman spectroscopies are relatively cheap and non-destructive techniques that are ideally suited to characterising solid compounds such as the precipitates formed in hydroponic nutrients.

Tetrahedral oxoanions such as phosphate and sulphate display four bands; symmetric (ν_1) and antisymmetric (ν_3) stretching and symmetric (ν_2) and antisymmetric (ν_4) bending modes (Farmer 1974). The ν_1 and ν_2 bands are only Raman active, whereas the ν_3 and ν_4 bands are both IR and Raman active. A difficulty with vibrational spectroscopy is that the positions of these bands for phosphate and sulphate ions occur in very similar regions.

Table 3.3-4 summarises the well-established and documented frequencies of SO_4^{2-} and PO_4^{3-} , illustrating how close these bands are.

	ν_1	ν_2	ν_3	ν_4
Activity	Raman only (cm^{-1})	Raman only (cm^{-1})	IR & Raman (cm^{-1})	IR & Raman (cm^{-1})
PO_4^{3-}	938	420	1017	567
SO_4^{2-}	983	450	1105	611

Table 3.3-4: Fundamental frequencies of SO_4^{2-} and PO_4^{3-} (Farmer 1974)

The Raman spectra of the precipitates are shown in Figure 3.3-5 and Figure 3.3-6, and the IR spectra are illustrated in Figure 3.3-7. XRD analysis indicates that the precipitates are a mixture of brushite and gypsum. Table 3.3-5 shows the IR and Raman bands for both minerals and demonstrates the similarities in the band positions for these compounds. The data in Table 3.3-5 correlates with Figure 3.3-5. Figure 3.3-6 and Figure 3.3-7. The Raman spectra contain a band at 1007 cm^{-1} which can be assigned to ν_1 peak in brushite. In gypsum, the ν_1 band is IR active. The strong band at 1100 cm^{-1} in

the IR spectra is most likely the sulphate antisymmetric (ν_3) stretching. The band at 413 cm^{-1} and 491 cm^{-1} in the Raman spectrum (Figure 3.3-5 & Figure 3.3-6) can be assigned to symmetric bending (ν_2) of gypsum. The 616 cm^{-1} and 668 cm^{-1} in the Raman spectrum can therefore be assigned to the antisymmetric (ν_4) bending modes of gypsum, in accordance with Table 3.3-5.

Activity	ν_1	ν_2	ν_3	ν_4
	IR Raman (cm^{-1})	IR Raman (cm^{-1})	IR Raman (cm^{-1})	IR Raman (cm^{-1})
CaHPO₄·2H₂O (Brushite)	1005	418 400	1135 1075	577
CaSO₄·2H₂O (Gypsum)	1006	492 413	1144 1138 1117	621 669 624

Table 3.3-5: Vibrational spectra of gypsum (CaSO₄·2H₂O) and brushite (CaHPO₄·2H₂O).

There are very subtle differences between the hard water and soft water formulations.

The IR spectrum of the soft water formulations, shown in Figure 3.3-7, also contains a band at 1014 cm^{-1} , which could be assigned to the antisymmetric (ν_3) stretching of the PO_4^{3-} ion (Table 3.3-4), with the symmetric (ν_1) stretching of PO_4^{3-} being masked by the large 1100 cm^{-1} band of the sulphate antisymmetric stretch (ν_3).

Furthermore, it is worth noting in Figure 3.3-7 the appearance of a band at 837 cm^{-1} in the spectra of the soft water bloom formulations. Within the literature, νPOH is mentioned and occurs between 834-900 cm^{-1} (Farmer 1974). The data from the ion chromatography, XRD and XRF, all show that there is a higher concentration of phosphate in the soft water formulation. This would suggest that the 837 cm^{-1} band is due to a POH vibration. .

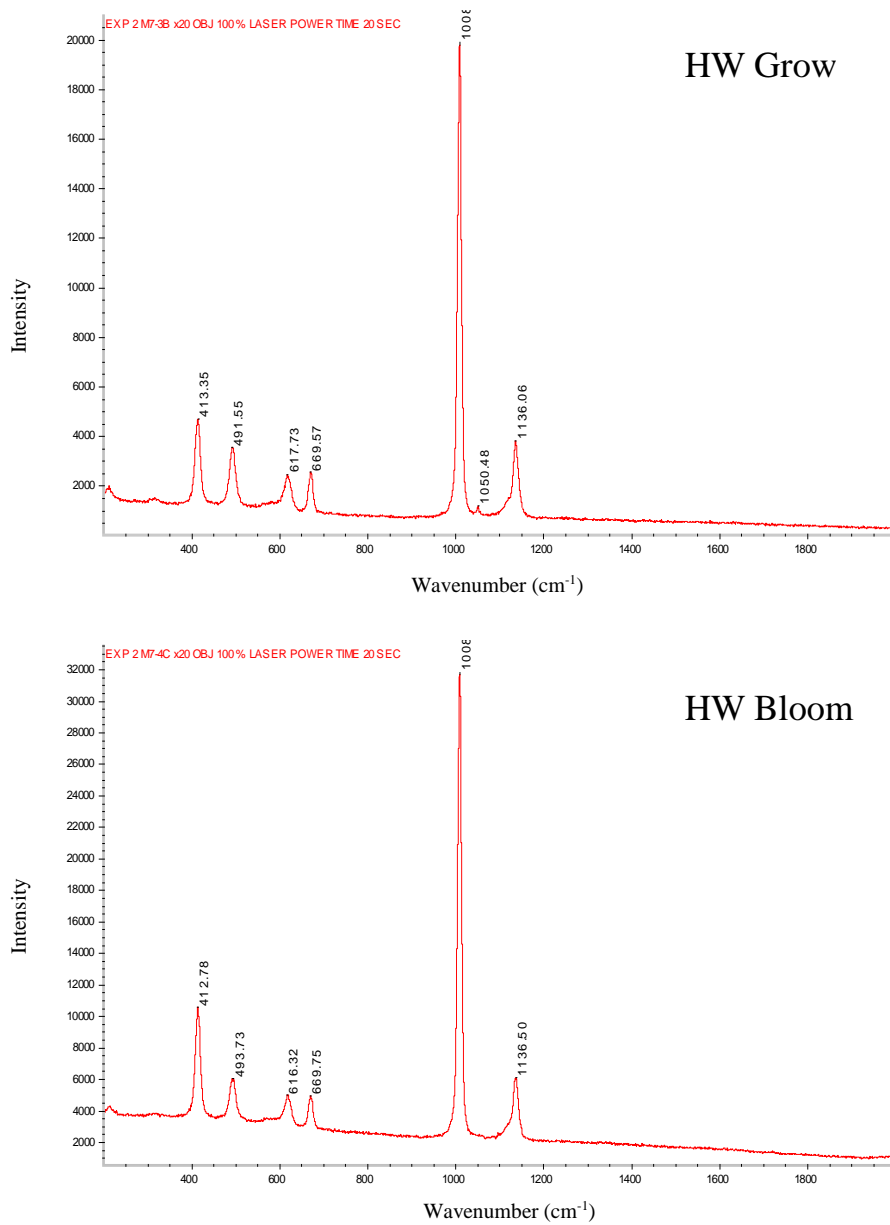


Figure 3.3-5: Raman spectra of the precipitate from Vita Link Hard Water Part A and Part B mixed

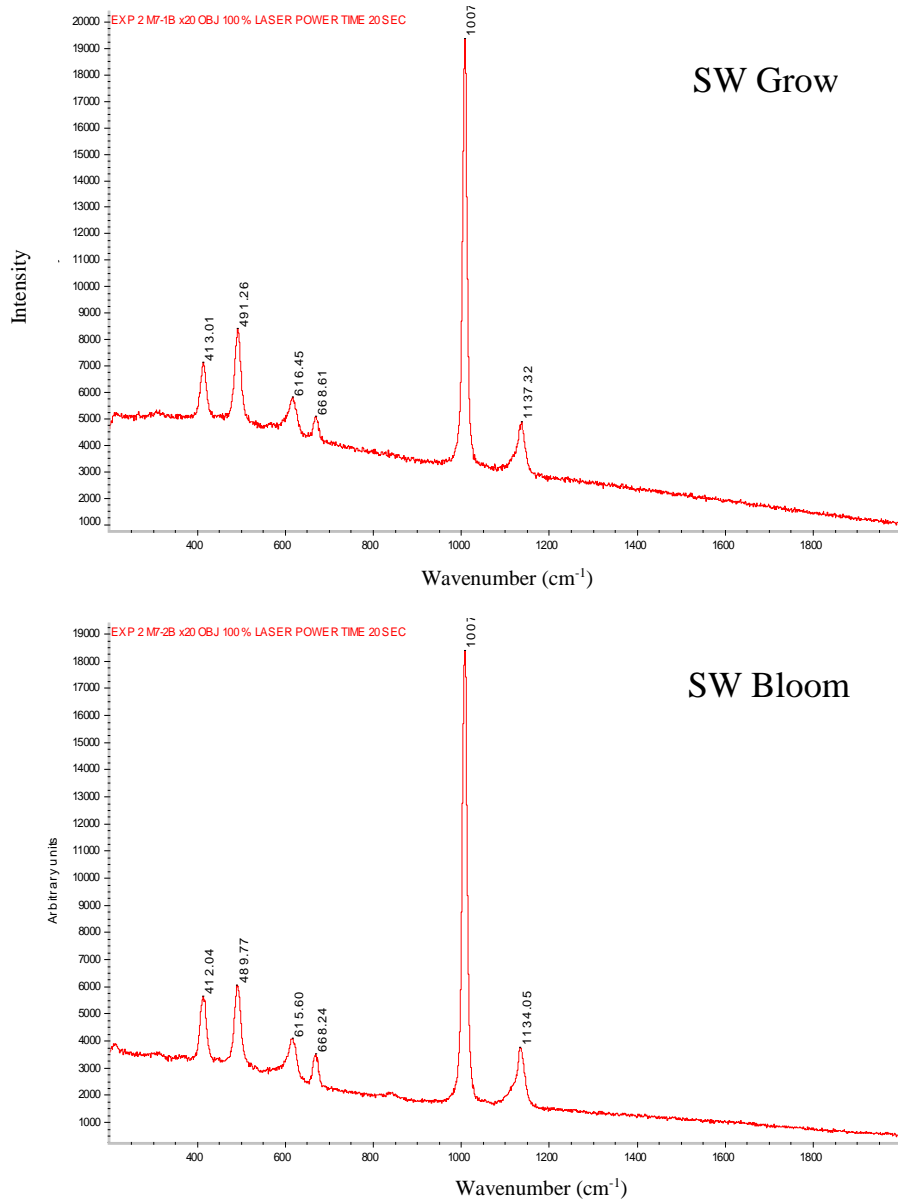


Figure 3.3-6: Raman spectra of the precipitates from Vita Link Max Soft Water Part A and Part B mixed.

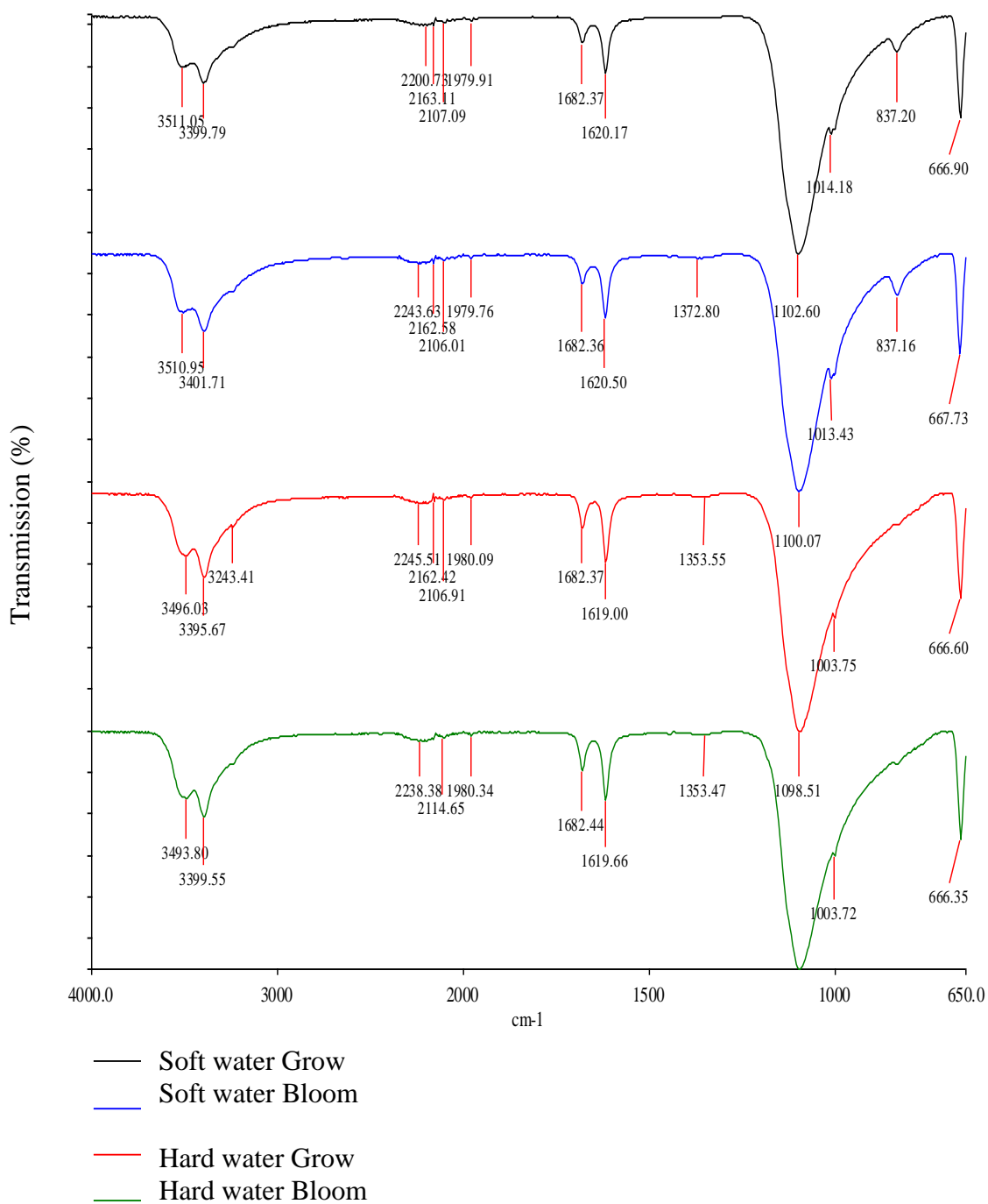


Figure 3.3-7: FT-IR spectra of the precipitates produced from the various formulation of Vita Link solutions.

3.3.2.5 Bioavailability reduction of ions by precipitate formation

From the data presented in this chapter, we can summarise and calculate the reduction in available ions to the plant due to the formation of the precipitate (Table 3.3-6, Table 3.3-7 and Table 3.3-8).

Ca ²⁺	Unit	SW Grow	SW Bloom	HW Grow	HW Bloom
pH		1.78	1.95	0.18	0.47
Amount of precipitate formed as a percentage of the total volume of nutrient solution.	% of the solution	2.233	2.223	1.466	1.08
Total solution content according to the label.	g/L	35	27.5	26.25	20
Quantity of Ca²⁺ determined by Ion Chromatography (IC)	% of the precipitate	-	-	-	-
Quantity of Ca²⁺ determined by XRF	%	34.92	34.56	34.93	33.72
Mean precipitate content from XRF & IC data.	% of precipitate	34.92	34.56	34.93	33.72
Ca²⁺ taken out of the solution due to precipitate formation.	g/L	7.80	7.68	5.12	3.64
% Ca²⁺ taken out of the total solution	% of the solution	22%	28%	20%	18%

Table 3.3-6: Calculation for the reduction in bioavailability of the cation Ca²⁺ (n = 3).

Table 3.3-6 demonstrates that there is between 18% and 28% reduction in the cation Ca²⁺ available to the plant, due to it being locked up in the precipitate formed. Table 3.3-7 shows that SO₄²⁻ availability is nearly completely reduced with 87% to 95% of the total SO₄²⁻ in the solution being locked up in the precipitate. The PO₄³⁻ is the least affected by the precipitate formation with a maximum reduction of 7% of the total solution concentration (Table 3.3-8).

SO_4^{2-}	Unit	SW Grow	SW Bloom	HW Grow	HW Bloom
pH		1.78	1.95	0.18	0.47
Amount of precipitate formed as a percentage of the total volume of nutrient solution.	% of the solution	2.233	2.223	1.466	1.08
Total solution content according to the label.	g/L	7.67	8.08	6.33	4.08
Quantity of SO_4^{2-} determined by Ion Chromatography (IC)	% of the precipitate	32.59	31.11	33.12	35.92
Quantity of SO_4^{2-} determined by XRF	%	32.89	33.68	42.39	33.82
Mean precipitate content from XRF & IC data.	% of precipitate	32.74	32.40	37.76	34.87
SO_4^{2-} taken out of the solution due to precipitate formation	g/L	7.31	7.20	5.53	3.77
% SO_4^{2-} taken out of the total solution.	% of the solution	95%	89%	87%	92%

Table 3.3-7: Calculation for the reduction in bioavailability of the anion SO_4^{2-} (n = 3).

PO_4^{3-}	Unit	SW Grow	SW Bloom	HW Grow	HW Bloom
pH		1.78	1.95	0.18	0.47
Amount of precipitate formed as a percentage of the total volume of nutrient solution.	% of the solution	2.233	2.223	1.466	1.08
Total solution content according to the label.	g/L	11.25	17.5	11.25	17.5
Quantity of PO_4^{3-} determined by Ion Chromatography (IC)	% of the precipitate	3.25	4.40	0.36	0.45
Quantity of PO_4^{3-} determined by XRF	%	3.45	4.44	0.5	0.8
Mean precipitate content from XRF & IC data.	% of precipitate	3.35	4.42	0.43	0.625
	<i>SD</i>	<i>0.1</i>	<i>0.02</i>	<i>0.07</i>	<i>0.175</i>
PO_4^{3-} taken out of the solution due to precipitate formation	g/L	0.75	0.98	0.06	0.07
% PO_4^{3-} taken out of the total solution.	% of the solution	7%	6%	1%	0%

Table 3.3-8: Calculation for the reduction in bioavailability of the anion PO_4^{3-} (n = 3)

Previous work published on the bioavailability of nutrients within solution has all been computational and theory based (De Rijck, Schrevens 1997, 1998a, 1998b, 1998c 1998e, 1998f, 1998g, 1999a and 1999b). Furthermore, this work has all been based on a solution which is to be irrigated directly to the plants, as opposed to the commercially available concentrate designed to be diluted (used in this study). Differences include pH, and total ionic concentration, therefore a direct comparison of the data is more difficult. Factors such as the solution pH, total ionic concentration, dissociation reactions, complexation reactions and precipitation reaction all effect the bioavailability and mineral composition of a solution and should all be considered when formulating a nutrient. The absorption of ions by plants is selective, and therefore complexation reactions, which form complex ions, reduce the freely available ions to the plant (De Rijck, Schrevens 1998e). This is also true for the precipitation reactions which occur in the solution. As stated by De Rijck and Schrevens 1998, with increased concentration comes an increased risk of precipitate formation over soluble complex ion formation.

The results presented in this chapter are supported by De Rijck work that the predominant constituent of the precipitate would be sulphate and calcium, with a small proportion of phosphate. De Rijck *et al* also state that the constituent of the precipitate will change under different conditions such as pH. Their work on the effect on elemental bioavailability in relation to dissociation reactions, stated that at a pH of 1, the predominate form of phosphorus is H_3PO_4 (De Rijck, Schrevens 1997). As the pH rises to 4, the species changes to H_2PO_4^- and becomes the dominate form in the solution. H_2PO_4^- is a much more reactive species and is more likely to form complexes and precipitates with the calcium in the solution. There are three distinct steps to the dissociation of H_3PO_4 which are demonstrated in Equation 3.16, Equation 3.17, and Equation 3.18. These are successive dissociations which are demonstrated in Figure

3.3-8, along with the pH at which each step occurs. The pH at which the dissociation occurs is known as the acid dissociation constant (pKa). Another useful tool for predicting what reaction and precipitations will take place.

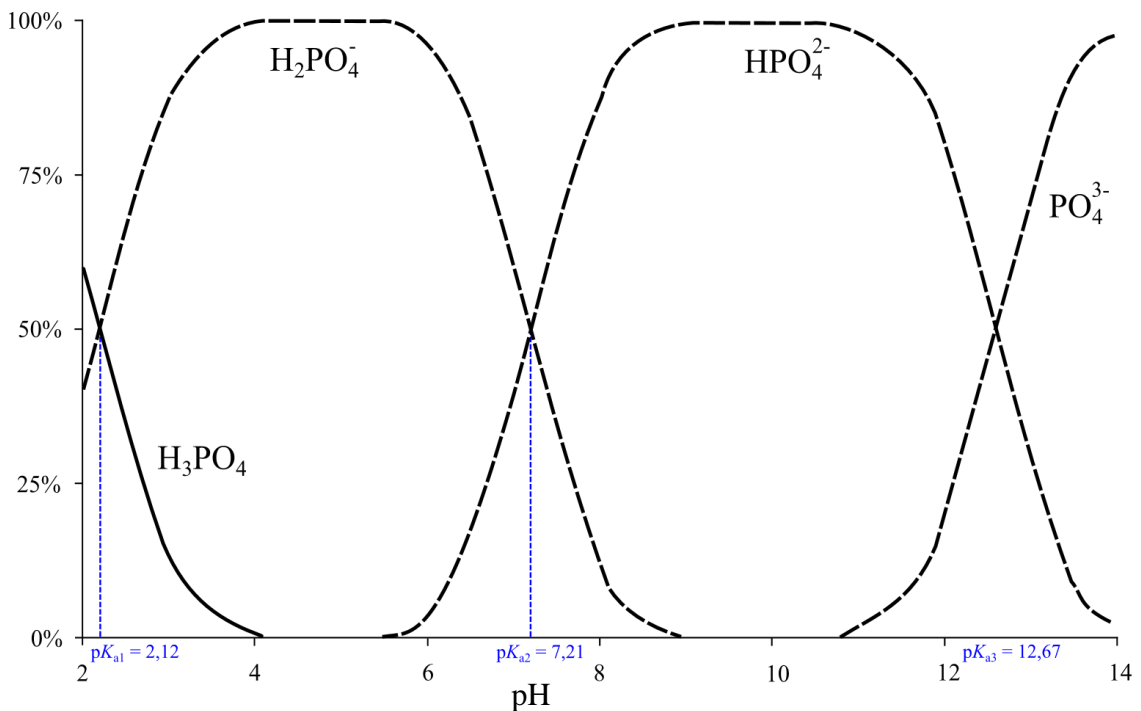
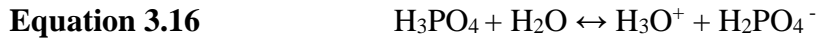


Figure 3.3-8: Dissociation of phosphoric acid.

Table 3.3-8 demonstrated the pH of the soft water formulation is approximately 2, therefore the solution has a higher fraction of H_2PO_4^- , giving reason to the higher concentration PO_4^{3-} in the precipitate. Both the hard water formulas are below pH 1, and the precipitate contains nearly 10 times less PO_4^{3-} than the soft water formulas.

When the dissociation reaction of sulphate is examined by De Rijck *et al*, at a pH of 1 the highest fraction of sulphate is found in the HSO_4^- form. This dissociates rapidly into SO_4^{2-} between a pH of 1 and 3. At a pH of 4 the only form found in the solution is SO_4^{2-} which does not undergo complexation or precipitation reactions with calcium ions and so does not affect the bioavailability of calcium (De Rijck, Schrevens 1997). Both the hard and the soft water formulations have a pH below 2, therefore complexation reactions between sulphate and calcium are more likely.

Since both the soft water formulations have higher concentration of sulphate in them both, it is difficult to say if the pH had an effect of the precipitate mass.

3.4 Conclusion

We can conclude from the work performed in this Chapter using a variety of destructive and non-destruction analytical techniques that the precipitate is a mixture of hydrates of calcium phosphate and calcium sulphate (gypsum). At pH below 1, calcium phosphate formation is dramatically reduced due to the species of the phosphate ion.

Calcium sulphate, in the form of gypsum, is used extensively in the construction industry. Although the amount of phosphate present in the nutrient solution precipitates is small, it has the potential to cause many problems. Phosphate is added to gypsum, in the dental profession and building industry to strengthen it (Swaintek, Han *et al*. 2005, Suwanprateeb, Suvannapruk *et al*. 2010, Lima, Airoldi 2004). The resulting material, phosphogypsum has much greater mechanical properties, such as hardness, than pure gypsum. This in turn can cause problems during the manufacturing of liquid fertilizers because the phosphogypsum precipitates are more difficult to resuspend in the solution

than pure gypsum. The formation of precipitates during the manufacture of liquid fertilizer is undesirable. Gypsum can be easily mixed into the solution to form a slurry. However, when large volumes, such as 2000 L are produced, an increased pressure from the liquid is exerted onto the solid precipitate, compressing it, and making it difficult to mix back into the solution. If the precipitates properties are altered so that it is strengthened, the effect of the compressions from the liquid becomes more problematic. The prevention and monitoring of phosphogypsum formation is therefore important, as the precipitate formed will be more difficult to resuspend.

The absorption of ions by plants is selective and any reduction in freely available ions will result in reduced bioavailability to the plant (De Rijck, Schrevens 1998e). The formation of complexes and precipitate dramatically reduces the free ions and will consequently lead to malnutrition in the plant.

Predicting the formation of a precipitate can be done with ease, saving time and money if factors such as common ion effect, the solubility product (K_{sp}) and ion product (Q_c) are examined and calculated beforehand. Unfortunately, these factors do not take into account some of the impurities that can be found in fertilizer chemicals, which can cause unpredictable reactions. However, these are tools which should be first considered before beginning large scale production of liquid fertilizers.

3.5 References

- BULDINI, P.L., TONELLI, D. and VALENTINI, F., 2009. Ion Chromatographic Analysis of Hydroxyapatite. *Analytical Letters*, **42**(3), pp. 483-491.
- COLINA, M. and GARDINER, P.H.E., 1999. Simultaneous determination of total nitrogen, phosphorus and sulphur by means of microwave digestion and ion chromatography. *Journal of Chromatography a*, **847**(1-2), pp. 285-290.
- DE RIJCK, G. and SCHREVEN, E., 1997. Elemental bioavailability in nutrient solutions in relation to dissociation reactions. *Journal of Plant Nutrition*, **20**(7-8), pp. 901-910.
- DE RIJCK, G. and SCHREVEN, E., 1999a. Anionic speciation in nutrient solutions as a function of pH. *Journal of Plant Nutrition*, **22**(2), pp. 269-279.
- DE RIJCK, G. and SCHREVEN, E., 1999b. Chemical feasibility region for nutrient solutions in hydroponic plant nutrition. *Journal of Plant Nutrition*, **22**(2), pp. 259-268.
- DE RIJCK, G. and SCHREVEN, E., 1998a. Application of mixture theory for the optimisation of the composition of nutrient solutions for hydroponic cropping: Practical use. *International Symposium on Growing Media and Hydroponics, Vols i and ii*, (481), pp. 205-212.
- DE RIJCK, G. and SCHREVEN, E., 1998b. Cationic speciation in nutrient solutions as a function of pH. *Journal of Plant Nutrition*, **21**(5), pp. 861-870.
- DE RIJCK, G. and SCHREVEN, E., 1998c. Comparison of the mineral composition of twelve standard nutrient solutions. *Journal of Plant Nutrition*, **21**(10), pp. 2115-2125.
- DE RIJCK, G. and SCHREVEN, E., 1998d. Distribution of nutrients and water in rockwool slabs. *Scientia Horticulturae*, **72**(3-4), pp. 277-285.
- DE RIJCK, G. and SCHREVEN, E., 1998e. Elemental bioavailability in nutrient solutions in relation to complexation reactions. *Journal of Plant Nutrition*, **21**(5), pp. 849-859.
- DE RIJCK, G. and SCHREVEN, E., 1998f. Elemental bioavailability in nutrient solutions in relation to complexation reactions. *Journal of Plant Nutrition*, **21**(5), pp. 849-859.
- DE RIJCK, G. and SCHREVEN, E., 1998g. Elemental bioavailability in nutrient solutions in relation to precipitation reactions. *Journal of Plant Nutrition*, **21**(10), pp. 2103-2113.
- FARMER, V.C., 1974. *Infrared Spectra of Minerals*. Mineralogical society.
- GORBE, E. and CALATAYUD, A., 2010. Optimization of Nutrition in Soilless Systems: A Review. *Advances in Botanical Research, Vol 53*, **53**, pp. 193-245.

GUPTA, P.K., 1999. Plant analysis. *Soil, Plant, Water and Fertiliser analysis*. India: Agrobios (India), pp. 264-266.

HOAGLAND, D. R., ARNON, D.I., 1938. *The Water-Culture Method for Growing Plants without Soil*. Berkeley, Calif.: University of California, College of Agriculture, Agricultural Experiment Station.

HOAGLAND, D.R. and ARNON, D.I., 1950. The water-culture method for growing plants without soil. *Circular. California Agricultural Experiment Station*, **347**(2nd edit),.

LIMA, C.B.A. and AIROLDI, C., 2004. Topotactic exchange and intercalation of calcium phosphate. *Solid State Sciences*, **6**(11), pp. 1245-1250.

LINDE, D.R (2004). CRC Handbook of Chemistry and Physics, 84rd Edition, CRC Press.

SUWANPRATEEB, J., SUVANNAPRUK, W. and WASOONTARARAT, K., 2010. Low temperature preparation of calcium phosphate structure via phosphorization of 3D-printed calcium sulfate hemihydrate based material. *Journal of Materials Science. Materials in Medicine*, **21**(2), pp. 419-429.

SWAINTEK, J.N., HAN, C.J., TAS, A.C. and BHADURI, S.B., 2005. SELF-SETTING ORTHOPEDIC CEMENT COMPOSITIONS BASED ON CaHPO₄ ADDITIONS TO CALCIUM SULPHATE. *Advances in Bioceramics and Biocomposites*, **26**(6), pp. 79-86.

WANG, H., SONG, Q., YANG, R., YAO, Q. and CHEN, C., 2010. [Study on microwave digestion of gypsum for the determination of multielement by ICP-OES and ICP-MS]. *Guang pu xue yu guang pu fen xi = Guang pu*, **30**(9), pp. 2560-3.

YASH KALRA (EDITOR), 1997. *Handbook of Reference Methods for Plant Analysis*. 1 edn. CRC Press.

Chapter 4

4. The use of zinc based seed coating in barley fodder production

4.1 Introduction

Production of feed for livestock has been extensively researched. One important feed is fodder, which can be grown hydroponically, as described extensively in Chapter 1 Section 1.5.3.(Al-Karaki, Al-Hashmi 2010, Dung, Godwin *et al.* 2010a, Fazaeli, Golmohammadi *et al.* 2011, Lopez-Aguilar, Murillo-Amador *et al.* 2009, Mansbridge, Gooch 1985, Peer, Leeson 1985a, Peer, Leeson 1985b,).

The nutritional content of the fodder is of great interest to farmers who want to ensure that their livestock is as healthy as possible. Microelements such as Co, Cu, Fe, I, Mn, Mo, Se and Zn are essential for maintaining the health and productivity of animals, such as dairy cows for milk production (López-Alonso 2012). Microelement deficiencies in livestock can lead to a number of diseases and reduced fertility. One particular element of interest is zinc, which is a key component in many important metabolic enzymes (Gómez-Galera, Rojas *et al.* 2010) . Zinc deficiency in livestock can lead to reduced growth rate, cracked hooves, skin lesions, reduced appetite, slow wound healing, and reduced fertility (Suttle 2010). Previous research (Cakmak 2008, Welch, Graham 2004) has shown that zinc in un-germinated cereal grains is less bioavailable due to the high concentrations of phytate in their starchy endosperm. Once germination has initiated, the phytate content decreases dramatically and continues to decrease (Azeke, Egielewa *et al.* 2011), increasing the zinc bioavailability of zinc to the animal. The zinc content of most forages is found to be low or marginal in comparison to the recommended content of 30 ppm found in dry matter (Suttle 2010). Environmental factors such as high pH, mineral nutrient concentrations (particularly calcium), organic content of the media, moisture content of the media, drought and heat stress all effect the availability to the plant.

Zinc is also an essential element for healthy plant growth and development and is one of the most common micronutrient deficiencies (Broadley, White *et al.* 2007). It is essential to produce thousands of plant proteins and is a cofactor for many enzymes. Zinc is taken up as Zn^{2+} by the roots of the plant, although it can also form organic ligand complexes in the surrounding media and be absorbed by the plant's roots this way (Gupta, Ram *et al.* 2016, Broadley, White *et al.* 2007, Hart, Norvell *et al.* 1998). Once zinc has entered the plant, it forms complexes with organic acids, enzymes, and forms Zn finger proteins. These zinc complexes aid the transportation around the plant via both the xylem and the phloem to the shoots (Broadley, White *et al.* 2007, Gupta, Ram *et al.* 2016).

Biofortification of crops has been extensively studied, with a number of different strategies applied (Gupta, Ram *et al.* 2016, Seppanen, Kontturi *et al.* 2010, Cakmak, Kalayci *et al.* 2010, Voogt, Holwerda *et al.* 2010, Cakmak 2008, Xue, Xia *et al.* 2016). One method of improving the elemental content of plants is with the use of a seed coat. This involves coating the seed with a quick drying solution, containing the elements of interest, which is applied prior to sowing. More detail on this can be found in Chapter 1.

The aim of this work is to establish if the seed coating Teprosyn Zn/P will increase the nutritional content of the shoot barley. The absorption of the seed treatment into the seed prior to germination will be investigated using mass spectrometry imaging techniques MALDI-MS and LA-ICP-MS. This will then indicate if the increase in zinc shoot content is due to absorption via the seed, occurring before germination, or if the residue from the coating is absorbed through the roots or shoots post germination. It is also the aim to establish if absorption into the seed is effective over time.

4.2 Material and methods

4.2.1 Cultivation - Barley for fodder production

The hydroponic system was supplied by HydroGarden (Coventry, UK) and produced by Fodder Solutions (Queensland, Australia) (Chapter 1, Section 1.5.3, Figure 1.5.7). The model supplied was the FS6/50, measuring 2.8 m x 1.6 m x 2.3 m (L x W x H), holding 12 trays in total, 4 trays tall; 3 trays deep; 1 tray wide. Each tray can grow 3 biscuits, with the dimensions 75 x 27 cm, giving a total capacity of 36 biscuits. Each biscuit requires 1.2 kg of barley seed (*Hordeum vulgare -Cassia*). The unit was fitted with a thermostatically controlled air conditioning unit and heater to maintain a temperature range of 18-23°C. Insulated walls were installed to improve efficiency. The seed was evenly distributed in the trays and placed in the fodder system. The growing seeds were held at a temperature of 18-23°C, with a humidity between 60-70% and with continuous illumination from 2 x 18 W fluorescent lights. They were irrigated with water for 30 seconds every 2 hours (Figure 4.2-1). Each irrigation delivered a total of 12 L of water over the seeds, with a total consumption of approximately 100 L per day. 24 hours after sowing, the trays were removed, photographed (Figure 4.2-2) and number of seeds germinated determined (Goodchild, Walker, 1971). This procedure was then repeated at 24-hour intervals from first sowing. After 144 hours (6 days) the biscuits were harvested and allowed to drip dry until all excess water had run off. The mass of each biscuit was recorded.



Figure 4.2-1:The spray head of the irrigation system delivering a fine mist of solution to the sprouted seeds.



Figure 4.2-2: Trays used in the fodder system, showing 3 sections filled with seeds to produce 3 individual “biscuits”. The growth after 6 days can be seen in the second image.

4.2.2 Experimental design – Treatments

The experiments performed involved the growth of barley using only water to irrigate.

The seed treatment, Teprosyn Zn/P, was applied at three concentrations, with an additional group with no seed treatment as the control (Table 4.2-1).

Teprosyn Zn/P was supplied by Yara and is a zinc/phosphorus seed treatment with a guaranteed analysis of 9% total nitrogen (in the form of urea), 15% phosphorus (in the form of phosphorus pentoxide (P₂O₅)) and 18% zinc (Zn). These elements are derived from urea, calcium phosphate and zinc phosphate. Teprosyn Zn/P has the appearance of a viscous pink suspension that dries very quickly.

Three series of experiments were completed using four different volumes of Teprosyn Zn/P seed treatment per 1.2 kg of barley seed (biscuit) (Table 4.2-1), as recommended by Yara. The Teprosyn was applied to the seed by placing 1.2 kg of the seeds into a sealable container and the volume stated in Table 4.2-1 added. This was then sealed and shaken for a minimum of 3 minutes. The coated seeds were then poured into the sections in the trays and grown as stated in Section 4.2.1.

Experiment	Procedure	Treatment – Volume of seed coat per 1.2 kg of seed (ml)
1	One treatment for complete system (36 replicate of each volume)	0
		1
		3.6
2	Random treatments run simultaneously (12 replicates of each volume)	0
		0.5
		1
3	Random treatments run simultaneously (9 replicates of each volume)	0
		0.5
		1
		3.6

Table 4.2-1: Treatments performed on the different experimental runs.

Each treatment was designed to supply a different concentration of P₂O₅ and Zn, but remaining in the same ratio (5:13) within the solution (Table 4.2-2).

Volume of seed treatment per 1.2 kg of seed(ml)	P ₂ O ₅ Concentration		Zn Concentration	
	(mM)	(mg/kg) of seed	(mM)	(mg/kg) of seed
0.0	0.000	000	0.000	000
0.5	0.856	101	2.225	121
1.0	1.712	203	4.451	243
3.6	6.163	729	16.023	873

Table 4.2-2: Elemental content of each treatment ($\pm 5\%$).

Before application of the Teprosyn Zn/P, all seeds, including the control group were surface sterilized; first with 70% ethanol, followed by 50% sodium hypochlorite and finally rinsed with sterile deionised water (Dung, Godwin *et al.* 2010a).

4.2.3 Fodder yield

4.2.3.1 Total fresh mass

Each biscuit at the point of harvest was weighed using a set of digital hanging scales to establish the fresh mass. The mass was recorded to 3 significant figures.

4.2.3.2 Percentage dry mass of sample shoots

A 10-cm diameter sample from each biscuit was taken (Figure 4.2-3), weighed, and shoots separated from the roots and the un-germinated seeds. Samples were dried at 70 °C for 72 hrs, to a constant mass, re-weighed and the mass recorded.

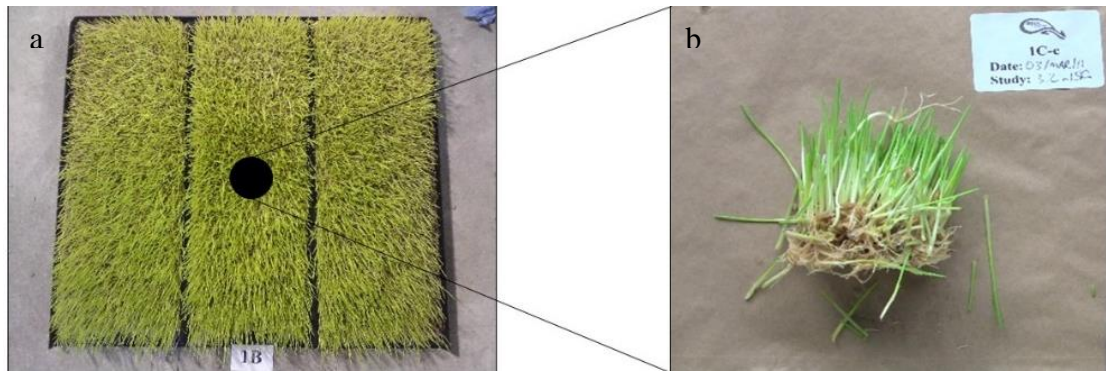


Figure 4.2-3: a) Three fully grown biscuits with the location of the sample. b) 10cm cut sample.

The % dry mass was calculated as follows:

Equation 4.2-1

$$\% \text{ dry mass} = \frac{\text{Dry mass}}{\text{Fresh mass}} \times 100$$

The ratio of fodder produced to seed plant was calculated as follows (Al-Karaki 2011):

Equation 4.2-2

$$\text{Ratio of fodder to seed} = \frac{\text{Total Fresh mass}}{\text{Mass of seed planted}}$$

The total number of samples taken from each treatment group and experimental run is summarized in Table 4.2-3.

		Number of samples in parameter measured (n)			
		Germination rate	Fresh mass	Dry mass	Elemental analysis
Volume of seed coating per 1.2 kg (ml)	0	31	57	21	31
	0.5	21	21	21	21
	1.0	32	57	57	37
	3.6	20	45	44	21
Experimental run	1	35	108	71	39
	2	35	36	36	35
	3	34	36	36	36
Totals		104	180	143	110

Table 4.2-3: Summary of samples taken.

4.2.4 Sample preparation

A 10-cm diameter sample from the centre of each biscuit was taken (Figure 4.2-3) weighed, and the shoots separated from the roots and the un-germinated seeds. The shoots and roots were then dried at 70 °C for 72 hrs, to a constant mass. The shoots were then ground in an electrical coffee grinder and passed through a 40-micron sieve to ensure homogeneity, ready for analysis.

Fresh leaves for imaging were prepared by placing samples between tissue paper and pressing between two glass slides. The slides were taped together and placed into a freeze drier at -36 °C until they reached a constant mass, taking approximately ten days. The dried leaves were mounted onto either aluminium target plates or glass slides using double sided carbon tape to adhere the sample.

4.2.4.1 Time dependent analysis sample preparation of seeds

Twenty seeds from each treatment group were removed and placed into separate falcon tubes. Four replicates of each treatment were prepared so that varying time periods from the treatment applications could be observed. These time periods included 0 days, 6 days, and 20 days after application of the seed treatment. All samples were placed in a dark, cool cupboard within the laboratory.

After the given time, each treatment group of seeds was snap frozen. This involved placing a propanol filled container first into liquid nitrogen to cool. The seeds were then placed into the pre-cooled propanol. Seeds were then stored at -80 °C before cryosectioning.

Three seeds from each group were sectioned (3-time points, 3 concentrations of Teprosyn plus a control group) with 6 sections per seed taken. The most homogenous,

in terms of thickness of section, shape and completeness of the material were chosen for analysis. A total of 30 sections were analysed by LA-ICP-MS.

4.2.4.2 Seed cryosections

Seeds were first embedded in 1% carboxymethyl cellulose (CMC) and placed into -80 °C freezer overnight. The frozen, embedded seeds were sectioned at a temperature of -24 °C to obtain 20 µm sections, which were then mounted onto glass slides using carbon tape as the adhesive (Figure 4.2-4).

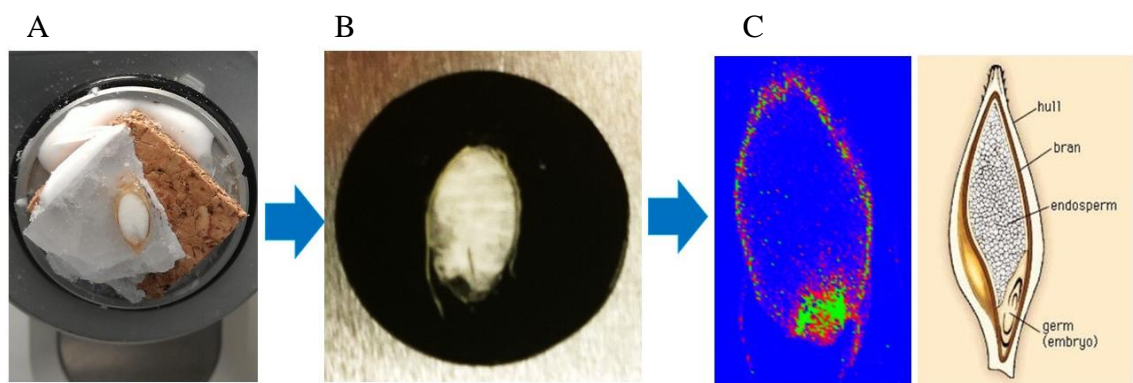


Figure 4.2-4: Schematic diagram of seed preparation for LA-ICP-MS imaging.

A) Embedded seed being cryosectioned B) Seed section mounted on carbon tape.

C) LA-ICP-MS image and seed anatomy diagram.

<http://www.britannica.com/topic/cereal-processing>

4.2.4.3 Matrix assisted laser desorption/ionisation matrix application (deposition)

Samples for MALDI were coated with a 5 mg/ml solution of CHCA in 70:30 methanol: water with 0.2% TFA using the Suncollect™ automated pneumatic sprayer (Sunchrom GmbH, Friedrichsdorf, Germany) in a series of 10 layers (Figure 4.2-5). The initial seeding layer was performed at 2 µl/minute and subsequent layers were performed at 3 µl/minute.

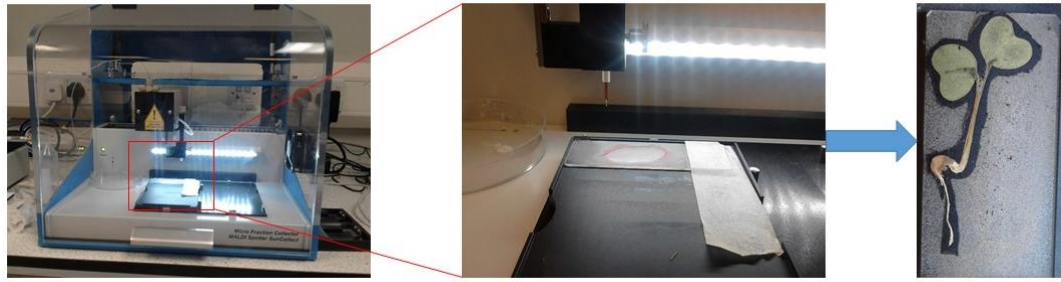


Figure 4.2-5: Suncollect automated pneumatic sprayer, coating plant tissue with matrix.

4.2.4.4 Reference material preparation for calibration of laser ablation ICP-MS

Matrix matched plant material was prepared as stated in Chapter 2, Section 2.4.5. A series of mixed element spikes were added to the material, before pressing into 3 mm diameter pellets. (Table 4.2-4)

Plant material	Reference	Concentration of standard solution (mg/L)
Barley leaf material	LD0	0
	LD5	5
	LD10	10
	LD20	20
	LD40	40
Barley seed material	SD0	0
	SD5	5
	SD10	10
	SD20	20
	SD40	40

Table 4.2-4: LA-ICP-MS reference material spike solution concentrations.

Carbon-13 was to be used as the internal standard to correct for instrument fluctuations, variation in sample thickness and water content (Wu, Zoriy *et al.* 2009a, Becker, Matusch *et al.* 2014, Cizdziel, Bu *et al.* 2012 Kotschau 2012). Previously, other elements have been used in research, including Sc (Gomes, Schenk *et al.* 2014), ^{12}C (Punshon, Jackson *et al.* 2004), Fe (Ward *et al.* 1992), Ag (Bauer, Limbeck. 2015), Ca

(Hanc *et al* 2013), Au, Rh (Compernelle *et al.* 2012) and Mg (Hirata *et al.* 2013), the selection should be based on the material being analysed.

Previous studies performed (O'Connor, Landon *et al.* 2007, Hare, Austin *et al.* 2012) added 25% w/w vanillic acid to help improve the signal to noise ratio. Vanillic acid is used as it is an organic chromophore and has a high absorbency at 213 nm, hence making it the ideal candidate for improving the signal to noise ratio. In this study, the effect of vanillic acid was also tested with spiked cellulose and analysing with LA-ICP-MS to test the effectiveness at improving the signal to noise ratio.

All the reference materials were microwave (MARS6) digested in triplicate (Section 4.2.4.5) before analysis by ICP-MS.

4.2.4.5 Digestion method

Microwave digestion methods (Yash *et al*, 1997) were adapted using 30% hydrogen peroxide (H₂O₂), concentrated trace analysis grade 69% nitric acid (HNO₃) and deionized water (DH₂O) solution for ICP-OES/MS analysis using 0.2 g (\pm 0.05 g) ground plant material. A specific method was used for each material (**Table 4.2-5**).

Material	Microwave unit used	HNO ₃ (ml)	DH ₂ O (ml)	H ₂ O ₂ (ml)	Microwave parameters	Analysis type
Leaf material	MDS2000	0.5	0	2	Table 4.2-6	ICP-OES
LA reference leaf material	MARS6	5	5	3	Table 4.2-7 Figure 4.2-7	ICP-MS
LA reference seed material	MARS6	5	0	2	Table 4.2-7 Figure 4.2-6	ICP-MS

Table 4.2-5: Digestion methods used for different plant material.

The MDS2000 microwave digestion system required programming, which can be seen in **Table 4.2-6**.

Stage	1	2	3	4	5
% Power *	47% (296W)	0	90% (595W)	0	90% (595W)
Pressure (psi)	20	20	20	20	20
Time (mins)	4:00	5:00	8:00	5:00	5:00
Fan speed	100	100	100	100	100

Table 4.2-6: Microwave (MDS2000) parameters for the digestion of barley leaf material for analysis by ICP-OES. * this is for a nominal 630W system. For a nominal 950 W system, multiply % power by 0.66.

The MARS6 used pre-programmed files to digest the different materials (Table 4.2-7).

Method	Feed Grain (MARSXpress)	Plant Material (MARSXpress)
Power	290-1800 W	290-1800 W
Ramp Time (mins)	20	20
Hold time (mins)	15	10
Cooling time (mins)	30	30
Temperature (°C)	200	200
Pressure (psi)	0	0

Table 4.2-7: The parameters of the MARS6 digestion methods.

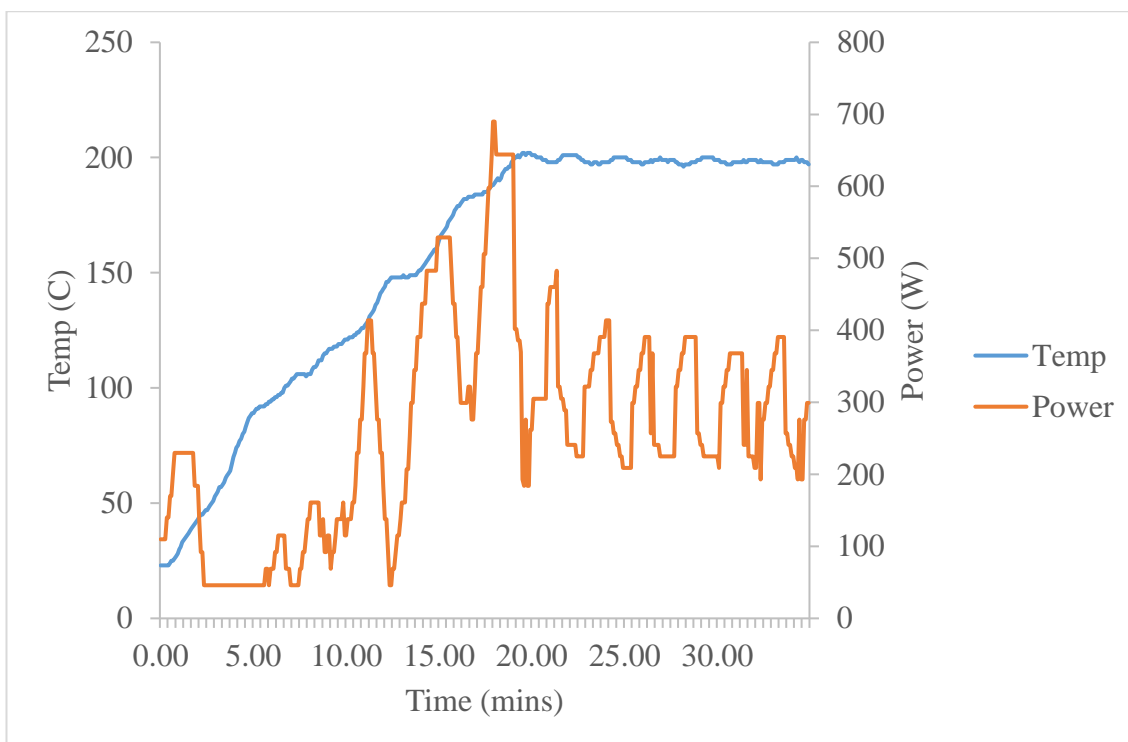


Figure 4.2-6: MARS6 microwave digestion parameters for the digestion of barley seeds.

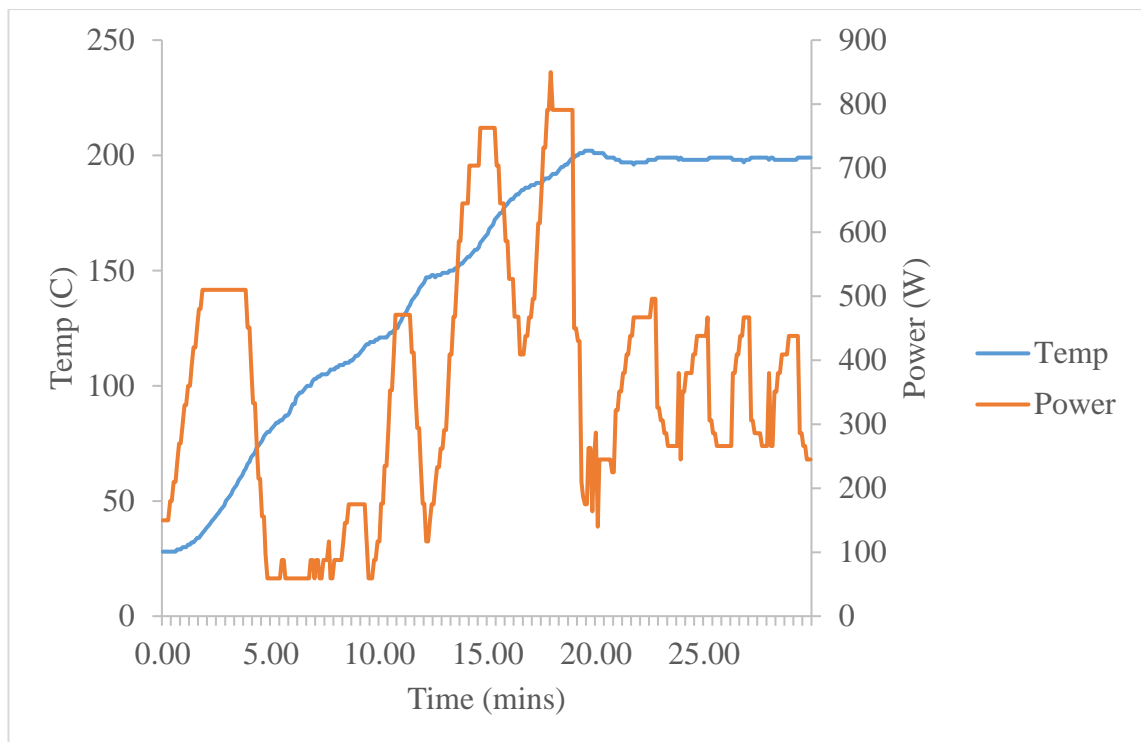


Figure 4.2-7: MARS6 microwave digestion run parameters for laser ablation reference barley leaf material.

After cooling for 30 minutes the contents of each tube were rinsed 3 times with deionized water into a 50-ml falcon tube and made up to 50 ml with deionised water. A further 1:4 dilution was then performed before analysis. The digest solutions were filtered using 30 mm, 0.2 μm syringe filters before analysis by ICP-OES. Samples were run in triplicate along with digestion blanks which contained no plant material.

All glassware and plastics were rinsed in 10% nitric acid before use (see Chapter 2, Section 2.3 and 2.4.1 for digestion tube preparation).

4.2.5 Analytical method (instrumentation)

Different analytical techniques were applied to the samples to monitor the distribution and elemental content of a variety of plant material and seed treatment solutions.

4.2.5.1 Matrix assisted laser desorption/ionisation mass spectrometry

Refer to Chapter 2, Section 2.5.9 for instrument specifications. MALDI-MS spectra were obtained in positive and negative ion mode in the mass range between m/z 50 and m/z 1000. Declustering potential 2 was set at 15 arbitrary units and the focus potential at 10 arbitrary units, with an accumulation time of 0.999 sec. Average spectra were acquired over a 0.5 cm² region on the leaves. The MALDI-MS/MS spectrum of the unknown precursor ions was obtained using argon as the collision gas; the declustering potential 2 was set at 15 and the focusing potential at 20, and the collision energy and the collision gas pressure were set at 20 and 5 arbitrary units, respectively.

4.2.5.2 Characterization of Teprosyn Zn/P

A powder of Teprosyn Zn/P was produced prior to analysis, by first snap freezing 4.5ml in liquid nitrogen, followed by freeze drying at a temperature of -52 °C, under vacuum at a pressure of 0.120 mBar until a constant mass was achieved. Characterization of Teprosyn Zn/P was performed using X-ray fluorescence spectroscopy (XRF). XRF was performed in the Material & Engineering Research Institute (MERI), at Sheffield Hallam University, UK.

4.2.5.3 Inductively coupled plasma optical emission spectroscopy (ICP-OES)

Samples were analysed for calcium, iron, magnesium, phosphorus, and zinc using ICP-OES, refer to Chapter 2, Section 2.5.1 for instrument specifications and parameters.

Zinc, iron, phosphorus, calcium, and magnesium were all analysed for.

4.2.5.4 Inductively coupled plasma mass spectrometry (ICP-MS)

Digested reference material of both leaves and seeds were analysed on a PerkinElmer NexIon 350X ICP-MS using an auto-sampler under normal operating conditions stated in Chapter 2, Section 2.5.7.2 and Table 4.2-8.

Parameter	Value
Nebulizer/carrier gas flow	0.98 L/min
Helium gas flow	4.4 L/min (3 L/min for Se)
Total integration time	0.5 s (1.5 s for Se)
Dwell time	10 ms (30 ms for Se)
Replicates per sample	3
Sweeps/Readings	50
Sample Flush	60 s
Read Delay	40 s
Wash	120 s
Mode	Collision
Isotopes	⁶⁶ Zn, ³¹ P, ⁷⁸ Se, ³⁹ K, ²⁴ Mg, ²³ Na, ⁶³ Cu, ⁵⁶ Fe, ⁴⁴ Ca, ¹⁰³ Rh (internal standard)
Sample uptake rate	300 µL/min

Table 4.2-8: ICP-MS operating conditions.

Calibration was performed using one multi-element calibration standard solution (Ultra Scientific, ICP/MS calibration standard #2) containing all required elements. The calibration standard ranges were based on the results of a semi-quantitative analysis performed on a non-spiked digested sample. The ranges for each element can be seen in Table 4.2-9.

Standard	Concentration of K (ppm)	Concentration of Ca, P, Mg (ppm)	Concentration of Se, Zn, Cu, Fe, Na (ppm)
1 (Blank)	0	0	0
2	0.05	0.01	0.001
3	0.5	0.1	0.01
4	5	1	0.1
5	25	5	0.5
6	50	10	1

Table 4.2-9: Calibration curve ranges.

Gold was added to all solutions at a final concentration of 200 µg/L to stabilize mercury and rhodium at a final concentration of 20 µg/L as the internal standard. Rhodium was used as the internal standard as this would not be found in the plant material.

4.2.5.5 Laser ablation inductively coupled plasma mass spectrometry

Laser ablation (LA) ICP-MS analysis was performed using a UP213 Universal Platform Laser Ablation System, utilizing a frequency quintupled NdYAG deep UV laser with the resulting wavelength of 213 nm. This was interfaced with the NexIon 350X via 5mm tubing and a trigger switch. Prior to sample analysis, the LA-ICP-MS was optimized for X-Y torch position, lens voltage and nebulizer gas flow by ablating a 0.1mm² raster of NIST 612 glass and monitoring the multi-element signal.

Three methods were employed, the first (Method 1) produced semi-quantitative 2D images of the control group and 3.6 ml treatment group, and did not apply reference materials for calibration. These conditions can be seen in Table 4.2-10.

Parameter	Value
Nebulizer/carrier gas flow	1.44 L/min
Helium gas flow	4.4 L/min
Dwell time	60 ms
Acquisition time	0.576 s
Replicates per sample	1
Reading/Replicate	Variable
Mode	Collision (KED)
Isotopes	⁶⁶ Zn, ³¹ P, ³⁹ K, ²⁴ Mg, ²³ Na, ⁶³ Cu, ⁵⁶ Fe, ⁴⁴ Ca, ³² S
LA Parameter	
Laser power	28%
Spot size	55 µm
Repetition rate	20 Hz
Laser energy/Fluence	0.06 J/cm ² (0.001mJ)
Scan speed	95.4 µm/s
Raster spacing	55 µm
Laser warm up time	20 s
Washout time	25 s

Table 4.2-10: Semi-quantitative parameters of the LA-ICP-MS (Method 1).

A spatial resolution of 62.64 μm in the x-direction and 55 μm in the y-direction was achieved for all elements in the images. Refer to Chapter 2, Section 2.5.10.1 for the calculation methods.

Once it was established that quantitative analysis was worth performing, further method optimisation was performed using pressed pellets of dried barley leaves which had been spiked with known concentrations of standard solution to produce matrix matched reference material (see Section 4.2.4.4 for preparation) (Method 2). The conditions for the quantitative analysis can be found in Table 4.2-11 and Chapter 2, Section 2.5.10. This method was also used for the seed study, only using matrix matched seed reference material.

ICP-MS Parameter	Value
Nebulizer gas flow	1.44 L/min
Helium gas flow	4.4 L/min
Dwell time	10 ms (60 ms for Zn)
Acquisition time	0.204 s
Replicates per sample	1
Readings/Replicate	variable
Mode	Collision (KED)
Isotopes	^{66}Zn , ^{31}P , ^{78}Se , ^{39}K , ^{24}Mg , ^{23}Na , ^{63}Cu , ^{56}Fe , ^{44}Ca , ^{13}C
LA Parameter	
Laser power	28%
Spot size	55 μm
Repetition rate	20 Hz
Fluence (Laser energy)	0.06 J/cm ² (0.001mJ)
Scan speed	269.6 $\mu\text{m/s}$
Raster spacing	55 μm
Laser warm up time	40 s
Washout time	40 s

Table 4.2-11: Full quantitative parameters of the LA-ICP-MS (Method 2&3).

Quantitative images were produced using method 2, by running identical consecutive ablations parallel to one another to produce a raster image. Prior to the analysis of the tissue of interest, a 60 second raster ablation of the reference materials, with a 30 second

gas blank period, before and after, was performed on the matrix matched reference materials. This was also performed after the tissue was completed. The fully quantitative method applied ^{13}C as an internal standard (Jurowski, Szewczyk *et al.* 2014, Kötschau, Büchel *et al.* 2013, Becker, Dietrich *et al.* 2008, Wu, Zoriy *et al.* 2009a) to compensate for the difference in the amount of material ablated (Wu, Zoriy *et al.* 2009a), and results normalised against the signal.

The third method (Method 3) involved the quantitative analysis of 13 mm pellets of dried barley leaf material performed for each of the treatment groups. This involved 10 consecutive lines, lasting 60 seconds, with a 30 second gas blank at the start and end, were performed using the parameters stated in Table 4.2-11. The mean, standard deviation (SD) and relative standard deviation (RSD) were then calculated. Reference material LD-40 was used in this analysis.

The limit of detection (LOD) for each element was calculated by Iolite 3.32 software (Paton, Hellstrom *et al.* 2011), based on previous work (Longerich, Jackson *et al.* 1996), using the reference materials. An average was calculated from a minimum of 8 replicates. The reference material lines from each run were used and an average taken over the whole experiment. The LOD for the quantitative data of the pellets was calculated separately, as this analysis was performed sometime after the images and the sensitivity of the instrument had decreased whilst tuning, due to cone damage.

The spatial resolution of the images in the y-direction was 55 μm and in the x-direction 76.6 μm for Zn and 63.1 μm for all other elements analysed (see section 2.5.10.1 for calculations).

4.2.6 Calculations - Elemental content

The following equation was used to calculate the elemental content within the digestion material.

The results are reported to the nearest 1 mg/kg:

Equation 4.2-3

$$\text{mg/kg analyte} = \left(\frac{\left(\text{Sample conc.} \left(\frac{\text{mg}}{\text{L}} \right) - \text{Digestion blank conc.} \left(\frac{\text{mg}}{\text{L}} \right) \right) \times \text{dilution}}{(1000 \div \text{Digestion volume (ml)}) \times \text{sample mass (g)}} \right) \times 1000$$

4.2.7 Germination rate

The germination rate was determined at 24-hour intervals by placing a thin plastic board (75 x 28 cm) with a 5 cm x 5 cm square cut out over the centre biscuit of each tray.

Photographs were taken daily. Using Microsoft Picture Manager, the shadow was reduced to -39 and a grid containing 25 x 1 cm² was superimposed over the picture (Figure 4.2-8).

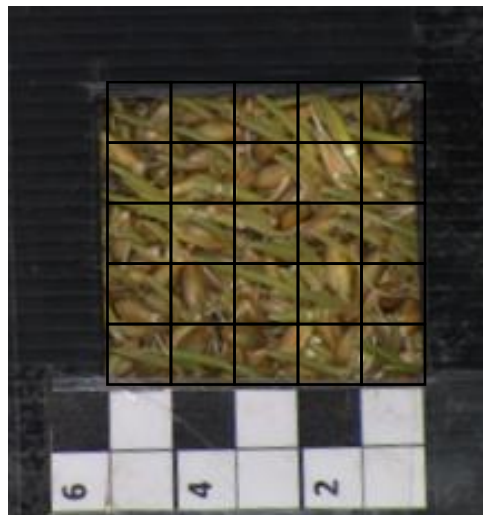


Figure 4.2-8: Germination rate grid

The number of germinated seeds (A) in each cm² was determined and the total within the sample section was then calculated. From this an estimated germination rate was calculated using the following equations:

Equation 4.2-4

$$\text{Estimated Germination rate} = \frac{\text{Number of seeds germinated (A)}}{\text{Number of seeds in a sample area (B)}}$$

Equation 4.2-5

$$\text{Number of seeds in sample area (B)} = \frac{\left(\frac{\text{mass of seed in one biscuit}}{\text{mean mass of 100 seeds}} \right)}{\text{Area of biscuit}} \times 25$$

4.2.8 Statistical analysis

Data was statistically analysed using two-way analysis of variance (ANOVA) according to the statistical package PASW (Predictive Analytics SoftWare) Statistics 18.0 from IBM. Probabilities of significance (p) among treatments (volume of seed coat) were used to compare means among treatments. The interaction between volume of seed coating and replicates was also tested. Post hoc tests (Tukey HSD and Bonferroni) were then performed on dependent variables (concentration of elements in plant tissue, % dry, % germination rate, fresh mass) that showed significances (p<0.05).

4.2.9 Data processing

Refer to Chapter 2, Section 2.6.1 for MALDI-MS and Section 2.6.2 for LA-ICP-MS software and procedure for data processing and image production.

4.3 Results and discussion

4.3.1 Characterization of Teprosyn Zn/P

To be able to identify if the Teprosyn Zn/P is either absorbed into the seed prior to planting, or taken up by the plant during growth, it is important to identify the key constituents of the substance before looking at the plant tissue. This also allows for the determination of uptake of the zinc and phosphate as either free ions or as bound form.

Table 4.3-1 states the guaranteed analysis of Teprosyn Zn/P.

Element	Concentration (%)	Concentration (g/L)
Total Nitrogen (N)	9%	146 g/L
Available Phosphate (P₂O₅)	15%	243 g/L
Zinc (Zn)	18%	291 g/L
Iron Oxide (Fe₂O₃)	1-2%	16-31 g/L
Urea (CO(NH₂)₂)	20-25%	311-389 g/L

Table 4.3-1: Teprosyn Zn/P guaranteed analysis according to the label.

The nitrogen present is derived from urea, and the zinc and phosphate is derived from zinc phosphate and calcium phosphate.

Initially, only a semi-quantitative XRF analysis was performed, revealing the presence of ZnO, P₂O₅, Na₂O, CaO, Fe₂O₃, SiO₂, and MgO (data not shown). A further quantitative XRF analysis (Table 4.3-2) was performed confirming this.

Compound	Na ₂ O	MgO	ZnO	P ₂ O ₅	Fe ₂ O ₃	CaO
Quantity (%)	1.34	0.03	28.74	17.03	1.62	5.00

Table 4.3-2: Quantitative XRF results of Teprosyn Zn/P seed treatment (± 0.005).

The results confirmed that the main constituents were zinc and phosphorus, with the addition of iron, magnesium, sodium, and calcium, all of which will be tracked in the plant tissue.

4.3.2 Germination rate

From the studies performed here on the effects of Teprosyn Zn/P on the germination rate of barley used for fodder production, it is clear that there is no beneficial effect. Photographs taken at 24-hour intervals over a 144-hour period, showed no visual difference in the time of germination or the rate of germination (Figure 4.3-1).

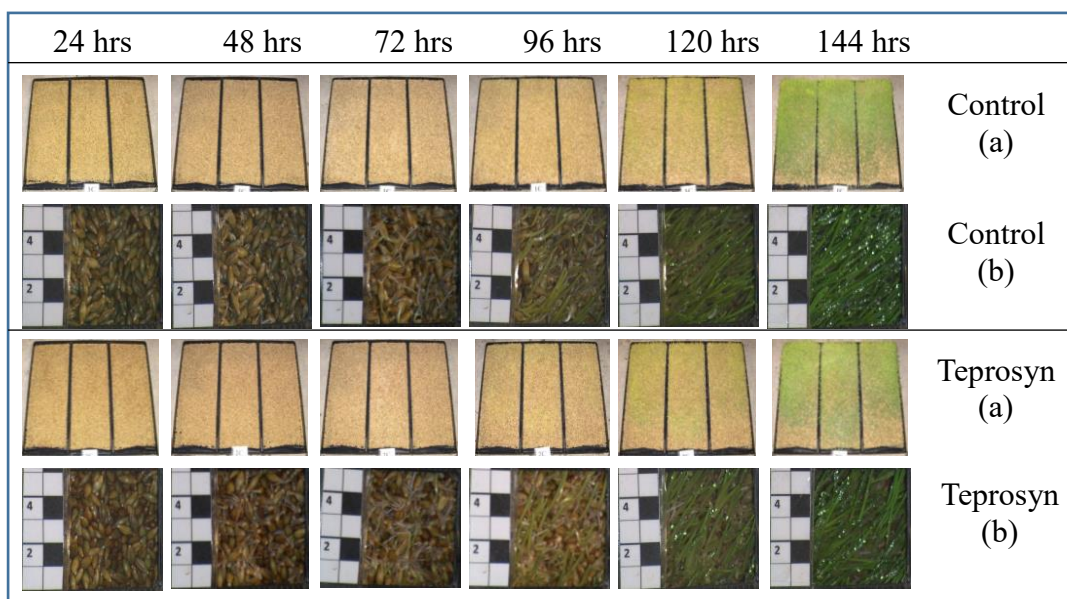


Figure 4.3-1: Comparison of the effect of Teprosyn Zn/P seed treatment on the germination rate over a 144-hour period, taken every 24hr.

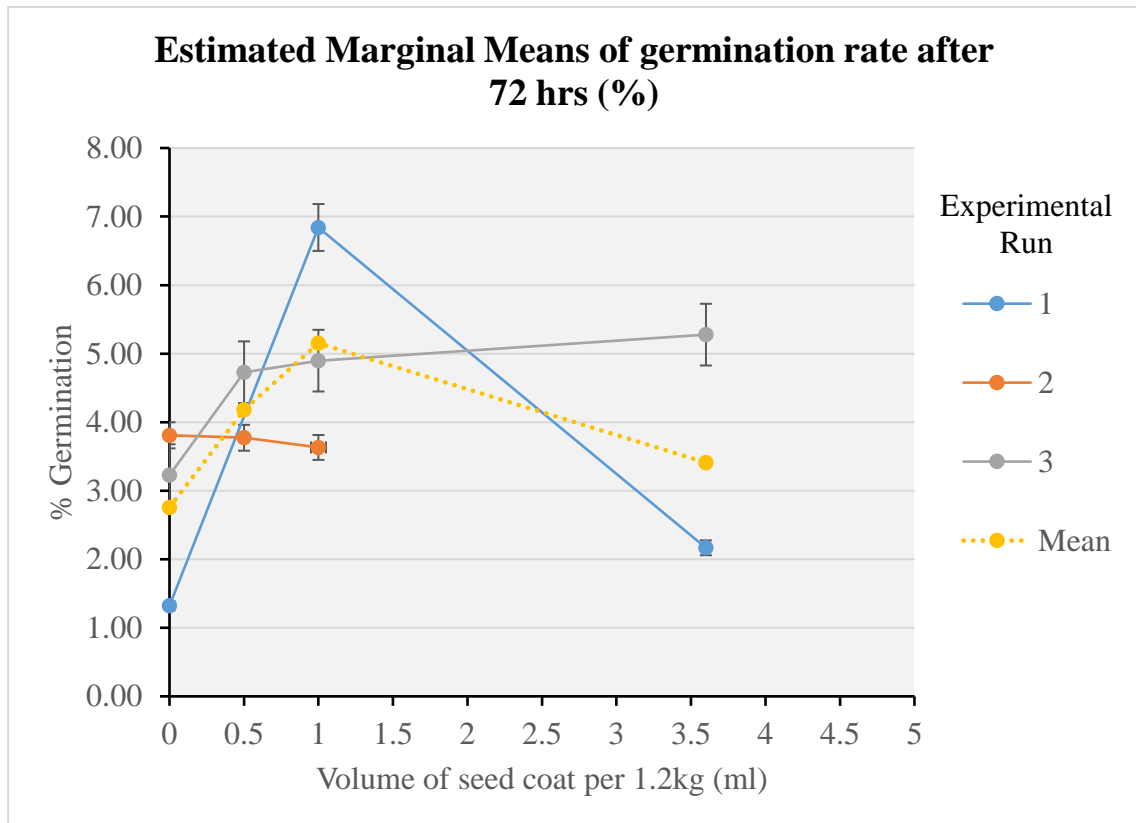


Figure 4.3-2: The effects of Teprosyn Zn/P seed treatment at various concentrations on germination rate (%) of barley in fodder production.

Figure 4.3-2 suggests that there is an increase in germination rate after 72 hrs with increasing Teprosyn Zn/P concentration, up to 1.0 mL per 1.2 kg of barley seed. Levels at 3.6 ml per 1.2 kg seeds appear to decrease germination and have a negative impact. Preliminary studies performed with higher levels of Teprosyn Zn/P (7.2 ml per 1.2 kg seed), had an adverse effect in the fodder system, completely preventing germination (data not shown). However, after statistical analysis of the variables, including replicates and concentrations, it can be concluded that there has been no significant ($p > 0.05$) impact on the germination rate (Table 4.3-3) with the use of seed coating and, therefore, the null hypothesis has been accepted.

Volume of seed coating per 1.2 kg	Experimental run	Mean (%)	Std. Deviation	N (number of samples)
0	1	1.321	0.465	11
	2	3.808	1.418	11
	3	3.228	0.511	9
	Mean	2.757	1.428	31 (Total)
0.5	2	3.773	1.271	12
	3	4.729	2.184	9
	Mean	4.182	1.741	21 (Total)
1.0	1	6.841	1.592	12
	2	3.632	1.020	12
	3	4.898	1.316	8
	Mean	5.152	1.917	32 (Total)
3.6	1	2.168	1.003	12
	3	5.278	1.673	8
	Mean	3.412	2.014	20 (Total)
Totals	1	3.504	2.704	35
	2	3.736	1.207	35
	3	4.500	1.680	34
p for the concentration = 0.512				

Table 4.3-3: The effects of Teprosyn Zn/P seed treatment at various concentrations on the germination rate after 72 hrs (%).

Previous studies performed on rice and sunflowers (Sankaran, Mani *et al.* 2002), cumin (Tookaloo, Mollafilabi *et al.* 2010) and oats (Oliveira, Tavares *et al.* 2014), all agree with our findings, that the effect of Teprosyn Zn/P is not significant on the germination rate. Interestingly, both Oliveira *et al.* and Tookaloo *et al.* also found that any positive effect of the seed coat was more pronounced at lower concentrations. These studies mentioned were performed under laboratory conditions, with the germination taking place between moist paper towels. These are classed as hydroponic conditions, though different from those within the fodder system used in our studies. For example, the seeds were less densely packed together in the previous studies performed and the irrigation intervals and methods differed. Contradictory to our finding, work performed on sunflowers (Chitdeshwari, Shanmugasundaram *et al.* 2002) and sugarcane (Rengel, Gil *et al.* 2011) found an increase in the germination with increasing concentration.

However, these studies were performed in soil not hydroponics, therefore making a true comparison difficult.

4.3.3 The effects on yield as dry and fresh mass.

The results presented here demonstrate that Teprosyn Zn/P at such early stages of plant development, has no impact on yield, with either fresh or dry mass.

After statistical analysis, it can be concluded that there has been no significant ($p>0.05$) impact on the % dry mass (Table 4.3-4 and Figure 4.3-5), fresh mass of biscuit (kg) and ratio of produced fodder/planted seed weight (Table 4.3-5) with the use of Teprosyn Zn/P seed coating and, therefore, the null hypothesis has been accepted.

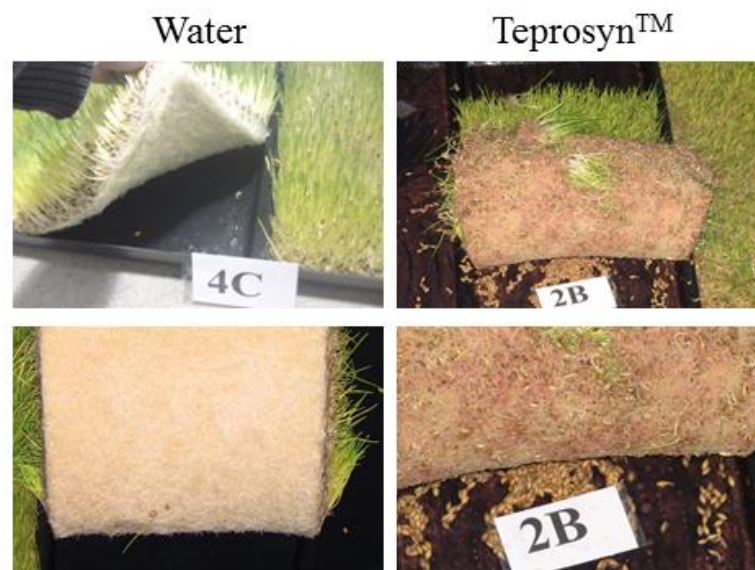


Figure 4.3-3: Comparison of root mat formation with the use of Teprosyn Zn/P at 3.6ml per 1.2kg of seed.

It was also observed that the formation of the biscuit was hindered with high levels of seed coat (Figure 4.3-3 & Figure 4.3-4) and, although root length was not measured in our studies, it was clear that there was a hindrance of root formation. These observations contradict two previous studies done using Teprosyn Zn/P with sunflowers (Sankaran,

Mani *et al.* 2002, Chitdeshwari, Shanmugasundaram *et al.* 2002), where they reported an increase in root length with increasing seed treatment concentrations. A possible reason for this might be because the studies were performed under different conditions. Our study was performed under hydroponic conditions, whereas Sankaran *et al.* and Chitdeshwari *et al.* grew their plants in soil and, therefore, the seeds were exposed to very different conditions. Soil naturally contains beneficial microorganisms that encourage greater root development, which are not found in hydroponic systems without inoculation (Sonneveld, Voogt 2009, Souza, Ambrosini *et al.* 2015, Lopez-Bucio, Pelagio-Flores *et al.* 2015, Tikhonovich, Provorov 2011, Hinsinger, Bengough *et al.* 2009, Fu, Zou *et al.* 2009). The use of a different species of plant (sunflowers) may also provide a reason for the contradictory results.

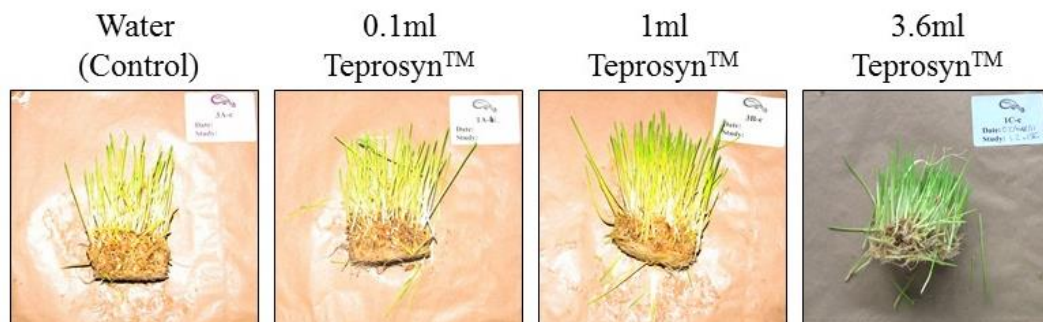


Figure 4.3-4: A cross sectional comparison of the barley development with varying concentration of Teprosyn.

Another previous study performed on barley using Teprosyn Zn/P (Akinci, Doran *et al.* 2008), reported that yield was increased in the later stage of the barley growth, as opposed to in the earlier stages of the plants development, agreeing with our results. Akinci *et al.* 2008, compare foliar application with seed application of zinc and reported a more significant increase in yield with seed application, concluding that this may be due to the ease of uptake of the zinc during germination.

Subsequent studies performed on wheat (Dogan, Cakmak *et al.* 2008), cumin (Tookaloo, Mollafilabi *et al.* 2010) and oats (Oliveira, Tavares *et al.* 2014) all concluded that a high concentration of Teprosyn Zn/P (Zn > 1.8 g/kg of seed), in fact, had a negative impact on the plants' yield. Although studies performed on sunflowers (Chitdeshwari, Shanmugasundaram *et al.* 2004, Chitdeshwari, Shanmugasundaram *et al.* 2002, Sankaran, Mani *et al.* 2002) found that increased concentration (max. Zn 2.4g/kg), increased yield. However, these previous studies mentioned did not find any of the results to be statistically significant.

Former studies on barley fodder production (Al-Karaki, Al-Hashmi 2010), using the same automated fodder machine method, recommend that there is no need to use chemical fertilization to increase yield as there was no significant effect due to the short period of growth, agreeing with the data presented here. Similar studies all concluded that the use of nutrients in this type of growing system had no significant impact on the yield (Dung, Godwin *et al.* 2010a, Dung, Godwin *et al.* 2010b, Peer, Leeson 1985b). Contradictory to this, another study (Al-Karaki 2011), investigating the effects of treated sewage waste water on barley forage production concluded that it was beneficial to the production and quality as the waste water was a good source of nutrients to encourage higher yields. This increase could be attributed to the microbes within the waste water, which may help to increase bioavailability of the nutrient.

Volume of seed coating per 1.2 kg (ml)	Experimental run	Dry mass (%)	Standard deviation	Number of samples (N)
0	1	-	-	
	2	18.980	2.557	12
	3	17.825	4.400	9
	mean	18.485	3.418	21 (total)
0.5	2	18.207	1.415	12
	3	16.722	1.020	9
	mean	17.571	1.444	21 (total)
1.0	1	16.257	1.531	36
	2	18.785	2.940	12
	3	16.722	1.020	9
	mean	16.863	2.084	57 (total)
3.6	1	21.713	1.882	35
	3	18.121	1.400	9
	mean	20.987	2.305	44 (total)
Totals	1	18.947	3.231	71
	2	18.657	2.348	36
	3	17.348	2.400	36
	mean	18.471	2.893	143 (total)

P for the concentration = 0.289

Table 4.3-4: The effects of Teprosyn Zn/P seed treatment at various concentrations on fodder yield as dry mass (%).

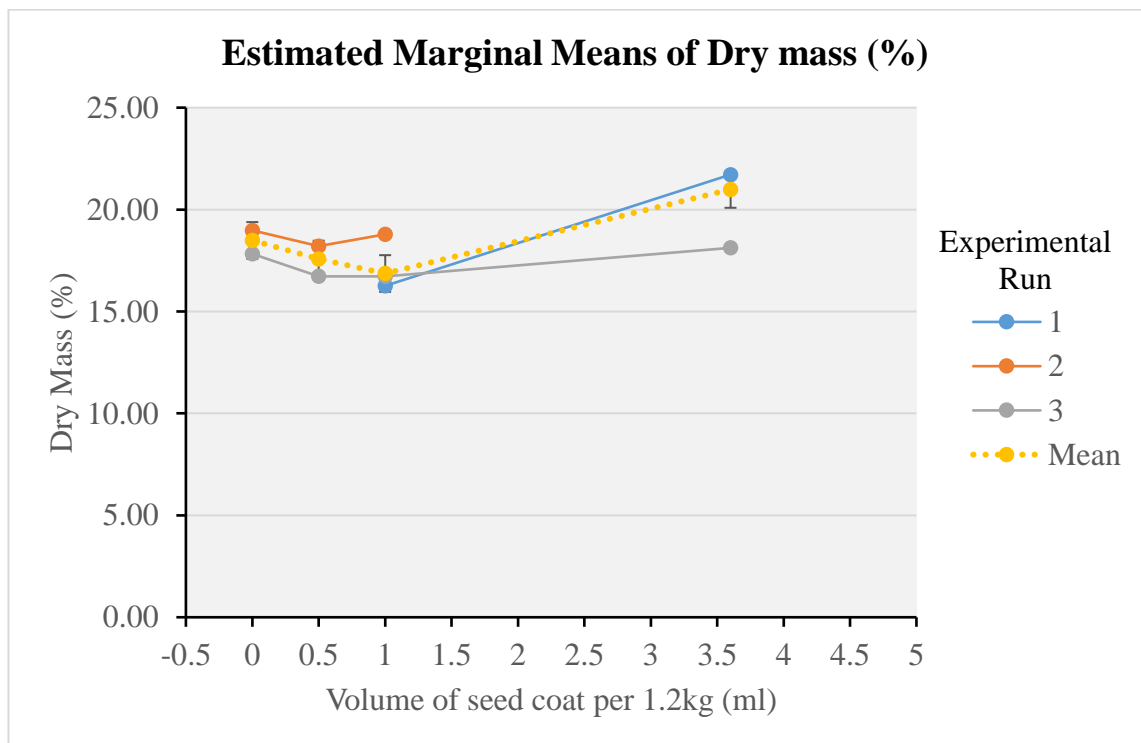


Figure 4.3-5: The effect of varying concentration of Teprosyn Zn/P on the dry mass (%) of barley grown for 6 days.

Volume of seed coating per 1.2 kg (ml)	Exp. run	Fresh mass of biscuit (Kg)	Standard deviation.	Number of samples (N)	Ratio of produced fodder/planted seed weight
0	1	5.682	0.416	36	4.735
	2	4.658	0.326	12	3.882
	3	4.783	0.495	9	3.986
	mean	5.325	0.624	57 (total)	4.438
0.5	2	4.658	0.287	12	3.882
	3	4.787	0.311	9	3.989
	mean	4.713	0.297	21 (total)	3.928
1.0	1	4.661	0.226	36	3.884
	2	4.798	0.338	12	3.998
	3	4.679	0.482	9	3.899
	mean	4.693	0.301	57 (total)	3.911
3.6	1	4.468	0.214	35	3.723
	3	4.457	0.284	9	3.714
	mean	4.466	0.226	44 (total)	3.722
Totals	1	4.937	0.612	108	4.114
	2	4.705	0.316	36	3.921
	3	4.676	0.410	36	3.897
	mean	4.839	0.540	180 (total)	4.033
P for the concentration = 0.417					

Table 4.3-5: The mean fresh mass (kg) of each experimental run testing the effects of Teprosyn Zn/P seed treatment at various concentrations.

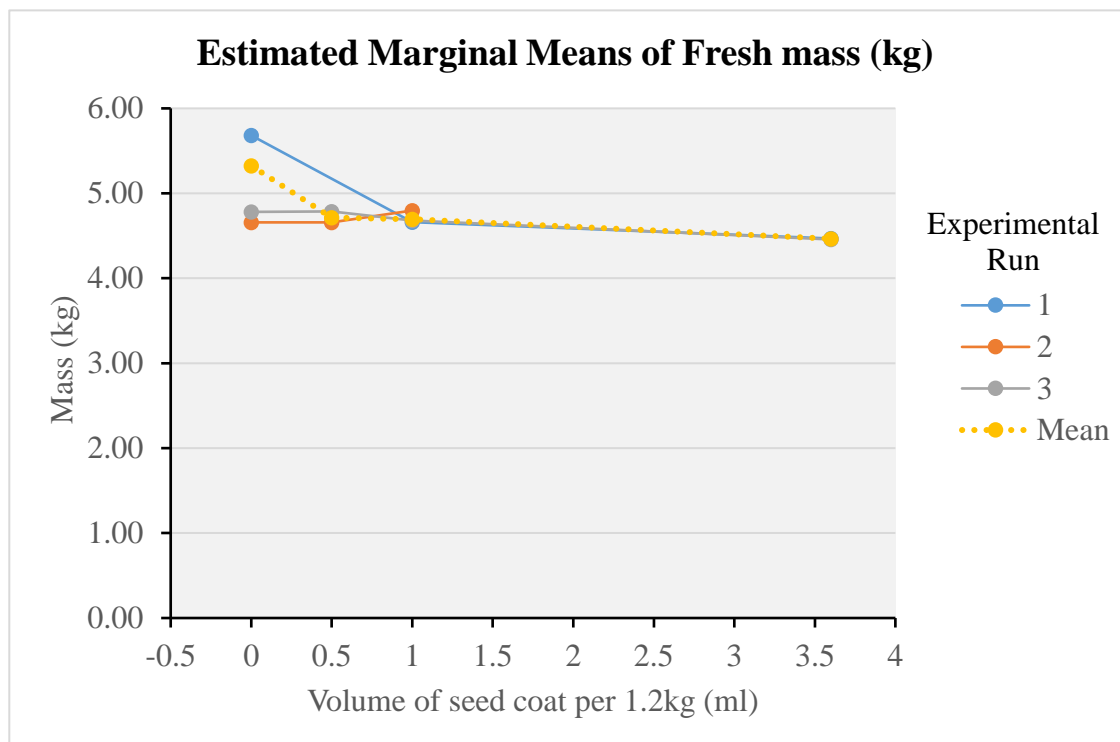


Figure 4.3-6: The effect of varying concentrations of Teprosyn Zn/P on fresh mass of barley grown for 6 days (kg).

It is worth noting that even though the differences between fresh mass of the biscuit were not found to be significant ($p > 0.05$), there is a trend with increased seed coating volume that there is a corresponding decrease in fresh mass (Figure 4.3-6). This would suggest that the Teprosyn Zn/P seed coat is possibly preventing water absorption by the seed, as the water uptake is what causes the fresh mass to increase dramatically under normal growing conditions (Peer, Leeson 1985b).

4.3.4 Elemental content of plant material

Two methods were used to quantify the elemental content of the leaf material, ICP-OES and LA-ICP-MS.

4.3.4.1 Quantitative analysis of ground leaf material after treatment with Teprosyn Zn/P using ICP-OES

The elemental content of the barley shoots is reported in Table 4.3-6. With the exception of Zn, there is no significant difference ($p > 0.05$) in the Fe, P, Ca, and Mg content of the barley shoots treated with seed coat. With increasing volumes of seed coat there is an almost linear increase in the Zn content of the barley shoots (Figure 4.3-7).

The Tukey's HSD homogeneous subset test (Table 4.3-7) is extremely strong evidence that the seed coating influenced the Zn content of the barley shoots. This also allows us to assume that, with increasing volumes of seed coat, there is an increase in the barley shoot Zn content.

Volume of seed coating per 1.2kg (ml)	Experimental run	Mean Elemental content of shoots (mg/kg)				
		Zn	Fe	P	Ca	Mg
0	1	24.88	43.22	4630	425	688
	2	15.64	22.31	3223	381	522
	3	19.73	21.36	3802	428	579
	mean	20.11*	29.45	3890	409	597
0.5	2	40.20	18.78	3515	401	550
	3	49.20	22.94	4336	492	636
	mean	44.06*	20.56	3867	440	587
1.0	1	89.84	19.68	4431	548	717
	2	58.13	21.92	3470	387	549
	3	49.55	23.47	4053	430	444
	mean	69.75*	21.33	4027	467	596
3.6	1	139.45	15.60	3157	377	475
	3	140.20	18.94	3948	446	569
	mean	139.77*	17.03	3496	407	515

Table 4.3-6: ICP-OES elemental content of barley shoots with varying volumes of seed coat.

* Means are significantly different at 1% probability level ($p > 0.01$).

Concentration of Zn in plant tissue						
	Volume of seed coating per 1.2 kg	N	Subset			
			1	2	3	4
Tukey HSD ^{a,b,c}	0.0 ml	31	20.105			
	0.5 ml	21		44.058		
	1.0 ml	37			69.754	
	3.6 ml	21				139.770
	Sig.			1.000	1.000	1.000
Means for groups in homogeneous subsets are displayed. Based on observed means. The error term is Mean Square (Error) = 299.08062.						
a. Uses Harmonic Mean Sample Size = 25.886.						
b. The group sizes are unequal. The harmonic mean of the group sizes is used. Type I error levels are not guaranteed.						
c. Alpha = 0.05.						

Table 4.3-7: Homogeneous subsets for Zinc in the plant tissues produced by the statistical package PASW.

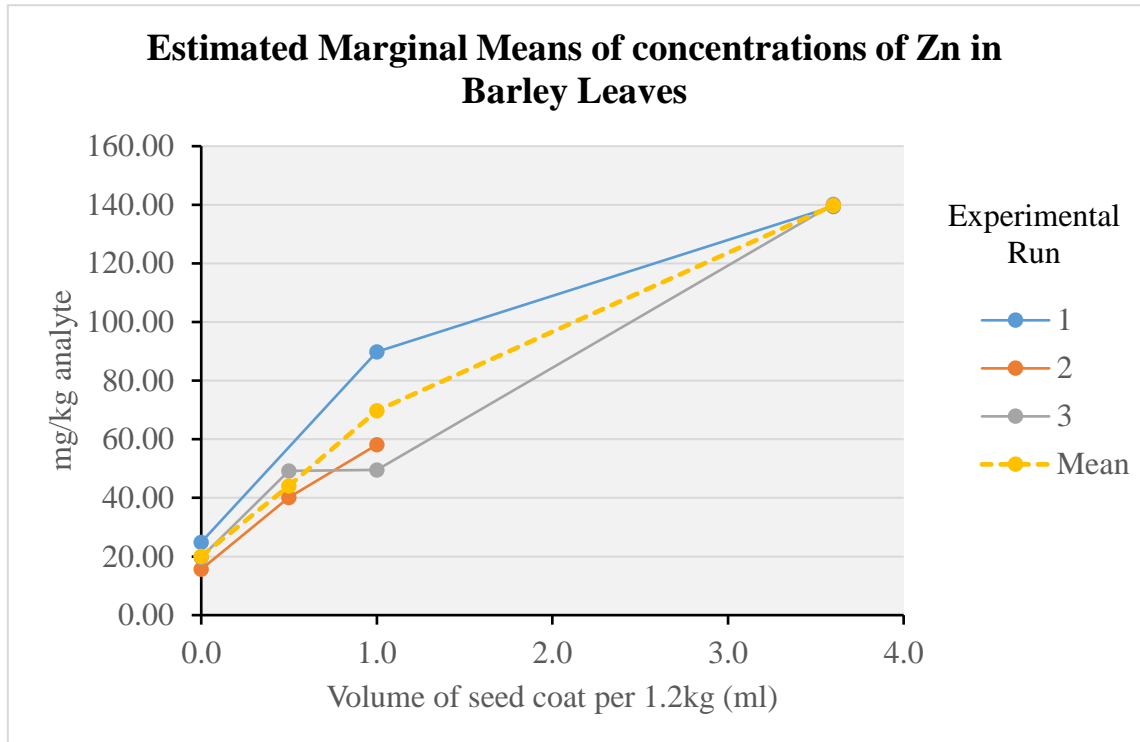


Figure 4.3-7: The effect of increasing concentration of Teprosyn Zn/P seed coat on Zn content of barley shoots.

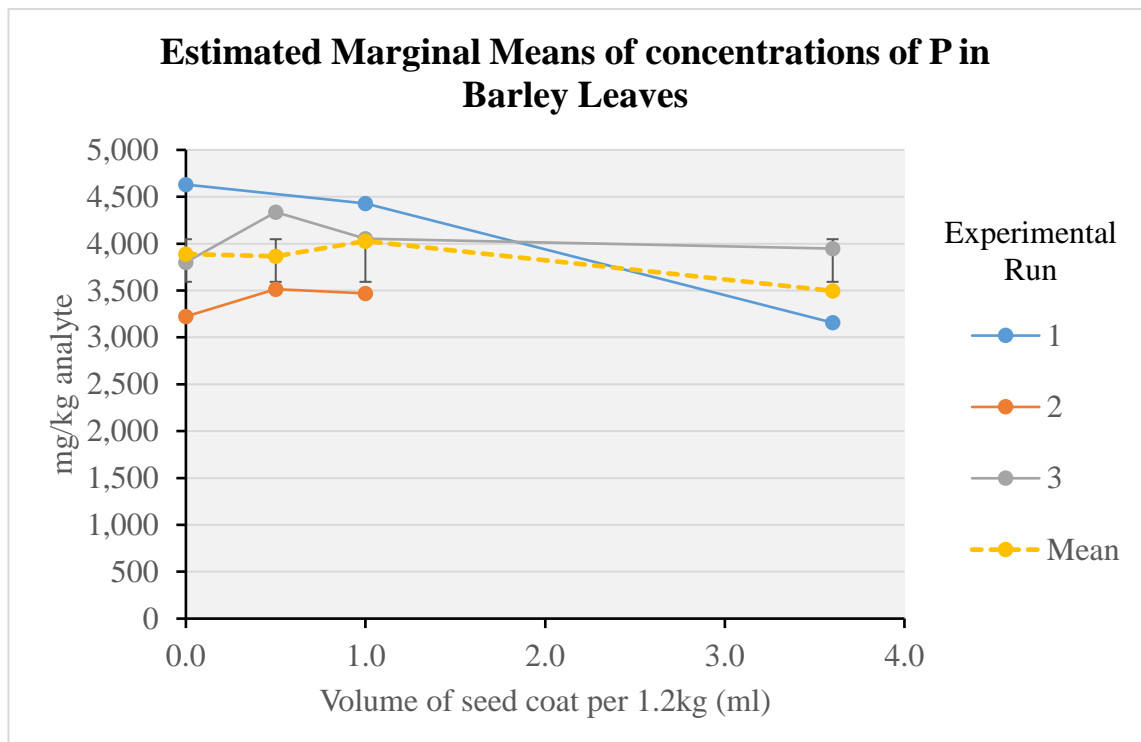


Figure 4.3-8: The phosphorus content of barley leaves after treatment with various concentrations of Teprosyn Zn/P.

The two major elemental constituents of Teprosyn Zn/P are zinc and phosphorus and, therefore, would be expected to increase in the tissue of the plant. Figure 4.3-7 and Figure 4.3-8 depict the change in the concentration of both elements in the plant material. Previous studies, demonstrated an increase in the uptake of both P and Zn into the plant with increasing concentrations of Teprosyn Zn/P (Chitdeshwari, Shanmugasundaram *et al.* 2002, Akinci, Doran *et al.* 2008). The results presented here, only agree with the Zn results of the previous studies. The lower, contradicting phosphorus uptake result, observed in our study, may be due to several reasons. The first of these being the age of the barley at the point of analysis. The previous studies mentioned, analysed plant material which had matured and been harvested weeks after germination, as opposed to six days after germination in our study. This, therefore, gave the plants more time to uptake and accumulate the P from the seed coat. The second reason is due to the cultivation method. The observations described in previous studies were from experiments performed in soil conditions, in contrast to the work reported here (Akinci, Doran *et al.* 2008, Chitdeshwari, Shanmugasundaram *et al.* 2002). It is well documented that a large proportion of the phosphorus in soil is poorly soluble, and for a plant to be able to uptake the phosphorus a symbiotic relationship with fungus must be formed (Fomina, Alexander *et al.* 2004, Lapeyrie, Ranger *et al.* 1991, Wallander, Wickman *et al.* 1997, Whitelaw 2000, Sonneveld, Voogt 2009, Broadley, White *et al.* 2007, Xue, Xia *et al.* 2016, Fomina, Alexander *et al.* 2004). Within the period of six days, in which the fodder production took place, a symbiotic relationship could not be formed. Therefore, solubilisation of the phosphate does not occur and is therefore not available to the barley.

It has also been observed in previous studies using the same method of cultivation as the work reported here (Dung, Godwin *et al.* 2010b) that the sprouted barley had a lower

nutritional content than that of the seeds. Another study (Peer, Leeson 1985b) into the nutrient content of hydroponically sprouted barley revealed that there was an increase in the Cu, Mg, Na, and Zn content of the leaves, whereas the Ca content was not affected and the P content decreased linearly. This was attributed to the leaching of the P from the plant and may explain why an increase was not seen in our study.

All the previous studies mentioned, and the work presented here, used a single species cropping method. A recent study (Xue, Xia *et al.* 2016) has looked at intercropping methods, where multiple crops are sown together and the effect on the uptake of elements such as Fe, Zn and P, (Xue, Xia *et al.* 2016) because very little work had been done previously. Xue *et al.* concluded that intercropping increases the P, Zn and Fe content of cereals and legumes, suggesting that this was due to increased solubilisation of P, Zn, and Fe by the increased release of exudates (e.g. protons, carboxylates, and phosphatases) from the roots and soil microbes under intercropping conditions. This may, also, help explain why an increase in P leaf content was not observed in the data presented here.

Previous studies performed on the effects of fertilizer treatment on fodder production using the same method in this study, revealed some interesting results. Treatment with waste water (Al-Karaki 2011) demonstrated no significant change in the P or Zn content of the barley shoots. Analysis of the waste water revealed that it did not contain any additional P, in comparison to the water, however the Zn content was nearly doubled in the waste water. Dung, Godwin, and Nolan 2010b also found this and concluded that the short growth cycle did not seem likely to be long enough for changes in the nutritional content of the sprouts to occur from the nutrient solution supplied.

A zinc leaf concentration exceeding 15-30 mg/kg dry matter (DM), is desirable for maximum yields in most crops (Gupta, Ram *et al.* 2016). Gupta *et al* 2016 state that concentrations in excess of 100-700 mg/kg will result in the inhibition of growth. At the treatment level of 3.6 ml Teprosyn Zn/P, the zinc leaf content of 139.77 mg/kg DM was achieved, giving reason to the reduction in yield within this treatment group (Figure 4.3-3, Figure 4.3-4 and Figure 4.3-6).

4.3.4.2 Quantitative analysis of ground leaf material after treatment with Teprosyn Zn/P using LA-ICP-MS.

The elemental content of the ground barley leaves, using LA-ICP-MS can be seen in Table 4.3-8. LA-ICP-MS analysis of Zn shows the same pattern as ICP-OES (Table 4.3-6, Figure 4.3-7 & Figure 4.3-9). This data supports the ICP-OES data with both techniques demonstrate that there is an increasing level of Zn in the plant tissues as increased concentrations of Teprosyn Zn/P is used on the seeds. The lower concentrations observed in LA-ICP-MS data may be due to the age of the samples as these had been stored for over 3 years in the -20°C freezer before analysis by LA-ICP-MS. The elemental content of the samples would have been kept more stable had they been stored at -80°C. However, lower results obtained from LA-ICP-MS, in comparison to digested ICP-OES data, has been previously reported (Gomes, Schenk *et al.* 2014, Jurowski *et al* 2014). With the main reason given being the differences in calibration strategies. Homogeneity of the particle size in the material being analysed by LA-ICP-MS is key to obtaining reliable results (Gomes, Schenk *et al.* 2014, Jurowski *et al* 2014). With ICP-OES the sample is digested, making homogeneity of the sample much easier to attain. It is still viewed with in the scientific community that the is still difficult

with the calibration methodology applied to LA-ICP-MS, with far extrapolation being employed to determine concentrations in non-spiked tissue (Jurowski *et al* 2014). With only one point used for calibration in LA-ICP-MS methodology there is an increase margin of error, therefore reducing the accuracy of the results. ICP-OES employees a multi-point calibration curves, resulting in a more accurate calibration method.

	Volume (ml) of Teprosyn Zn/P per 1.2Kg			
	0	0.5	1	3.6
³¹P	1595	2018	2166	2328
<i>SD</i>	581	245	128	133
<i>RSD</i>	36%	12%	6%	6%
²⁴Mg	382	417	430	419
<i>SD</i>	124	48	116	112
<i>RSD</i>	32%	12%	27%	27%
⁵⁶Fe	8.438	7.182	28.140	7.327
<i>SD</i>	0.622	3.331	36.108	1.926
<i>RSD</i>	7%	46%	128%	26%
⁶⁶Zn	16.163	39.800	48.930	83.390
<i>SD</i>	2.957	4.432	16.332	22.956
<i>RSD</i>	18%	11%	33%	28%
⁴⁴Ca	68.857	85.200	114.429	56.286
<i>SD</i>	34.721	2.786	95.181	29.310
<i>RSD</i>	50%	3%	83%	52%

Table 4.3-8: LA-ICP-MS quantitative data of ground barley leaf which has been treated with increasing concentration of Teprosyn seed coating (mg/Kg). (n = 10)

The P LA-ICP-MS data (Table 4.3-8 & Figure 4.3-10) show that the levels of P increase with increased concentration of Teprosyn Zn/P, contradicting the ICP-OES results (Table 4.3-6 & Figure 4.3-8) Analysis by LA-ICP-MS reports lower levels of elements than ICP-OES, but this is probably due to differences between the techniques, instruments and limits of detection (LOD). ICP-OES has a much higher LOD than ICP-MS, at 100 ppm and 1 ppm respectively. However, the results in Table 4.3-9, demonstrate that the LOD for P when using LA-ICP-MS, with this method is still high at 87.5 mg/Kg, but still lower than the 165 mg/Kg of the ICP-OES data (data not

shown). The wavenumber used in the ICP-OES method for P was 213.618 nm and is not the most sensitive and suffers from severe interference from Cu and Mo, elements which are found in plant material. This maybe a reason for the differences in the results. Another reason could be the collision cell on the LA-ICP-MS being utilized within the analysis and therefore minimising the interference experienced. However, it is well documented that matrix interferences do provide more issues with ICP-MS than with optical spectrometry, however this should have been solved by the collision cell. This may also be the reason for the differences in results.

The data obtained for Mg and Fe from LA-ICP-MS did not support the ICP-OES data, however the Ca data, though lower did support the same pattern, with an increase in content and then a drop. Further supporting data would have been attend using microwave digestion and ICP-MS on the sample plant material, unfortunately a lack of sample material dictated to this not being performed. ICP-MS also provides a better detection limit, increasing the sensitivity and accuracies of the results, but does suffer with more serious issues of matrix interference than optical spectrometry. However, this should have been minimised using the collision cell installed on the ICP-MS.

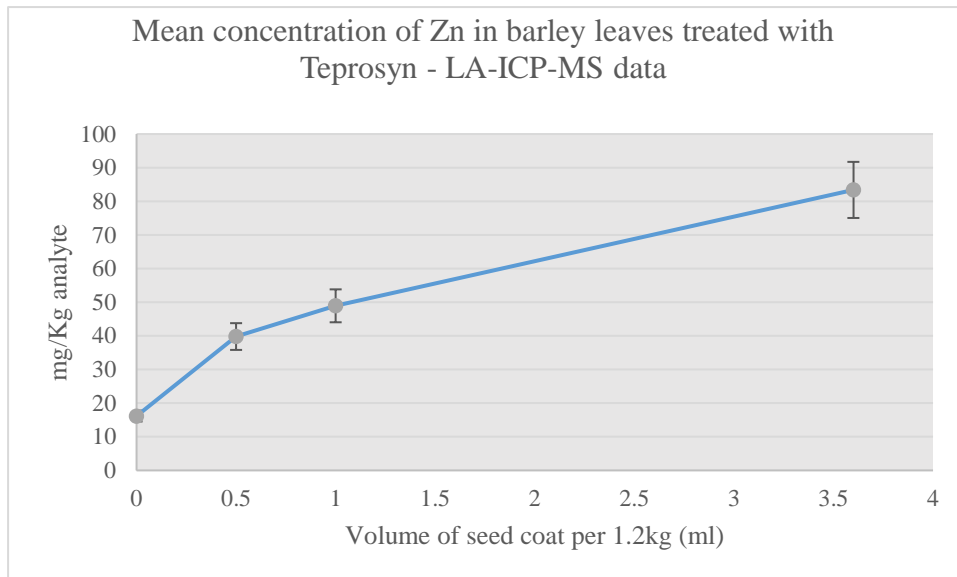


Figure 4.3-9: LA-ICP-MS mean Zn concentration of pelleted barley leaf treated with varying concentrations of Teprosyn Zn/P seed treatment.

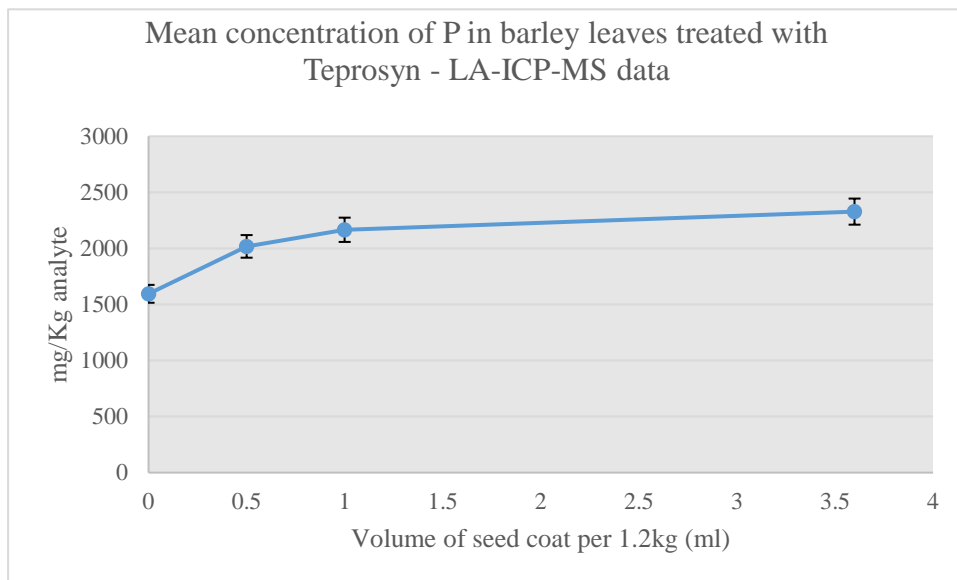


Figure 4.3-10: LA-ICP-MS mean P concentration of pelleted barley leaf treated with varying concentrations of Teprosyn Zn/P seed treatment.

The data obtained for Mg and Fe from LA-ICP-MS did not support the ICP-OES data, however the Ca data, though lower did support the same pattern, with an increase in content and then a drop. Further supporting data would have been attend using microwave digestion and ICP-MS on the sample plant material, unfortunately a lack of

sample material dictated to this not being performed. It is well documented that ICP-MS which are fitted with collision cells are less prone to interference than ICP-OES. ICP-MS also provides a better detection limit, increasing the sensitivity and accuracies of the results.

	³¹ P	⁶⁶ Zn	³⁶ Cu	⁴⁴ Ca	³⁹ K	²³ Na	⁵⁶ Fe	²⁴ Mg	⁷⁸ Se
Mean (mg/Kg)	87.5	0.208	0.096	26.5	14.25	8.75	0.475	1.45	8.5
SD	12.85	0.03	0.04	5.68	2.63	3.55	0.06	0.35	0.00
RSD	15%	17%	40%	21%	18%	41%	13%	24%	0%

Table 4.3-9: LOD for LA-ICP-MS of pelleted barley leaves. (n=10)

The LOD for each element for the LA-ICP-MS method used for quantitative analysis of barley leaf pellets using LD40 as the reference material are displayed in Table 4.3-9. All the elements analysed with LA-ICP-MS achieved RSD above 10% for the LOD analysis, proving that further development is still required for the calibration strategies to be able to use this method as a reliable quantitative method.

4.3.4.3 The use of vanillic acid to improve of laser ablation inductively coupled plasma mass spectrometry analysis.

The addition of vanillic acid to the reference material as a binding agent, in accordance with O'Connor, Landon *et al.* 2007, clearly had a beneficial effect on the data produced.

Figure 4.3-11 displays the average CPS of 9 elements from a 60s ablation line run on a spiked cellulose. The control samples were just cellulose, the VA samples had 25% w/w vanillic acid mixed with them. These were run in triplicate.

The effect was most pronounced with ⁵⁶Fe, but a positive effect can also be seen with ⁶⁶Zn, ³⁹K and ⁷⁸Se. The effect on ³¹P is positive, though not significant, as the standard deviation is so large (shown by the errors bars). It would appear from the result that there is no real effect on ⁴⁴Ca, ²⁴Mg and ²³Na. The most surprising results was the ⁶³Cu,

where the addition of vanillic acid appears to have a signal suppressing effect. Table 4.3-9 reports that the RSD of the LOD for ^{63}Cu and ^{23}Na are above 40%, suggesting that the method was not fully optimised for these elements.

The addition of a binding material is to help compensate for differences in the physical properties of the calibration standard. This in turn reduces variation in the ablation and transport efficiency from the sample to the plasma and finally the detector (Bauer, Limbeck, 2015). Previous studies performed (O'Connor, Landon *et al.* 2007, Hare, Austin *et al.* 2012) added 25% w/w vanillic acid to help improve the signal to noise ratio. Vanillic acid is used as it is an organic chromophore and has a high absorbency at 213 nm, hence making it the ideal candidate for improving the signal to noise ratio. This is due to the phenolic group present in the compound. Other compounds such as PVA, nicotinic acid and pyrazinoic acid have also been investigated by O'Connor's group. Vanillic acid has a much greater molar absorptivity, than the other agents they investigated by O'Connor *et al.* and concluded that a vast increase in sensitivity is seen. This agrees with our findings; however, this paper did not report on specific elemental effects of vanillic acid.

One of the issues with introducing a binding agent is the diluting effect on the sample, making analysis of elements with higher LOD more difficult. In the study presented here, the reference material was replaced with 25% vanillic acid. As this was a chromophore, the signal to noise ratio was reduced, increasing the sensitivity and therefore compensated for the reduction in material. Binding agents such as cellulose alone decrease the sensitivity in comparison to using in conjunction with a chromophore (Stankova *et al.* 2011).

Other binding agents used in LA-ICP-MS reference material preparation, which are not chromophores, include sodium tetraborate. When used in conjunction with silver oxide as an internal standard, more homogenous results were observed with environmental samples (Bauer *et al.* 2015). This was attributed to increased efficiency of particle transport, however the addition a chromophore binding agent increased the sensitivity helping to compensate for the diluting effect of the binding agent its self (Stankova *et al.* 2011). However, Bauer did report issues with polyatomic interference with ^{63}Cu by $^{40}\text{Ar}^{23}\text{Na}$, due to the increased Na from the sodium tetraborate. They also reported possible interferences from contamination of the binding agents, which may give reason to the variation in the results reported in this chapter. The application of kinetic energy discrimination (KED) and collision cell with in the work presented here should have minimised this effect though.

Caffeic acid (Bauer, Limbeck, 2015), caffeine, cinnamic acid and maleic acid (Stankova *et al.* 2011) have all been investigated as chromophore binding agents. Positive effects have been reported for maleic acid, vanillic acid, pyrazinoic acid, nicotinic acid and caffeic acid due to their high absorbency at 213 nm. The main reason the increased sensitivity is the improved coupling between the laser beam energy and the sample. At the point of ablation smaller particles are produced and the efficiency of ablation is improved. This in turn makes the transportation of the particle to the plasma more efficient and fully processed by the plasma, therefore reducing the elemental fractionation (O'Connor *et al.* 2007).

It can be concluded that the use of a chromophore binding agent increases the sensitivity of the analysis, reducing the detection limit and improving quantitation. Binding agents improve the mechanical stability of the pressed disc which produce more reliable results.

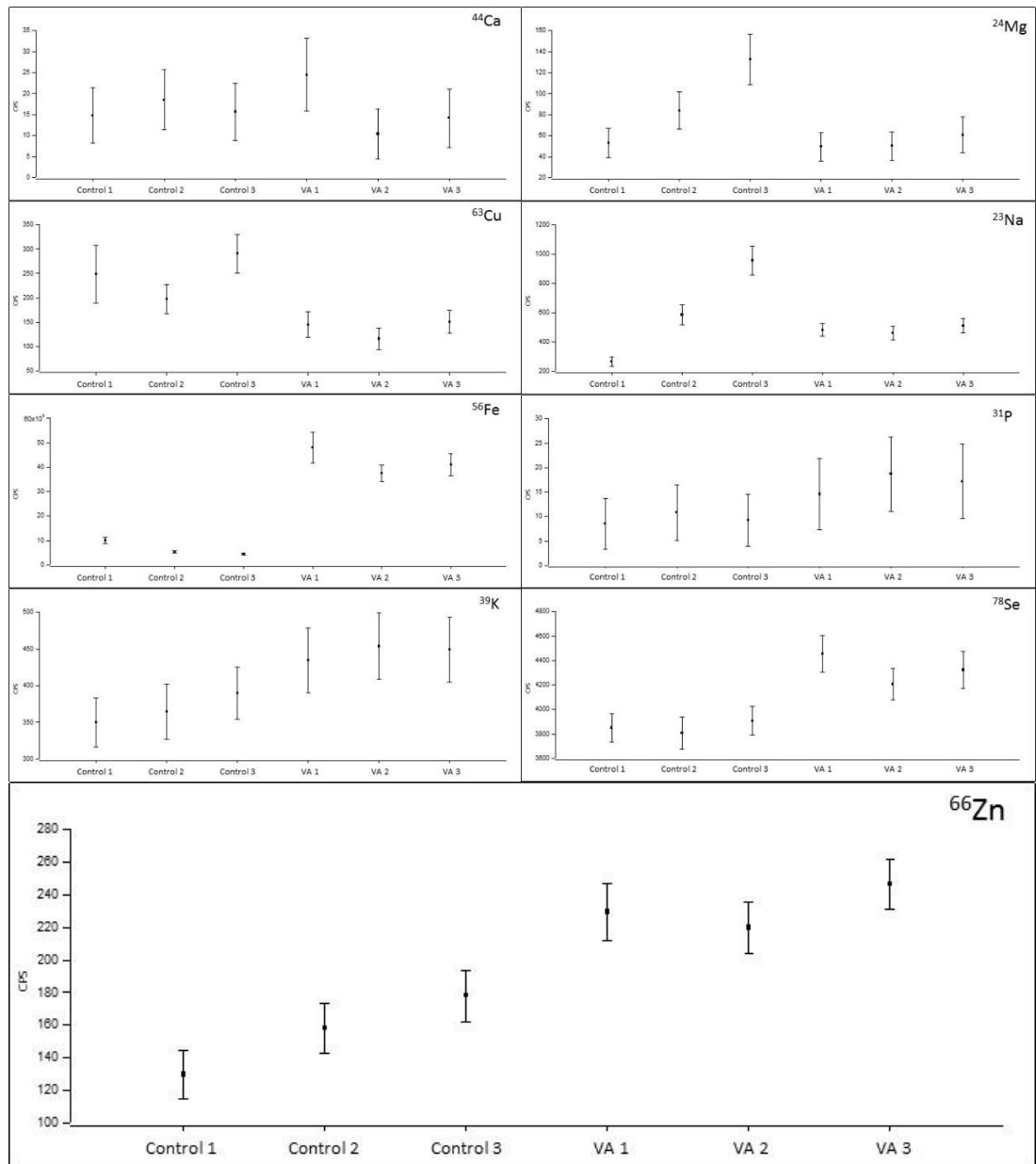


Figure 4.3-11: A comparison of the stat summaries of the effects of vanillic acid on the sensitivity of LA-ICP-MS. *VA = Vanillic acid

4.3.5 Quantitative analysis of laser ablation inductively coupled plasma mass spectrometry reference leaf tissue

Following semi-quantitative analysis, matrix match reference materials were prepared, digested and analysed using ICP-MS for their elemental content. The results are presented in Table 4.3-10 as an average of the triplicates.

Sample	³¹ P	⁶⁶ Zn	⁶³ Cu	⁴⁴ Ca	³⁹ K	²³ Na	⁵⁶ Fe	²⁴ Mg	⁷⁸ Se
	mg/kg	mg/kg	mg/kg	mg/kg	mg/kg	mg/kg	mg/kg	mg/kg	mg/kg
LD0	4540	31.12	4.84	299.7	12072	140.0	34.03	833	0.05
RSD	2%	12%	2%	4%	2%	3%	1%	1%	45%
LD5	5622	40.72	81.27	314.6	12123	168.9	103.1	1032	3.35
RSD	2%	6%	2%	10%	1%	1%	4%	1%	3%
LD10	5522	44.05	78.52	310.7	11862	164.8	111.0	1009	6.73
RSD	2%	3%	2%	9%	2%	3%	4%	2%	2%
LD20	4573	38.17	16.01	340.3	11753	162.7	46.62	812	12.58
RSD	0%	5%	1%	3%	2%	4%	1%	0%	0%
LD40	5625	61.62	98.64	420.3	11751	188.7	130.4	1007	24.64
RSD	0%	2%	6%	6%	1%	5%	12%	1%	2%

Table 4.3-10: Barley leaf reference material elemental content (n = 3).

(Note: LD refers to the sample reference, Leaf Disk and then concentration of standard)

The ¹³C content was reported to be 1.082% in all barley leaf material and was used as the internal standard. These results were entered into the Iolite 3.32 software (Paton, Hellstrom *et al.* 2011) and used to quantify the images produced.

Figure 4.3-12 provides visual representation of the results in the form of the standard calibration curves, which would be used for quantification with liquid ICP-MS. The only elements which follows a linear increase are ⁷⁸Se. ⁶⁶Zn, ⁴⁴Ca and ²³Na also show a linear increase with increasing spike standard concentration. ³¹P, ⁶³Cu, ⁵⁶Fe and ²⁴Mg, all displayed similar patterns with a dramatic drop with LD20, but demonstrated an increase again with LD40. ³⁹K demonstrates a drop in elemental concentration with the increase in spike standard concentration.

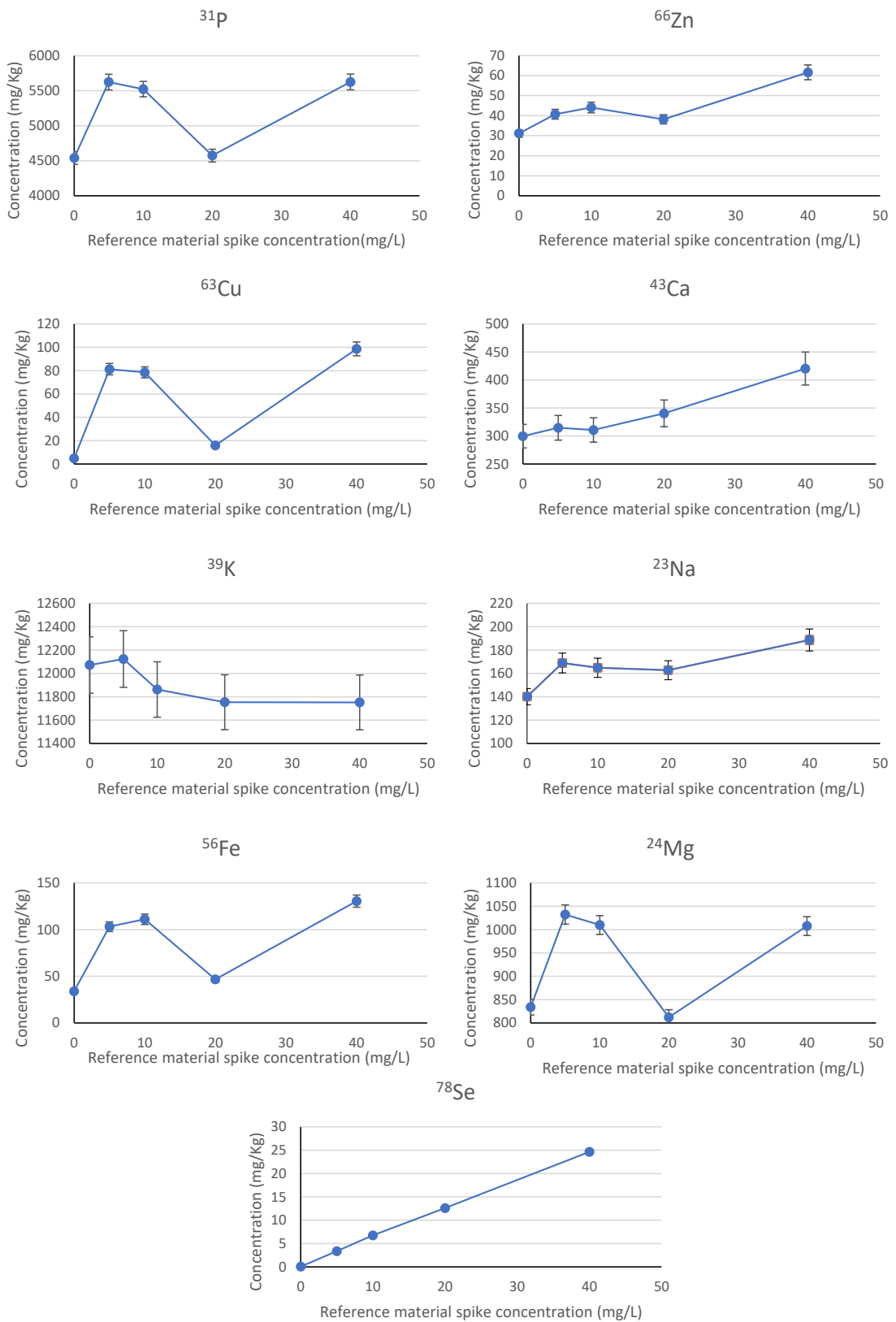


Figure 4.3-12: LA-ICP-MS calibration curves of barley leaf reference material.

These results confirm the lack of homogeneity in the reference material before spike standard addition. This makes the production of calibration curve more difficult and therefore software is required to extrapolate the data. This can give rise to a reduction in the accuracy in the results, when compared with digestion methods. More work is required on the development of standard reference materials preparation, to ensure homogeneity between the matrix.

4.3.5.1 Limit of Detection (LOD) for laser ablation inductively coupled plasma mass spectrometry

The LOD for each element for the LA-ICP-MS method used for quantitative analysis of barley leaves and the seeds are displayed in Table 4.3-11.

	³¹ P	⁶⁶ Zn	⁶³ Cu	⁴⁴ Ca	³⁹ K	²³ Na	⁵⁶ Fe	²⁴ Mg	⁷⁸ Se
	mg/kg	mg/kg	mg/kg	mg/kg	mg/kg	mg/kg	mg/kg	mg/kg	mg/kg
LD0	68.38	0.17	0.10	16.41	12.55	1.63	0.26	1.26	10.08
LD5	69.88	0.16	0.08	16.99	12.61	1.41	0.22	1.37	8.85
LD10	57.67	0.15	0.09	15.25	11.33	1.23	0.22	0.99	8.72
LD20	49.89	0.13	0.08	12.59	9.96	2.73	0.18	0.69	8.90
LD40	60.00	0.17	0.06	14.24	10.96	1.17	0.22	1.04	9.59
Mean	61.16	0.156	0.084	15.09	11.48	1.634	0.221	1.072	9.227
SD	7.329	0.017	0.014	1.573	1.004	0.570	0.024	0.237	0.520
RSD	12.0%	10.8%	16.8%	10.4%	8.7%	34.9%	10.7%	22.1%	5.6%

Table 4.3-11: LOD for each element analysed with LA-ICP-MS.

As the quantitative analysis of the pelleted barley leaves was performed at a different time point to when the images were produced, a drop-in instrument sensitivity had occurred, therefore the LOD were also calculated separately for these, using the reference material LD40. The results can be seen in Table 4.3-9.

4.3.6 Monitoring the distribution in leaf material using laser coupled mass spectrometry imaging

Barley produces monocotyledon leaves which are acicular in shape and have a very simple anatomy, consisting of parallel veins with the lamina in-between. The images presented in this chapter clearly show this anatomy and the distribution of various elements.

4.3.6.1 Matrix assisted laser desorption/ionisation mass spectrometry imaging of leaf material

Teprosyn Zn/P was initially analysed with MALDI-MS to establish strong mass candidates for tracking into the plant. Various ions were picked and fragmentation of those ions was performed. These ions were then monitored within the plant material, using the fragmentation patterns to confirm these were the same compounds

The two major metabolites which were also studied, were phytic acid (659.85 m/z) (Mestek, Polak *et al.* 2008, Loennerdal, Mendoza *et al.* 2011) and zinc orthophosphate, $Zn_3(PO_4)_2$ (387.17 m/z). Various parameters and techniques were applied to the leaves and seed sections, this included variation in matrix concentrations and laying quantities. On fragmentation of the chosen masses most turned out to be matrix peaks. Isotopic patterns were also examined along with various different adducts. Negative mode was also tried with no success.

Figure 4.3-13 shows what was believed to be the phytic acid Zn adduct at mass 756.82.

Further analysis with fragmentation MS/MS revealed it to be a matrix peak.

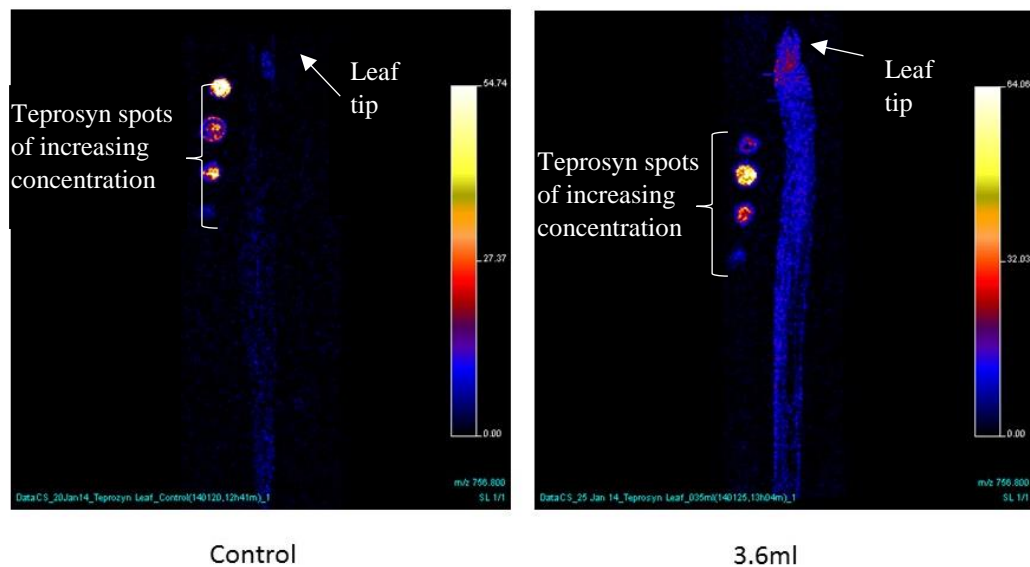


Figure 4.3-13: MALDI-MS images of barley leaf of 756.82 m/z, believed to be phytic acid Zn adduct.

It was concluded that MALDI-MS was not suitable for imaging the distribution of Teprosyn Zn/P in the plant tissue.

4.3.6.2 Semi-quantitative laser ablation inductively coupled plasma mass spectrometry imaging of barley leaves.

Preliminary semi quantitative LA-ICP-MS analysis involved comparing the counts per second (CPS) of ^{63}Cu , ^{44}Ca , ^{56}Fe , ^{39}K , ^{24}Mg , ^{23}Na , ^{31}P and ^{66}Zn within the leaf tissue of the control and the 3.6ml Teprosyn Zn/P group. This revealed some interesting results. As imaging of the tissues would be involved, the elements ^{63}Cu , ^{39}K , and ^{23}Na were added to the analysis, to evaluate the effects on the distribution within the plant.

Initially, Iolite 3.32 calculates the mean CPS of each raster line, and summarises the mean across all the raster lines. Table 4.3-12 summarizes these results and demonstrates

with the proportion as a factor (Diff - Table 4.3-12), that the only significant result is for zinc. As would be expected, the treated group showed an increase in the zinc, at 3.59 times greater intensity than the control group.

	Mean CPS		*Diff (Proportion)
	Control	0.36ml Teprosyn Zn/P	
⁴⁴ Ca	13	19	1.46
⁶³ Cu	170	170	1
⁵⁶ Fe	310	270	0.87
³⁹ K	33000	31000	0.94
²⁴ Mg	1410	1220	0.87
²³ Na	1280	1700	1.33
³¹ P	340	350	1.03
⁶⁶ Zn	128	460	3.59
* The proportion is calculated by dividing the CPS of 3.6ml by the control CPS.			

Table 4.3-12: A comparison of the mean total CPS of treated and non- treated barley leaves.

The distribution of ⁴⁴Ca, ⁶³Cu, ⁵⁶Fe, ³⁹K, ²⁴Mg, ²³Na, ³¹P and ⁶⁶Zn within the control leaf and treated leaf are compared in Figure 4.3-14 and Figure 4.3-15 respectively. It can be clearly seen that the ⁶⁶Zn content in the treated leaf is considerably greater than that in the control group, providing further evidence for increased zinc concentrations with the use of Teprosyn Zn/P.

Figure 4.3-16 and Figure 4.3-17 demonstrate the 3D distribution of the ⁶⁶Zn in the control group and the treated group, showing the greatest distribution in the growth tip of the leaf.

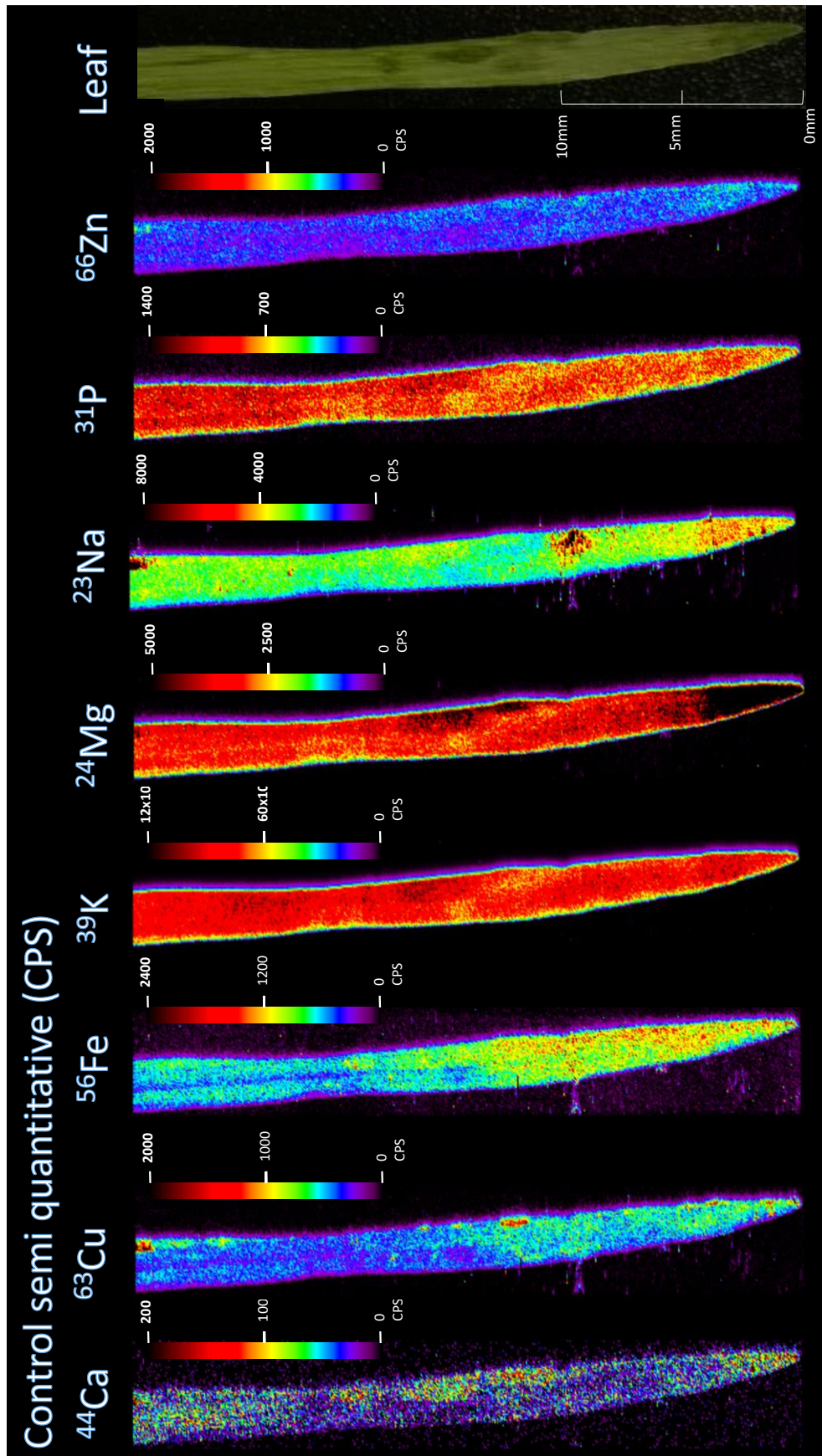


Figure 4.3-14: Semi-quantitative LA-ICP-MS image of control barley leaf.

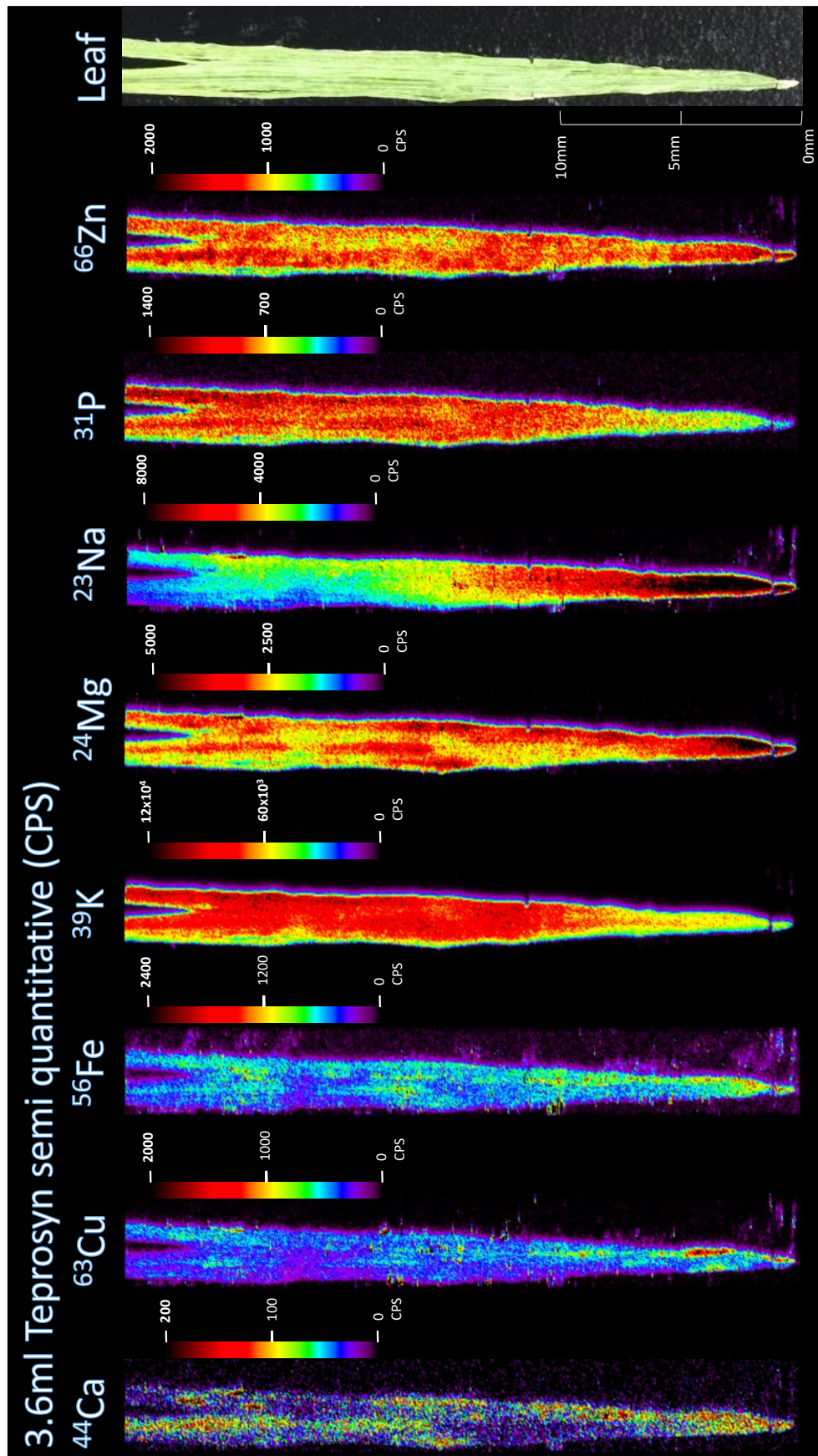


Figure 4.3-15: Semi-quantitative LA-ICP-MS image of barley leaf treated with 3.6ml Teprosyn Zn/P.

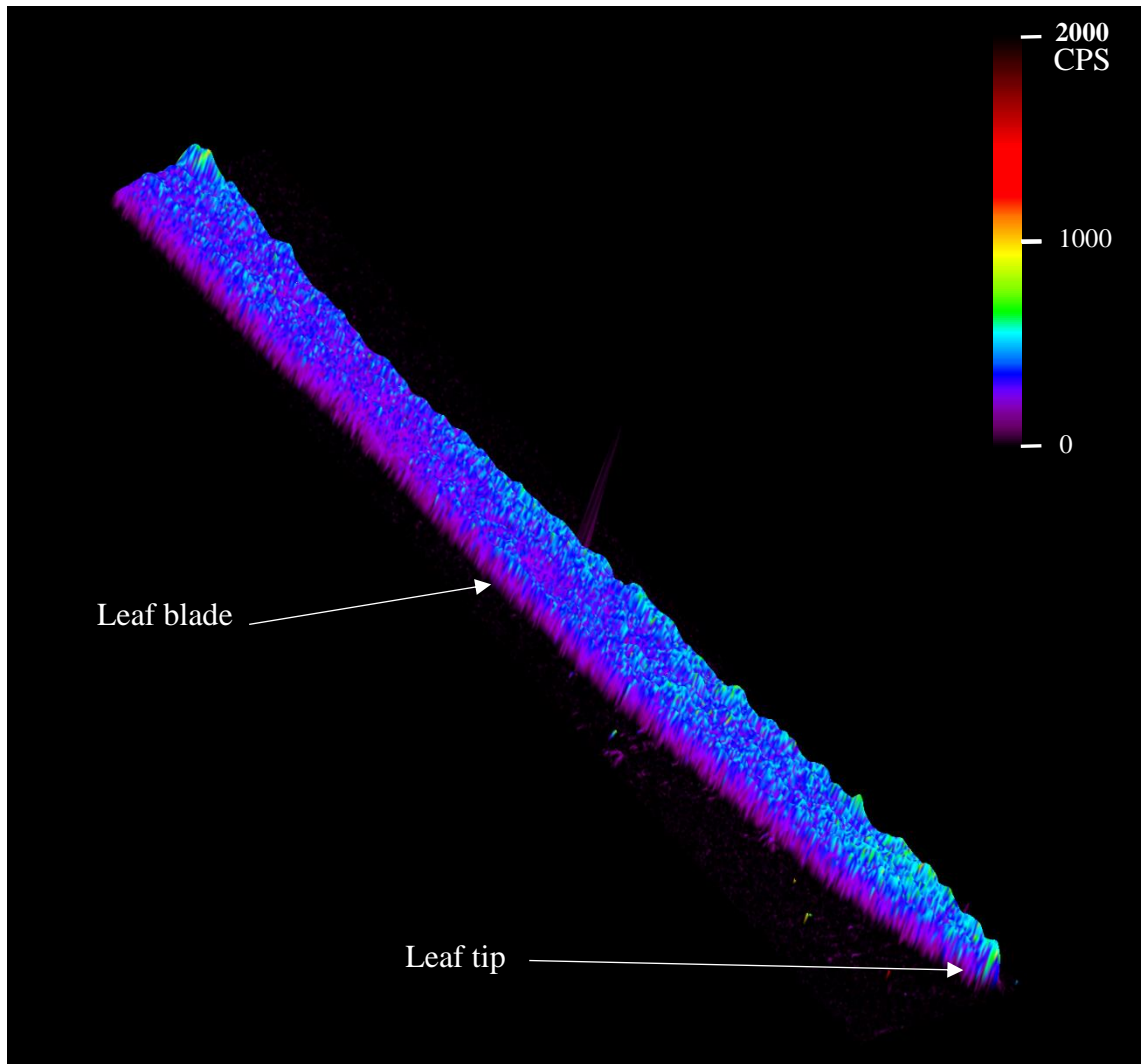


Figure 4.3-16: Semi-quantitative 3D LA-ICP-MS image of ^{66}Zn distribution in the barley leaves in the control group.

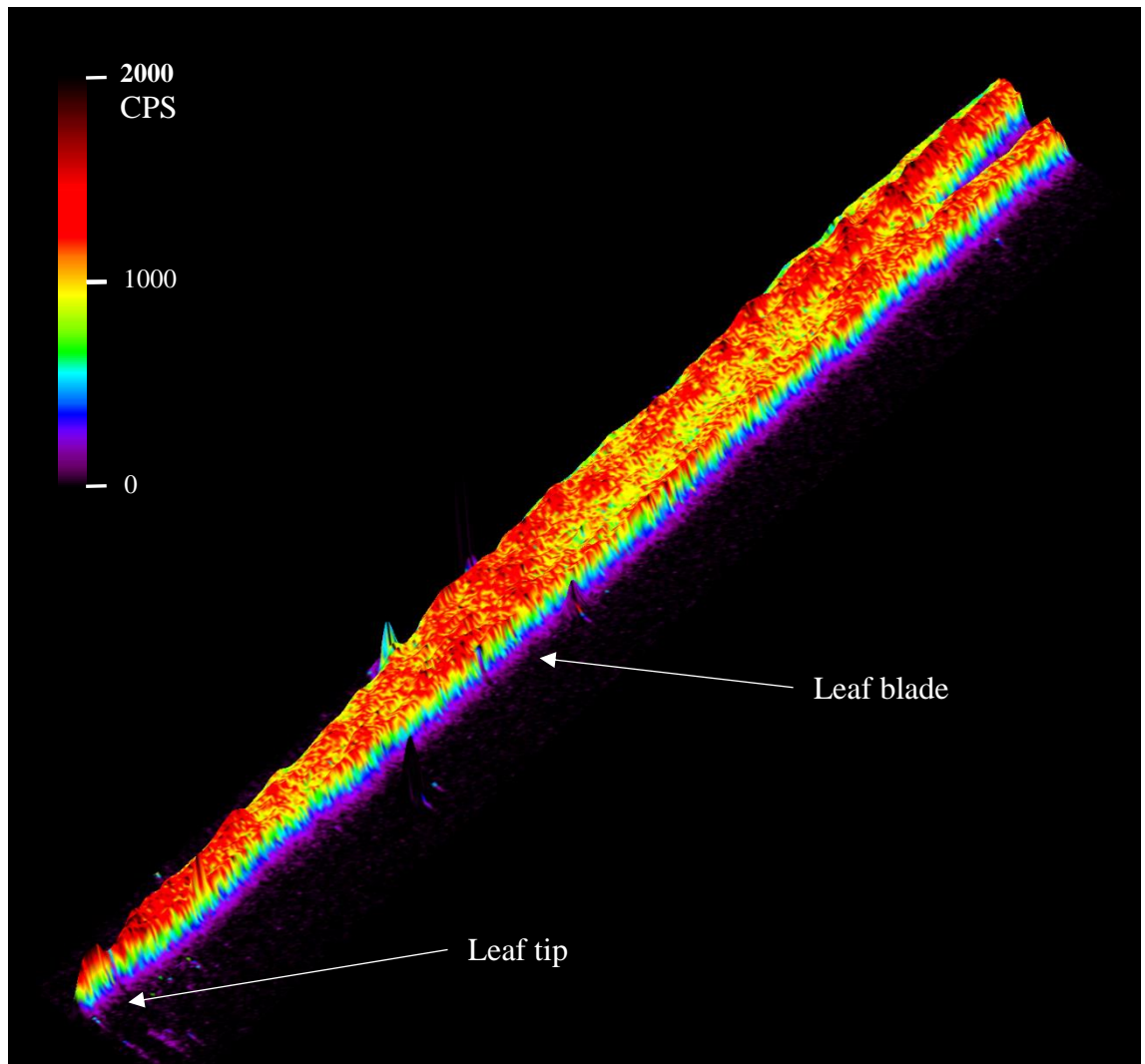


Figure 4.3-17: 3D LA-ICP-MS image of ^{66}Zn distribution in the barley leaves treated with 3.6ml Teprosyn.

Further evidence can be seen in the plotted version of the Summary stats data (Figure 4.3-18) and the stack plot histograms (Figure 4.3-19). Figure 4.3-18 displays the average CPS of ^{66}Zn for each raster line run on the LA-ICP-MS for both leaves untreated and leaves treated. Each point represents the average CPS of one raster line along with the standard deviation as the error bar. The solid black line that runs through the middle denotes the plot average and the grey area represents the plot uncertainty (the standard deviation of the total run). The barley leaf treated with Teprosyn Zn/P, clearly show higher levels of zinc.

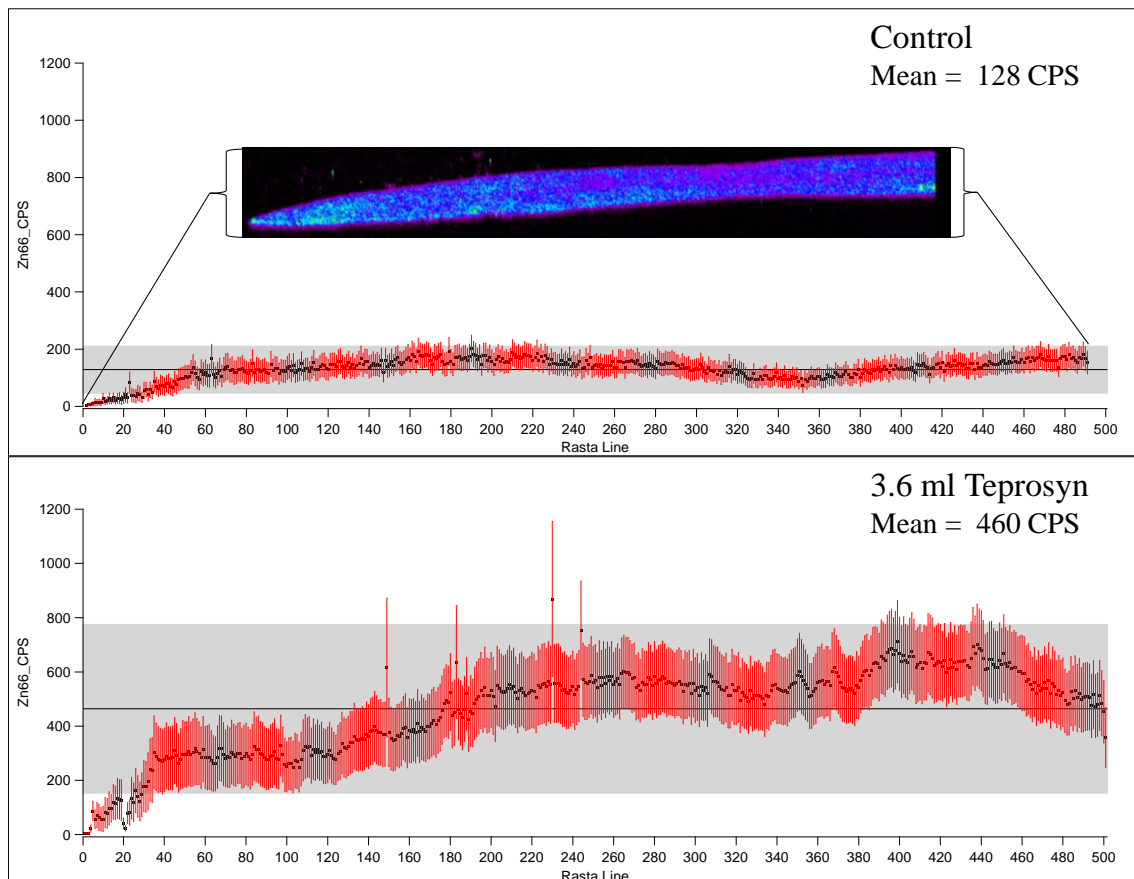


Figure 4.3-18: A comparison of the summary statistical plot of ^{66}Zn for the control group and treated group of barley leaf.

Each red point represents the average concentration a single raster line and the standard deviation is represented by the error bar. The grey area represents the standard deviation of the whole sample and the mean represented by the horizontal line.

The plot histograms (Figure 4.3-19) depict the frequency of ^{66}Zn CPS ranges, at increments of 30 CPS for the control group and 75 CPS for the treated group. This allows for the whole tissue to be assessed for Zn levels, as opposed to regions where the concentration may be elevated. The mean and the median of the averages are also expressed as green and red lines respectively, Figure 4.3-19 illustrates that the control group has a higher frequency of low CPS for Zn than the treated group, therefore resulting in an increase mean and median for the treated group.

^{31}P distribution and content, however, showed no viable differences between the control and treated group. All other elements analysed for did not show any differences between the treated and control group. It is worth noting though, that the images also demonstrate high concentrations of ^{39}K , ^{24}Mg and ^{23}Na , in the tip of the leaves, with the distribution being interveinal within the lamina (i.e. between the veins of the leaf).

Dwell time for each element is 60ms, therefore decreasing the laser speed. This in turn improves the quality of the image data. The dwell times were reviewed for the quantitative analysis and in order to decrease the analysis time, as these images were taking 12 hours to run. According to Longerich *et al* the dwell time for each element should be 6 times the settling time of the quadrupole. For the NexIon 350X the settling time is 0.2ms, therefore the dwell time should be 1.2ms for each element. Refer Chapter 2, section 2.5.10 for further details.

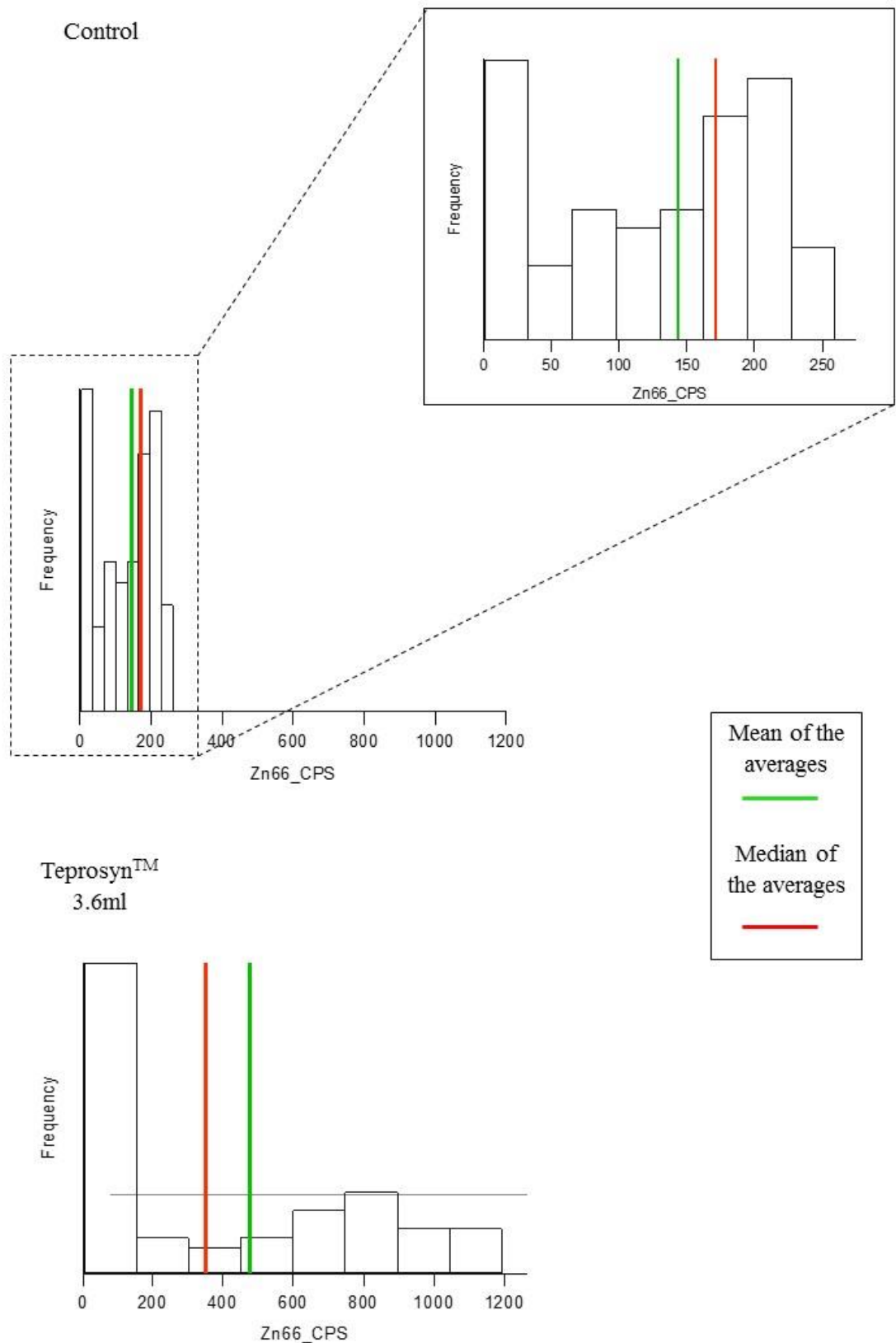


Figure 4.3-19: Comparison of ^{66}Zn stack plots of control group and treated.

The stack plot represents the tissue as a whole and demonstrates the frequency of a particular concentration within the whole tissue. The total mean is shown as a green line and the median as a red line.

4.3.6.3 Quantitative laser ablation inductively coupled plasma mass spectrometry imaging of barley leaves

The distribution and concentration of various elements within barley leaves can be seen in Figure 4.3-20, Figure 4.3-21, Figure 4.3-22 and Figure 4.3-23. LA-ICP-MS was used to produce these images and compare the effects of varying concentrations of Teprosyn Zn/P seed treatment on the uptake and distribution of various elements within the leaf tissue of barley seeding, 6 days after germination.

The zinc can be seen to be interveinal very clearly from Figure 4.3-24 and the 3D image in Figure 4.3-25. The accumulation of the zinc can be seen in the base of the 3.6ml treatment group in Figure 4.3-24, with further distribution spreading into the leaf.

From all of the images it can be seen that highest concentrations of K, Mg and Na can be found in the tips of the leaves, with the distribution being interveinal within the lamina.

LA-ICP-MS to monitor the distribution have been performed on a variety of plants. There are two ways in which the data can be collected and presented. The first involves between three and five replicate raster lines within a small area of interest, and only gives a general overview of the concentrations within that area of the tissue. Previous studies of this method have been performed on plants such as lettuce (*Lactuca sativa*) to monitor heavy metal uptake, Creosote, Ocotillo, Texas-Ebony, Lantana, Autumn sage, Brittle-bush and desert willow (Cizdziel, Bu *et al.* 2012). The second method involves producing a full distribution map by running multiple parallel raster lines across the whole tissue. Previous studies using this method have produced images of plants such as *Elsholtzia splendens* (Wu, Zoriy *et al.* 2009b), *Kosteletzkya virginica* (Han, Quinet *et al.* 2013), and *Nicotiana tabacum* (Tobacco) (Becker, Zoriy *et al.* 2008).

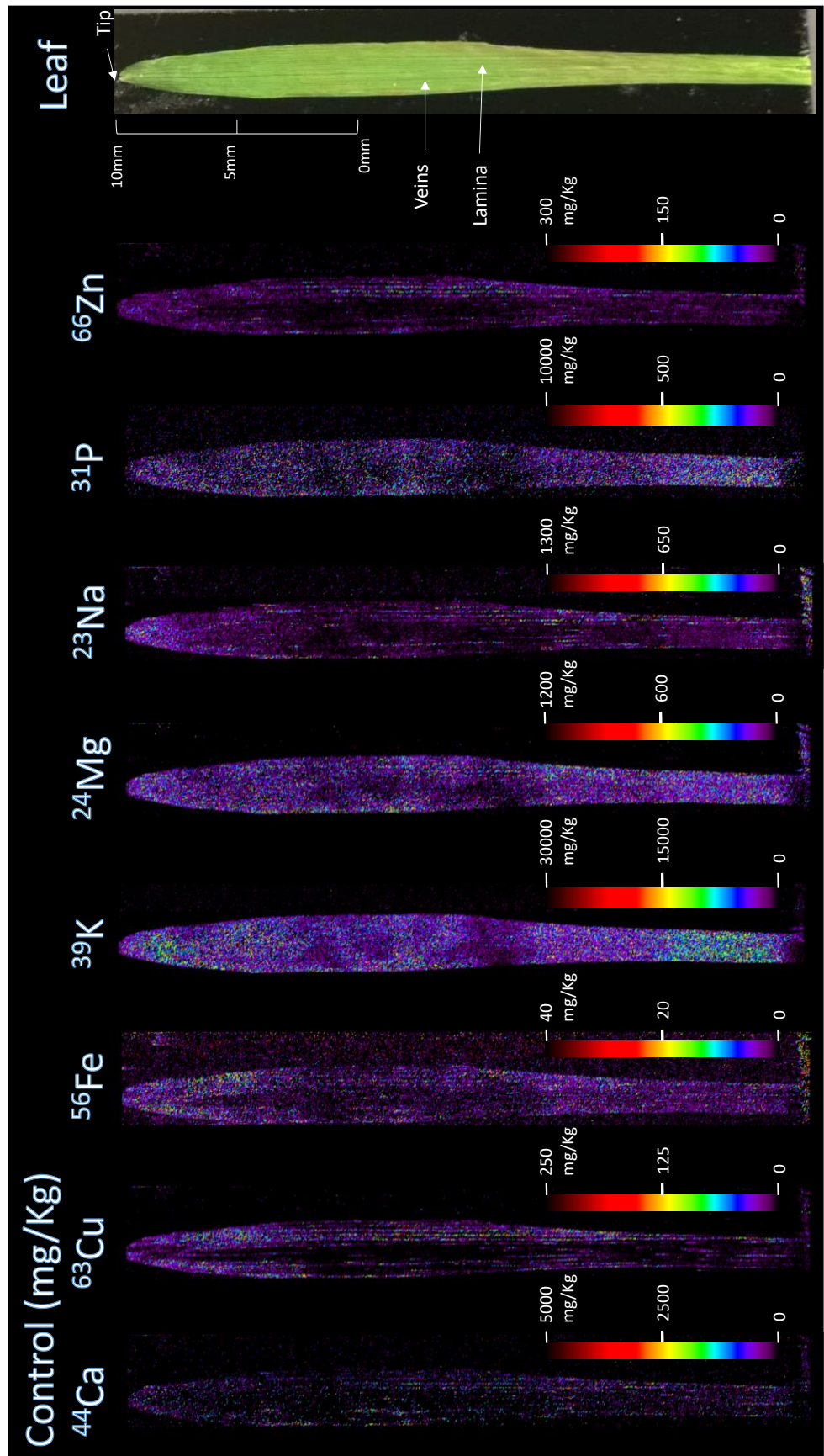


Figure 4.3-20: Quantitative LA-ICP-MS elemental distribution images of control group barley leaf (mg/Kg).

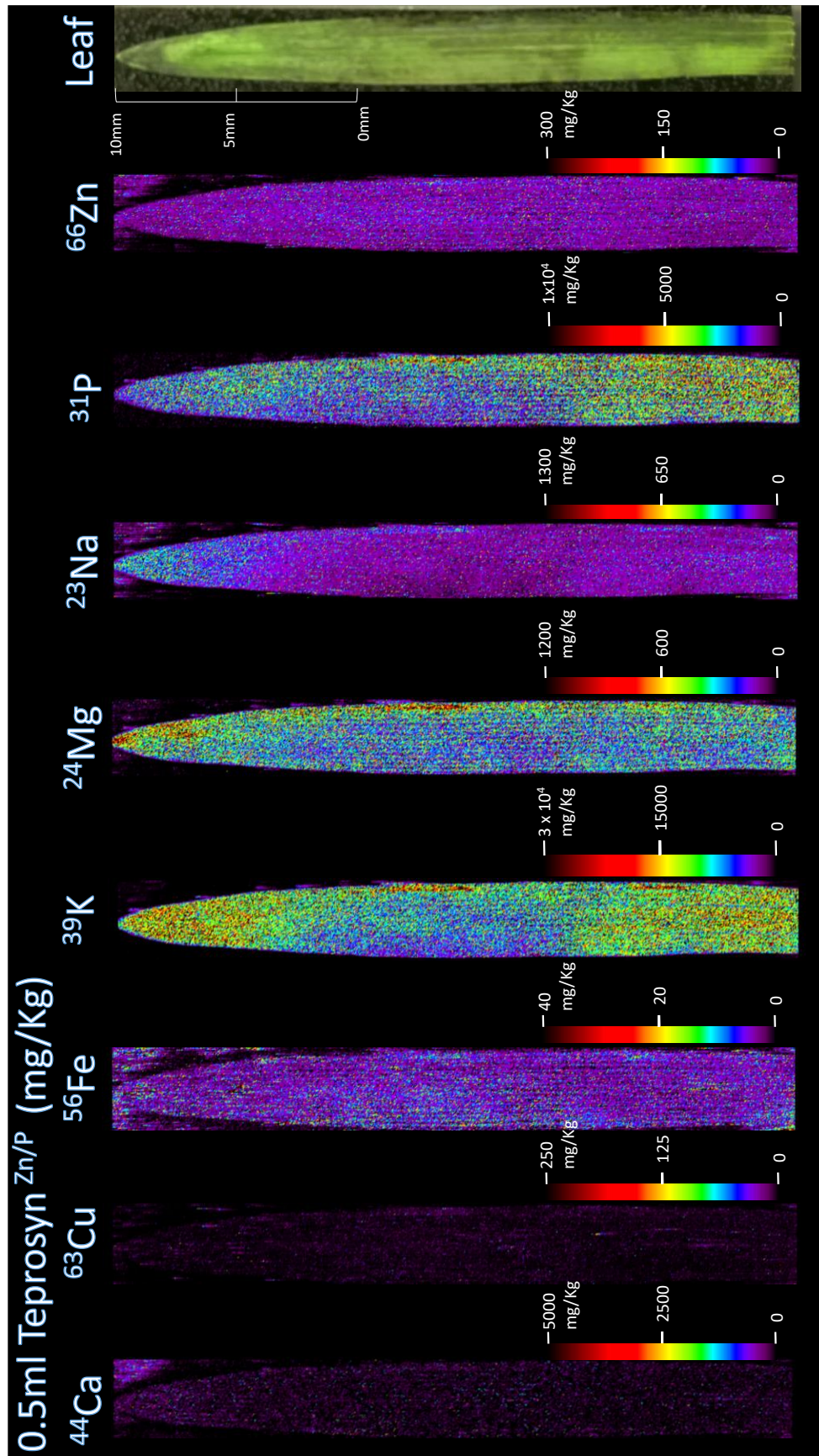


Figure 4.3-21: Quantitative LA-ICP-MS elemental distribution images of barley leaf 0.5ml Teprosyn treatment group (mg/Kg).

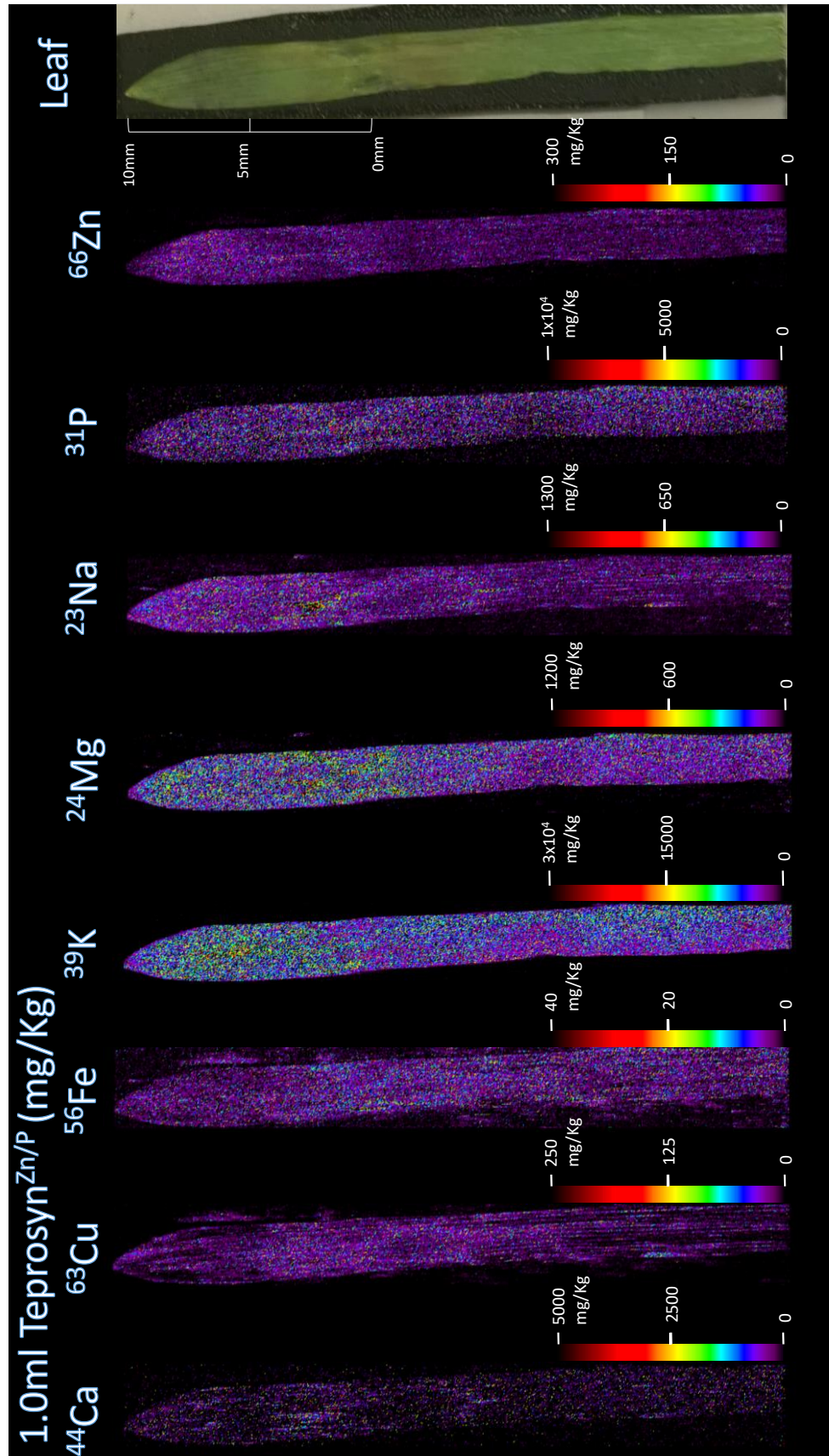


Figure 4.3-22: LA-ICP-MS elemental distribution images of 1.0ml Teprosyn treatment group.

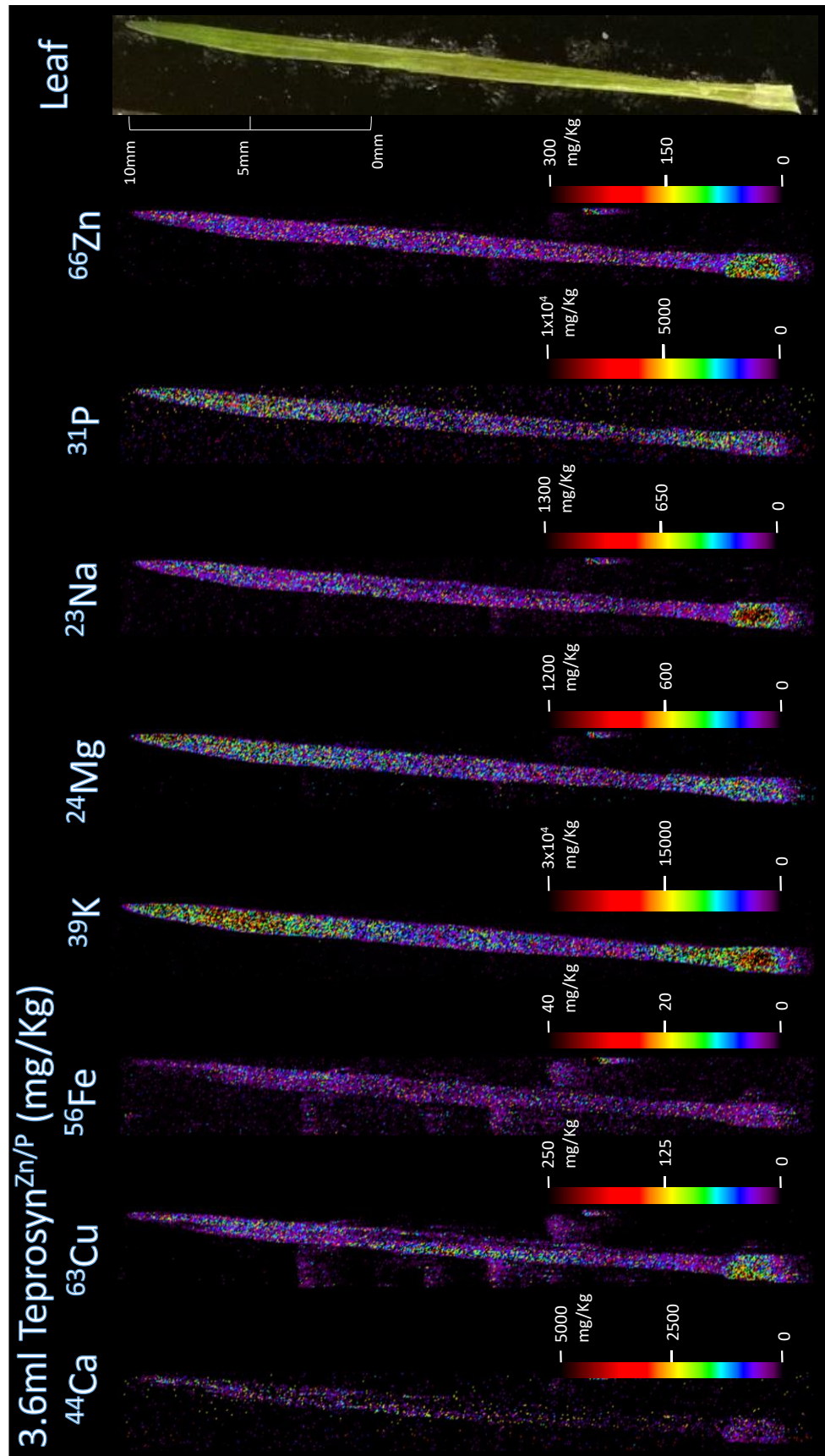


Figure 4.3-23: LA-ICP-MS elemental distribution images of 3.6ml Teprosyn treatment group.

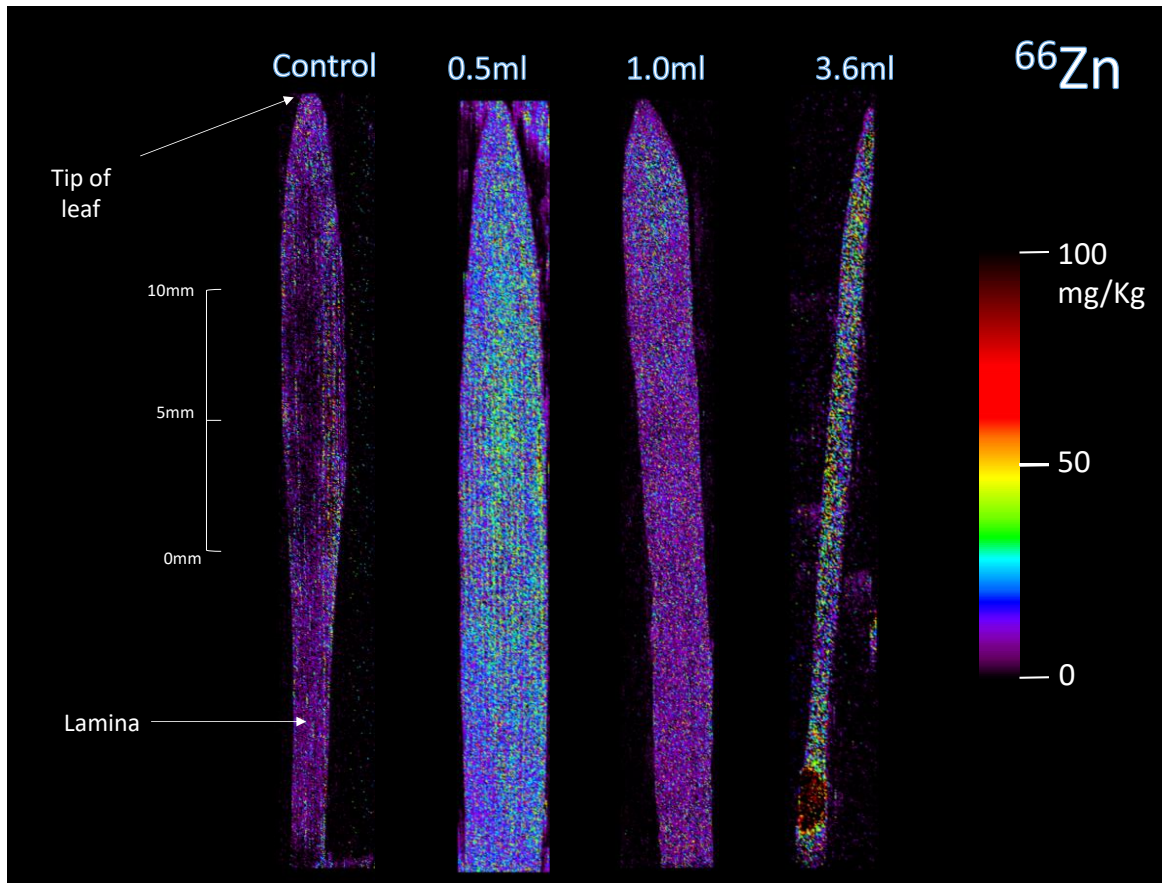


Figure 4.3-24: Comparison of the Zn content of barley leaf with increasing concentration treatment of Teprosyn. Elemental distribution images produced using LA-ICP-MS.

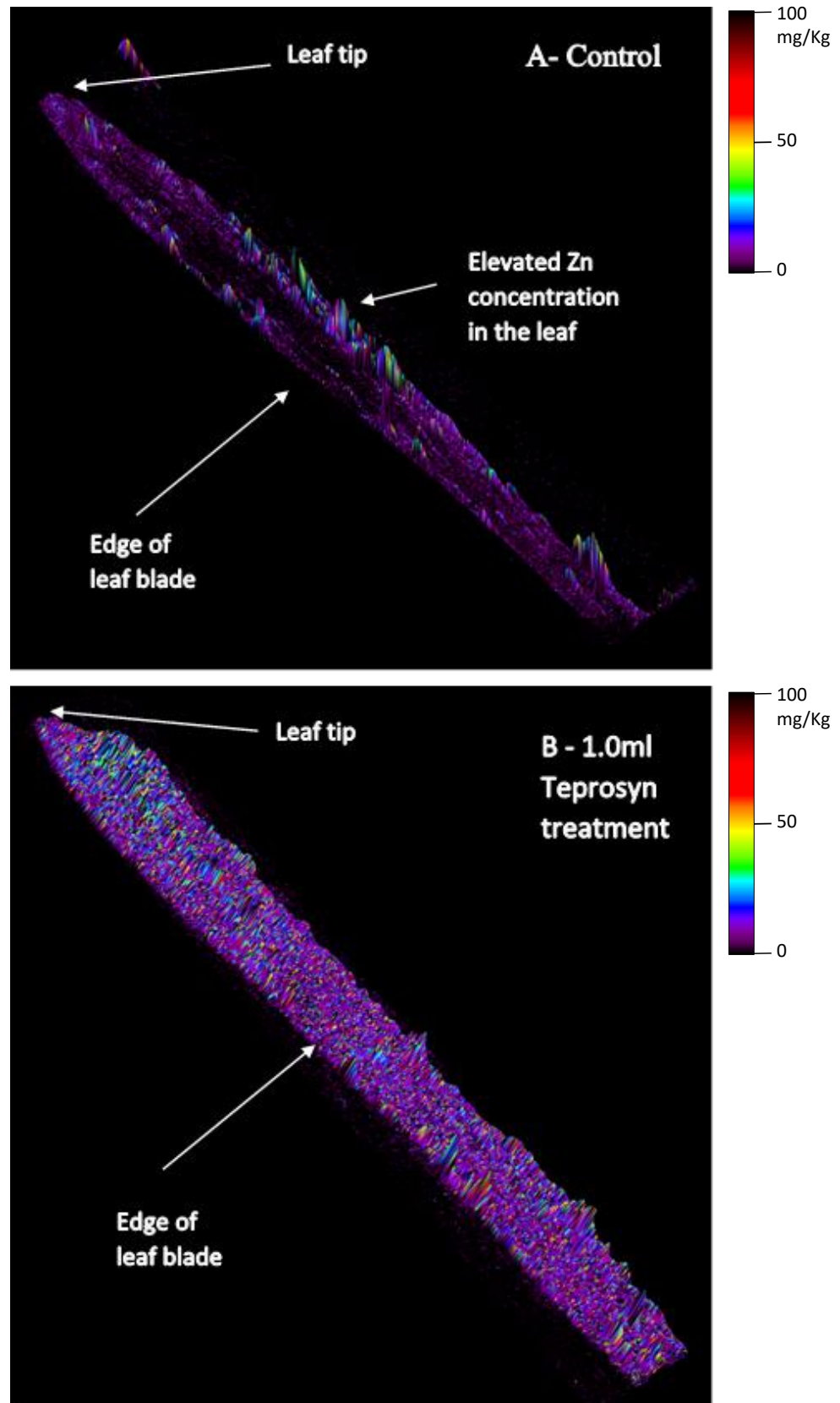


Figure 4.3-25: LA-ICP-MS 3D image of the distribution of Zn in a) Control b) 1.0ml treatment group from Figure 4.3-24.

The reference materials were analysed with the control and 3.6ml treatment group together, with the addition of the 1.0ml and 0.5ml treatment groups. Initially Iolite 3.32 calculates the mean concentrations of each raster line, and summarises the mean across all the raster lines (Table 4.3-13).

Element	Mean Concentrations (mg/kg)			
	Control	0.5ml Teprosyn Zn/P	1.0ml Teprosyn Zn/P	3.6ml Teprosyn Zn/P
⁴⁴ Ca	54	57.1	85	35
³⁶ Cu	6.4	2.02	8.3	10.6
⁵⁶ Fe	1.69	5.27	3.54	0.88
³⁹ K	2260	10020	4770	2570
²⁴ Mg	72	328	171	72
²³ Na	36	126	81.2	52.7
³¹ P	416	2760	711	569
⁶⁶ Zn	4.4	22.2	8.41	12
¹³ C (CPS)	260 <i>RSD 5.3%</i>	901 <i>RSD 2.8%</i>	377 <i>RSD 3.2%</i>	289.5 <i>RSD 7.7%</i>

Table 4.3-13: The effect of Teprosyn Zn/P on the average elemental concentrations (mg/kg) in the whole barley leaf using LA-ICP-MS.

A graphical representation can be seen of these in Figure 4.3-26, Figure 4.3-27 and Figure 4.3-28. As these were an average over the entire tissue, the results are not conclusive and do not truly represent the content of the leaves. The fact that the leaves are different sizes and shapes also effects the accuracy of the results. Despite this it can be seen that there is an increase in Zn content with increased use of Teprosyn Zn/P.

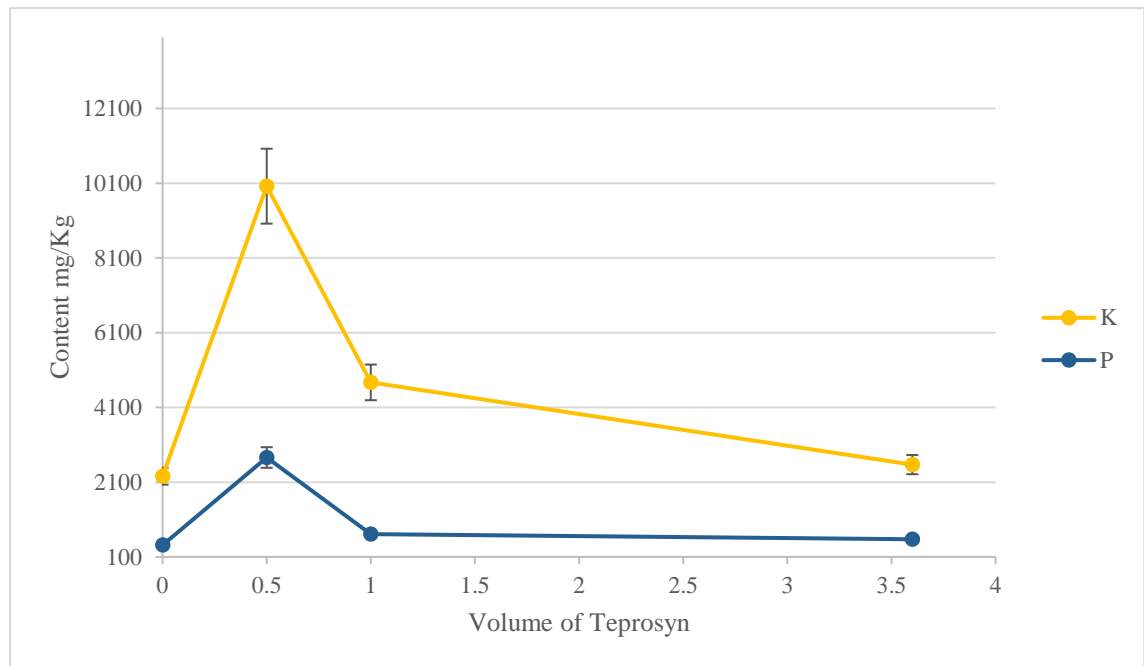


Figure 4.3-26: Graphical representation of the average elemental content of barley leaves treated with various concentrations of Teprosyn, using LA-ICP-MS imaging.

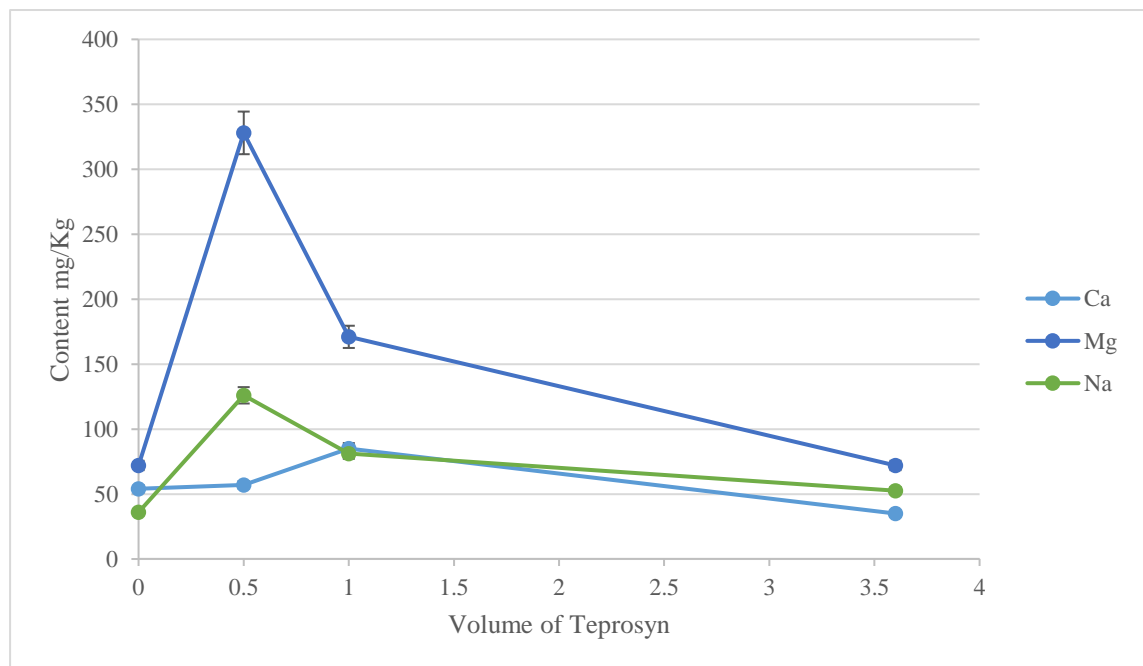


Figure 4.3-27: Graphical representation of the average elemental content of barley leaves treated with various concentrations of Teprosyn Zn/P, using LA-ICP-MS imaging.

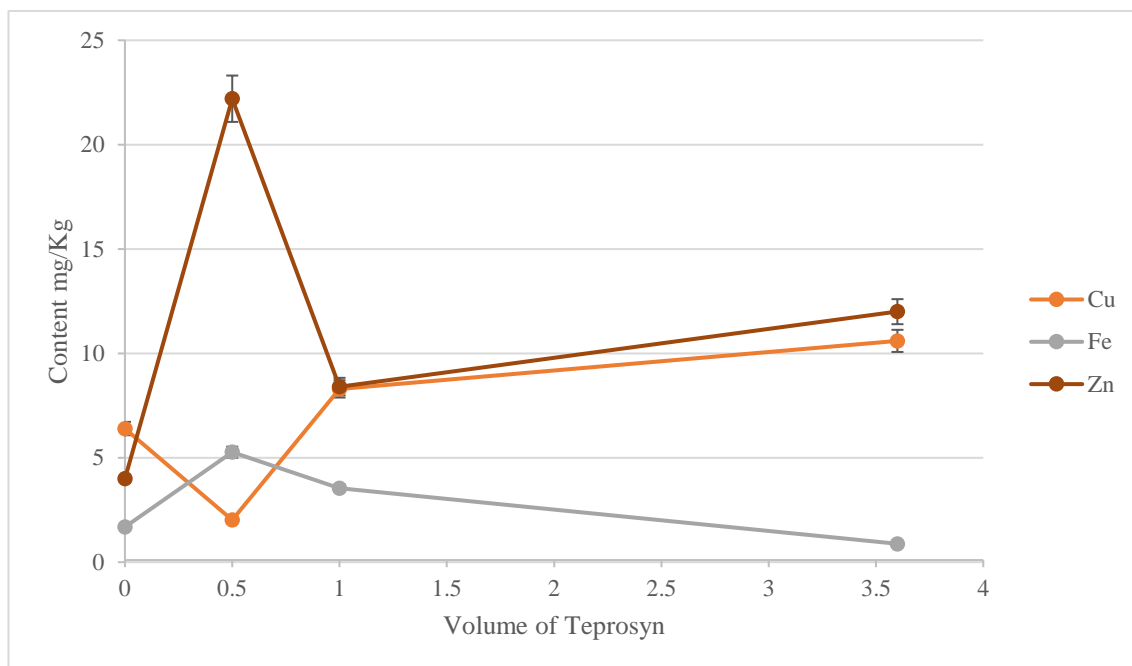


Figure 4.3-28: Graphical representation of the average elemental content of barley leaves treated with various concentrations of Teprosyn Zn/P, using LA-ICP-MS imaging.

The internal standard ^{13}C produced RSD below 10% (Table 4.3-13), helping to correct for variation between tissues. It is also worth noting that Se is not displayed, as the parameters were not optimised, primarily the He gas flow.

Figure 4.3-29 and Figure 4.3-30 give a more comprehensive demonstration of the Zn content. Each point on the graphs in Figure 4.3-29 represent an individual raster line on the tissue. The mean of these raster lines has been calculated to produce Figure 4.3-26. Visual representation of this data can be found in Figure 4.3-20, Figure 4.3-21, Figure 4.3-22, Figure 4.3-23, Figure 4.3-24 and Figure 4.3-25, clearly demonstrating the distribution of the eight elements within the different barley groups. Other than the ^{66}Zn , there was no significant difference between the treatment groups in the concentration of the other elements in the leaves.

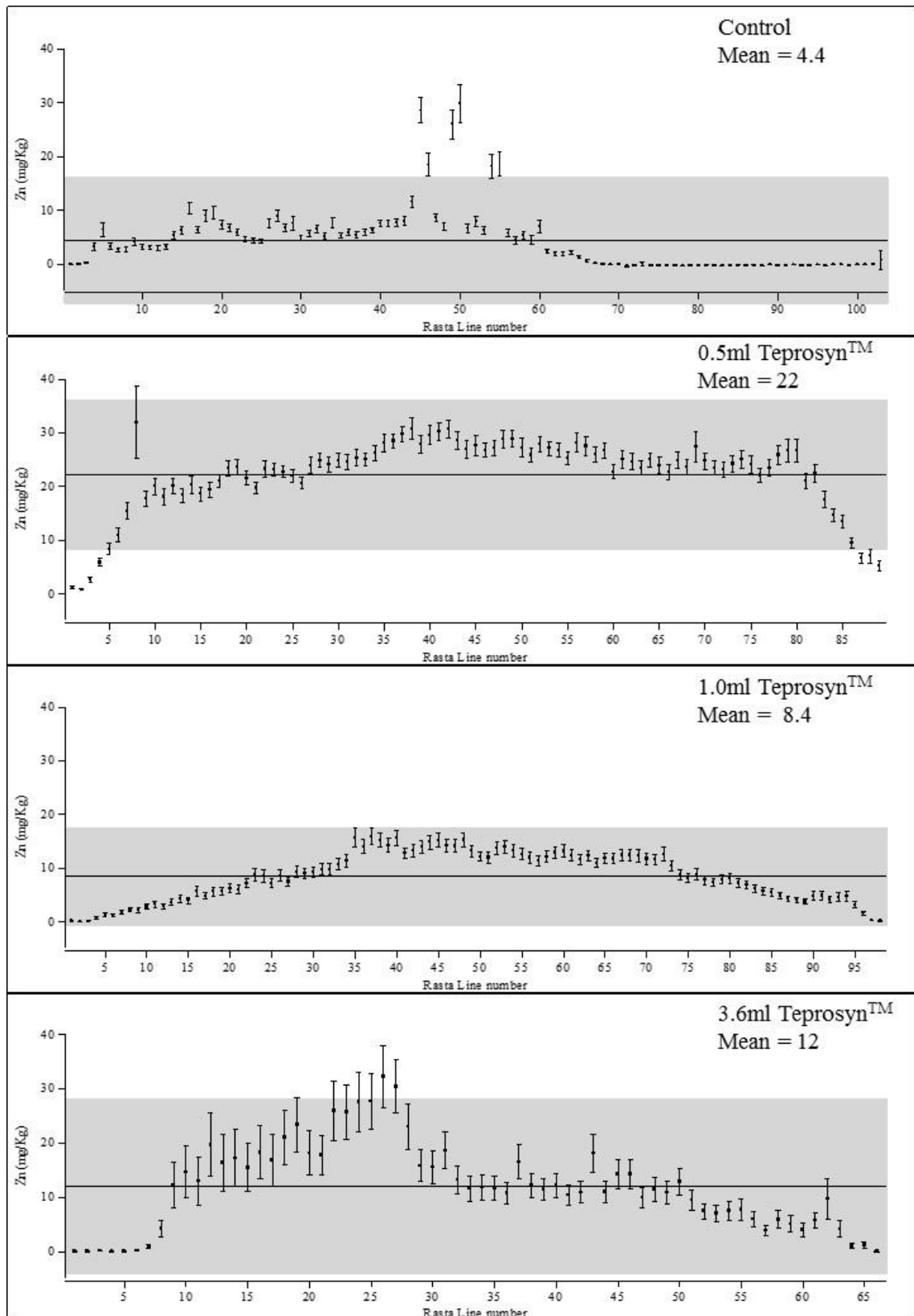


Figure 4.3-29: Comparison of the statistical summary plots of ^{66}Zn for all the treatments of Teprosyn Zn/P on barley seedlings.

Each point represents the average concentration a single raster line and the standard deviation is represented by the error bar. The grey area represents the standard deviation of the whole sample and the mean represented by the horizontal line.

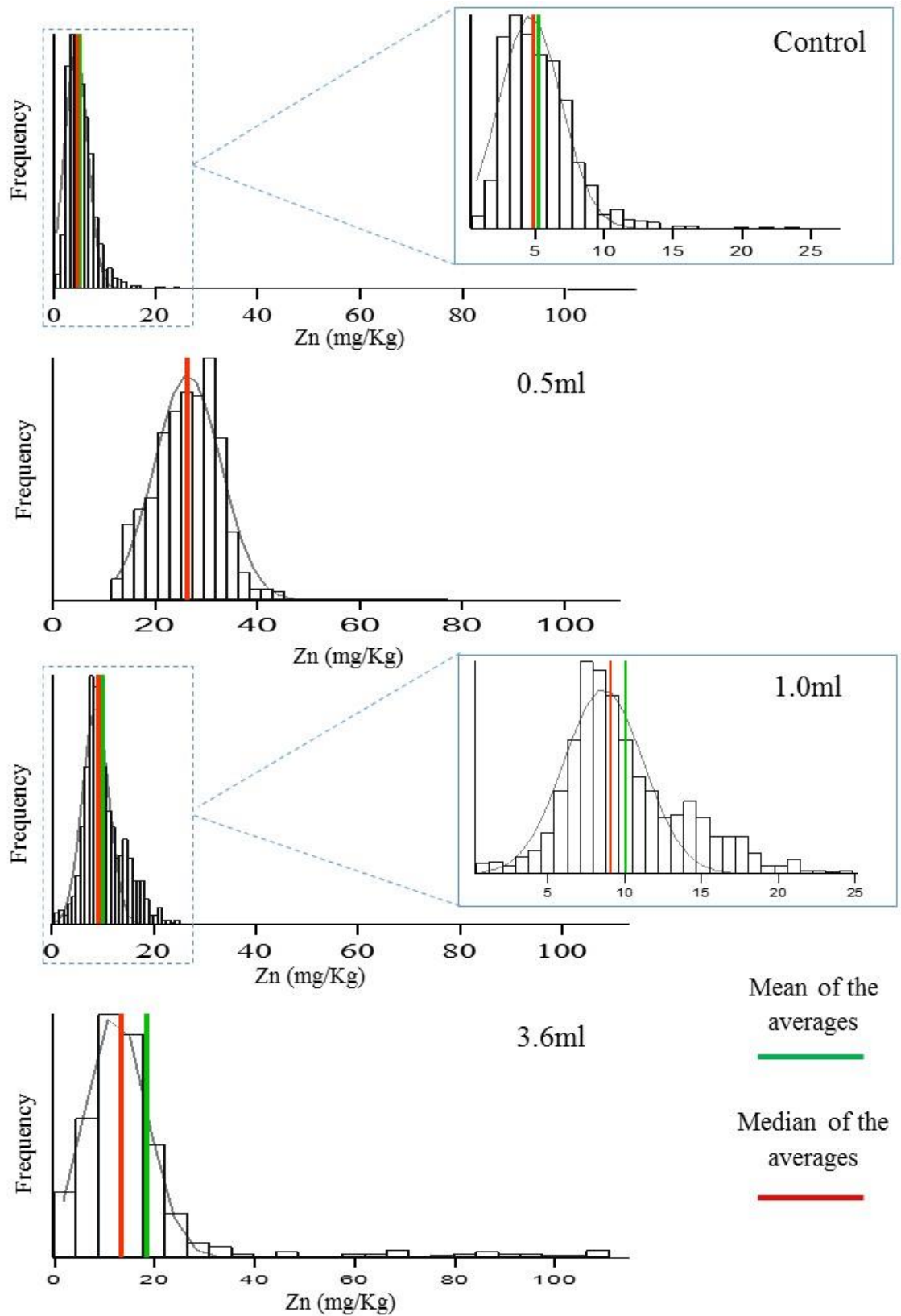


Figure 4.3-30: Histograms to compare the frequency of ^{66}Zn in barley leaves treated with Teprosyn.

The stack plot represents the tissue as a whole and demonstrates the frequency of a particular concentration within the whole tissue. The total mean is shown as a green line and the median as a red line.

4.3.7 Monitoring the uptake of seed coat over time by pre-germinated seeds using laser coupled mass spectrometry imaging

Barley seeds have a very distinctive monocot structure (Figure 4.3-31). All the images for each element clearly show the seed coat, endosperm and the germ (radicle, epicotyl and cotyledon).

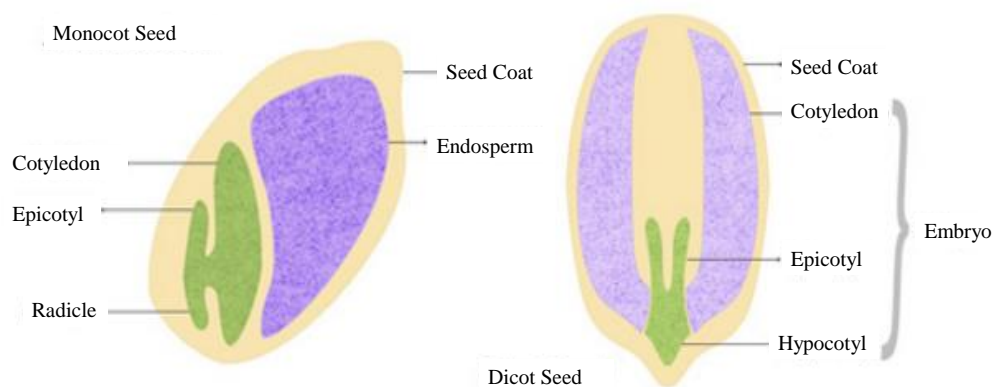


Figure 4.3-31: Structure of a monocot and dicot seed.

4.3.7.1 Matrix assisted laser desorption/ionisation mass spectrometry imaging of seeds

Teprosyn Zn/P was initially analysed with MALDI-MS to establish strong mass candidates for tracking into the plant. Various masses were picked and fragmentation of those masses were performed. These masses were then monitored within the plant material, using the fragmentation patterns to confirm these were the same compounds.

The two major metabolites which were also studied, were phytic acid ($659.85 m/z$) (Mestek, Polak *et al.* 2008, Loennerdal, Mendoza *et al.* 2011) and zinc orthophosphate, $Zn_3(PO_4)_2$ ($387.17 m/z$). Various parameters and techniques were applied to leaves and seed sections. This included variation in matrix concentrations and laying quantities. On fragmentation of the chosen masses most turned out to be matrix peaks. Isotopic

patterns were also examined along with various different adducts. Negative mode was also tried with no success. Therefore, it was concluded that MALDI-MS could not be used to image Teprosyn Zn/P in seeds.

4.3.7.2 Quantitative analysis of laser ablation inductively coupled plasma mass spectrometry reference seed material.

Matrix match reference materials were prepared, digested and analysed for their elemental content (Table 4.3-14). The results are presented in Table 4.3-14 as an average of the triplicates. Figure 4.3-32 depicts these as graphs.

Sample	³¹ P	⁶⁶ Zn	⁶³ Cu	⁴³ Ca	³⁹ K	²³ Na	⁵⁶ Fe	²⁴ Mg	⁷⁸ Se
	mg/kg	mg/kg	mg/kg	mg/kg	mg/kg	mg/kg	mg/kg	mg/kg	mg/kg
SD0	2066.18	15.60	8.69	148.44	3021.43	151.07	28.58	653.61	0.00
<i>RSD</i>	3%	17%	5%	1%	2%	7%	19%	2%	1038%
SD5	1907.82	18.37	11.88	163.97	2729.62	139.08	27.40	573.50	3.00
<i>RSD</i>	3%	13%	1%	16%	0%	4%	8%	0%	1%
SD10	2038.54	21.47	15.85	201.97	2918.43	160.26	33.87	623.02	6.07
<i>RSD</i>	3%	8%	5%	8%	1%	1%	15%	2%	2%
SD20	2049.66	27.49	21.38	227.57	2877.21	162.05	36.33	616.66	11.73
<i>RSD</i>	2%	1%	3%	7%	3%	4%	4%	2%	2%
SD40	2044.08	30.95	25.29	251.47	2822.95	166.10	42.41	614.51	15.42
<i>RSD</i>	1%	4%	2%	3%	1%	3%	7%	2%	2%

Table 4.3-14: Barley seed reference material elemental content. (n =3)

(Note: LD refers to the sample reference, Seed Disk and then concentration of standard)

The ¹³C content was reported to be 1.081% in all barley seed material and was used as the internal standard. Refer to Chapter 2, Section 2.5.11 for more details. These results were entered into the Iolite 3.32 software (Paton, Hellstrom *et al.* 2011) and used to quantify the images produced.

C1

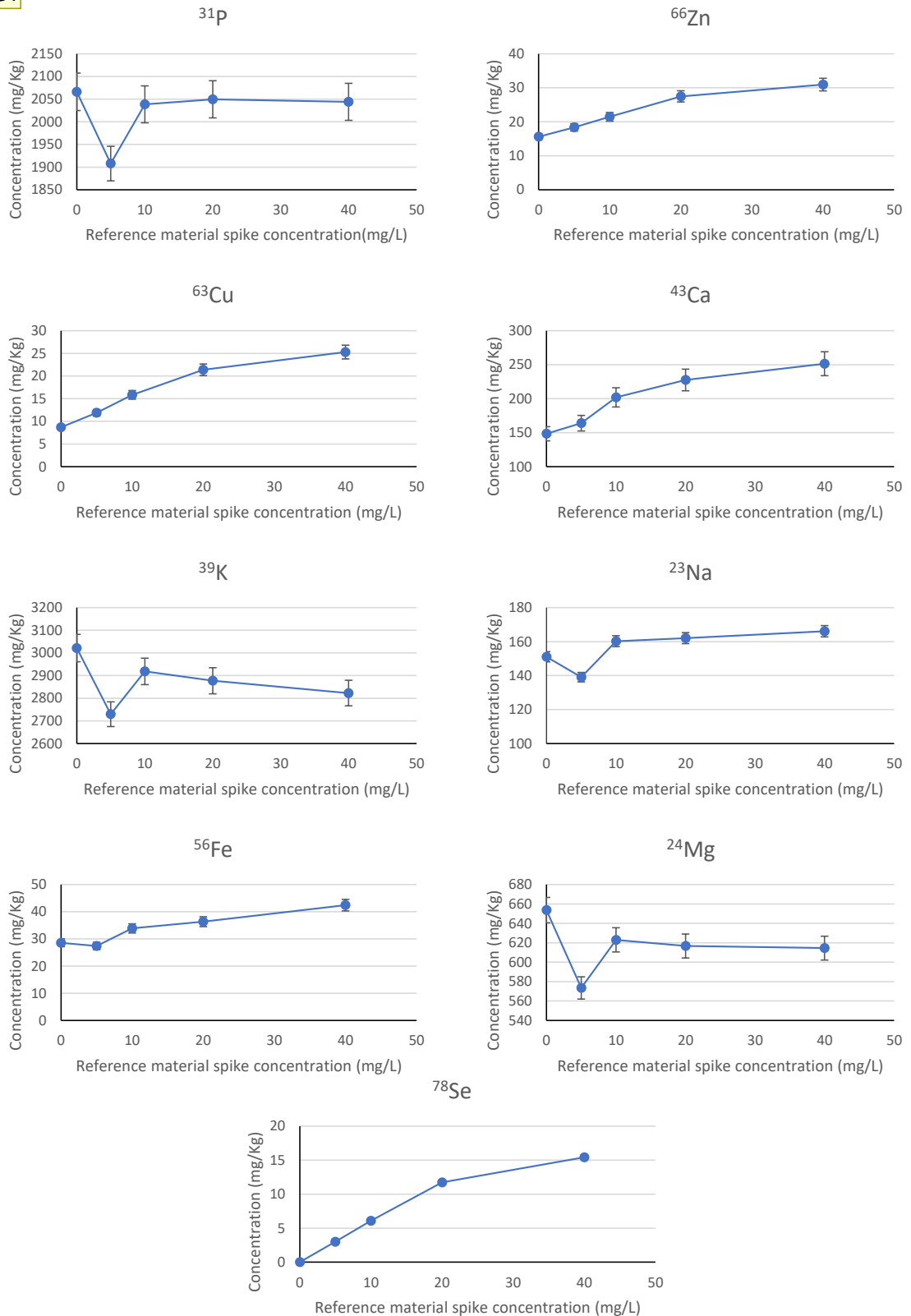


Figure 4.3-32: LA-ICP-MS calibration curve of seed material spiked with standard solutions.

Figure 4.3-32 illustrates the lack in the homogeneity in the concentrations of particular elements with the seed reference material. The elements that showed non-linear curves were ^{31}P , ^{39}K , ^{24}Mg and ^{23}Na . These elements followed a similar pattern, with the unspiked material containing higher concentrations than the spiked material. These elements are macro-elements and are found naturally in the seeds in the range of 100-2000 mg/Kg. Therefore, the addition of such low concentrations (maximum 40 mg/L) will therefore have a lower impacted on the overall concentration with in the reference material. Higher concentrations of the spike solution should therefore be used in the future for these elements. In contrast ^{78}Se , ^{56}Fe , ^{43}Ca and ^{63}Cu produced more linear curves, as these are found in lower concentrations (<100 mg/Kg) within the base seed material. The only exception to this can be seen with ^{43}Ca , which is a macro-element and is normally found at concentrations above 100mg/Kg within seeds, all of these other elements are microelements. The addition the spiked solution therefore has a greater impact on the overall concentration within the reference material. The same conclusion from section 4.3.5 can be drawn, that due to the lack of homogeneity between the reference materials, the use of software to extrapolate the data in a more reliable method for quantitative analysis using LA-ICP-MS.

4.3.7.3 Quantitative laser ablation inductively coupled plasma mass spectrometry imaging of barley seeds

Within this section the data from the analysis with LA-ICP-MS of the seeds that had been treated with various concentrations of Teprosyn Zn/P over a period of time is presented. Figure 4.3-33 demonstrates the distribution of the ^{66}Zn in seeds. Teprosyn Zn/P application, as would be expected, caused an increase in ^{66}Zn content within the seed, which rose with increasing application concentration (Figure 4.3-33). The control group in Figure 4.3-33 shows very little ^{66}Zn in the seed, with the highest

concentrations residing in the hull/seed coat. Increasing the application concentration of the Teprosyn Zn/P, appears to increase the ^{66}Zn in the endosperm and into the germ as a whole. The ^{66}Zn is concentrated in the germ (embryo) and the hull of the seeds. Over time though, there appears to be a degradation of the Teprosyn Zn/P when applied to seeds. However, it does start off being absorbed into the seed.

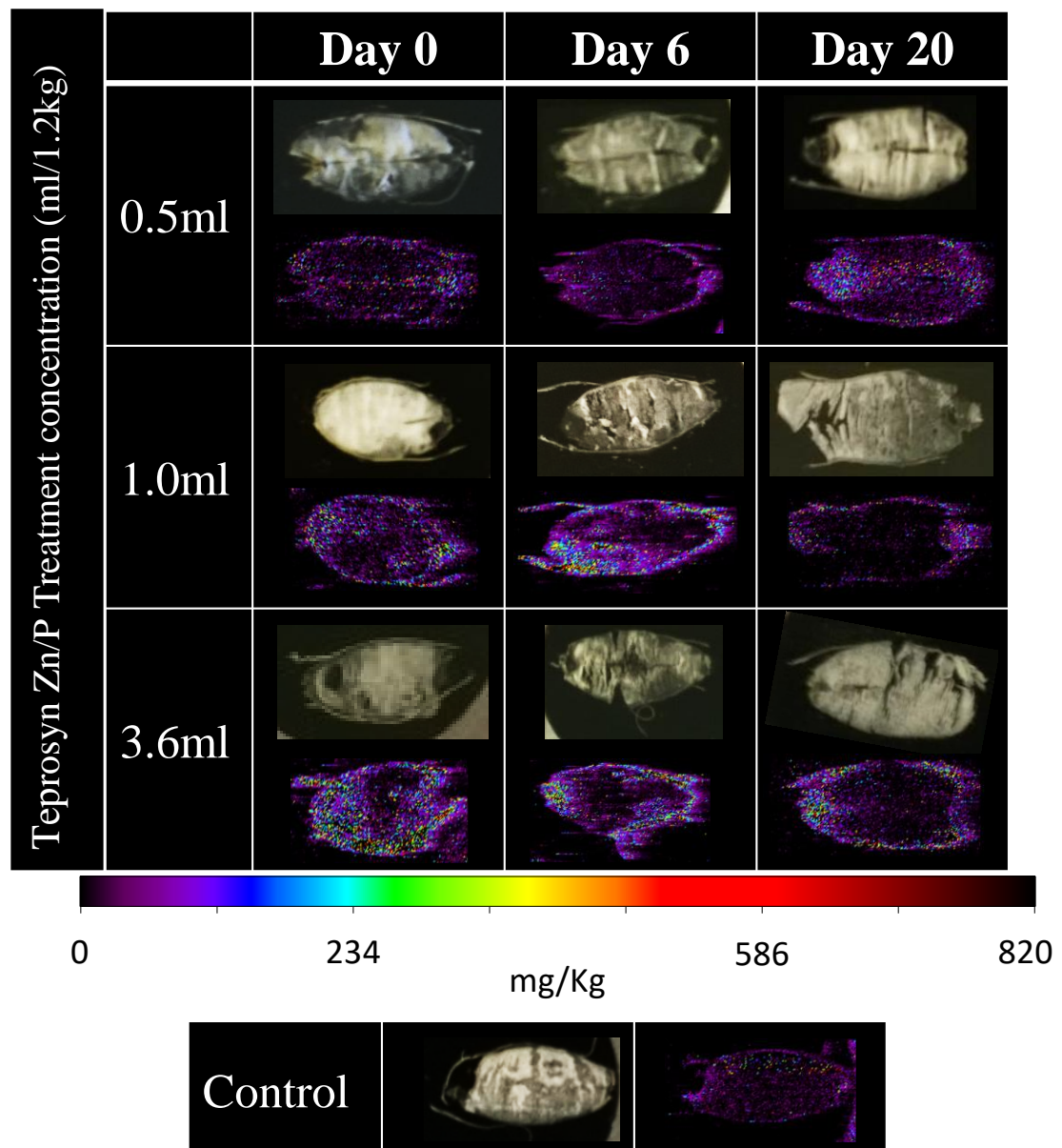


Figure 4.3-33: ^{66}Zn LA-ICP-MS distribution map of barley seeds treated with varying concentrations of Teprosyn Zn/P.

Figure 4.3-34 clearly shows the germ in the seed has high concentrations of ^{31}P and is the most concentrated region. The hull of the seeds also displays high concentrations of ^{31}P with lower concentrations in the endosperm. The ^{31}P within the Teprosyn Zn/P does not appear to be absorbed into the seed and, therefore, may be a reason why there is not an increase in the leaf.

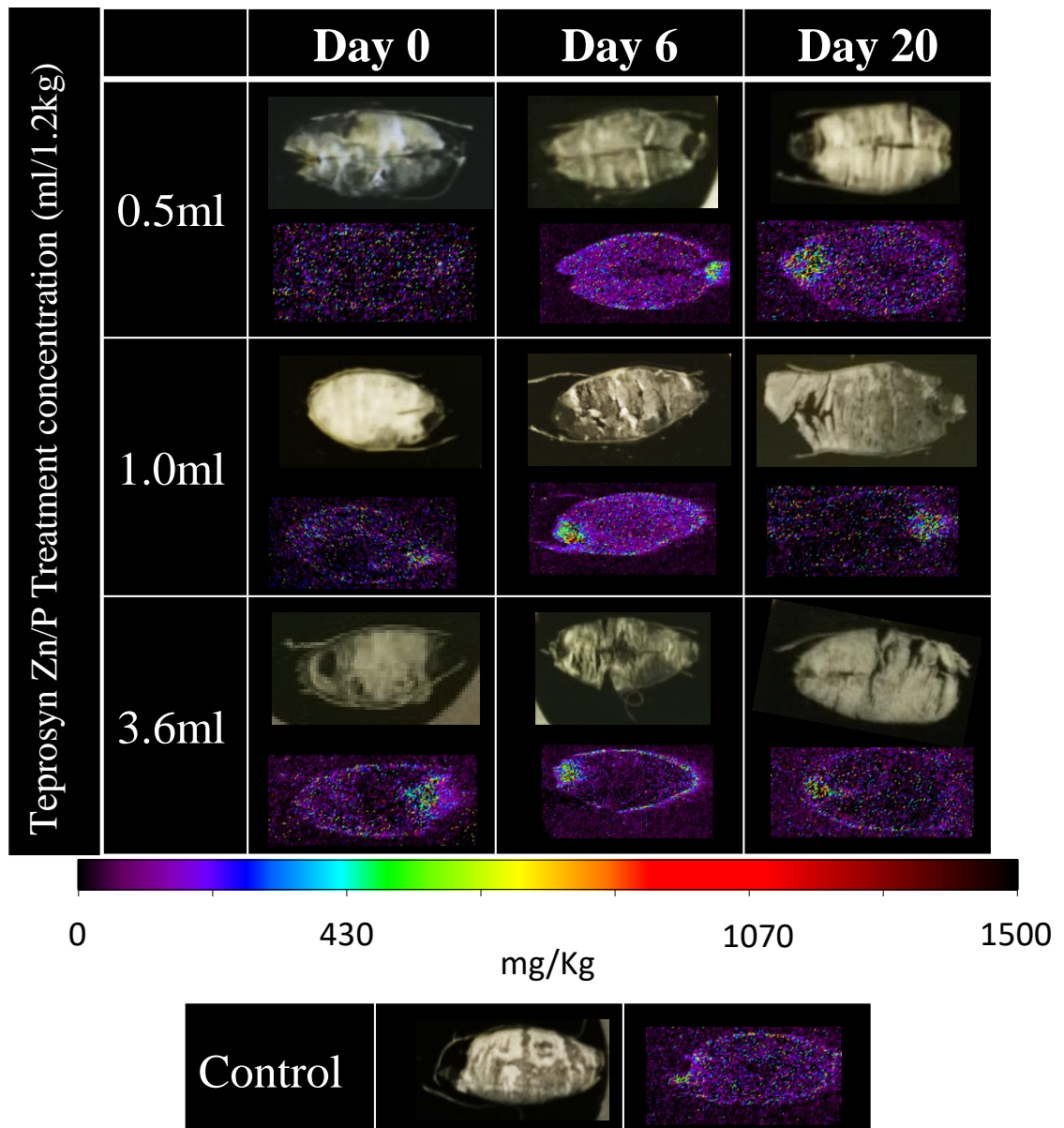


Figure 4.3-34: ^{31}P LA-ICP-MS distribution map of barley seeds treated with varying concentrations of Teprosyn Zn/P.

Figure 4.3-35 reveals that the highest concentration of Fe appears to be in the seed coat, as can be seen from the control group. As would be expected, with increasing concentration of Teprosyn Zn/P, there is an increase in the iron content in the seed coat and into to the germ. At day six there is a significant increase in the content with a slow absorption in to the endosperm. By day 20, though, there appears to be a degradation of the iron content, however the greatest content being in the 3.6ml treatment group.

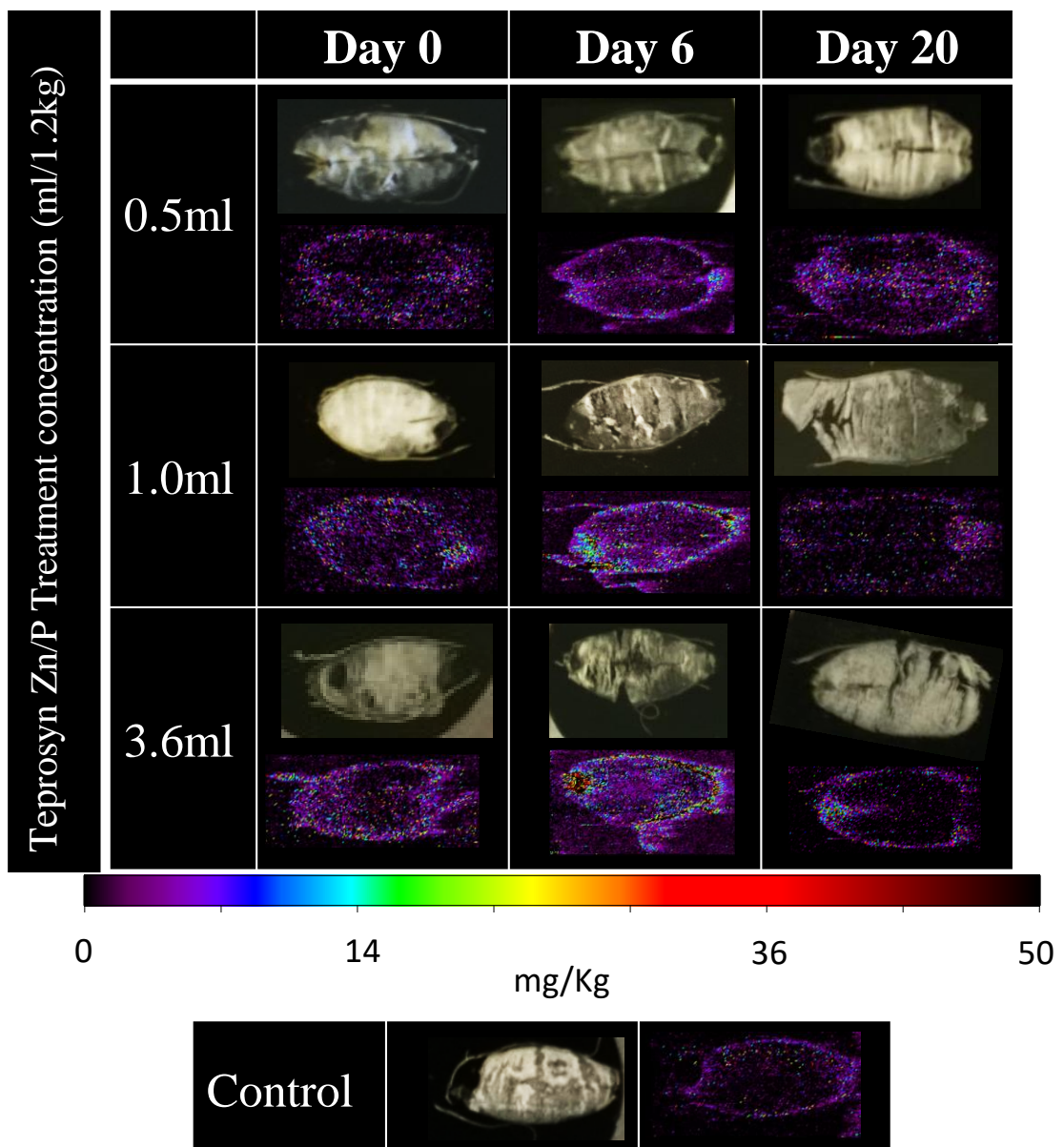


Figure 4.3-35: ^{56}Fe LA-ICP-MS distribution map of barley seeds treated with varying concentrations of Teprosyn Zn/P.

Other elements analysed for, were not affected by the application of the Teprosyn Zn/P at all concentrations. However, the data presented in Figure 4.3-36, Figure 4.3-37, Figure 4.3-38 and Figure 4.3-39 all demonstrate the application potential this technique offers. The ^{39}K (Figure 4.3-37) and ^{24}Mg (Figure 4.3-38) content of the seeds is very similar, with very high concentrations in the hull and the germ, with the endosperm containing much less. The ^{44}Ca (Figure 4.3-36) content is mainly distributed in the hull of the seeds and surrounding the germ. Whereas the ^{63}Cu (Figure 4.3-39) distributions appears to run through the centre of the endosperm progressing from the germ.

Only a limited number of papers have been published on the elemental mapping of seeds using LA-ICP-MS (Basnet, Amarasiriwardena *et al.* 2014, Bittencourt, Lana *et al.* 2012, Cakmak, Kalayci *et al.* 2010, Han, Quinet *et al.* 2013, Wu, Andersch *et al.* 2013a, Wu, Andersch *et al.* 2013b), with even less of full images (Wu, Andersch *et al.* 2013b, Basnet, Amarasiriwardena *et al.* 2014). Therefore, the work presented in this chapter further demonstrates the potential application for LA-ICP-MS in agricultural studies. It demonstrates the viability for this technique to be used to support other more destructive techniques such as microwave digestion followed ICP-MS analysis. It also provides an image of the distribution of a variety of elements and the monitoring of the movement of elements within plants.

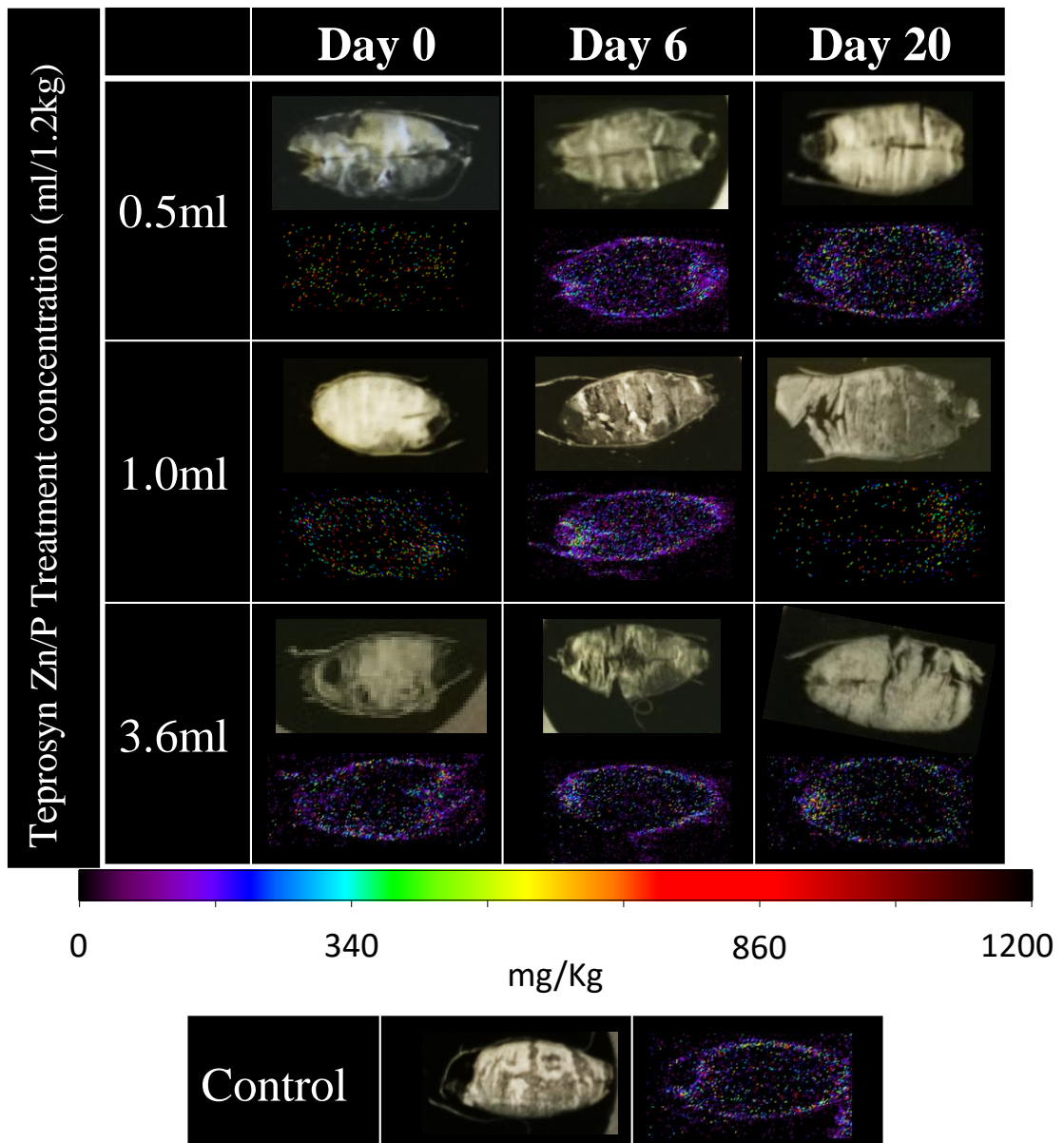


Figure 4.3-36: ^{44}Ca LA-ICP-MS distribution map of barley seeds treated with varying concentrations of Teprosyn Zn/P.

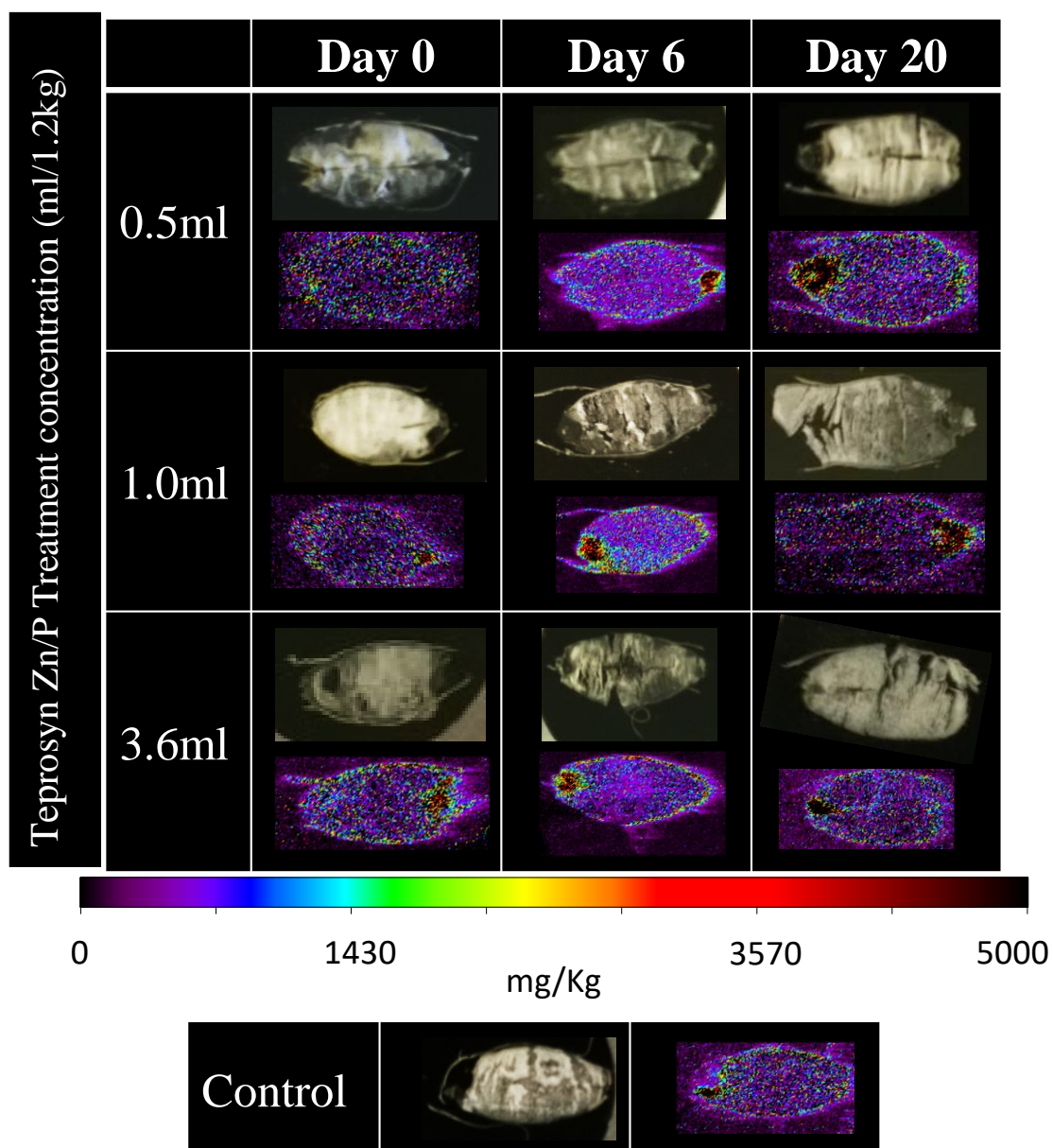


Figure 4.3-37: ^{39}K LA-ICP-MS distribution map of barley seeds treated with varying concentrations of Teprosyn Zn/P.

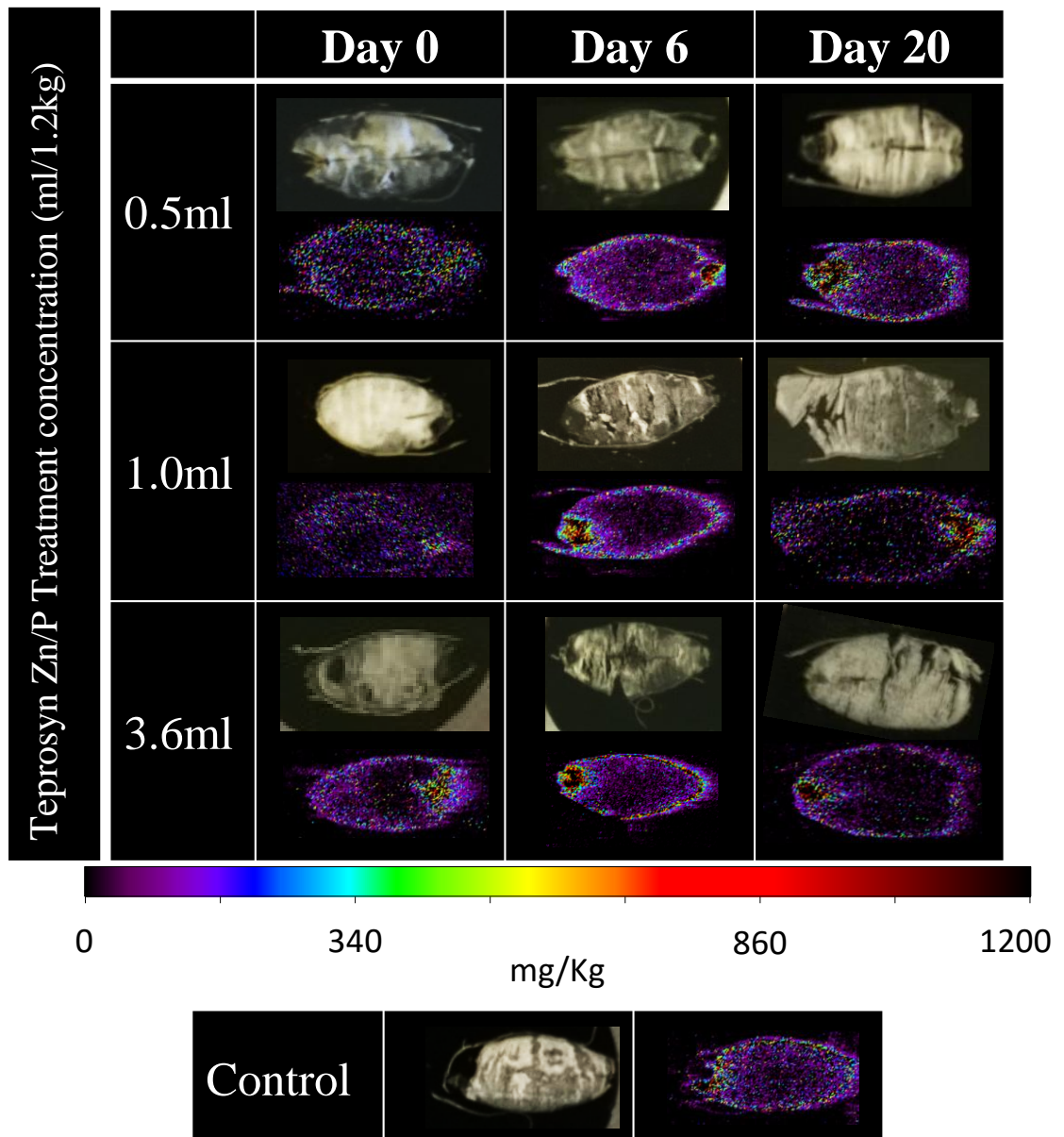


Figure 4.3-38: ^{24}Mg LA-ICP-MS distribution map of barley seeds treated with varying concentrations of Teprosyn Zn/P.

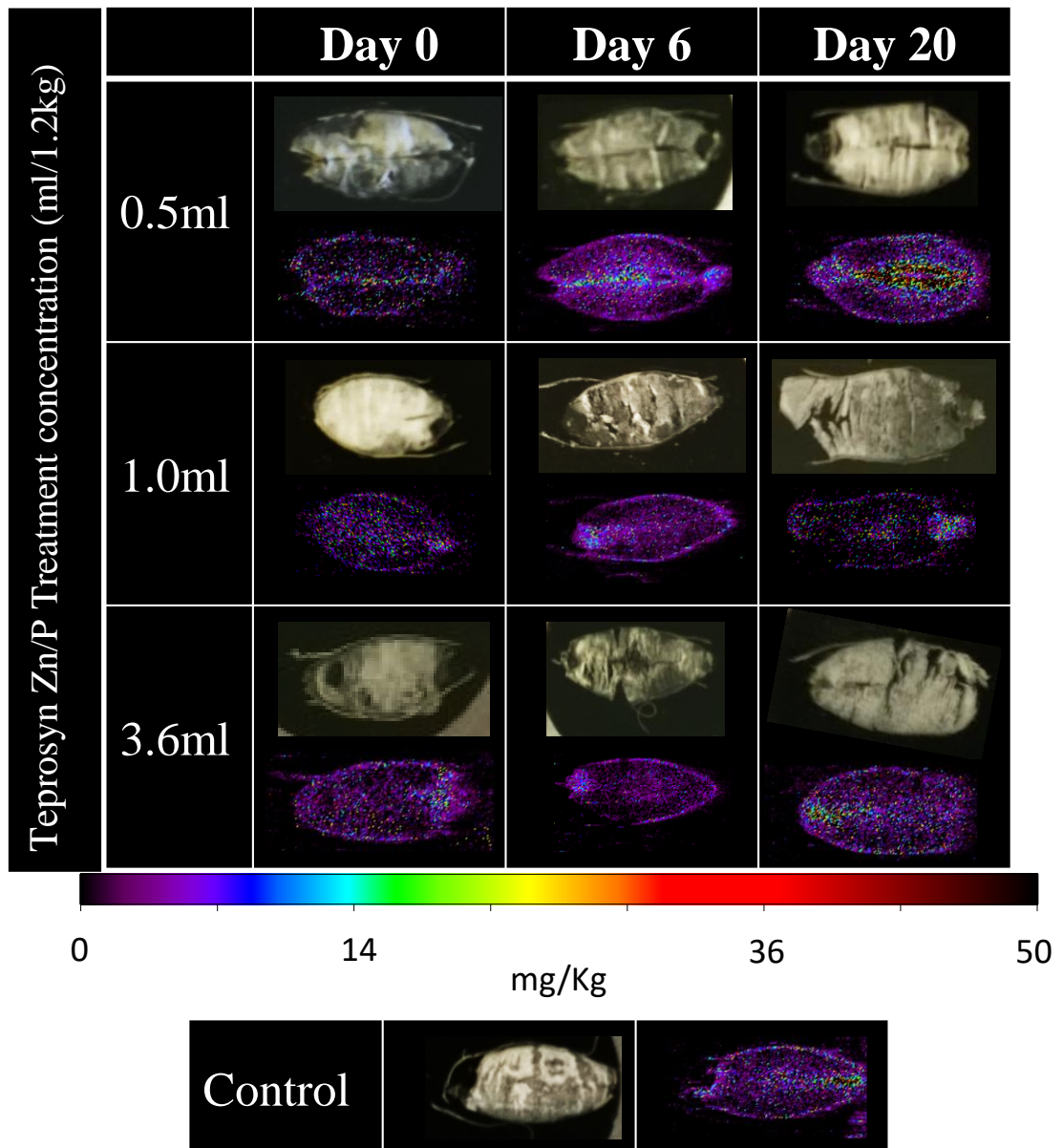


Figure 4.3-39: ^{63}Cu LA-ICP-MS distribution map of barley seeds treated with varying concentrations of Teprosyn Zn/P.

4.3.8 Distribution of zinc in broccoli sprouts

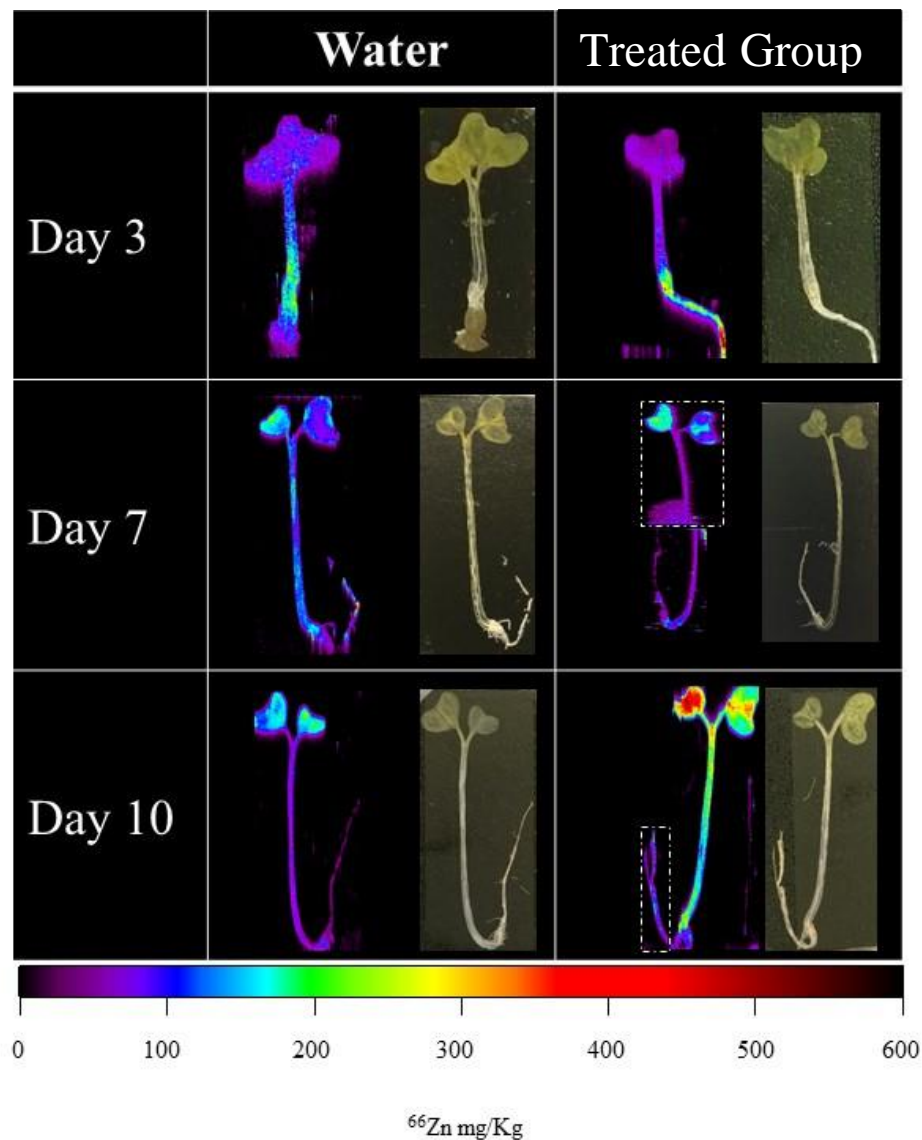


Figure 4.3-40: ^{66}Zn distribution in broccoli seedling over a 10-day period using LA-ICP-MS imaging technique. NB. The white dotted marks the separate imagers boarder

In addition to the barley, the distribution of zinc was also monitored in broccoli sprouts irrigated with sodium selenate over a 10-day period. Figure 4.3-40 demonstrates how the distribution of the Zn moves through the seedling over a period. Initially the highest concentration of the zinc can be seen in the root system at day three. The zinc by day seven has started to migrate up the stem on the seedling, leaving very little in the root system. By day 10 the highest concentration of zinc can be seen in the leaves (Figure 4.3-41 and Figure 4.3-42).

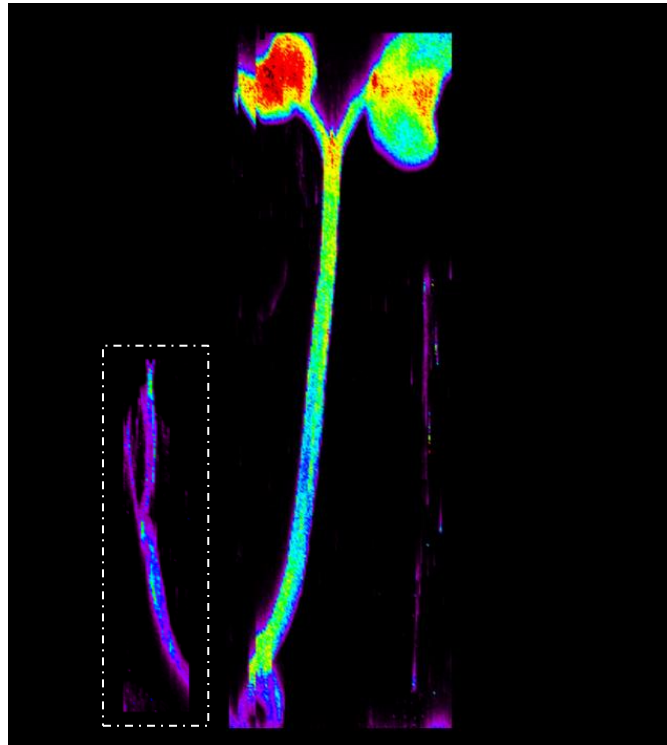


Figure 4.3-41:Distribution of ^{66}Zn in 10-day old broccoli seedling using LA-ICP-MS imaging technique. *NB. The white dotted marks the separate imagers boarder.*

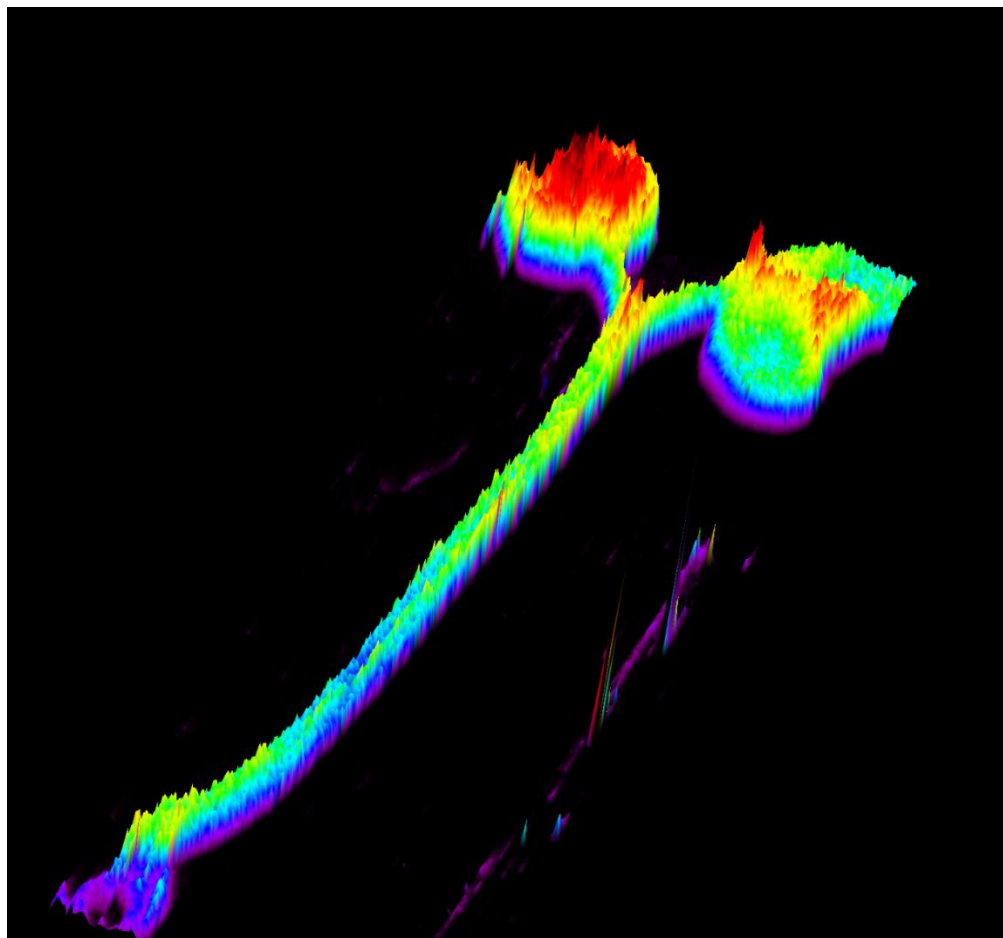


Figure 4.3-42: A 3D distribution map of ^{66}Zn in a 10-day old broccoli seedling using LA-ICP-MS imaging technique.

4.4 Conclusion

From this study, it can be assumed that with increased volumes of the seed coat Teprosyn Zn/P used there is an increase in the uptake of Zn into the shoot with no significant impact on the yield of the fodder, both fresh and dry. Root mat formation was hindered with larger volumes, with residue left.

It is worth noting that all previous studies performed using Teprosyn Zn/P (Sankaran, Mani *et al.* 2002, Chitdeshwari, Shanmugasundaram *et al.* 2002, Chitdeshwari, Shanmugasundaram *et al.* 2004, Dogan, Cakmak *et al.* 2008, Tookaloo, Mollafilabi *et al.* 2010, Akinci, Doran *et al.* 2008, Rengel, Gil *et al.* 2011, Oliveira, Tavares *et al.* 2014) were all performed in field trials, using soil as the media, as opposed to pure hydroponics where no media is used. Germination rate studies (Chitdeshwari, Shanmugasundaram *et al.* 2002, Tookaloo, Mollafilabi *et al.* 2010, Sankaran, Mani *et al.* 2002, Rengel, Gil *et al.* 2011, Oliveira, Tavares *et al.* 2014) all used paper tissue for the germination studies or soil (Chitdeshwari, Shanmugasundaram *et al.* 2002). These are different conditions to that of the fodder system, where the seeds are clustered together in a tray and sprayed at 2 hourly intervals. This could account for reduction in germination rate with increased use of Teprosyn Zn/P, which contradicted the previous studies.

From an analytical point of view, it can be concluded that laser ablation coupled with ICP-MS is an excellent technique for imaging and monitoring the distribution of fertilizers in plants. Though there are still challengers with regards to the accuracy of the quantification of the data produced from LA-ICP-MS, in comparison to the results obtained from digested material analysed using ICP-MS. These differences can be attributed to the difference in homogeneity of the reference materials used LA-ICP-MS. The seed reference material produced lower RSD within the results, in comparison to

the leaf reference material, making the seed data more accurate than the leaf data. The seed material did appear to be finer and more uniform in the reference material, it could be the reason for the differences in the RSD between them. The calibration methodology for these two techniques is also different, with LA-ICP-MS relying on the extrapolation of one point. Digestion of plant material and analysis with ICP-MS employs a 5-point calibration curve, which increases the accuracy of the results generated. Sample preparation for LA-ICP-MS is reduced, much easier and safer than ICP-MS sample preparation once the reference material has been prepared. As the samples enter the plasma in a dry state with LA-ICP-MS, the interferences caused by solvents used in “wet” samples introductions are decreased dramatically, offering another advantage (Bauer, Limbeck, 2015). Unfortunately, MALDI-MS for this study and type of compound was not suitable.

LA-ICP-MS is still mainly utilized for environmental samples and its main application lying in the geosciences (Limbeck, *et al* 2015). Recent developments in samples preparation, calibration strategies and reference material preparation have allowed the analysis of a larger variety of biological tissues (Miliszkiewicz *et al*, 2015, Becker *et al*, 2014). However, reliability quantification still remains a challenge. One of the biggest issues with LA-ICP-MS is the matrix composition which affects interaction of the laser beam and the sample. This in turn affects the quantity and size of the particles/aerosol generated to enter the plasma before detection (Bauer, Limbeck, 2015). Other issues result from differences in ionization efficiency in the plasma, variation in transfer efficiency of the sample from the cell to the plasma and differences between sample ablation, all of which are discussed in detail by Limbeck *et al* 2015.

Further work needs to be performed on increasing the homogeneity of the reference material used in LA-ICP-MS in order to produce results which are as accurate as ICP-

MS results. Along with this, further investigation into binding agents and internal standards used in the references material to remove interference and increase the sensitivity of the method.

LA-ICP-MS can be used for isotope ratio analysis and the creation high resolution images. The images produced using LA-ICP-MS give a better understand of the distribution and movement of elements within plant material, even though more work is required on achieving accurate and reproducible quantitative data.

4.5 References

- AKINCI, C., DORAN, I., YILDIRIM, M. and GUEL, I., 2008. Effects of different zinc doses on zinc and protein contents of barley. *Asian Journal of Chemistry*, **20**(3), pp. 2293-2301.
- AL-KARAKI, G.N. and AL-HASHMI, M., 2010. Effect of mineral fertilization and seeding rate on barley green fodder production and quality under hydroponic conditions. *International Conference & Exhibition on Soilless Culture*, 8-13 March 2010.
- AL-KARAKI, G.N., 2011. Utilization of treated sewage wastewater for green forage production in a hydroponic system. *Emirates Journal of Food and Agriculture*, **23**(1), pp. 80-94.
- AZEKE, M.A., EGIELEWA, S.J., EIGBOGBO, M.U. and IHIMIRE, I.G., 2011. Effect of germination on the phytase activity, phytate and total phosphorus contents of rice (*Oryza sativa*), maize (*Zea mays*), millet (*Panicum miliaceum*), sorghum (*Sorghum bicolor*) and wheat (*Triticum aestivum*). *Journal of Food science and Technology*, **48**(6), pp. 724-729.
- BASNET, P., AMARASIRIWARDENA, D., WU, F., FU, Z. and ZHANG, T., 2014. Elemental bioimaging of tissue level trace metal distributions in rice seeds (*Oryza sativa* L.) from a mining area in China. *Environmental Pollution*, **195**, pp. 148-156.
- BECKER, J.S., DIETRICH, R.C., MATUSCH, A., POZEBON, D. and DRESSIER, V.L., 2008. Quantitative images of metals in plant tissues measured by laser ablation inductively coupled plasma mass spectrometry. *Spectrochimica Acta Part B-Atomic Spectroscopy*, **63**(11), pp. 1248-1252.
- BECKER, J.S., MATUSCH, A. and WU, B., 2014. Bioimaging mass spectrometry of trace elements – recent advance and applications of LA-ICP-MS: A review. *Analytica Chimica Acta*, **835**(0), pp. 1-18.
- BECKER, J.S., ZORIY, M., DRESSLER, V.L., WU, B. and BECKER, J.S., 2008. Imaging of metals and metal-containing species in biological tissues and on gels by laser ablation inductively coupled plasma mass spectrometry (LA-ICP-MS): A new analytical strategy for applications in life sciences. *Pure and Applied Chemistry*, **80**(12), pp. 2643-2655.
- BITTENCOURT, L.M., LANA, D.A.P.D., AUGUSTI, R., COSTA, L.M., PIMENTA, A.M.C., DOS SANTOS, A.V. and GONCALVES, A.P.F., 2012. Determination of Cu, Fe, Mn, Zn and total protein content in wheat and soybean samples after sequential extraction procedure. *Quimica Nova*, **35**(10), pp. 1922-1926.
- BROADLEY, M.R., WHITE, P.J., HAMMOND, J.P., ZELKO, I. and LUX, A., 2007. Zinc in plants. *New Phytologist*, **173**(4), pp. 677-702.

- BAUER, G., LIMBECK, A., 2015. Quantitative analysis of trace elements in environmental powders with laser ablation inductively coupled mass spectrometry using non-sample-corresponding reference materials for signal evaluation. *Spectrochimica Acta Part B*, **113**, pp 63-69.
- CAKMAK, I., 2008. Enrichment of cereal grains with zinc: agronomic or genetic biofortification? *Plant and Soil*, **302**(1-2), pp. 1-17.
- CAKMAK, I., KALAYCI, M., KAYA, Y., TORUN, A.A., AYDIN, N., WANG, Y., ARISOY, Z., ERDEM, H., YAZICI, A., GOKMEN, O., OZTURK, L. and HORST, W.J., 2010. Biofortification and Localization of Zinc in Wheat Grain. *Journal of Agricultural and Food Chemistry*, **58**(16), pp. 9092-9102.
- CHITDESHWARI, T., SHANMUGASUNDARAM, R., POONGOTHAI, S. and SAVITHRI, P., 2004. Effect of teprosyn micronutrient formulations on the yield of sunflower and nutrient uptake. *Agricultural Science Digest*, **24**(1), pp. 9-12.
- CHITDESHWARI, T., SHANMUGASUNDARAM, R., POONGOTHAI, S. and SAVITHRI, P., 2002. Effect of teprosyn micronutrient formulations on the yield and yield attributes of sunflower. *The Madras Agricultural Journal*, **89**(1-3), pp. 121-124.
- CIZDZIEL, J., BU, K. and NOWINSKI, P., 2012. Determination of elements in situ in green leaves by laser ablation ICP-MS using pressed reference materials for calibration. *Analytical Methods*, **4**(2), pp. 564.
- COMPERNOLLE, S., WAMANUKUL, W., DE RAEDT, I. AND VANHAECKE, F. (2012). Evaluation of a combination of isotope dilution and single standard addition as an alternative calibration method for the determination of precious metals in lead fire assay buttons by laser ablation-inductively coupled plasma-mass spectrometry. *Spectrochimica Acta Part B: Atomic Spectroscopy*, **67**, pp 50-56.
- DOGAN, R., CAKMAK, F., YAGDI, K. and KAZAN, T., 2008. Effect of zinc compound (teprosyn F-2498) on wheat (*Triticum aestivum* L.). *Asian Journal of Chemistry*, **20**(3), pp. 1795-1800.
- DUNG, D.D., GODWIN, I.R. and NOLAN, J.V., 2010a. Nutrient Content and In sacco Degradation of Hydroponic Barley Sprouts Grown Using Nutrient Solution or Tap Water. *Journal of Animal and Veterinary Advances*, **9**(18), pp. 2432-2436.
- DUNG, D.D., GODWIN, I.R. and NOLAN, J.V., 2010b. Nutrient Content and in sacco Digestibility of Barley Grain and Sprouted Barley. *Journal of Animal and Veterinary Advances*, **9**(19), pp. 2485-2492.
- FAZAELI, H., GOLMOHAMMADI, H.A., SHOAYEE, A.A., MONTAJEBI, N. and MOSHARRAF, S., 2011. Performance of Feedlot Calves Fed Hydroponics Fodder Barley. *Journal of Agricultural Science and Technology*, **13**(3), pp. 367-375.
- FOMINA, M., ALEXANDER, I.J., HILLIER, S. and GADD, G.M., 2004. Zinc Phosphate and Pyromorphite Solubilization by Soil Plant-Symbiotic Fungi. *Geomicrobiology Journal*, **21**(5), pp. 351-366.

- FU, S., ZOU, X. and COLEMAN, D., 2009. Highlights and perspectives of soil biology and ecology research in China. *Soil Biology & Biochemistry*, **41**(5), pp. 868-876.
- GOMES, M.S., SCHENK, E.R., SANTOS JR., D., KRUG, F.J. and ALMIRALL, J.R., 2014. Laser ablation inductively coupled plasma optical emission spectrometry for analysis of pellets of plant materials. *Spectrochimica Acta Part B: Atomic Spectroscopy*, **94-95**(0), pp. 27-33.
- GÓMEZ-GALERA, S., ROJAS, E., SUDHAKAR, D., ZHU, C., PELACHO, A.M., CAPELL, T. and CHRISTOU, P., 2010. Critical evaluation of strategies for mineral fortification of staple food crops. *Transgenic Research*, **19**(2), pp. 165-180.
- GOODCHILD, N.A. and WALKER, M.G., 1971. A Method of Measuring Seed Germination in Physiological Studies. *Annals of Botany*, **35**(3), pp. 615-621.
- GUPTA, N., RAM, H. and KUMAR, B., 2016. Mechanism of Zinc absorption in plants: uptake, transport, translocation and accumulation. *Reviews in Environmental Science and Bio/Technology*, **15**(1), pp. 89-109.
- HAN, R., QUINET, M., ANDRE, E., VAN ELTEREN, J.T., DESTREBECQ, F., VOGEL-MIKUS, K., CUI, G., DEBELJAK, M., LEFEVRE, I. and LUTTS, S., 2013. Accumulation and distribution of Zn in the shoots and reproductive structures of the halophyte plant species *Kosteletzkya virginica* as a function of salinity. *Planta*, **238**(3), pp. 441-457.
- HANĆ, A, OLSZEWSKA, A. and BARAŁKIEWICZ, D. (2013). Quantitative analysis of elements migration in human teeth with and without filling using LA-ICP-MS. *Microchemical Journal*, **110** 61-69.
- HARE, D., AUSTIN, C. and DOBLE, P., 2012. Quantification strategies for elemental imaging of biological samples using laser ablation-inductively coupled plasma-mass spectrometry. *Analyst*, **137**(7), pp. 1527-1537.
- HART, J.J., NORVELL, W.A., WELCH, R.M., SULLIVAN, L.A. and KOCHIAN, L.V., 1998. Characterization of zinc uptake, binding, and translocation in intact seedlings of bread and durum wheat cultivars. *Plant Physiology*, **118**(1), pp. 219-226.
- HINSINGER, P., BENGOUGH, A.G., VETTERLEIN, D. and YOUNG, I.M., 2009. Rhizosphere: biophysics, biogeochemistry and ecological relevance. *Plant and Soil*, **321**(1-2), pp. 117-152.
- HIRATA, J., TAKAHASHI, K. and TANAKE, M (2013). Determination Method of Multi Elements in Ferromanganese Samples by LA-ICP-MS. *Analytical Sciences*, **29** (1), pp. 151-155.
- JUROWSKI, K., SZEWCZYK, M., PIEKOSZEWSKI, W., HERMAN, M., SZEWCZYK, B., NOWAK, G., WALAS, S., MILISZKIEWICZ, N., TOBIASZ, A. and DOBROWOLSKA-IWANIEK, J., 2014. A standard sample preparation and calibration procedure for imaging zinc and magnesium in rats' brain tissue by laser

ablation-inductively coupled plasma-time of flight-mass spectrometry. *Journal of Analytical Atomic Spectrometry*, **29**(8), pp. 1425-1431.

KÖTSCHAU, A., BÜCHEL, G., EINAX, J.W., FISCHER, C., VON TÜMPLING, W. and MERTEN, D., 2013. Mapping of macro and micro elements in the leaves of sunflower (*Helianthus annuus*) by Laser Ablation–ICP–MS. *Microchemical Journal*, **110**(0), pp. 783-789.

LAPEYRIE, F., RANGER, J. and VAIRELLES, D., 1991. Phosphate-Solubilizing Activity of Ectomycorrhizal Fungi In vitro. *Canadian Journal of Botany-Revue Canadienne De Botanique*, **69**(2), pp. 342-346.

LIMECK, A., GALLER, P., BONTA, M., BAUER, G., NISCHKAUER, W., and VANHAECKE, F., 2015. Recent advances in quantitative LA-ICP-MS analysis: challenges and solutions in the life sciences and environmental chemistry, *Analytical Biochemistry*. **407**, pp. 6593-6617.

LOENNERDAL, B., MENDOZA, C., BROWN, K.H., RUTGER, J.N. and RABOY, V., 2011. Zinc Absorption from low phytic acid Genotypes of Maize (*Zea mays* L.), Barley (*Hordeum vulgare* L.), and Rice (*Oryza sativa* L.) Assessed in a Suckling Rat Pup Model. *Journal of Agricultural and Food Chemistry*, **59**(9), pp. 4755-4762.

LONGERICH, H.P., JACKSON, S.E. and GUNTHER, D., 1996. Inter-laboratory note. Laser ablation inductively coupled plasma mass spectrometric transient signal data acquisition and analyte concentration calculation. *Journal of Analytical Atomic Spectrometry*, **11**(9), pp. 899-904.

LOPEZ-AGUILAR, R., MURILLO-AMADOR, B. and RODRIGUEZ-QUEZADA, G., 2009. Hydroponic Green Fodder (Hgf): an Alternative for Cattle Food Production in Arid Zones. *Interciencia*, **34**(2), pp. 121-126.

LÓPEZ-ALONSO, M., 2012. Trace minerals and livestock: not too much not too little. *ISRN veterinary science*, **2012**.

LOPEZ-BUCIO, J., PELAGIO-FLORES, R. and HERRERA-ESTRELLA, A., 2015. Trichoderma as biostimulant: exploiting the multilevel properties of a plant beneficial fungus. *Scientia Horticulturae*, **196**, pp. 109-123.

MANSBRIDGE, R.J. and GOOCH, B.J., 1985. A Nutritional Assessment of Hydroponically Grown Barley for Ruminants. *Animal Production*, **40**(JUN), pp. 569-570.

MESTEK, O., POLAK, J., KOPLIK, R., SANTRUCEK, J. and KODICEK, M., 2008. Isolation of ligands of trace metals from plant samples by immobilized metal affinity chromatography. *Analytical Letters*, **41**(8), pp. 1459-1467.

MILISZKIEWICZ, N., WALAS, S. AND TOBIASZ, A., 2015. Current approaches to calibration of LA-ICP-MS analysis. *Journal of Analytical Atomic Spectrometry*, **30**, 327-338.

- O'CONNOR, C., LANDON, M.R. and SHARP, B.L., 2007. Absorption coefficient modified pressed powders for calibration of laser ablation inductively coupled plasma mass spectrometry. *Journal of Analytical Atomic Spectrometry*, **22**(3), pp. 273-282.
- OLIVEIRA, S.D., TAVARES, L.C., LEMES, E.S., BRUNES, A.P., DIAS, I.L. and MENEGHELLO, G.E., 2014. Seed treatment of *Avena sativa* L. with zinc: physiological quality and performance of initial plants. *Semina-Ciencias Agrarias*, **35**(3), pp. 1131-1142.
- PATON, C., HELLSTROM, J., - PAUL, B., - WOODHEAD, J. and -HERGT, J., 2011. Iolite: Freeware for the visualisation and processing of mass spectrometric data. *Journal of Analytical Atomic Spectrometry*, **26**(12), pp. 2508.
- PEER, D.J. and LEESON, S., 1985a. Feeding Value of Hydroponically Sprouted Barley for Poultry and Pigs. *Animal Feed Science and Technology*, **13**(3-4), pp. 183-190.
- PEER, D.J. and LEESON, S., 1985b. Nutrient Content of Hydroponically Sprouted Barley. *Animal Feed Science and Technology*, **13**(3-4), pp. 191-202.
- PUNSHON, T., JACKSON, B., BERTSCH, P. and BURGER, J., 2004. Mass loading of nickel and uranium on plant surfaces: application of laser ablation-ICP-MS. *Journal of Environmental Monitoring*, **6**(2), pp. 153-159.
- RENGEL, M., GIL, F. and MONTAÑO, J., 2011. Efecto del tratamiento de semilla con zinc y ácido giberélico sobre la emergencia y el crecimiento inicial de las plantas de caña de azúcar. *Agronomía Tropical*, **61**(1), pp. 37-45.
- SANKARAN, M., MANI, S. and SAVITHRI, P., 2002. Effect of teprosyn and other zinc sources on germination characteristics of sunflower and rice. *The Madras Agricultural Journal*, **89**(1-3), pp. 124-126.
- SEPPANEN, M.M., KONTTURI, J., LOPEZ HERAS, I., MADRID, Y., CAMARA, C. and HARTIKAINEN, H., 2010. Agronomic biofortification of Brassica with selenium-enrichment of Se-Met and its identification in Brassica seeds and meal. *Plant and Soil*, **337**(1-2), pp. 273-283.
- SONNEVELD, C. and VOOGT, W., 2009. *Plant Nutrition of Greenhouse Crops*. 1 edn. Springer.
- SOUZA, R.D., AMBROSINI, A. and PASSAGLIA, L.M.P., 2015. Plant growth-promoting bacteria as inoculants in agricultural soils. *Genetics and Molecular Biology*, **38**(4), pp. 401-19.
- STANKOVA, A. GILON, N. DUTRUCH, L. and KANICKY, V. 2011. Comparison of LA-ICP-MS and ICP-OES for the analysis of some elements in fly ashes. *Journal of Analytical Atomic Spectrometry*, **26**, pp 443-449.
- STROHALM, M., KAVAN, D., NOVAK, P., VOLNY, M. and HAVLICEK, V., 2010. mMass 3: A Cross-Platform Software Environment for Precise Analysis of Mass Spectrometric Data. *Analytical Chemistry*, **82**(11), pp. 4648-4651.

- SUTTLE, N.F., 2010. *Mineral nutrition of livestock*. Cabi.
- TIKHONOVICH, I.A. and PROVOROV, N.A., 2011. Microbiology is the basis of sustainable agriculture: an opinion. *Annals of Applied Biology*, **159**(2), pp. 155-168.
- TOOKALLOO, M.R., MOLLAFILABI, A. and PAKNEJAD, F., 2010. Influence of Zn Teprosyn Seed Treatment on Rate of Germination and Grain Yield of Cuminum (Cuminum cyminum L.). *International Symposium on Medicinal and Aromatic Plants - Sipam2009*, **853**, pp. 53-56.
- TRIM, P.J., DJIDJA, M., ATKINSON, S.J., OAKES, K., COLE, L.M., ANDERSON, D.M.G., HART, P.J., FRANCESE, S. and CLENCH, M.R., 2010. Introduction of a 20 kHz Nd:YVO4 laser into a hybrid quadrupole time-of-flight mass spectrometer for MALDI-MS imaging. *Analytical and Bioanalytical Chemistry*, **397**(8), pp. 3409-3419.
- VOOGT, W., HOLWERDA, H.T. and KHODABAKS, R., 2010. Biofortification of lettuce (*Lactuca sativa* L.) with iodine: the effect of iodine form and concentration in the nutrient solution on growth, development and iodine uptake of lettuce grown in water culture. *Journal of the Science of Food and Agriculture*, **90**(5), pp. 906-913.
- WALLANDER, H., WICKMAN, T. and JACKS, G., 1997. Apatite as a P source in mycorrhizal and non-mycorrhizal *Pinus sylvestris* seedlings. *Plant and Soil*, **196**(1), pp. 123-131.
- WARD, N.I. DURRANT, S.F. and GRAY, A.L., 1992. Analysis of biological standard reference materials by laser ablation inductively coupled plasma mass spectrometry. *Journal of Analytical Atomic Spectrometry*, **7**, pp. 1139-1146.
- WELCH, R.M. and GRAHAM, R.D., 2004. Breeding for micronutrients in staple food crops from a human nutrition perspective. *Journal of Experimental Botany*, **55**(396), pp. 353-364.
- WHITELAW, M.A., 2000. Growth promotion of plants inoculated with phosphate-solubilizing fungi. *Advances in Agronomy*, Vol 69, **69**, pp. 99-151.
- WU, B., ANDERSCH, F., WESCHKE, W., WEBER, H. and BECKER, J.S., 2013a. Diverse accumulation and distribution of nutrient elements in developing wheat grain studied by laser ablation inductively coupled plasma mass spectrometry imaging. *Metallomics*, **5**(9), pp. 1276-1284.
- WU, B., ZORIY, M., CHEN, Y. and BECKER, J.S., 2009a. Imaging of nutrient elements in the leaves of *Elsholtzia splendens* by laser ablation inductively coupled plasma mass spectrometry (LA-ICP-MS). *Talanta*, **78**(1), pp. 132-137.
- XUE, Y., XIA, H., CHRISTIE, P., ZHANG, Z., LI, L. and TANG, C., 2016. Crop acquisition of phosphorus, iron and zinc from soil in cereal/legume intercropping systems: a critical review. *Annals of Botany*, **117**(3), pp. 363-77.

Chapter 5

5. Selenium biofortification of broccoli sprouts

5.1 Introduction

5.1.1 Selenium and human health

Selenium is an element that is beneficial to human health and is an essential cofactor in approximately 50 enzymes. It plays an important role in the function of an enzyme that converts thyroxine into triiodothyronine, therefore deficiencies can result in hypothyroidism (Gómez-Galera, Rojas *et al.* 2010). Other enzymes selenium is integral to include, glutathione peroxidase, which reduces antioxidant enzymes and thyroid hormone deiodinases which removes mineral ions from other proteins (Lyons, Stangoulis *et al.* 2003, Rayman, Infante *et al.* 2008).

Selenium is usually acquired via diet at very low concentrations, and in developed countries deficiencies are rare. However, selenium has a very narrow therapeutic range (100-200 µg/day) meaning that toxicity is very easily achieved if daily intake exceeds 700µg (Mao, Hu *et al.* 2012, Toler, Charron *et al.* 2007). The toxicity and availability are not dependent on the total amount of selenium, rather the species in which the selenium exists. Selenium can be found in the inorganic form (selenate, selenite) or as organic selenium compounds (seleno-amino acids, seleno-peptides and seleno-proteins) (Mao, Hu *et al.* 2012). The inorganic forms tend to be more toxic than the more bioavailable organic forms of selenium. It is therefore important that biofortification of plants for human consumption is monitored, optimized and in a non-toxic form.

5.1.2 Selenium biofortification

Biofortification is the improvement of a crops nutritional quality through various methods including plant breeding, genetic engineering, fertilization and crop and soil

management (Xue, Xia *et al.* 2016). In areas where food is scarce, it is important that the food that is available has the best possible nutritional content. Biofortification can also be used to target a population with nutritional deficiencies, such as zinc (Zn) and iron (Fe) in Africa and selenium (Se) in central China, New Zealand, Denmark, Finland, and central Siberia. In these areas the soils are deficient in Se, with a content of 0.1-0.6mg/kg (Lyons, Stangoulis *et al.* 2003). In China, the mountainous region soil is very low in selenium and there is a high rate of diseases such as cardiomyopathy, thyroid dysfunction, cancer and various inflammatory conditions (Lyons, Stangoulis *et al.* 2003). With the increasing population of China, comes increased incidence of disease due to nutritional deficiencies. However, this is not just an issue for developing countries; within almost all European countries selenium intake is below the daily recommended amount (Yadev, Gupta *et al.* 2007).

Some plants readily up-take particular elements, storing large reserves of them within the plant tissue without showing any visible symptoms of toxicity. The concentrations which are stored in the aerial parts of the plants can be extremely high and would normally be toxic. These plants are known as hyper-accumulators and have high tolerance to trace element accumulation (Verbruggen, Hermans *et al.* 2009) . Examples include sunflowers with copper, Indian mustard with zinc, and broccoli with selenium. These plants are able to grow in conditions which are not favourable to other plants, with soil containing very high levels of the elements. By growing these types of plants in the areas where there are nutritional deficiencies they can, in turn, help to increase the dietary levels of elements in humans.

A crop of particular interest is broccoli, *Brassica oleracea*. Not only is it a selenium hyper-accumulator, but also, it has been well documented that selenium encourages the formation of sulphoraphane, glucosinolates, phenolic acid and other compounds that

display anticancer properties (Robbins, Keck *et al.* 2005, Hauder, Winker *et al.* 2011, Matusheski, Wallig *et al.* 2001, Fahey, Zhang *et al.* 1997, Li, Wu *et al.* 2008, Zhang, Svehlikova *et al.* 2003, Li, Wang *et al.* 2012, Finley, Ip *et al.* 2001, Finley, Sigrid-Keck *et al.* 2005).

5.1.3 Selenium uptake and metabolism by plants.

Selenium is absorbed by the roots predominately as selenate (SeO_4^{2-}) but is also taken up as selenite (SeO_3^{2-}) and organic Se (Sors, Ellis *et al.* 2005, Hajiboland, Amjad 2008, Germ, Stibilj *et al.* 2007). Factors such as pH, temperature and organic content of the soil regulate the absorption of Se into plants via the roots. Within the roots it is absorbed via sulphate transporters and then translocated to the chloroplasts in the leaves via the xylem and accumulates in the shoots and the leaves, rather than the roots (Germ, Stibilj *et al.* 2007, Lyons, Stangoulis *et al.* 2003, Oseas da Silva, Lopez de Andrade *et al.* 2011). Once selenium enters a plant it is metabolised into a number of organic species including selenium amino acids, which are incorporated into proteins (Encinar, Sliwka-Kaszynska *et al.* 2003, Lyons, Stangoulis *et al.* 2003, Sors, Ellis *et al.* 2005, Uden, Bird *et al.* 1998, Fahey, Zhang *et al.* 1997, Bianga, Govasmark *et al.* 2013, Sathe, Mason *et al.* 1992, Haberhauer-Troyer, Alvarez-Llamas *et al.* 2003, Robbins, Keck *et al.* 2005, Thiry, Ruttens *et al.* 2012, Kolachi, Kazi *et al.* 2010a, Kim, Juvik 2011). The principle seleno-amino acid found in plants is selenomethionine (Se-Met) with others also being produced (Olivas, Donard *et al.* 1996a).

Figure 5.1-1 (Germ, Stibilj *et al.* 2007) displays the main steps in Se metabolism within plants, demonstrating how first selenate (SeO_4^{2-}) is reduced to selenite (SeO_3^{2-}) before becoming free Se^{2-} within the plant. The free Se^{2-} is then converted into seleno-cysteine

(Se-Cys), after which, it can be metabolised into other amino acids such as Se-methylselenocysteine (Methyl-SeCys) or Se-methionine (Se-Met) and then incorporated into seleno-proteins. It can, however, also be converted from Se-Met to dimethylselenide (DMSe), a volatile form of Se which can be released from the plant.

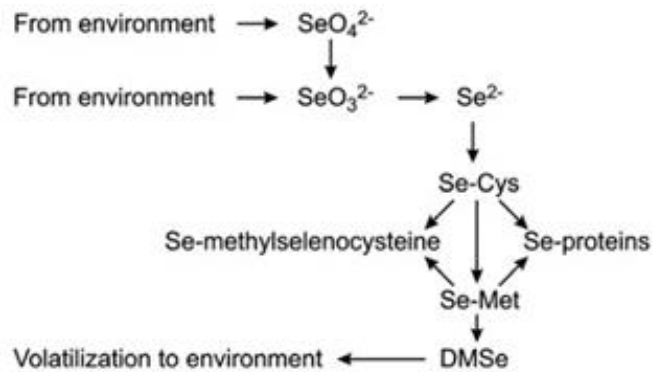


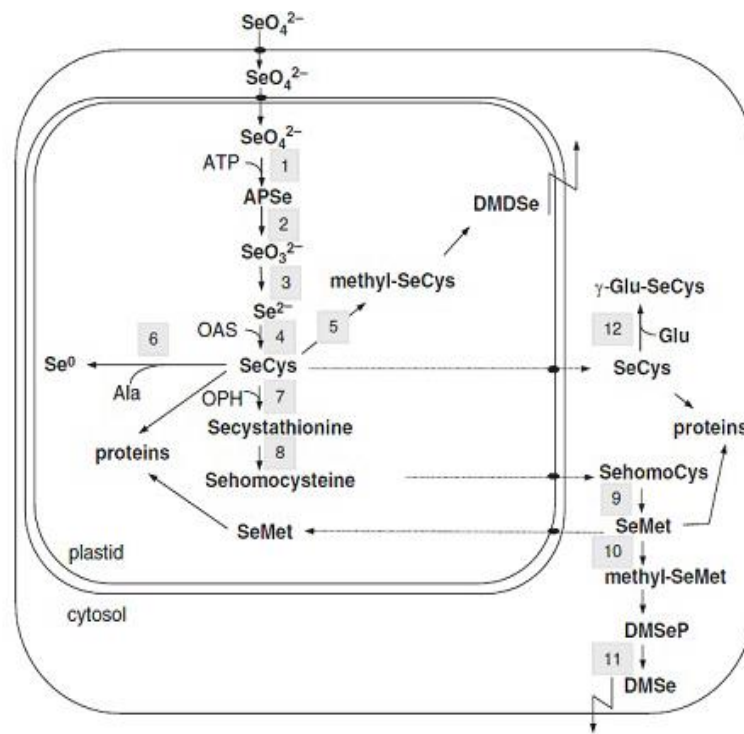
Figure 5.1-1: Schematic representation of the main steps in Se metabolism within plants (Germ, Stibilj and Kreft 2007).

Se-Met = Se-methionine; Se-Cys = seleno-cysteine; DMSe = dimethylselenide

Figure 5.1-2 (Pilon-Smits, Quinn 2010) demonstrates in greater detail how selenium is metabolised by the plant and the enzymes involved. Selenate is taken into the cytosol of the cell and then the plastid before being reduced to selenite. A more comprehensive list of some of the other seleno-amino acids can be seen in Table 5.1-1, along with their formulae and relative molecular mass.

Adduct	Compound	Formula	Mass	M/Z				
				M+H-H2O	M+H	M+Li	M+Na	M+K
				-17	1.01	7.015	23	39
	Selenocysteine	C ₃ H ₇ NO ₂ Se	162.97	145.97	163.98	169.99	185.97	201.97
	Methylselenopyruvate	C ₄ H ₆ O ₃ Se	181.95	164.95	182.96	188.96	204.95	220.95
	Se-methylselenocysteine	C ₄ H ₉ NO ₂ Se	182.98	327.92	183.99	189.99	205.98	221.98
	Selenohomocysteine	C ₄ H ₉ NO ₂ Se	182.98	165.98	183.99	189.99	205.98	221.98
	Selenomethyl selenocysteine	C ₄ H ₉ NO ₂ Se	182.98	165.98	183.99	189.99	205.98	221.98
	Se-methionine	C ₅ H ₁₁ NO ₂ Se	197.00	180.00	198.01	204.01	220.00	236.00
	Methylselenocysteine Se-oxide	C ₄ H ₉ NO ₃ Se	198.97	181.97	199.98	205.99	221.97	237.97
	Selenocysteine seleninic acid	C ₃ H ₇ NO ₄ Se	200.95	183.95	201.96	207.97	223.95	239.95
	Se-Methylselenomethionine	C ₆ H ₁₃ NO ₂ Se	211.01	194.01	212.02	218.03	234.01	250.01
	Selenomethionine Se-oxide	C ₅ H ₁₁ NO ₃ Se	212.99	195.99	214.00	220.01	235.99	251.99
	Se-Propenylselenocysteine Se-oxide	C ₆ H ₁₁ NO ₃ Se	224.99	207.99	226.00	232.01	247.99	263.99
	Selenocystathionine	C ₇ H ₁₄ N ₂ O ₄ Se	270.01	253.01	271.02	277.03	293.01	309.01
	1-Methylseleno-N-acetyl-D-galactosamine	C ₉ H ₁₇ NO ₅ Se	299.03	282.03	300.04	306.04	322.03	338.03
	Gamma-Glutamyl-Se-methylselenocysteine	C ₉ H ₁₆ N ₂ O ₅ Se	312.02	295.02	313.03	319.04	335.02	351.02
	Selenocystine	C ₆ H ₁₂ N ₂ O ₄ Se ₂	335.91	318.91	336.92	342.93	358.91	374.91
	Selenohomocystine	C ₈ H ₁₆ N ₂ O ₄ Se ₂	363.94	346.94	364.95	370.96	386.94	402.94
	Glutathioselenol	C ₁₀ H ₁₇ N ₃ O ₆ SSe	387.00	370.00	388.01	394.02	410.00	426.00
	Se-Adenosylselenohomocysteine	C ₁₄ H ₂₀ N ₆ O ₅ Se	432.07	415.07	433.08	439.08	455.07	471.07
	Se-Adenosylselenomethionine	C ₁₅ H ₂₂ N ₆ O ₅ Se	446.08	429.08	447.09	453.10	469.08	485.08
	Selenodiglutathione	C ₂₀ H ₃₂ N ₆ O ₁₂ S ₂ Se	692.07	675.07	693.08	699.08	715.07	731.07

Table 5.1-1: Seleno-amino acid with the formula, relative molecular mass and the mass to charge ratio (m/z) of 5 adducts.



Compounds	Enzymes
APSe = adenosine phosphor selenate.	1 = ATP sulfurylase
SAT = serine acetyl transferase.	2 = Adenosine phosphosulfate reductase.
OAS = O-acetylserine	3 = Sulfite reductase (or glutathione).
OPH = O-phosphoserine.	4 = OAS thiol lyase.
Se-Cys = selenocysteine	5 = SeCys methyltransferase.
Se-Met = selenomethionine	6 = SeCys lyase.
Methyl-SeCys = Se-methylselenocysteine	7 =cystathionine- γ -synthase.
DMSeP = dimethylselenopropionate.	8 = cystathionine- β -lyase.
DMSe = dimethylselenide	9 = methionine synthase.
DMDSe =dimethyldiselenide.	10 = methionine methyltransferase.
	11 = DMSP lyase
	12 = γ -glutamyl-cysteine synthetase.

Figure 5.1-2: Se metabolism within plant cells (Pilon-Smits and Quinn 2010).

5.1.4 Selenium and the production of medically beneficial compounds.

It has been documented that Se fortification of broccoli encourages the production of anticancer compounds (Abdulah, Faried *et al.* 2009, Fahey, Zhang *et al.* 1997, Finley, Ip *et al.* 2001, Finley, Sigrid-Keck *et al.* 2005, Gu, Guo *et al.* 2012, Hauder, Winker *et al.* 2011, Kolachi, Kazi *et al.* 2010a, Li, Wang *et al.* 2012, Li, Wu *et al.* 2008, Matusheski, Wallig *et al.* 2001, Robbins, Keck *et al.* 2005, Zhang, Svehlikova *et al.* 2003).

In recent years a number of studies have been performed on the biofortification of broccoli with selenium (Abdulah, Faried *et al.* 2009, Banuelos 2002, Fahey, Zhang *et al.* 1997, Finley, Ip *et al.* 2001, Finley, Sigrid-Keck *et al.* 2005, Gu, Guo *et al.* 2012, Hauder, Kim, Juvik 2011, Hsu, Li, Wu *et al.* 2008, Mahn, Zamorano *et al.* 2012, Matusheski, Wallig *et al.* 2001, Pedrero, Elvira *et al.* 2007, Robbins, Keck *et al.* 2005, Winker *et al.* 2011, Wirtz *et al.* 2011, Xue, Xia *et al.* 2016,).

The aim of the work presented in this Chapter is to establish if the application of Se as part of the fertilization regime, increases seleno-amino acid such as Se-Met, Methyl-SeCys and inorganic Se within broccoli sprouts. Initially, a comparison between the total selenium content of a treated group and control was conducted and then the optimum time period from planting to harvest was assessed using the selenium content of the sprouts as an indication. The germination rate, along with the dry and fresh mass was also measured and recorded to gauge if selenium has a positive effect on the plants' productivity. The distribution of Se and organic seleno-molecules within the seedlings was monitored using various mass spectrometry imaging techniques.

5.2 Material and methods

5.2.1 Cultivation method

The broccoli was grown in a self-contained miniature replicate of the fodder system from Chapter 4, using a reflective, insulated tent and two modified propagators to administer different treatments (Figure 5.2-1)

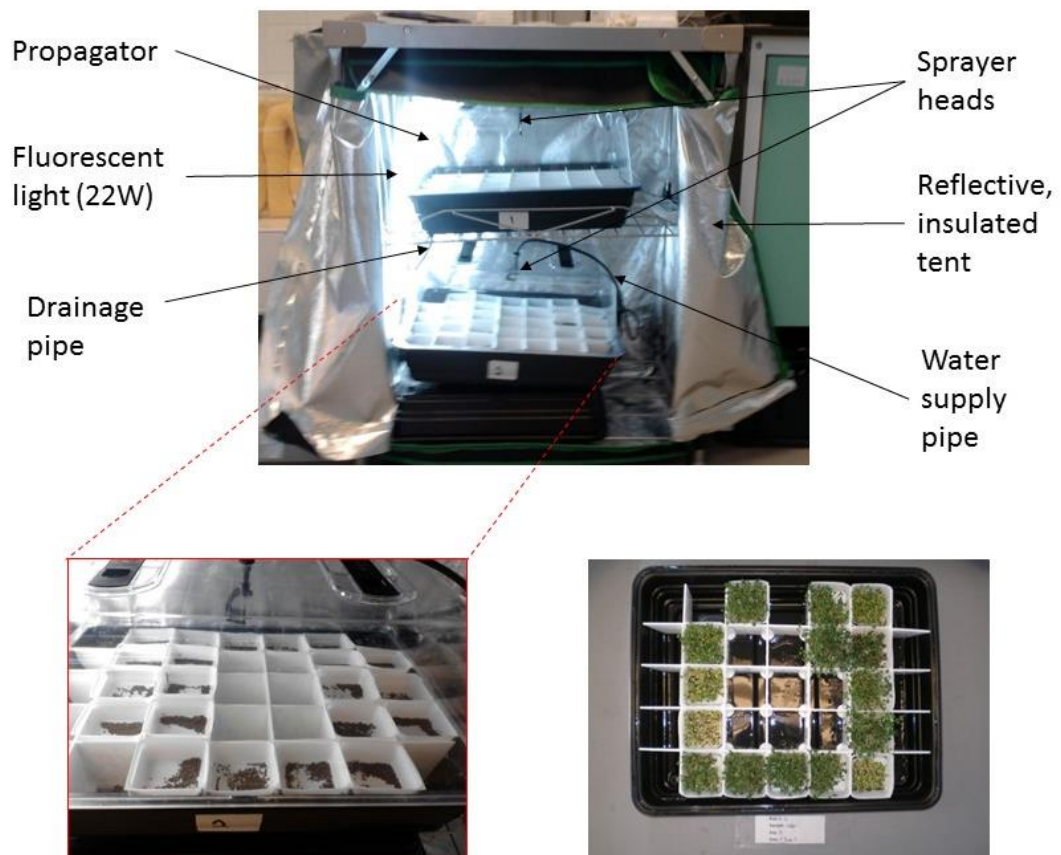


Figure 5.2-1: Hydroponic growing system.

The system was illuminated with 22 W of fluorescent light constantly. $3\text{g} \pm 0.05\text{g}$ of broccoli seeds were weighed on calibrated scales and poured into a 5cm^2 weighing boat, which had been adapted with drainage holes. This was repeated 36 times, and half placed into one propagator and the remaining 18 placed into a second propagator.

The study was performed using a hydroponic system which sprayed a solution over the seeds every two hours over a 21-day period. The sprouts were then harvested periodically at day 3, 5,7,10 and 14 after sowing.

Two groups were set-up; a control group, which was only fed water, the other was fed 20µg/L (0.02ppm) of Se in the form of sodium selenate. Three replicates per day were grown and harvested. Further details about this procedure can be found in Section 5.2.2. The experiment was repeated, only swapping the treatment given from the top shelf to the bottom.

5.2.2 Sample preparation

Three of the weighing boats containing the germinated broccoli were removed randomly from the system periodically. The shoots were washed thoroughly, for a minimum of 3 times with deionised water and separated from the un-germinated seeds. After air drying for a short period (approx. 30mins) and removing the excess water with paper towels, the shoots were weighed and the fresh mass recorded. The un-germinated seeds and shoots were freeze dried separately to a constant mass. The dry mass was recorded and the percentage (%) of the fresh mass was calculated along with the percentage of the original mass sown. The shoots were then ground in an electrical coffee grinder and passed through a 40-micron sieve to ensure homogeneity, ready for analysis.

The germination rate was calculated by first determining the number of un-germinated seeds, using the following equations:

Equation 5.2-1

$$\text{Approx. number of un-germinated seeds (U)} = \frac{\text{Freeze dried mass of seeds from sample}}{\text{Mass of one freeze dried seed}}$$

Equation 5.2-2

$$\text{Approximate germination rate (\%)} = \left(\frac{\text{Number of seeds sown} - U}{\text{Number of seeds sown}} \right) \times 100$$

5.2.2.1 Seedlings for imaging

Leaves for imaging were prepared by placing fresh samples between tissue paper and pressing between two glass slides. The slides were taped together and placed into a freeze drier at -36°C until they reached a constant mass, taking approximately ten days. The dried leaves were mounted onto either aluminium target plates or glass slides using double sided carbon tape to adhere the sample.

Due to the size of some of the plant tissue, samples were cut in half and analysed as two sections. The point at which the two images are joined can be clearly seen on each image with the white dashed line. Refer to Section 2.5.10 for the full explanation.

5.2.2.2 Reference material preparation for calibration of LA-ICP-MS

Matrix matched plant material was prepared as stated in Section 2.4.5. A series of mixed element spikes were added to the material, before pressing into 3 mm diameter pellets (Table 5.2-1).

Sample ID	Concentration of Se in standard solution used to spike reference plant material (mg/L)
Br0	0
Br5	10
Br10	20
Br25	50
Br50	100

Table 5.2-1: Standard concentrations add to each of the ground broccoli reference material for LA-ICP-MS analysis.

Carbon-13 was used as the internal standard to correct for instrument fluctuations, variation in sample thickness and water content (Becker, Matusch *et al.* 2014, Cizdziel, Bu *et al.* 2012, Kotschau 2012 Wu, Zoriy *et al.* 2009). Other elements that have been used as internal standards in plant analysis include Sc (Gomes, Schenk *et al.* 2014), ^{12}C (Punshon, Jackson *et al.* 2004) and Fe (Ward *et al.* 1992). For other materials internal standard such as Ag (Bauer, Limbeck. 2015), Ca (Hanc *et al.* 2013), Au, Rh (Compernelle *et al.* 2012) and Mg (Hirata *et al.* 2013), the selection should be based on the material being analysed.

5.2.2.3 Microwave digestion for total Se content

Microwave digestion methods (Montes-Bayon, Molet *et al.* 2006) were adapted using 30% hydrogen peroxide (H_2O_2), concentrated trace analysis grade 69% nitric acid (HNO_3) and deionized water (DH_2O). Ground plant material ($0.2\text{g} \pm 0.05\text{g}$) was weighed directly into the precleaned digestion vessels (Chapter 2, Section 2.3 & 2.4.1), 1.5ml HNO_3 and 1.5ml H_2O_2 were then added to each tube. This was performed in triplicate. To ensure complete drenching of the samples the mixture was gently swirled and allowed to predigest for 10 minutes with the lid on. A blank solution containing no sample was also prepared before placing all vessels into the microwave unit. The MDS2000 microwave digestion system required programming, which can be seen in Table 5.2-2.

Once the program completed, the vessels were removed and allowed to cool for 5 minutes before transferring the contents to 15ml tubes, rinsing the digestion tube a minimum of 3 times with deionised water. Final volume was then made up with deionised water.

Stage	1	2	3	4	5
% Power *	40% (240W)	0	40% (240W)	100% (625W)	0%
Pressure (psi)	20	20	20	20	20
Time (mins)	1:00	2:00	2:00	7:30	15:00
Fan speed	100	100	100	100	100

Table 5.2-2: MDS2000 microwave digestion parameter for the digestion of broccoli shoots.

*** this is for a nominal 630W system. For a nominal 950W system, multiply % power by 0.66.**

5.2.2.4 Seleno-amino acid Extraction

The method developed by Montes-Bayon *et al* 2006, was adapted for the speciation of selenium compounds, as a gentler method of extraction is required. Refer to Chapter 2 Section 2.4.6 for exact procedure performed.

5.2.3 Inductively coupled plasma mass spectrometry for total Se content.

Hewlett Packard (HP) 4500 series ICP-MS was used for the analysis of the total Se in the broccoli. Standard operating parameters were applied and can be found in Chapter 2, Section 2.5.7.1 and Table 2.5.1. The ICP-MS utilized the Chemstation 4500 series software to produce data and Microsoft Excel was used to process the data.

External calibration was performed using one multi-element calibration standard solution (Ultra Scientific, ICP/MS calibration standard #2) containing all required elements. The calibration standard ranges were based on the results of a semi-quantitative analysis performed on a non-spiked digested sample. The ranges for each element can be seen in Table 5.2-3.

Standard	Concentration of Se and Zn (ppm)
1 (Blank)	0
3	0.0001
4	0.001
5	0.001
6	0.01
7	0.02
8	0.1

Table 5.2-3: Calibration curve ranges.

Selenium experiences a number of polyatomic and isobaric interferences with ICP-MS (Table 5.2-4). There are three methods to combat this (Simmons, Kryukova *et al.* 2008):

1) use an instrument fitted with a collision cell (Gilbert, Danyushevsky *et al.* 2014, McCurdy, Woods 2004, Quarles, Jones *et al.* 2014) . The use of a collision gas such as helium helps to remove interference from other isotopes of the same mass, before they reach the detector.

2) use an interference free isotope.

3) apply correction equation factors (Gilbert, Danyushevsky *et al.* 2014, McCurdy, Woods 2004, Quarles, Jones *et al.* 2014, Rodriguez-Castrillon, Reyes *et al.* 2008, Simmons, Kryukova *et al.* 2008,).

Unfortunately, this particular instrument does not possess a collision cell, so correction equations were used and manual calculations were performed on the ratio of isotopes.

Isotope	Interference	Abundance
⁷⁶ Se	Ge, ³⁶ Ar ⁴⁰ Ar, ArS, Sm ²⁺ , Eu ²⁺ , Gd ²⁺	9.37
⁷⁷ Se	³⁷ ArCl, Ar ₂ H, Gd ²⁺ , Sm ²⁺ , Gd ²⁺	7.63
⁷⁸ Se	⁴⁰ Ar ³⁸ Ar ⁺ , Gd ²⁺ , Gd ²⁺ , Dy ²⁺	23.77
⁸⁰ Se	⁸⁰ Kr, ⁴⁰ Ar ⁴⁰ Ar, BrH, Gd ²⁺ , Dy ²⁺ ,	49.61
⁸² Se	⁸¹ BrH ⁺ , ⁸² Kr, Ar ₂ H, Ho ²⁺ , Dy ²⁺ , Er ²⁺	8.73

Table 5.2-4: Se isotope interferences experienced using ICP-MS.

5.2.4 Inductively coupled plasma mass spectrometry analysis of the laser ablation reference material.

Digested reference material for the broccoli were analysed on a PerkinElmer NexIon 350X ICP-MS using an auto-sampler under normal operating conditions (Chapter 2 Section 2.5.7.2 and Table 5.2-5.).

External calibration was performed using one multi-element calibration standard solution (Ultra Scientific, ICP/MS calibration standard #2) containing all required elements. The calibration standard ranges were based on the results of a semi-quantitative analysis performed on a non-spiked digested sample. The ranges for each element can be seen in Table 5.2-6.

Parameter	Value
Nebulizer/carrier gas flow	0.98L/min
Helium gas flow	4.4L/min (3.0 L /min for all Se isotopes)
Total integration time	0.5s (1.5s for Se)
Dwell time	30ms
Replicates per sample	3
Sweeps/Readings	50
Sample Flush	60s
Read Delay	40s
Wash	120s
Mode	Collision
Isotopes	⁶⁶ Zn, ⁷⁷ Se, ⁷⁸ Se, ⁸² Se, ¹³ C, ¹⁹⁷ Au and ¹⁰³ Rh (internal standard)

Table 5.2-5: ICP-MS operating conditions.

Standard	Concentration of Se and Zn (ppm)
1 (Blank)	0
2	0.0001
3	0.0005
4	0.001
5	0.005
6	0.01
7	0.05
8	0.1
9	1

Table 5.2-6: Calibration curve ranges.

Gold was added to all solutions at a final concentration of 200µg/L to stabilize mercury and rhodium at a final concentration of 20µg/L as the internal standard. Further details of the experimental procedure can be found in Chapter 2 Section 2.2.

5.2.5 Reversed phase high performance liquid chromatography inductively coupled plasma mass spectrometry.

Instrumentation specification and conditions can be found in Chapter 2, Section 2.5.8.

Due to seleno-amino acids being too hydrophilic to be retained and separated under typical C8 reverse phase condition, ion pairing was employed. The ion pairing agent was heptafluorobutyric acid (HFBA), and has been well documented to be better than trifluoroacetic acid (TFA) providing considerable enhanced resolution over TFA and allowing the separation of many additional organo-selenium species (Bianga, Govasmark *et al.* 2013, Bird, Ge *et al.* 1997. Casal, Far *et al.* 2010, Kotrebai, Birringer *et al.* 1999b, Kotrebai, Birringer *et al.* 1999c, Mao, Hu *et al.* 2012, Matusheski, Wallig *et al.* 2001, Montes-Bayon, Molet *et al.* 2006, Olivas, Donard *et al.* 1996b, Olivas, Kotrebai, Tyson *et al.* 2000 Uden, Bird *et al.* 1998, Wu, Prior 2005.).

Gradient analysis was used with a mobile phase 5% MeOH + 0.1% HFBA, for more details see Chapter 2, Section 2.5.8.1. All data was normalised against ¹²¹Sb.

5.2.6 Matrix assisted laser desorption/ionisation time of flight mass spectrometry

Instrumentation specification and conditions can be found in Chapter 2 Section 2.5.9.

MALDI-MS spectra were obtained in positive and negative ion mode in the mass range

between m/z 50 and m/z 1000. Declustering potential 2 was set at 15 arbitrary units and the focus potential at 10 arbitrary units, with an accumulation time of 0.999 sec.

Average spectra were acquired over a 0.5 cm² region on the leaves. The MALDI-MS/MS spectrum of the unknown precursor ions was obtained using argon as the collision gas; the declustering potential 2 was set at 15 and the focusing potential at 20, and the collision energy and the collision gas pressure were set at 20 and 5 arbitrary units, respectively.

5.2.7 Laser ablation inductively coupled plasma mass spectrometry

The PerkinElmer NexIon 350X ICP-MS unit was connected via a trigger switched to the UP-213 laser ablation unit. Standard operating parameters were applied and can be found in Chapter 2, Section 2.5.10. and Table 5.2-7.

Pressed pellets of dried broccoli leaves which had been spiked with known concentrations of standard, to produce matrix matched reference material (see Chapter 2, Section 2.4.5 and Chapter 4, Section 4.2.4.4 for preparation).

Quantitative analysis of 13 mm pellets was also performed for each of the sample groups analysed with digestion and ICP-MS. Ten consecutive lines, lasting 60 seconds, with a 30 second gas blank before and after, were performed and the mean, SD and RSD calculated.

Quantitative images were produced by running identical consecutive ablations parallel to one another to produce a raster image. Prior to the analysis of the tissue of interest, a 60 second raster ablation of the reference materials, with a 30 second gas blank period, before and after, was performed on the matrix matched reference materials. This was

also performed after the tissue was completed. The fully quantitative method applied ^{13}C as an internal standard (Becker, Dietrich *et al.* 2008, Jurowski, Szewczyk *et al.* 2014, Kötschau, Büchel *et al.* 2013, Wu, Zoriy *et al.* 2009) to compensate for the difference in the amount of material ablated (Wu, Zoriy *et al.* 2009), and results normalised against the signal. ^{13}C was found to be 1.08139 % using the method stated in Chapter 2, Section 2.5.11.

ICP-MS Parameter	Value
Nebulizer gas flow	1.44 L/min
Helium gas flow	3.5 L/min
Dwell time	30 ms
Acquisition time	0.204 s
Replicates per sample	1
Readings/Replicate	variable
Mode	Collision (KED)
Isotopes	^{66}Zn , ^{77}Se , ^{78}Se , ^{82}Se , ^{13}C
LA Parameter	
Laser power	28%
Spot size	100 μm
Repetition rate	20 Hz
Fluence (Laser energy)	0.06 J/cm ² (0.001mJ)
Scan speed	490 $\mu\text{m/s}$
Laser warm up time	40 s
Washout time	40 s

Table 5.2-7: LA-ICP-MS parameters.

The limit of detection (LOD) for element was calculated by Iolite 3.32 software (Paton, Hellstrom *et al.* 2011), based on previous work, using the reference materials (Longerich, Jackson *et al.* 1996). An average was calculated from a minimum of eight replicates. The reference material lines from each run were used and an average taken over the whole experiment. The LOD for the quantitative data of the pellets was calculated separately, as this analysis was performed sometime after the images and the sensitivity of the instrument had decreased whilst tuning, due to cone damage.

A spatial resolution in the x-direction was achieved at 124.5 μm and 100 in the y-direction.

5.2.8 Statistical analysis

Data was statistically analysed using two-way analysis of variance (ANOVA) according to GraphPad Prism version 7.00 for Windows, GraphPad Software, La Jolla California USA, www.graphpad.com. Probabilities of significance (p) between control and treatment were used to compare means. The interaction between treatment and replicates was also tested. Post hoc tests (Tukey HSD and Bonferroni) were then performed on dependent variables (concentration of elements in plant tissue, % dry mass, % germination rate, and fresh mass) that showed significances ($p < 0.05$).

5.2.9 Data processing

Refer to Chapter 2, Section 2.6.1 for MALDI-MS and Section 2.6.2 for LA-ICP-MS software and procedure for data processing and image production.

5.3 Results and discussion

When selenium is taken up by the plant, it is via the root system and translocation occurs via the xylem to the aerial parts of the plant (Lyons, Stangoulis *et al.* 2003). From there that it is converted into various organo-seleno molecules.

Due to the conditions within the growth chamber, at day 14 of growth, a fungus took hold and result in the seedling starting to decay, therefore all results are only reported up to day 14. Two methods of quantification were used to establish the total selenium content of the broccoli sprouts and establish which day was optimal for harvest.

5.3.1 Total selenium content by inductively coupled plasma mass spectrometry

Figure 5.3-1 clearly demonstrates that with time there is an exponential increase in the selenium content of the broccoli irrigated with sodium selenate. There is a slight increase in the selenium content in the group irrigated with water, which is negligible. The results are shown to be very significant ($p < 0.01$) for both the treatment and over time. This confirms that broccoli is a hyper-accumulator of selenium and agrees with many previous studies (Abdulah, Faried *et al.* 2009, Banuelos 2002, Fahey, Zhang *et al.* 1997, Finley, *et al.* 2001, Finley, Sigrid-Keck *et al.* 2005, Hsu, Wirtz *et al.* 2011, Kim, Juvik 2011, Mahn, Zamorano *et al.* 2012, Pedrero, Elvira *et al.* 2007, Robbins, Keck *et al.* 2005, Verbruggen, Hermans *et al.* 2009).

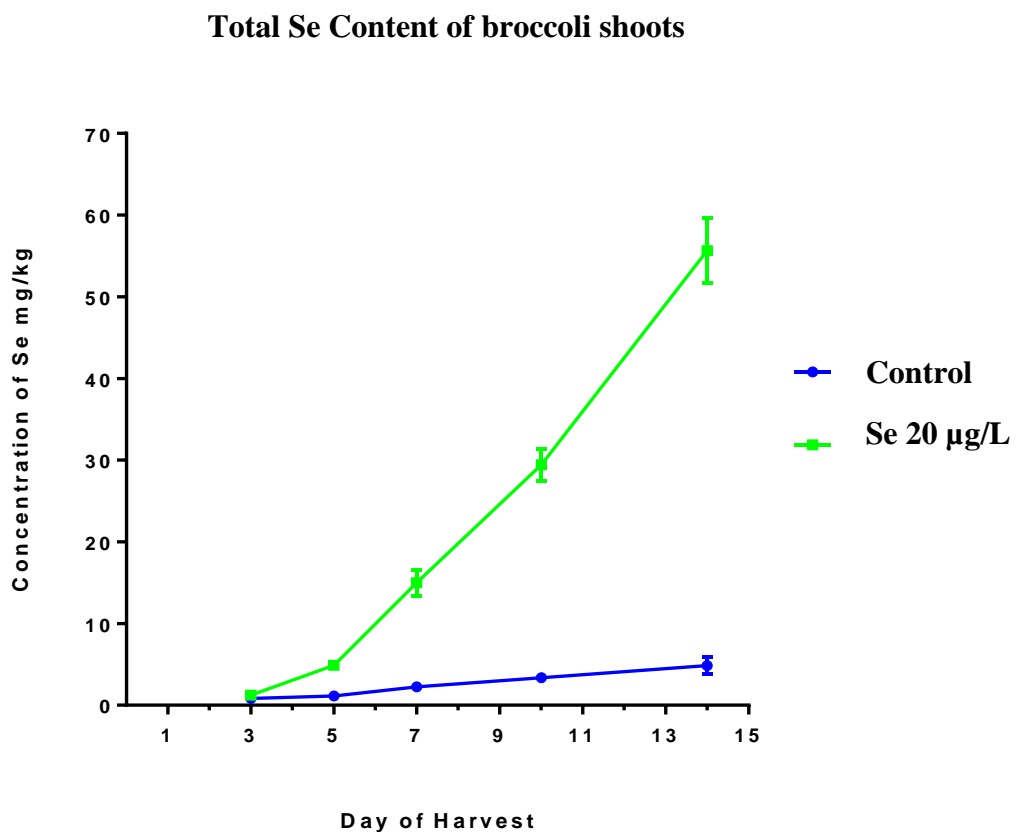


Figure 5.3-1: Comparison of the total selenium content of broccoli sprouts irrigated with either water or sodium selenate.

Previous studies (Abdulah, Faried *et al.* 2009) saw similar results, after 7-day exposure to 10ppm sodium selenite, reporting a total Se content of 10.24 mg/kg with the treated group and the control only showing 0.01mg/kg. The broccoli was germinated in a 10ppm solution of sodium selenite compared to regular irrigations with fresh solution, as described here.

Another previous study on broccoli in hydroponics (Lyi, Heller *et al.* 2005) used 40 μ M sodium selenate (7.5ppm). However, the study was done on mature broccoli, which will naturally have higher levels of Se. The leaf content was found to be 900mg/kg after 4-weeks of growth with one application of sodium selenate for 1 week. In this study, they also grew the control group in a separate room to avoid exposure of phytovolatilized Se to them. Lyi *et al* also found that selenate exposure produced more Methyl-SeCys within the broccoli.

Sodium selenate concentration (ppm)	Se content dry weight (mg/kg)	Time of harvest after planting	Number of applications	Reference
7.5	900	28 days	1	(Lyi, Heller <i>et al.</i> 2005)
1	270	24 days	Continuous from day 7 Fresh nutrient solution prepared 3 times.	(Charron, Kopsell <i>et al.</i> 2001)
2	479			
3	512			
6	440			
7.2	750			
9	731			
25	62.3	6 days	2	(Finley, Ip <i>et al.</i> 2001)
7.5	130	21 days	1	(Hsu, Wirtz <i>et al.</i> 2011)
	220	28 days	2	
	300	35 days	3	
	420	42 days	4	
0.5	178	30 days	Continuous from day 7 Fresh nutrient solution prepared 3 times	(Toler, Charron <i>et al.</i> 2007)
0.75	218			
1	280			
1.5	360			

Table 5.3-1: Previous studies investigating the effects of sodium selenate on the total Se content of broccoli.

Table 5.3-1 consolidates previously published work on sodium selenate applications to broccoli, outlining the differences between the methods. Interestingly, the application concentration of sodium selenate within the data presented in this Chapter was only 0.02ppm, however this was applied every 2 hours. Finley *et al*, is the only experiment to expose the seeds, pre-germination, to sodium selenate, by first soaking them for 4 hours in 25ppm sodium selenate (seed priming) and then spraying once with the same solution before allowing them to grow for 6 days. This would appear to be a much more efficient use of the nutrient and water, with more dramatic effects on the Se content. Though Charron *et al*, reported chlorosis on the leaves with older plants at concentration above 14.3ppm. It is evident though, from all of the data that broccoli accumulates Se in its tissues with time and increased exposure.

5.3.2 Quantitative analysis of laser ablation inductively coupled plasma mass spectrometry reference material.

The results are presented in Table 5.3-2 as an average of the triplicates.

Sample Id	Concentration of Se in standard solution used to spike the standards (mg/L)				
	⁶⁶ Zn (mg/kg)	⁷⁸ Se (mg/kg)	⁷⁷ Se (mg/kg)	⁸² Se (mg/kg)	
Br0	0	250.492	0.365	0.601	0.547
<i>SD</i>		7.42	0.01	0.03	0.02
<i>RSD</i>		2.96%	3.98%	4.56%	3.26%
Br5	10	130.957	11.967	13.260	12.132
<i>SD</i>		3.63	0.45	0.46	0.40
<i>RSD</i>		2.78%	3.72%	3.51%	3.27%
Br10	20	137.563	22.630	23.968	22.873
<i>SD</i>		1.42	0.71	0.47	0.70
<i>RSD</i>		1.03%	3.14%	1.96%	3.06%
Br25	50	124.308	49.691	52.654	49.589
<i>SD</i>		4.60	0.56	0.17	0.61
<i>RSD</i>		3.70%	1.13%	0.33%	1.22%
Br50	100	127.140	110.899	118.294	110.782
<i>SD</i>		0.57	1.25	1.17	1.49
<i>RSD</i>		0.45%	1.13%	0.99%	1.34%

Table 5.3-2: Quantitative results of the of laser ablation inductively coupled plasma mass spectrometry reference material. (n = 3)

The ^{13}C content was reported to be 1.081% in all broccoli leaf material and was used as the internal standard. These results were entered into the Iolite 3.32 software (Paton, Hellstrom *et al.* 2011) and used to quantify the images produced.

5.3.3 Total selenium content by laser ablation inductively coupled plasma mass spectrometry

The data presented in Figure 5.3-2 clearly demonstrates that the addition of sodium selenate to the irrigation solution increases the total selenium content of the broccoli.

The dried samples, when analysed by this method, had been stored at -80°C for 2 years prior to analysis, and this is possibly the reason for the decrease in Se content, in comparison to the ICP-MS data. The volatility and poor stability of selenium compounds has been documented (Olivas, Quevauviller *et al.* 1998, Cuderman, Stibilj 2010, Moreno, Quijano *et al.* 2002). A similar study, using LA-ICP-MS to track Se in sunflowers, stated that it is necessary to emphasize that Se may have been lost during sample preparation procedure as compounds such as dimethylselenide and dimethylselenide are very volatile and can be lost (Oseas da Silva, Zezzi Arruda 2013).

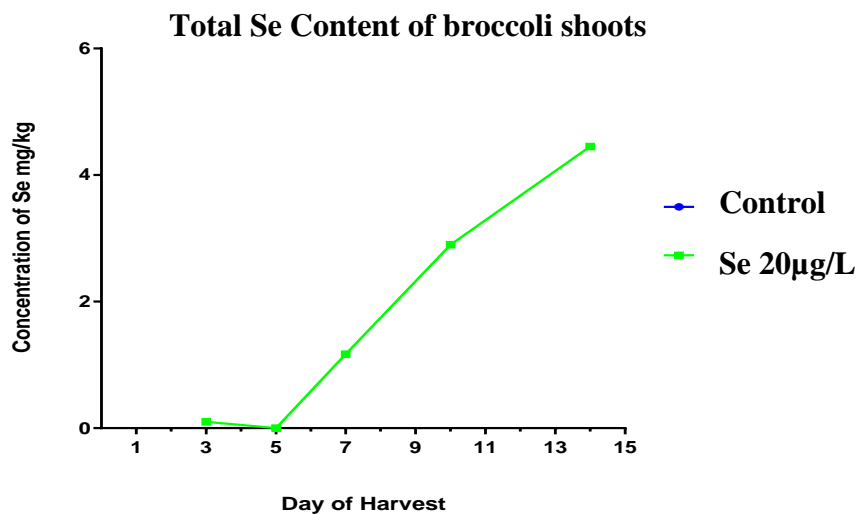


Figure 5.3-2: LA-ICP-MS quantitative data of broccoli shoots.

However, it is still evident from the data that there is an increase in the Se content over time, with the application of selenium fertilizer. All of the control group results were below the limit of detection for the method and therefore no data is presented in Figure 5.3-2.

5.3.4 Limit of detection for laser ablation method

The LOD for each element for the LA-ICP-MS method used for quantitative analysis of pelletised broccoli shoots are displayed in Table 5.3-3.

	⁶⁶ Zn	⁷⁷ Se	⁷⁸ Se	⁸² Se
Mean (mg/Kg)	0.232	0.839	1.357	1.406
SD	0.071	0.214	0.316	0.678
RSD (%)	30%	26%	23%	48%

Table 5.3-3: LOD for LA-ICP-MS method.

5.3.5 Selenium speciation

The identification and quantification of the selenate, selenite, Se-methionine and Se-methylselenocysteine (Methyl-SeCys) was first established by Montes-Bayon (Montes-Bayon, Molet *et al.* 2006).

Figure 5.3-3A shows the retention times of the Se compounds of interest. Figure 5.3-3B reveals four additional peaks, two of which are prominent, denoted peak B and peak C. There are a number of other seleno-amino acids and derivatives, including γ -glutamyl-Se-methylselenocysteine, selenocysteine and selenocysteine (Table 5.1-1) which these could be. A similar study performed on chives (Kápolna, Shah *et al.* 2007) and on biological extracts (Kotrebai, Birringer *et al.* 1999a), employing the same type of C8 column and conditions, demonstrated the position of selenocysteine in relation to the other selenium species with a mixed standard solution of seleno-amino acids. Peak B in

Figure 5.3-3B corresponds to the same retention time and positions in relation to the other known peaks on the spectra of Kotrebai and Kápolna, allowing the tentative deduction that peak B is selenocysteine. However, within this study, the main focus was on Se-methionine and Se-methylselenocysteine and confirmation would be required with a known standard.

Seleno-amino acids are zwitterions and they can, therefore, be present as positively charged, negatively charged or neutral forms (Mahn, Zamorano *et al.* 2012, Mao, Hu *et al.* 2012). The form they are present in is dictated by the pH. This can present a number of problems when it comes to separating the different Se species, particularly separating inorganic and organic species via one chromatography method (Olivas, Donard *et al.* 1996a). The resolution achieved with RP-HPLC-ICP-MS of particular Se-amino acids is also affected by the pH of the mobile phase, with previous studies optimising these conditions (Mahn, Zamorano *et al.* 2012, Olivas, Donard *et al.* 1996a, Uden, Bird *et al.* 1998, Li, Hu *et al.* 2008). Other factors that have been reported to affect the resolution and retention behaviour of selenium species, including column temperature and organic content of the mobile phase (Mahn, Zamorano *et al.* 2012, Mao, Hu *et al.* 2012). These are all factors that may have influenced the change of species within the sample as well as affected the separation of the Se-amino acids and the sensitivity of the method.

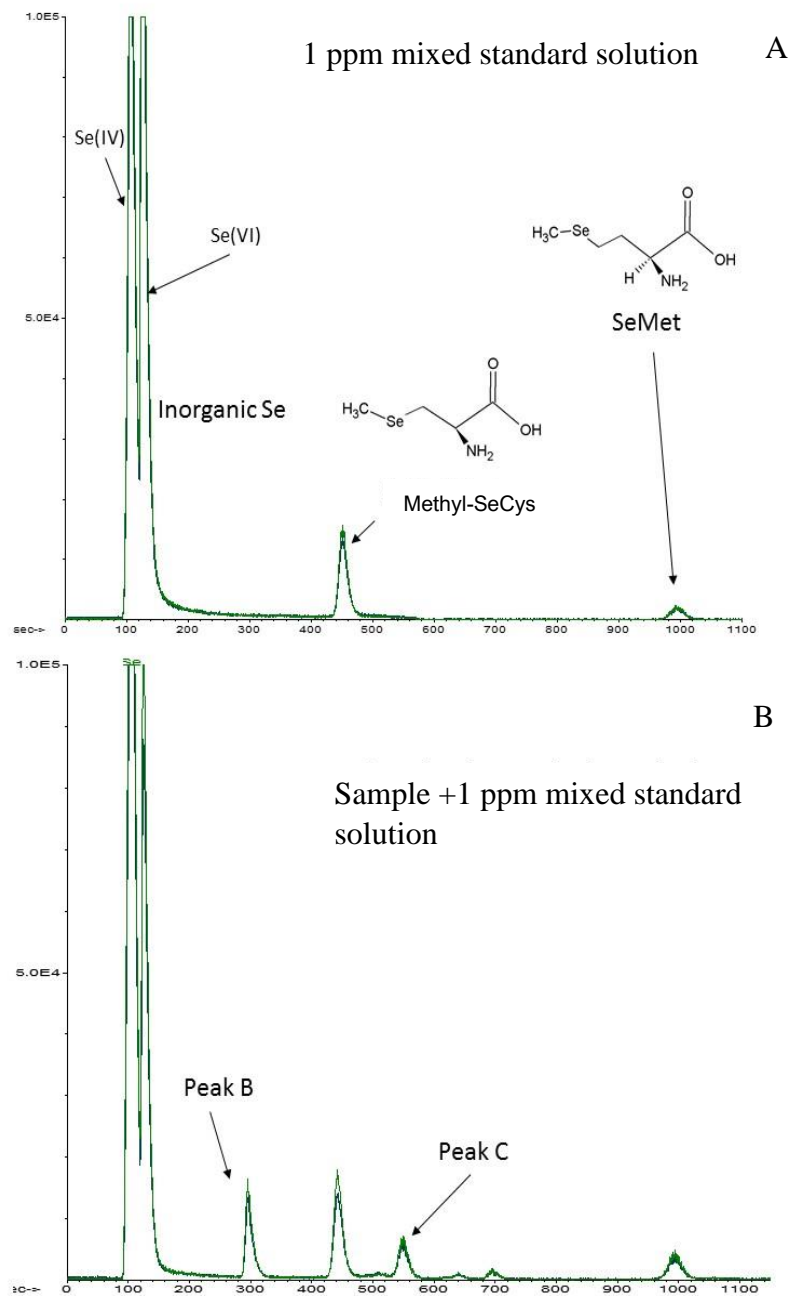


Figure 5.3-3: HPLC chromatograms for the detection of various seleno-amino acids .A) Standard solution of inorganic Se and Se-amino acids B) Broccoli extract spiked with standard solution.

5.3.6 Accumulation of Se species over time

Figure 5.3-4 displays all of the Se species identified in Section 5.3.5, comparing the content of broccoli sprouts irrigated with water and 20 μ g/L sodium selenate over a 10-day period. The results presented here show that irrigating broccoli with sodium selenate had a very significant ($P < 0.01$) effect on the content of Se-methionine (Figure 5.3-4B), showing an increase in the content, as would be expected. Over time the Se-Met was also increased, however this was not found to be statistically significant ($p > 0.05$). The inorganic selenium (Figure 5.3-4E) was also found to be affected significantly ($p < 0.01$) however, the application of sodium selenate caused the inorganic content to drop and was not affected by increased time of exposure. The unidentified peak C (Figure 5.3-4C) was also found to be significantly increased with the application of sodium selenate.

Lyi reported an increase in the Methyl-SeCys with selenate exposure (Lyi, Heller *et al.* 2005), however, these plants were 5 weeks old at the point of harvest and were exposed to much higher concentrations of sodium selenate 40 μ M (7.54ppm). Interestingly the group which was treated with 10 μ M (1.88ppm) only showed a small increase, indicating that higher concentration of sodium selenate are required having an impact on Methyl-SeCys.

Se-methylselenocysteine (Figure 5.3-4A) content was not significantly ($p > 0.05$) affected by sodium selenate fertigation or over time. It is worth noting that the highest content was found to be on day 3 for both the treated and control group, however this was not seen to be significant. Other studies have reported that Methyl-SeCys is highest in germinated seeds, compared to mature plants (Abdulah, Faried *et al.* 2009).

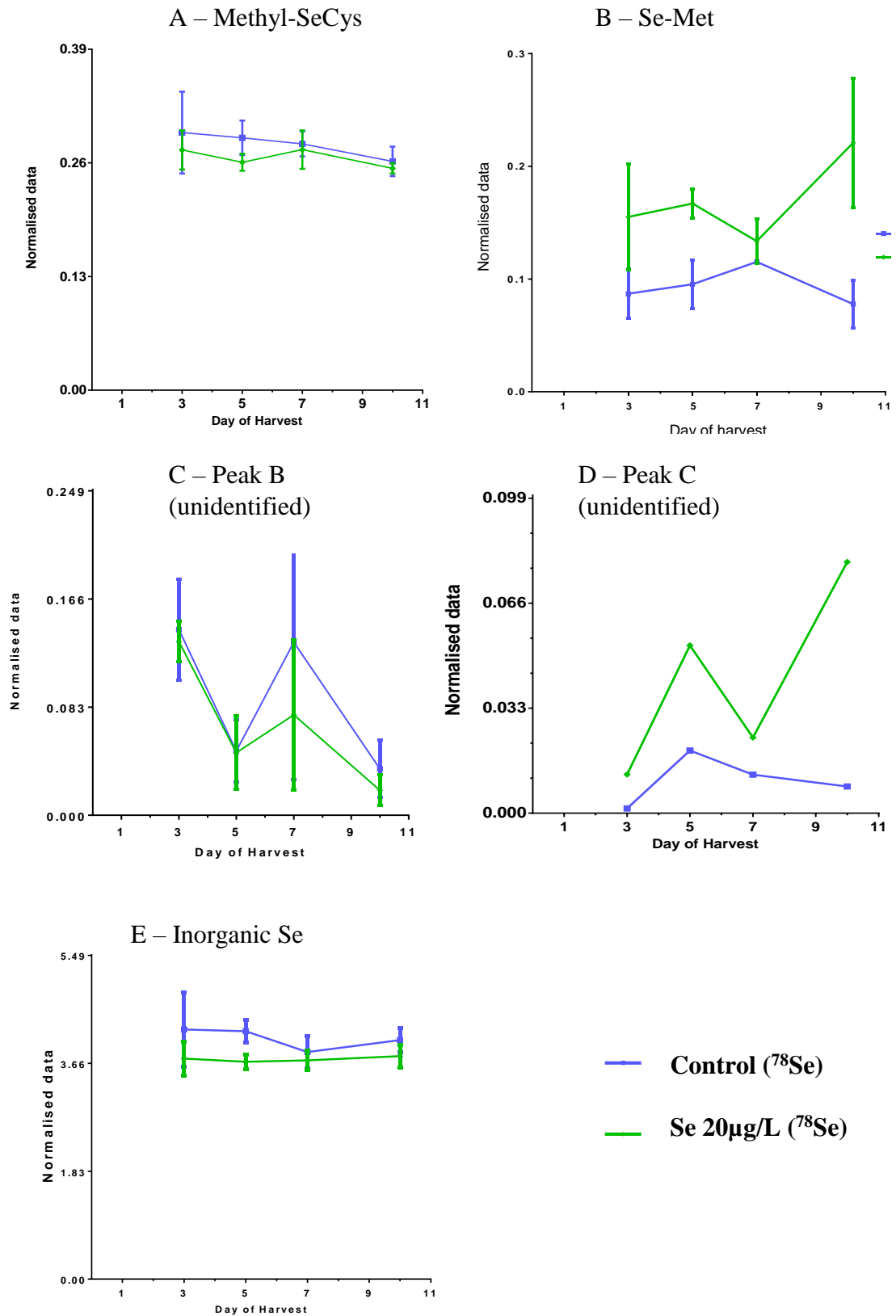


Figure 5.3-4: Comparison of various Se-amino acids in broccoli sprout irrigated with sodium selenate or water over a 10-day period; A) Methyl-SeCys; B) Se-Met; C) Unidentified Peak B; D) Unidentified peak C; E) Inorganic Se.

The unidentified peak B (Figure 5.3-4C) was not affected by the treatment, however the content did drop significantly ($p < 0.05$) over time in both the control and the treated group. It would be expected that there are no Se-amino acids present in the control group, however, the control group in the data presented here did show the presence of Se in the total Se content, which could have come from volatile Se compounds released from the treated group. Analysis of the seeds pre-germination would allow a definitive reason to for the presence of Se in the control group.

5.3.7 The effect of sodium selenate on plant yield and germination rate.

In order to assess the effect of sodium selenate on the productivity of the broccoli sprouts over time, four parameters were measured. This included the fresh mass (Figure 5.3-5A), dry mass as a percentage of the fresh mass (Figure 5.3-5B), germination rate (%) (Figure 5.3-5C) and fresh to dry mass ratio (Figure 5.3-5D). The 2-way analysis of variation revealed that that the treatment with $20\mu\text{g/L}$ sodium selenate did not affect any of the parameters significantly ($p > 0.05$).

The results presented in Figure 5.3-5A are in agreement with previous studies which showed that sodium selenate treatment on broccoli does not have a significant effect on the fresh mass (Hsu, Wirtz *et al.* 2011, Toler, Charron *et al.* 2007) . Hsu *et al* 2011 reported that the dry mass was also not affected, and concluded that selenate fertilization did not affect young plant development. Toler *et al.* 2007 reported a drop in dry mass with the application of sodium selenate, however the concentrations applied were much higher, with the lowest at 0.5mg/L selenate and the plants were also harvested after 30 days.

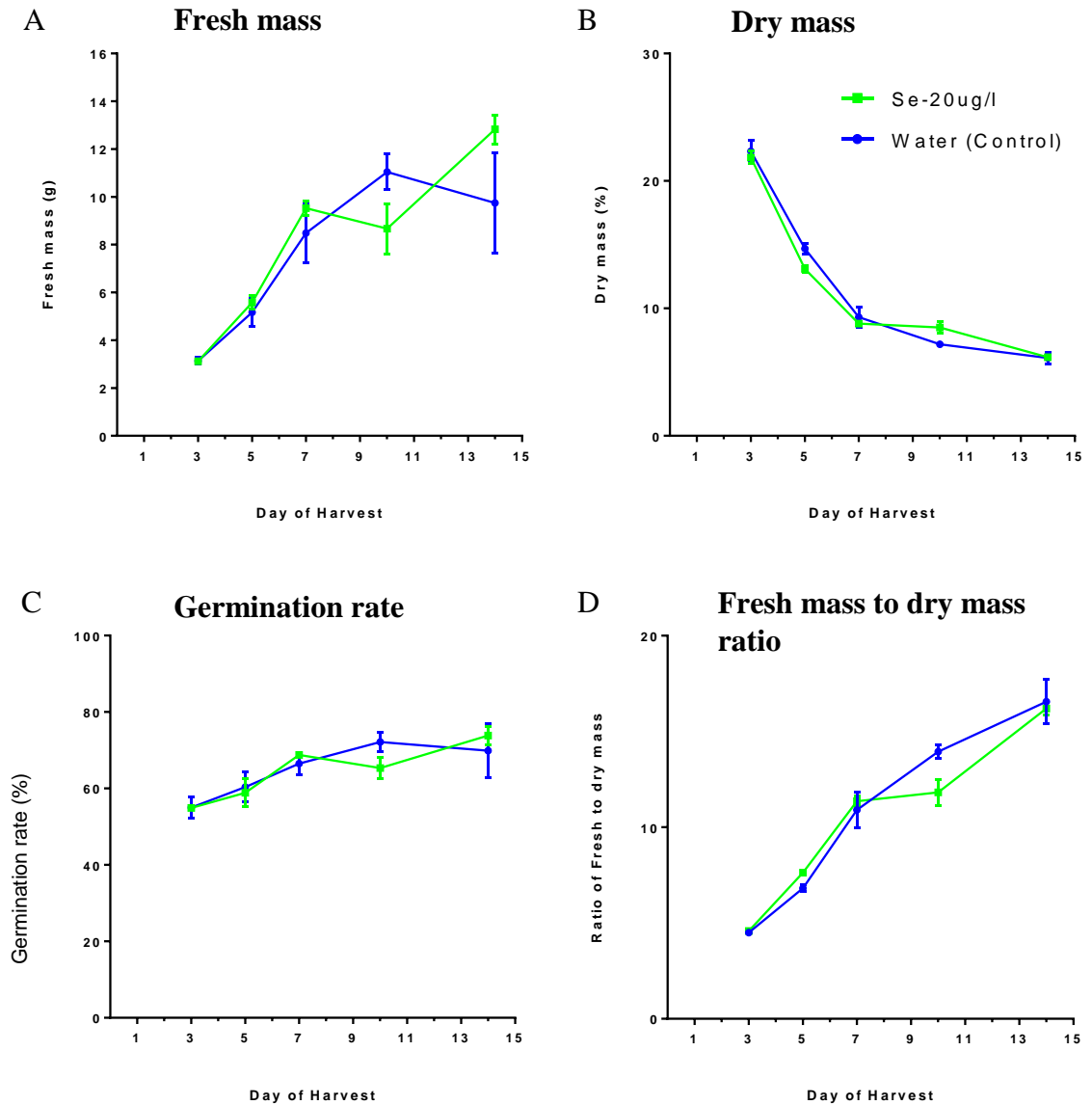


Figure 5.3-5: Comparison of broccoli sprouts irrigated with 20 µg/L sodium selenate or water on productivity parameters A) Fresh Mass; B) % Dry mass; C) Germination rate (%); D) Fresh to Dry mass ratio

5.3.8 Monitoring the distribution within plant using Matrix assisted laser desorption/ionisation mass spectrometry imaging

Table 5.1-1 displays the seleno-amino acids and the adducts which were strong mass candidates for tracking in to the plant. Various ions of seleno-amino acids were selected and fragmentation of those ions was performed. These masses were then monitored within the plant material, using the fragmentation patterns to confirm these were the same ions.

Various parameters and techniques were applied to the seedlings. This included variation in matrix concentrations and laying quantities. On fragmentation of the chosen masses most turned out to be matrix peaks rather than ions of interest. Isotopic patterns were also examined along with various different adducts. Negative mode was also tried with no success.

Figure 5.3-6 is of m/z 204 and was believed to be the Na adduct of Se-methionine. Fragmentation of the data revealed it to be matrix peaks.

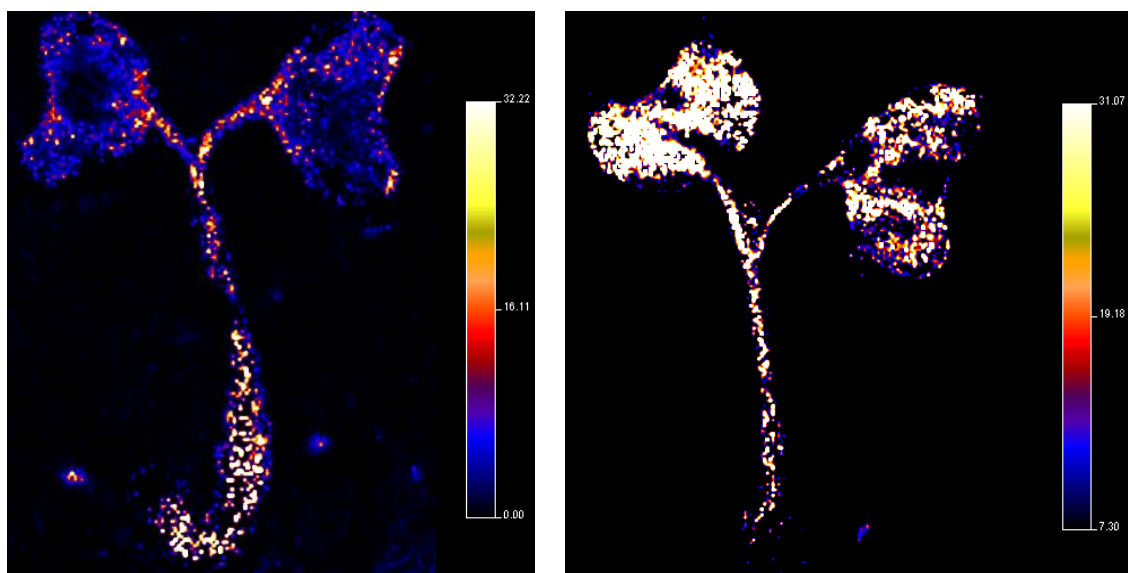


Figure 5.3-6: MALDI-MS image of broccoli sprouts treated with Se at day 10 after sowing.

The molecules of interest are very small and have similar mass to charge ratio (m/z) as many of the matrix peaks.

A review by Lobinski, Schaumlöffel *et al.* 2006 discusses the use of MALDI-MS for the speciation of Se compounds, stating that preservation of metal complexes under MALDI ionization condition is difficult and that electrospray MS is a more appropriate technique. Due to the acidic matrices and the ionisation mechanism the complexes of the seleno-amino acids can be lost. Future studies would use this technique to help support the data present in this chapter.

5.3.9 Distribution within plant using laser ablation inductively coupled plasma mass spectrometry

Figure 5.3-7 shows clearly that the broccoli irrigated with sodium selenate has an increased selenium content. The content also increases with time, concurring with the previously presented data in Section 5.2.3.

Figure 5.3-7 and Figure 5.3-8 clearly shows that the roots is where the highest concentration is, with the selenium working its way up the stem and to the leaves. Supporting evidence can be seen in Figure 5.3-12, displaying the highest concentration of Se in any of the plant material (Se = 0.95mg/kg of dry mass).

Figure 5.3-9 reveals a large margin of error with the control/water group on day 3, which can be also seen in the image produced in Figure 5.3-7, as there appears to be a large amount of background noise in the image. There appears to be no real significant difference between the control group and the treated group after 3 days of application. At day 7 though, it can be seen that the treated group has increased in Se content. The image of the day 7 treated group in Figure 5.3-7, demonstrated the uptake of the Se.

This is further supported by Figure 5.3-10, clearly showing a mean content of Se (0.352 ± 0.037 ppm) in the treated group, compared with the control group (0.045 ± 0.019 ppm).

A further increase in the Se content over time can be seen from Figure 5.3-11, with the day 10 treated leaves containing an average content of 0.47 ± 0.71 ppm, compared with the control group at 0.023 ± 0.82 ppm.

This observation is very interesting due to the way the sodium selenate was delivered to the plant via a sprinkler system, as opposed to root irrigation. However, the roots were exposed to the solution, unlike previous studies on carrots (Kápolna, Hillestrøm *et al.* 2009), where the effect on exclusively foliar application of sodium selenate was investigated and found that the leaves had the highest Se content.

Previous work performed on broccoli which investigated the distribution of Se in the plant (Pedrero, Elvira *et al.* 2007), using digestion and quantitative analysis with ICP-MS, reported that the roots had the highest concentration, similar to the data reported here. Pedrero also reported that this increased with time. Contradictory to this, Hsu *et al.* found that the highest concentration of Se in fortified broccoli was found in the shoots, however, this study did not apply the Se until 2 weeks after planting and the analysis was performed on mature plants which were 6 weeks old (Hsu, Wirtz *et al.* 2011).

Studies with soybeans (Chan, Afton *et al.* 2010) and chives (Kápolna, Shah *et al.* 2007) also reported that the roots had the highest concentration of Se in comparison to the leaves. Interestingly, Silva reported that in sunflowers the leaves had the highest concentration, however this study ran for 44 days before harvest (Oseas da Silva, Lopez de Andrade *et al.* 2011).

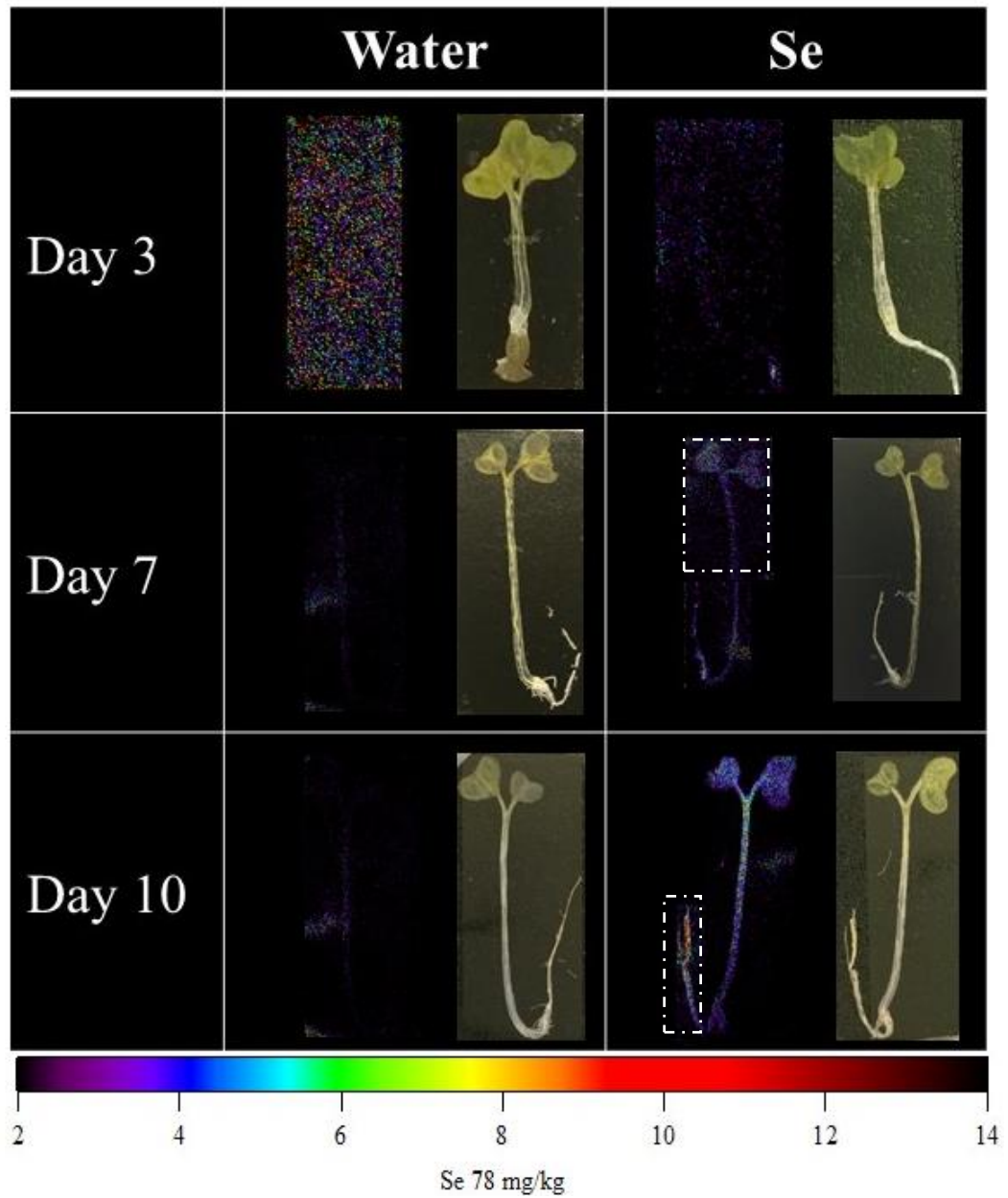


Figure 5.3-7: LA-ICP-MS images of broccoli irrigated with water or sodium selenate.

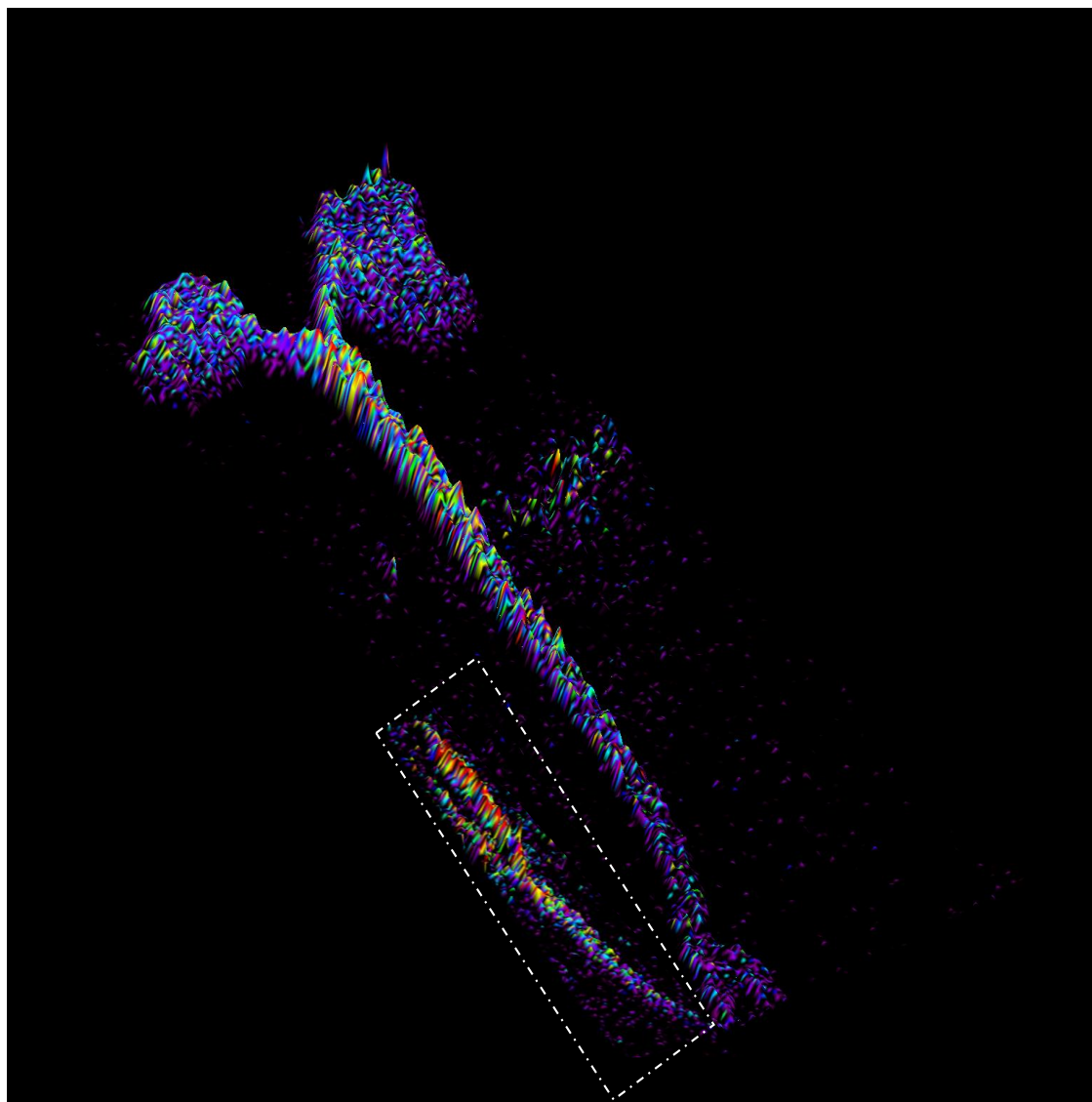


Figure 5.3-8: 3D distribution map of ^{78}Se in broccoli sprout irrigated with sodium selenate for 10 days using LA-ICP-MS.

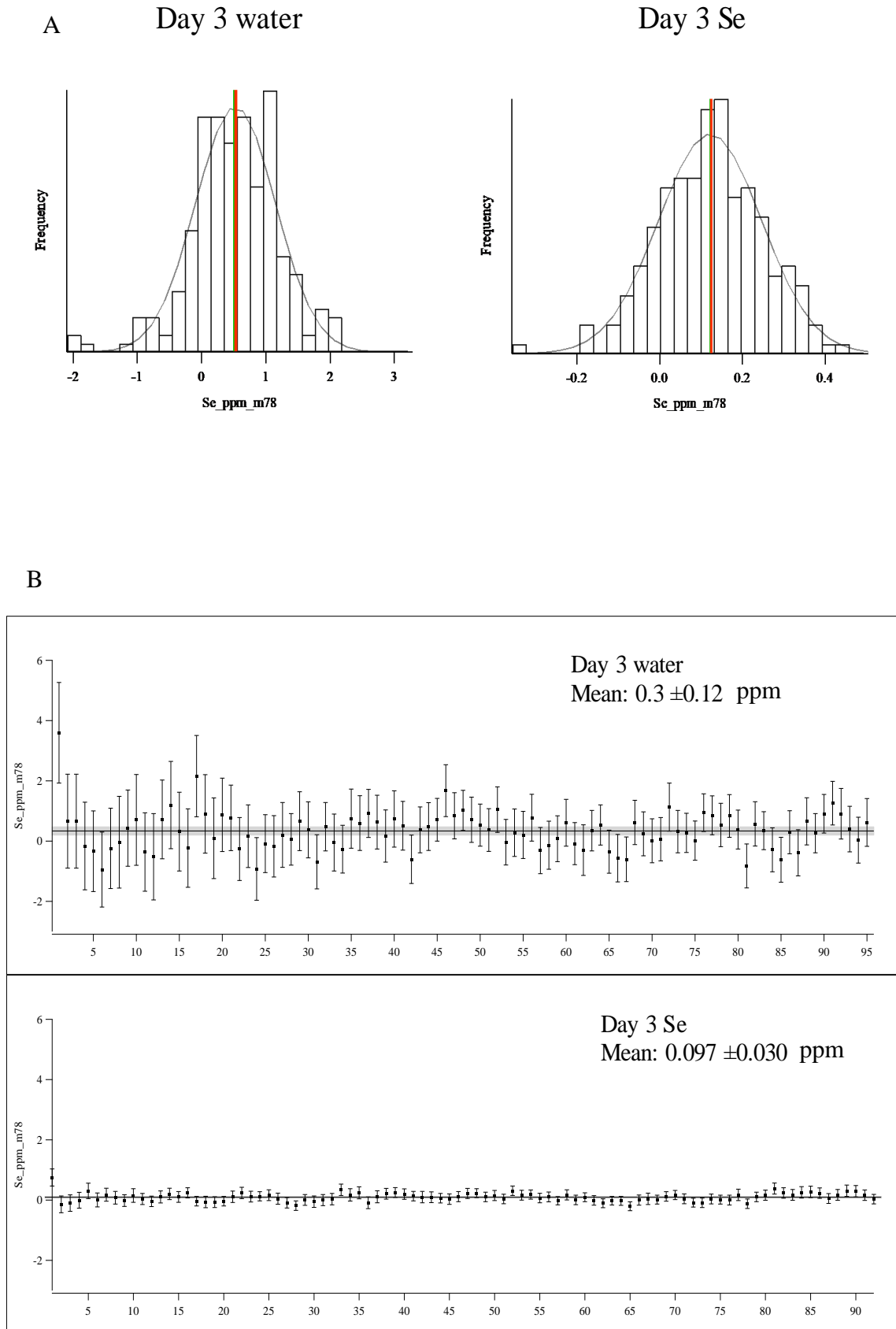


Figure 5.3-9: Iolite 3.32 software Statistical comparison of the Se content and distribution within broccoli sprouts, 3 days after germination within the control and selenium treated A) histograms B) stats summary from LA-ICP-MS analysis.

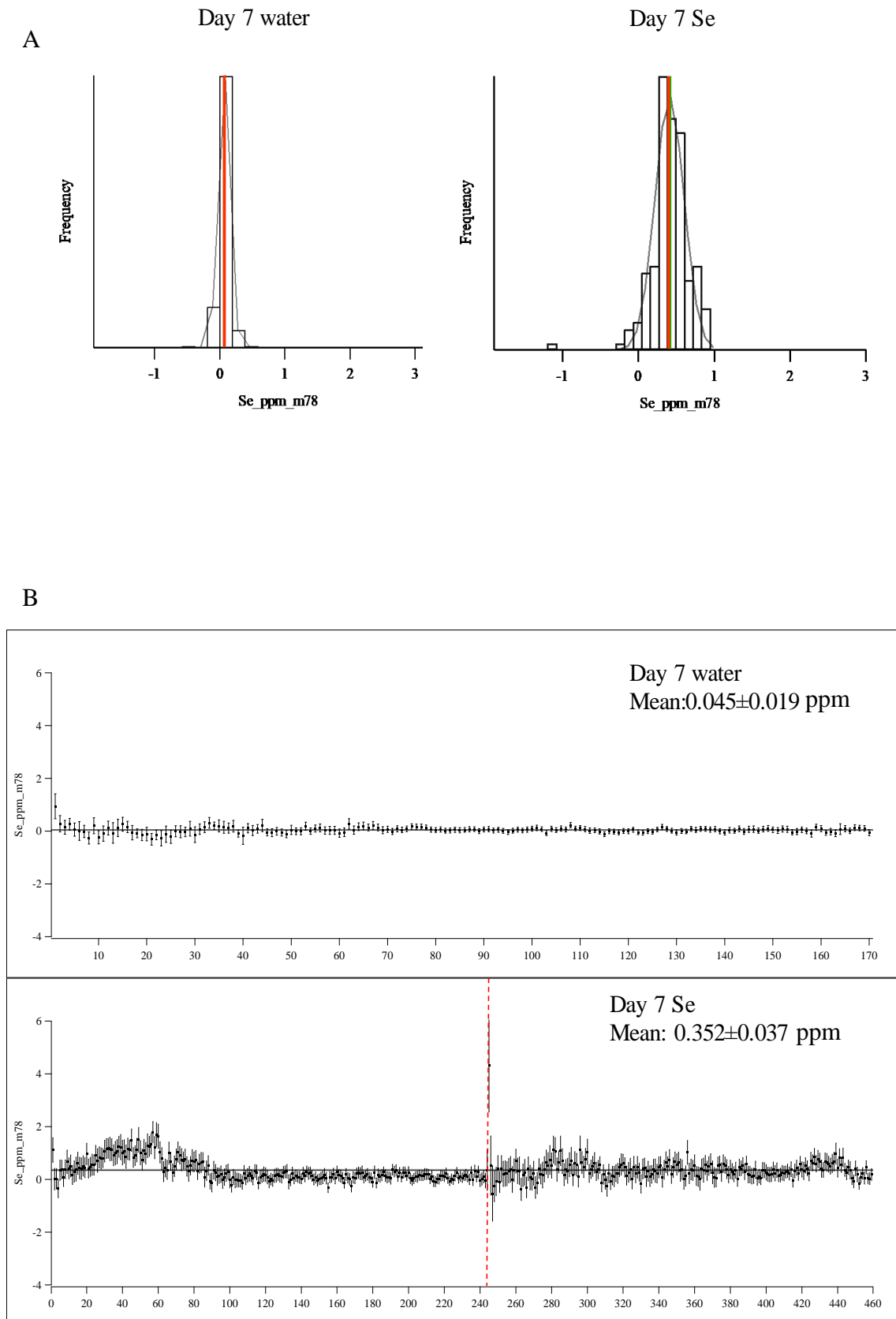


Figure 5.3-10: Iolite 3.32 software Statistical comparison of the Se content and distribution within broccoli sprouts, 7 days after germination within the control and selenium treated A) histograms B) stats summary from LA-ICP-MS analysis. NB: The red dotted line represents where the two images were stuck together.

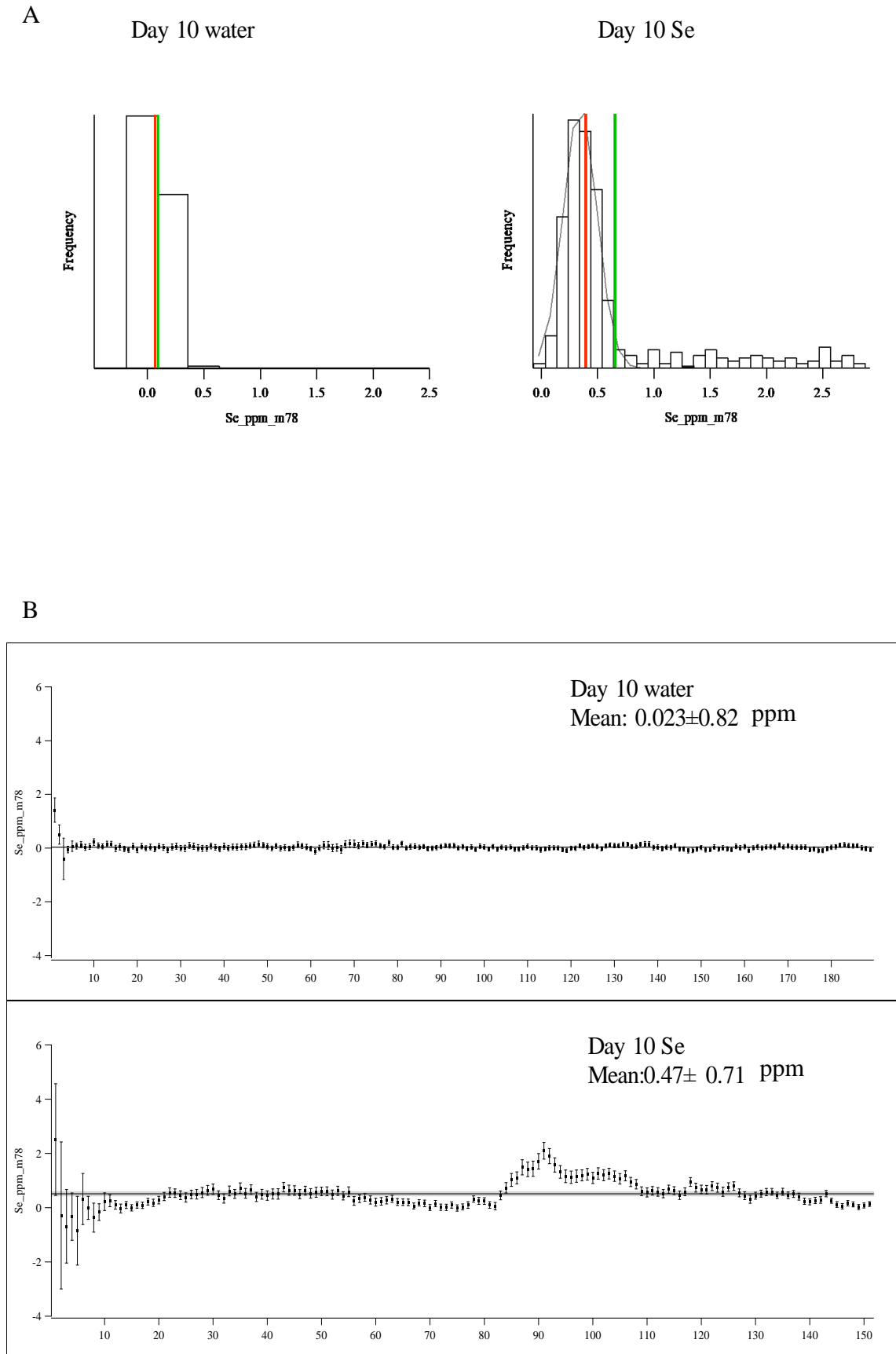


Figure 5.3-11: Iolite 3.32 software statistical comparison of the Se content and distribution within broccoli sprouts, 10 days after germination within the control and selenium treated A) histograms B) stats summary from LA-ICP-MS analysis.

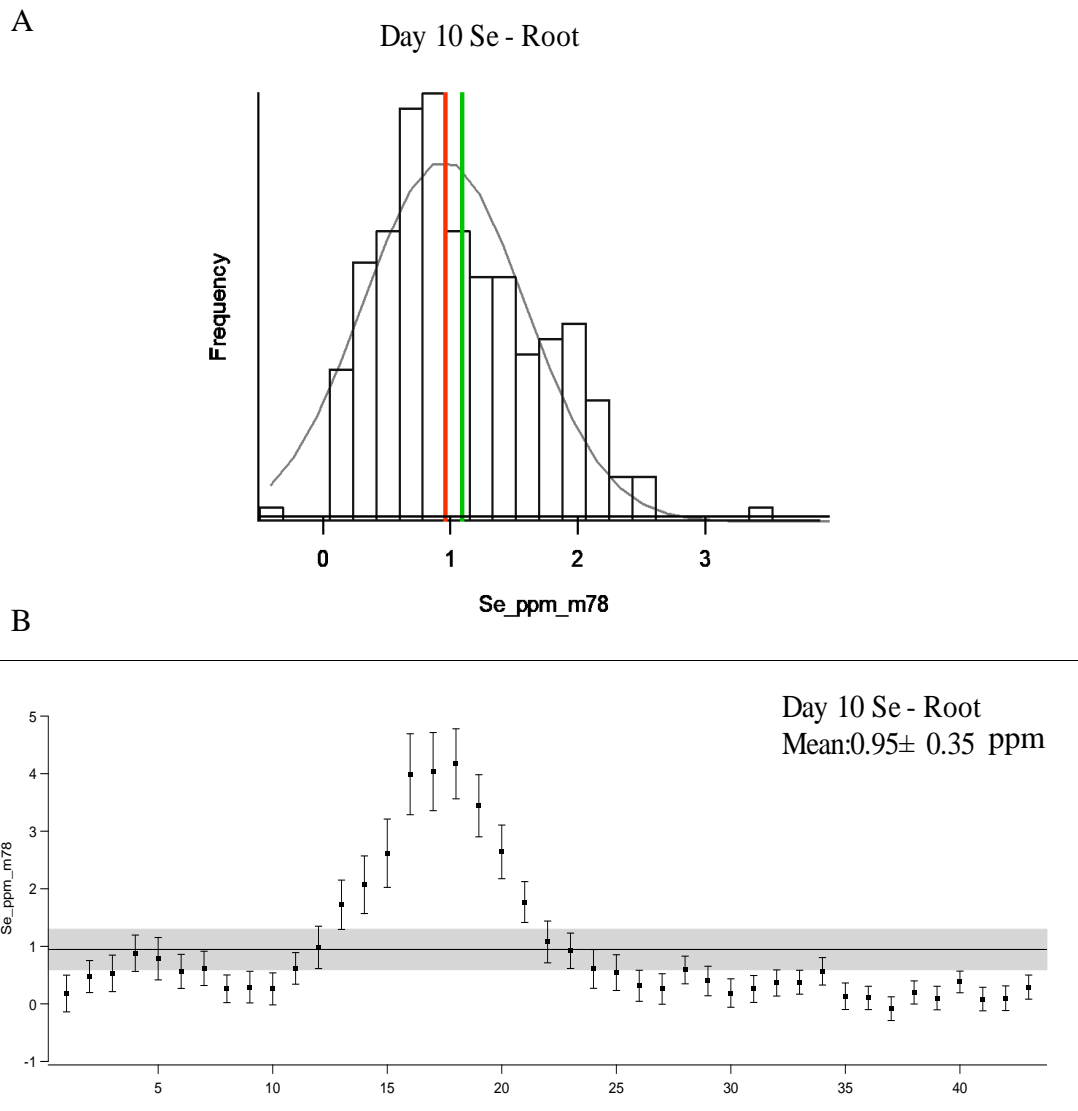


Figure 5.3-12: Iolite 3.32 software statistical comparison of the Se content and distribution within broccoli roots, 10 days after germination in the selenium treat group A) histograms B) stats summary from LA-ICP-MS analysis.

Very few studies have been performed on Se distribution maps within plants using laser ablation ICP-MS and the only work to date is of sunflower leaves (Oseas da Silva, Zezzi Arruda 2013). Within this study, sodium selenite was used as the source of selenium rather than sodium selenate used in this investigation. It is also worth noting that these researchers used a dynamic reaction cell, with oxygen as the reaction gas, to combat the interference that ^{80}Se experiences. The species, therefore, monitored was

$^{80}\text{Se}^{16}\text{O}^+$. It can be concluded that LA-ICP-MS is an excellent technique for mapping of elements such as Se within plant tissue. Other work on soybean leaves, which monitored the Se speciation using 3D gel and LA-ICP-MS, has been reported (Oliveira, Arruda 2015). This work however did not produce any images. Most of the previous work on LA-ICP-MS imaging maps of Se has been performed on mouse brains (Becker, Zoriy *et al.* 2008, Bishop, Clases *et al.* 2016).

5.3.9.1 Limit of detection

The LOD for each element for the LA-ICP-MS method used for quantitative analysis of broccoli leaves and the seeds are displayed in Table 5.3-4.

Average	^{77}Se mg/kg	^{78}Se mg/kg	^{82}Se mg/kg	^{66}Zn mg/kg
RMBr 5	0.52	0.53	0.69	0.18
RMBr 0	0.62	0.65	0.83	0.09
RMBr 10	0.62	0.59	0.68	0.10
RMBr 25	0.69	0.56	0.70	0.09
RMBr 50	0.81	0.65	0.80	0.10
Mean	0.613	0.597	0.742	0.112
SD	0.060	0.045	0.062	0.032
RSD	9.9%	7.6%	8.4%	28.8%

Table 5.3-4: LOD for ^{77}Se , ^{78}Se , ^{82}Se and ^{66}Zn for the LA-ICP-MS imaging method

The data presented in Table 5.3-4 demonstrates that a decrease in collision gas (He) flow rate to 3.5L/min dramatically improves the limit of detection for ^{78}Se . Table 4.3-11 in Chapter 4, Section 4.3.5.1, reports a LOD for ^{78}Se of 9.22mg/kg at a collision gas flow rate of 4.4L/min. However, this improvement is not observed with ^{66}Zn , as similar LOD were seen at both collision gas flow rates.

5.4 Conclusion

The work presented in this Chapter demonstrates that broccoli sprouts are hyper-accumulators of Se and produce Se-amino acids, which are known to have anticancer properties. It has also been demonstrated that LA-ICP-MS is a very suitable imaging technique for tracking Se isotope movement in plant material. LA-ICP-MS has been used for a number of different applications for plant studies including monitoring the uptake by hyper-accumulators (Callahan, Hare *et al.* 2016, Wu, Becker 2012) and for Se content in plants (Oliveira, Arruda 2015, Oseas da Silva, Zezzi Arruda 2012, Oseas da Silva, Zezzi Arruda 2013). Very little work has been performed on Se and distribution imaging on plants.

Accurate determination of Se will always be problematic due to low concentrations of Se in the sample and instability of Se compounds during analysis (Cuderman, Stibilj 2010). Stability of selenium species has been well documented over the years, including long term stability studies in aqueous solution (Olivas, Quevauviller *et al.* 1998), oyster extracts (Moreno, Quijano *et al.* 2002) and plant extracts (Cuderman, Stibilj 2010). Various strategies have been implemented for the sample preparation (Mahn, Zamorano *et al.* 2012, Mesko, Hartwig *et al.* 2011), to produce the most accurate selenium speciation results, including enzyme digestion (Mao, Hu *et al.* 2012), acid extraction (Montes-Bayon, Molet *et al.* 2006), buffer extraction (Montes-Bayon, Molet *et al.* 2006) and microwave digestion (Kolachi, Kazi *et al.* 2010a, Kolachi, Kazi *et al.* 2010b, Kolachi, Kazi *et al.* 2011, Chan, Afton *et al.* 2010). Montes-Bayon *et al.* 2006 concluded that there was no significant difference between enzymic, acid or buffer extraction when identifying selenium species. For this reason, LA-ICP-MS offers a great advantage, as very little sample preparation is required and the risk of conversion to other species and destruction of the Se is reduced. The HPLC data presented in this

Chapter is inconclusive and repeats would have to be performed. A number of other studies have successfully employed ESI MS (electrospray MS) to identify various organo-seleno molecules (Bianga, Govasmark *et al.* 2013, Kápolna, Hillestrøm *et al.* 2009, Zhou, Smith *et al.* 2000, Kotrebai, Tyson *et al.* 2000, Kotrebai, Birringer *et al.* 1999a, Casal, Far *et al.* 2010).

More recent studies have been on the effects of the more toxic Se compound, sodium selenite (Na_2SeO_3), and the uptake and metabolism in comparison to applying sodium selenate (Wang, Wang *et al.* 2012).

Hydroponics is an excellent method for biofortification of plants as there is more control over the exposure of the plant to the element of interest. The human recommended daily intake (RSI) for Se is 55-400 μg per day, with toxicity occurring above 700 μg per day (Gómez-Galera, Rojas *et al.* 2010). Previous studies (Table 5.3-1) have shown very high application levels, resulting in tissue concentration being above the RSI, although these plants could be used for the production of pharmaceuticals and extraction of anticancer compounds. It is clear from this study and previous studies, that the application method of the sodium selenate influences the accumulation, and further investigation into the effects of the application method on the production of the various seleno-amino acids is required. Analysis of the seeds for Se content and species, pre-germination would also be beneficial and allow a better understanding on the metabolism and accumulation.

As no negative effect on productivity from the application of sodium selenate at 20 $\mu\text{g}/\text{l}$ was observed, it can be concluded that this method of application and at this concentration Se enriched broccoli sprouts can be grown.

5.5 References

- ABDULAH, R., FARIED, A., KOBAYASHI, K., YAMAZAKI, C., SURADJI, E.W., ITO, K., SUZUKI, K., MURAKAMI, M., KUWANO, H. and KOYAMA, H., 2009. Selenium enrichment of broccoli sprout extract increases chemosensitivity and apoptosis of LNCaP prostate cancer cells. *BMC Cancer*, **9**, pp. 414.
- BANUELOS, G.S., 2002. Irrigation of broccoli and canola with boron- and selenium-laden effluent. *Journal of Environmental Quality*, **31**(6), pp. 1802-1808.
- BECKER, J.S., DIETRICH, R.C., MATUSCH, A., POZEBON, D. and DRESSIER, V.L., 2008. Quantitative images of metals in plant tissues measured by laser ablation inductively coupled plasma mass spectrometry. *Spectrochimica Acta Part B-Atomic Spectroscopy*, **63**(11), pp. 1248-1252.
- BECKER, J.S., MATUSCH, A. and WU, B., 2014. Bioimaging mass spectrometry of trace elements – recent advance and applications of LA-ICP-MS: A review. *Analytica Chimica Acta*, **835**(0), pp. 1-18.
- BECKER, J.S., ZORIY, M., DRESSLER, V.L., WU, B. and BECKER, J.S., 2008. Imaging of metals and metal-containing species in biological tissues and on gels by laser ablation inductively coupled plasma mass spectrometry (LA-ICP-MS): A new analytical strategy for applications in life sciences. *Pure and Applied Chemistry*, **80**(12), pp. 2643-2655.
- BIANGA, J., GOVASMAR, E. and SZPUNAR, J., 2013. Characterization of Selenium Incorporation into Wheat Proteins by Two-Dimensional Gel Electrophoresis-Laser Ablation ICP MS followed by capillary HPLC-ICP MS and Electrospray Linear Trap Quadrupole Orbitrap MS. *Analytical Chemistry*, **85**(4), pp. 2037-2043.
- BIRD, S.M., GE, H.H., UDEN, P.C., TYSON, J.F., BLOCK, E. and DENOYER, E., 1997. High-performance liquid chromatography of selenoamino acids and organo selenium compounds - Speciation by inductively coupled plasma mass spectrometry. *Journal of Chromatography a*, **789**(1-2), pp. 349-359.
- BISHOP, D.P., CLASES, D., FRYER, F., WILLIAMS, E., WILKINS, S., HARE, D.J., COLE, N., KARST, U. and DOBLE, P.A., 2016. Elemental bio-imaging using laser ablation-triple quadrupole-ICP-MS. *Journal of Analytical Atomic Spectrometry*, **31**(1), pp. 197-202.
- BAUER, G., LIMBECK, A., 2015. Quantitative analysis of trace elements in environmental powders with laser ablation inductively coupled mass spectrometry using non-sample-corresponding reference materials for signal evaluation. *Spectrochimica Acta Part B*, **113**, pp 63-69.
- CALLAHAN, D.L., HARE, D.J., BISHOP, D.P., DOBLE, P.A. and ROESSNER, U., 2016. Elemental imaging of leaves from the metal hyperaccumulating plant *Nocca caerulea* shows different spatial distribution of Ni, Zn and Cd. *RSC Advances*, **6**(3), pp. 2337-2344.

- CASAL, S.G., FAR, J., BIERLA, K., OUERDANE, L. and SZPUNAR, J., 2010. Study of the Se-containing metabolomes in Se-rich yeast by size-exclusion-cation-exchange HPLC with the parallel ICP MS and electrospray orbital ion trap detection. *Metallomics*, **2**(8), pp. 535-548.
- CHAN, Q., AFTON, S.E. and CARUSO, J.A., 2010. Selenium speciation profiles in selenite-enriched soybean (Glycine Max) by HPLC-ICPMS and ESI-ITMS. *Metallomics*, **2**(2), pp. 147-153.
- CHARRON, C., KOPSELL, D., RANDLE, W. and SAMS, C., 2001. Sodium selenate fertilisation increases selenium accumulation and decreases glucosinolate concentration in rapid-cycling Brassica oleracea. *Journal of the Science of Food and Agriculture*, **81**(9), pp. 962-966.
- CIZDZIEL, J., BU, K. and NOWINSKI, P., 2012. Determination of elements in situ in green leaves by laser ablation ICP-MS using pressed reference materials for calibration. *Analytical Methods*, **4**(2), pp. 564.
- COMPERNOLLE, S., WAMANUKUL, W., DE RAEDT, I. AND VANHAECKE, F. (2012). Evaluation of a combination of isotope dilution and single standard addition as an alternative calibration method for the determination of precious metals in lead fire assay buttons by laser ablation-inductively coupled plasma-mass spectrometry. *Spectrochimica Acta Part B: Atomic Spectroscopy*, **67**, pp 50-56.
- CUDERMAN, P. and STIBILJ, V., 2010. Stability of Se species in plant extracts rich in phenolic substances. *Analytical and Bioanalytical Chemistry*, **396**(4), pp. 1433-1439.
- ENCINAR, J.R., SLIWKA-KASZYNSKA, M., POLATAJKO, A., VACCHINA, V. and SZPUNAR, J., 2003. Methodological advances for selenium speciation analysis in yeast. *Analytica Chimica Acta*, **500**(1-2), pp. 171-183.
- FAHEY, J.W., ZHANG, Y.S. and TALALAY, P., 1997. Broccoli sprouts: An exceptionally rich source of inducers of enzymes that protect against chemical carcinogens. *Proceedings of the National Academy of Sciences of the United States of America*, **94**(19), pp. 10367-10372.
- FINLEY, J.W., IP, C., LISK, D.J., DAVIS, C.D., HINTZE, K.J. and WHANGER, P.D., 2001. Cancer-protective properties of high-selenium broccoli. *Journal of Agricultural and Food Chemistry*, **49**(5), pp. 2679-2683.
- FINLEY, J.W., SIGRID-KECK, A., ROBBINS, R.J. and HINTZE, K.J., 2005. Selenium enrichment of broccoli: Interactions between selenium and secondary plant compounds. *Journal of Nutrition*, **135**(5), pp. 1236-1238.
- GERM, M., STIBILJ, V. and KREFT, I., 2007. Metabolic importance of selenium for plants. *Eur J Plant Sci Biotechnol*, **1**(1), pp. 91-97.
- GILBERT, S.E., DANYUSHEVSKY, L.V., RODEMANN, T., SHIMIZU, N., GURENKO, A., MEFFRE, S., THOMAS, H., LARGE, R.R. and DEATH, D., 2014. Optimisation of laser parameters for the analysis of sulphur isotopes in sulphide

minerals by laser ablation ICP-MS. *Journal of Analytical Atomic Spectrometry*, **29**(6), pp. 1042-1051.

GOMES, M.S., SCHENK, E.R., SANTOS JR., D., KRUG, F.J. and ALMIRALL, J.R., 2014. Laser ablation inductively coupled plasma optical emission spectrometry for analysis of pellets of plant materials. *Spectrochimica Acta Part B: Atomic Spectroscopy*, **94–95**(0), pp. 27-33.

GÓMEZ-GALERA, S., ROJAS, E., SUDHAKAR, D., ZHU, C., PELACHO, A.M., CAPELL, T. and CHRISTOU, P., 2010. Critical evaluation of strategies for mineral fortification of staple food crops. *Transgenic Research*, **19**(2), pp. 165-180.

GU, Y., GUO, Q., ZHANG, L., CHEN, Z., HAN, Y. and GU, Z., 2012. Physiological and Biochemical Metabolism of Germinating Broccoli Seeds and Sprouts. *Journal of Agricultural and Food Chemistry*, **60**(1), pp. 209-213.

HABERHAUER-TROYER, C., ALVAREZ-LLAMAS, G., ZITTING, E., RODRIGUEZ-GONZALEZ, P., ROSENBERG, E. and SANZ-MEDEL, A., 2003. Comparison of different chloroformates for the derivatisation of seleno amino acids for gas chromatographic analysis. *Journal of Chromatography a*, **1015**(1-2), pp. 1-10.

HAJIBOLAND, R. and AMJAD, L., 2008. The effects of selenate and sulfate supply on the accumulation and volatilization of Se by cabbage, kohlrabi and alfalfa plants grown hydroponically. *Agricultural and Food Science*, **17**(2), pp. 177-189.

HANĆ, A., OLSZEWSKA, A. and BARAŁKIEWICZ, D. (2013). Quantitative analysis of elements migration in human teeth with and without filling using LA-ICP-MS. *Microchemical Journal*, **110** 61-69.

HAUDER, J., WINKER, S., BUB, A., RUEIFER, C.E., PIGNITTER, M. and SOMOZA, V., 2011. LC-MS/MS Quantification of Sulforaphane and Indole-3-carbinol Metabolites in Human Plasma and Urine after Dietary Intake of Selenium-Fortified Broccoli. *Journal of Agricultural and Food Chemistry*, **59**(15), pp. 8047-8057.

HIRATA, J. TAKAHASHI, K. and TANAKE, M. (2013). Determination Method of Multi Elements in Ferromanganese Samples by LA-ICP-MS. *Analytical Sciences*, **29** (1), pp. 151-155.

HSU, F., WIRTZ, M., HEPPEL, S.C., BOGS, J., KRAEMER, U., KHAN, M.S., BUB, A., HELL, R. and RAUSCH, T., 2011. Generation of Se-fortified broccoli as functional food: impact of Se fertilization on S metabolism. *Plant Cell and Environment*, **34**(2), pp. 192-207.

JUROWSKI, K., SZEWCZYK, M., PIEKOSZEWSKI, W., HERMAN, M., SZEWCZYK, B., NOWAK, G., WALAS, S., MILISZKIEWICZ, N., TOBIASZ, A. and DOBROWOLSKA-IWANEK, J., 2014. A standard sample preparation and calibration procedure for imaging zinc and magnesium in rats' brain tissue by laser ablation-inductively coupled plasma-time of flight-mass spectrometry. *Journal of Analytical Atomic Spectrometry*, **29**(8), pp. 1425-1431.

- KÁPOLNA, E., SHAH, M., CARUSO, J.A. and FODOR, P., 2007. Selenium speciation studies in Se-enriched chives (*Allium schoenoprasum*) by HPLC-ICP-MS. *Food Chemistry*, **101**(4), pp. 1398-1406.
- KÁPOLNA, E., HILLESTRØM, P.R., LAURSEN, K.H., HUSTED, S. and LARSEN, E.H., 2009. Effect of foliar application of selenium on its uptake and speciation in carrot. *Food Chemistry*, **115**(4), pp. 1357-1363.
- KIM, H.S. and JUVIK, J.A., 2011. Effect of Selenium Fertilization and Methyl Jasmonate Treatment on Glucosinolate Accumulation in Broccoli Florets. *Journal of the American Society for Horticultural Science*, **136**(4), pp. 239-246.
- KOLACHI, N.F., KAZI, T.G., AFRIDI, H.I., KHAN, S., WADHWA, S.K., SHAH, A.Q., SHAH, F., BAIG, J.A. and SIRAJUDDIN, 2010a. Determination of selenium content in aqueous extract of medicinal plants used as herbal supplement for cancer patients. *Food and Chemical Toxicology*, **48**(12), pp. 3327-3332.
- KOLACHI, N.F., KAZI, T.G., AFRIDI, H.I., KHAN, S., BAIG, J.A., WADHWA, S.K., SHAH, A.Q. and SHAH, F., 2011. Development of Extraction Methods for Speciation Analysis of Selenium in Aqueous Extracts of Medicinal Plants. *Journal of AOAC International*, **94**(4), pp. 1069-1075.
- KOLACHI, N.F., KAZI, T.G., BAIG, J.A., KANDHRO, G.A., KHAN, S., AFRIDI, H.I., KUMAR, S. and SHAH, A.Q., 2010b. Microwave-Assisted Acid Extraction of Selenium from Medicinal Plants Followed by Electrothermal Atomic Absorption Spectrometric Determination. *Journal of AOAC International*, **93**(2), pp. 694-702.
- KOTREBAI, M., TYSON, J.F., BLOCK, E. and UDEN, P.C., 2000. High-performance liquid chromatography of selenium compounds utilizing perfluorinated carboxylic acid ion-pairing agents and inductively coupled plasma and electrospray ionization mass spectrometric detection. *Journal of Chromatography A*, **866**(1), pp. 51-63.
- KOTREBAI, M., BIRNINGER, M., TYSON, J.F., BLOCK, E. and UDEN, P.C., 1999a. Identification of the principal selenium compounds in selenium-enriched natural sample extracts by ion-pair liquid chromatography with inductively coupled plasma- and electrospray ionization-mass spectrometric detection. *Analytical Communications*, **36**(6), pp. 249-252.
- KOTREBAI, M., BIRNINGER, M., TYSON, J.F., BLOCK, E. and UDEN, P.C., 1999b. Selenium speciation in enriched and natural samples by HPLC-ICP-MS and HPLC-ESI-MS with perfluorinated carboxylic acid ion-pairing agents. *Analyst*, **125**(1),.
- KÖTSCHAU, A., BÜCHEL, G., EINAX, J.W., FISCHER, C., VON TÜMPLING, W. and MERTEN, D., 2013. Mapping of macro and micro elements in the leaves of sunflower (*Helianthus annuus*) by Laser Ablation-ICP-MS. *Microchemical Journal*, **110**(0), pp. 783-789.
- LI, Y., HU, B., HE, M. and XIANG, G., 2008. Simultaneous speciation of inorganic selenium and antimony in water samples by electrothermal vaporization inductively

coupled plasma mass spectrometry following selective cloud point extraction. *Water Research*, **42**(4), pp. 1195-1203.

LI, D., WANG, W., SHAN, Y., BARRERA, L.N., HOWIE, A.F., BECKETT, G.J., WU, K. and BAO, Y., 2012. Synergy between sulforaphane and selenium in the up-regulation of thioredoxin reductase and protection against hydrogen peroxide-induced cell death in human hepatocytes. *Food Chemistry*, **133**(2), pp. 300-307.

LI, D., WU, K., HOWIE, A.F., BECKETT, G.J., WANG, W. and BAO, Y., 2008. Synergy between broccoli sprout extract and selenium in the upregulation of thioredoxin reductase in human hepatocytes. *Food Chemistry*, **110**(1), pp. 193-198.

LIMECK, A., GALLER, P., BONTA, M., BAUER, G., NISCHKAUER, W., and VANHAECKE, F., 2015. Recent advances in quantitative LA-ICP-MS analysis: challenges and solutions in the life sciences and environmental chemistry, *Analytical Biochemistry*, **407**, pp. 6593-6617.

LOBINSKI, R., SCHAUMLOFFEL, D. and SZPUNAR, J., 2006. Mass spectrometry in bioinorganic analytical chemistry. *Mass Spectrometry Reviews*, **25**(2), pp. 255-289.

LONGERICH, H.P., JACKSON, S.E. and GUNTHER, D., 1996. Inter-laboratory note. Laser ablation inductively coupled plasma mass spectrometric transient signal data acquisition and analyte concentration calculation. *Journal of Analytical Atomic Spectrometry*, **11**(9), pp. 899-904.

LYI, S., HELLER, L., RUTZKE, M., WELCH, R., KOCHIAN, L. and LI, L., 2005. Molecular and biochemical characterization of the selenocysteine Se-methyltransferase gene and Se-methylselenocysteine synthesis in broccoli. *Plant Physiology*, **138**(1), pp. 409-420.

LYONS, G., STANGOULIS, J. and GRAHAM, R., 2003. High-selenium wheat: biofortification for better health. *Nutrition Research Reviews*, **16**(1), pp. 45-60.

MAHN, A., ZAMORANO, M., BARRIENTOS, H. and REYES, A., 2012. Optimization of a process to obtain selenium-enriched freeze-dried broccoli with high antioxidant properties. *LWT - Food Science and Technology*, **47**(2), pp. 267-273.

MAO, X., HU, B., HE, M. and CHEN, B., 2012. High polar organic-inorganic hybrid coating stir bar sorptive extraction combined with high performance liquid chromatography-inductively coupled plasma mass spectrometry for the speciation of seleno-amino acids and seleno-oligopeptides in biological samples. *Journal of Chromatography A*, **1256**(0), pp. 32-39.

MATUSHESKI, N.V., WALLIG, M.A., JUVIK, J.A., KLEIN, B.P., KUSHAD, M.M. and JEFFERY, E.H., 2001. Preparative HPLC method for the purification of sulforaphane and sulforaphane nitrile from *Brassica oleracea*. *Journal of Agricultural and Food Chemistry*, **49**(4), pp. 1867-1872.

MCCURDY, E. and WOODS, G., 2004. The application of collision/reaction cell inductively coupled plasma mass spectrometry to multi-element analysis in variable

sample matrices, using He as a non-reactive cell gas. *Journal of Analytical Atomic Spectrometry*, **19**(5), pp. 607-615.

MESKO, M.F., HARTWIG, C.A., BIZZI, C.A., PEREIRA, J.S.F., MELLO, P.A. and FLORES, E.M.M., 2011. Sample preparation strategies for bioinorganic analysis by inductively coupled plasma mass spectrometry. *International Journal of Mass Spectrometry*, **307**(1-3), pp. 123-136.

MILISZKIEWICZ, N., WALAS, S. AND TOBIASZ, A., 2015. Current approaches to calibration of LA-ICP-MS analysis. *Journal of Analytical Atomic Spectrometry*, **30**, 327-338.

MONTES-BAYON, M., MOLET, M.J.D., GONZALEZ, E.B. and SANZ-MEDEL, A., 2006. Evaluation of different sample extraction strategies for selenium determination in selenium-enriched plants (*Allium sativum* and *Brassica juncea*) and Se speciation by HPLC-ICP-MS. *Talanta*, **68**(4), pp. 1287-1293.

MORENO, P., QUIJANO, M., GUTIÉRREZ, A., PÉREZ-CONDE, M. and CAMARA, C., 2002. Stability of total selenium and selenium species in lyophilised oysters and in their enzymatic extracts. *Analytical and Bioanalytical Chemistry*, **374**(3), pp. 466-476.

OLIVAS, R.M., QUEVAUVILLER, P. and DONARD, O.F., 1998. Long term stability of organic selenium species in aqueous solutions. *Fresenius' Journal of Analytical Chemistry*, **360**(5), pp. 512-519.

OLIVAS, R., DONARD, O., GILON, N. and POTINGAUTIER, M., 1996b. Speciation of organic selenium compounds by high-performance liquid chromatography inductively coupled plasma mass spectrometry in natural samples. *Journal of Analytical Atomic Spectrometry*, **11**(12), pp. 1171-1176.

OLIVEIRA, S.R. and ARRUDA, M.A.Z., 2015. Application of laser ablation (imaging) inductively coupled plasma mass spectrometry for mapping and quantifying Fe in transgenic and non-transgenic soybean leaves. *Journal of Analytical Atomic Spectrometry*, **30**(2), pp. 389-395.

OSEAS DA SILVA, M.A., LOPEZ DE ANDRADE, S.A., MAZZAFERA, P. and ZEZZI ARRUDA, M.A., 2011. Evaluation of sunflower metabolism from zinc and selenium addition to the culture: A comparative metallomic study. *International Journal of Mass Spectrometry*, **307**(1-3), pp. 55-60.

OSEAS DA SILVA, M.A. and ZEZZI ARRUDA, M.A., 2013. Laser ablation (imaging) for mapping and determining Se and S in sunflower leaves. *Metallomics*, **5**(1), pp. 62-67.

OSEAS DA SILVA, M.A. and ZEZZI ARRUDA, M.A., 2012. Identification of selenium in the leaf protein of sunflowers by a combination of 2D-PAGE and laser ablation ICP-MS. *Microchimica Acta*, **176**(1-2), pp. 131-136.

PATON, C., HELLSTROM, J., - PAUL, B., - WOODHEAD, J. and -HERGT, J., 2011. Iolite: Freeware for the visualisation and processing of mass spectrometric data. *Journal of Analytical Atomic Spectrometry*, **26**(12), pp. 2508.

PEDRERO, Z., ELVIRA, D., CAMARA, C. and MADRID, Y., 2007. Selenium transformation studies during Broccoli (*Brassica oleracea*) growing process by liquid chromatography-inductively coupled plasma mass spectrometry (LC-ICP-MS). *Analytica Chimica Acta*, **596**(2), pp. 251-256.

PILON-SMITS, E.A. and QUINN, C.F., 2010. Selenium metabolism in plants. *Cell biology of Metals and Nutrients*. Springer, pp. 225-241.

PUNSHON, T., JACKSON, B., BERTSCH, P. and BURGER, J., 2004. Mass loading of nickel and uranium on plant surfaces: application of laser ablation-ICP-MS. *Journal of Environmental Monitoring*, **6**(2), pp. 153-159.

QUARLES, C.D., Jr., JONES, D.R., JARRETT, J.M., SHAKIROVA, G., PAN, Y., CALDWELL, K.L. and JONES, R.L., 2014. Analytical method for total chromium and nickel in urine using an inductively coupled plasma-universal cell technology-mass spectrometer (ICP-UCT-MS) in kinetic energy discrimination (KED) mode. *Journal of Analytical Atomic Spectrometry*, **29**(2), pp. 297-303.

RAYMAN, M.P., INFANTE, H.G. and SARGENT, M., 2008. Food-chain selenium and human health: spotlight on speciation. *British Journal of Nutrition*, **100**(2), pp. 238-253.

ROBBINS, R.J., KECK, A.S., BANUELOS, G. and FINLEY, J.W., 2005. Cultivation conditions and selenium fertilization alter the phenolic profile, glucosinolate, and sulforaphane content of broccoli. *Journal of Medicinal Food*, **8**(2), pp. 204-214.

RODRIGUEZ-CASTRILLON, J., REYES, L.H., MARCHANTE-GAYON, J., MOLDOVAN, M. and GARCIA ALONSO, J.I., 2008. Internal correction of spectral interferences and mass bias in ICP-MS using isotope pattern deconvolution: Application to the determination of selenium in biological samples by isotope dilution analysis. *Journal of Analytical Atomic Spectrometry*, **23**(4), pp. 579-582.

SATHE, S.K., MASON, A.C., RODIBAUGH, R. and WEAVER, C.M., 1992. Chemical Form of Selenium in Soybean (*Glycine-Max L*) Lectin. *Journal of Agricultural and Food Chemistry*, **40**(11), pp. 2084-2091.

SIMMONS, J., KRYUKOVA, A., XIE, Q. and MOODY, R., 2008. Interferences in ICP-MS Analysis and How to Deal With Them, 2008.

SORS, T., ELLIS, D. and SALT, D., 2005. Selenium uptake, translocation, assimilation and metabolic fate in plants. *Photosynthesis Research*, **86**(3), pp. 373-389.

STANKOVA, A. GILON, N. DUTRUCH, L. and KANICKY, V. 2011. Comparaison of LA-ICP-MS and ICP-OES for the analysis of some elements in fly ashes. *Journal of Analytical Atomic Spectrometry*, **26**, pp 443-449.

- THIRY, C., RUTTENS, A., DE TEMMERMAN, L., SCHNEIDER, Y. and PUSSEMIER, L., 2012. Current knowledge in species-related bioavailability of selenium in food. *Food Chemistry*, **130**(4), pp. 767-784.
- TOLER, H.D., CHARRON, C.S., SAMS, C.E. and RANDLE, W.R., 2007. Selenium increases sulfur uptake and regulates glucosinolate metabolism in rapid-cycling Brassica oleracea. *Journal of the American Society for Horticultural Science*, **132**(1), pp. 14-19.
- UDEN, P., BIRD, S., KOTREBAI, M., NOLIBOS, P., TYSON, J., BLOCK, E. and DENOYER, E., 1998. Analytical selenoamino acid studies by chromatography with interfaced atomic mass spectrometry and atomic emission spectral detection. *Fresenius Journal of Analytical Chemistry*, **362**(5), pp. 447-456.
- VERBRUGGEN, N., HERMANS, C. and SCHAT, H., 2009. Molecular mechanisms of metal hyperaccumulation in plants. *New Phytologist*, **181**(4), pp. 759-776.
- WANG, Y., WANG, X. and WONG, Y., 2012. Proteomics analysis reveals multiple regulatory mechanisms in response to selenium in rice. *Journal of proteomics*, **75**(6), pp. 1849-1866.
- WARD, N.I. DURRANT, S.F. and GRAY, A.L., 1992. Analysis of biological standard reference materials by laser ablation inductively coupled plasma mass spectrometry. *Journal of Analytical Atomic Spectrometry*, **7**, pp. 1139-1146.
- WU, B. and BECKER, J.S., 2012. Imaging techniques for elements and element species in plant science. *Metallomics*, **4**(5), pp. 403-416.
- WU, B., ZORIY, M., CHEN, Y. and BECKER, J.S., 2009. Imaging of nutrient elements in the leaves of *Elsholtzia splendens* by laser ablation inductively coupled plasma mass spectrometry (LA-ICP-MS). *Talanta*, **78**(1), pp. 132-137.
- WU, X.L. and PRIOR, R.L., 2005. Identification and characterization of anthocyanins by high-performance liquid chromatography-electrospray ionization-tandem mass spectrometry in common foods in the United States: Vegetables, nuts, and grains. *Journal of Agricultural and Food Chemistry*, **53**(8), pp. 3101-3113.
- XUE, Y., XIA, H., CHRISTIE, P., ZHANG, Z., LI, L. and TANG, C., 2016. Crop acquisition of phosphorus, iron and zinc from soil in cereal/legume intercropping systems: a critical review. *Annals of Botany*, **117**(3), pp. 363-77.
- YADEV, S., GUPTA, S., PRAKASH, R., SPALLHOLZ, J. and PRAKAS, N., 2007. Selenium uptake by *Allium cepa* grown in Se-spiked soils. *American-Eurasian Journal of Agriculture and Environment Science*, **2**(1), pp. 80-84.
- ZHANG, J.S., SVEHLIKOVA, V., BAO, Y.P., HOWIE, A.F., BECKETT, G.J. and WILLIAMSON, G., 2003. Synergy between sulforaphane and selenium in the induction of thioredoxin reductase 1 requires both transcriptional and translational modulation. *Carcinogenesis*, **24**(3), pp. 497-503.

ZHOU, Z.S., SMITH, A.E. and MATTHEWS, R.G., 2000. L-selenohomocysteine: One-step synthesis from L-selenomethionine and kinetic analysis as substrate for methionine synthases. *Bioorganic & Medicinal Chemistry Letters*, **10**(21), pp. 2471-2475.

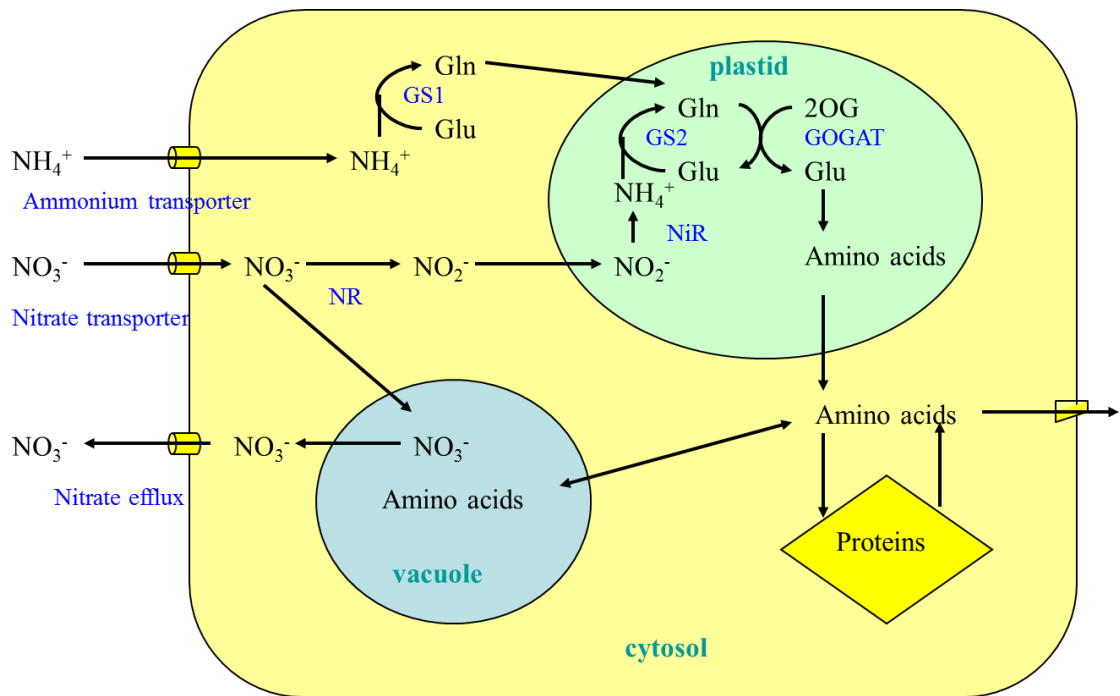
Chapter 6

6. The “Afterlife Experiment”: Use of MALDI-MS imaging for the study of the nitrogen cycle within plants

6.1 Introduction

In May 2011, the MS Imaging group at Sheffield Hallam University was approached by the BBC to take part in a project to demonstrate the science of decay (BBC 2011). Set up in Edinburgh Zoo in summer 2011, a fully equipped kitchen and garden, together with all the detritus from a family barbeque, was sealed in a glass box. As part of the experiment, the programme makers wished to demonstrate that decay and decomposition was only part of the story, with atoms and molecules from dead plants and animals being incorporated into new life. The television programme was given the title 'AfterLife: The strange science of decay', and was first aired on BBC4 on 6th December 2011 (<http://www.bbc.co.uk/programmes/b012w66t>). The MS imaging data was subsequently published (Seaman, Flinders *et al.* 2014).

The element nitrogen is a ubiquitous component of all living systems and is located, primarily, in amino acids, proteins, nucleic acids and, in plants, chlorophyll. Nitrogen is one of the principal nutritional requirements of all plants which acquire it through their root systems, usually in the form of nitrates or ammonia. Once the inorganic nitrogen has entered the plant either via passive or active transporters in the roots, a process of assimilation and reduction within the plant cells occurs (Figure 6.1-1). In the plant, the nitrate is quickly converted into nitrite and then ammonium ions which can be incorporated into amino acids or stored (Scott 2008). In the 1650's a German-Dutch chemist, Joanne Rudolph Glauber, first describes “nitrum” (nitrogen) as the “soul” or “embryo” of nitrate salts, known then as saltpetre (Keeney, Hatfield 2008).



Amino Acids

Gln = Glutamine

Glu = Glutamic acid

Enzymes

NiR = Ferredoxin dependent nitrite reductase

2OG = 2-Oxoglutarate

GOGAT = Glutamine oxoglutarate aminotransferase

GS1 = Glutamine synthase

GS2 = Glutamate synthase

NR = Nitrate reductase

Figure 6.1-1: A model of absorption and metabolism of ammonium and nitrate in plant root cell. (Image taken from :<http://www.intechopen.com/books/a-comprehensive-survey-of-international-soybean-research-genetics-physiology-agronomy-and-nitrogen-relationships/soybean-seed-production-and-nitrogen-nutrition>)

The nitrogen cycle (Figure 6.1-2) has been extensively documented, with research into the nitrogen cycle first started in the 19th century, (Table 6.1-1) with scientists, such as Boussingault, shaping modern agrochemistry (Keeney, Hatfield 2008).

Date	Scientist	Development
1780	Cavendish	Discovered that nitrogen from air would combine with oxygen to give oxides
1813	Davy	First recognised the beneficial effects of legumes on soil nitrogen production.
1830-1860	Boussingault	Determined that manures fertilizing properties came from the ammonium formed in the soil and taken up by plant roots.
1857	Liebig, Lawes, Gilbert & Pugh	First attempted to prove biological nitrogen fixation.
1882	Gayon & Dupetite	First demonstration of denitrification
1980-1890	Hellriegel & Wilfarath	Confirmed biological nitrogen fixation
1888	Beijerinck	Isolated <i>Rhizobia</i>
1890	Winogradsky	Identified <i>Clostridium</i>
1901	Beijerinck	Isolated <i>Azotobacter</i>
1902	King & Whitson	Documented: a) the effects of environmental variables on the rate of nitrification, b) the effects of cropping on profile nitrate concentrations, c) leaching of nitrates.
1910-1912	Beijerinck & Minkman. Suzuki	Identification of nitric oxide and nitrous oxide as being obligatory intermediates in denitrification and that organic matter was the major electron donor.
1913	Lohnis	First modern “N Cycle” published.
1917	Blair	Evaluation of fertilizer values of manures and compost leading to the publication of a “N cycle” that included abiotic reaction more ecosystems orientated.
1926	Lohnis	Identification of heterotrophic nitrification.
1927	Allison	Discovered the first nitrification inhibitors. (Cyanamides)
1940-1950	Bremner, Burris, Broadbent & Norman	Major developments in the use of the stable isotope ¹⁵ N in fertilizer research utilizing mass spectrometry.
1958	Jansson	Identification of ammonium playing the central role in mineralization-immobilization.
1965	Jansson & Persson	Confirmation of mineralization and immobilization of soil nitrogen.
1970		First computer generated mathematical models of the “N cycle”.
1982	Lad & Jackson	Reviewed the biochemistry of ammonification, proving the presence of extracellular enzymes such as soil urease.

Table 6.1-1: The history of the development of the nitrogen cycle (adapted from Keeney and Hatfield 2008).

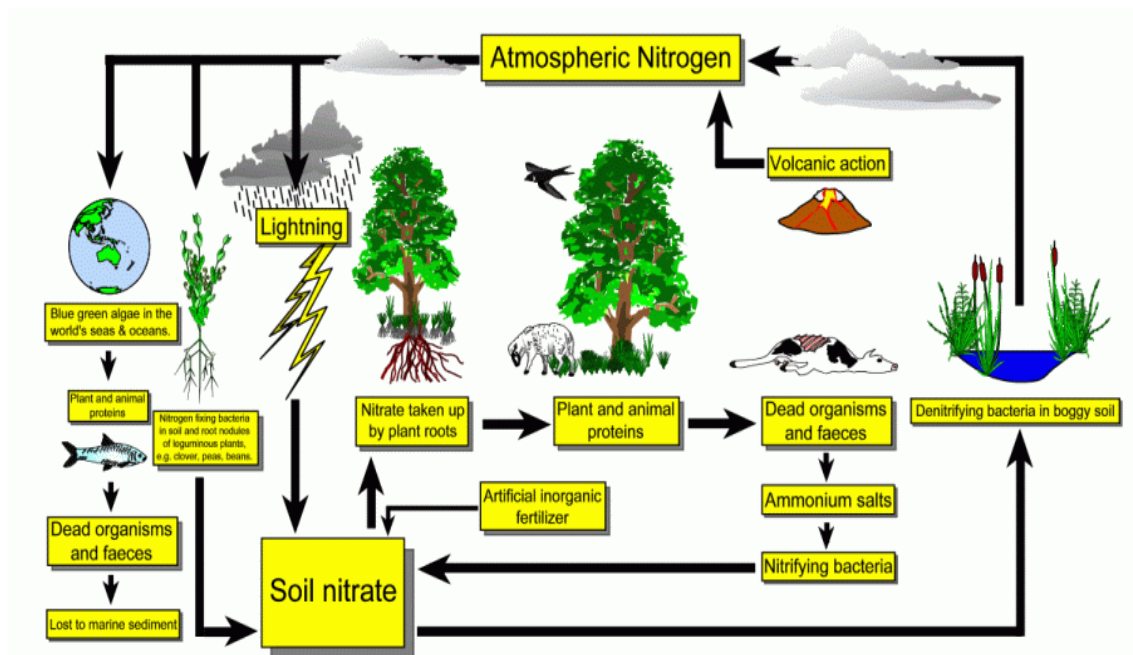


Figure 6.1-2: A diagrammatic representation of the nitrogen cycle.

(image taken from: <http://gozoneguide.com/nitrogen-cycle-diagram-worksheet/>)

There have been many studies of the uptake and metabolism of nitrogen by plants and many of these utilise the isotope ^{15}N ; this is a rare but stable isotope, with a natural abundance of 0.366% (0.00366 mole fractions) (Berglund, Wieser 2011, Dawson, Mambelli *et al.* 2002). Plant studies utilizing ^{15}N enriched KNO_3 material as a tracer in isotopic analysis are well documented, with techniques such as gas chromatography–mass spectrometry (GC-MS) (Keeney, Hatfield 2008) showing the quantitative analysis of proteins and metabolites, inductively coupled plasma-optical emission spectroscopy (ICP-OES) for routine analysis in agriculture (Fiedler, Proksch 1972), microwave induced plasma-optical emission spectroscopy (MIP-OES) for studies into soil ecology (Heltai, Jozsa 1995), nuclear magnetic resonance (NMR) to monitor microbial degradation (Knicker, Lüdemann 1995), liquid chromatography-tandem mass spectrometry (LC-MS/MS) in quantitative protein studies (Engelsberger, Erban *et al.*

2006), multi-isotope imaging mass spectrometry (MIMS) for the quantitative imaging of nitrogen fixation (Lechene, Luyten *et al.* 2007) and secondary ion mass spectrometry (SIMS) to demonstrate the localization of elements in leaves (Grignon, Halpern *et al.* 1997) have all been employed. Furthermore, it has been used in agricultural research to trace mineral nitrogen compounds (particularly fertilizers) in the environment and is also a very important tracer for describing the fate of nitrogenous organic pollutants (Marsh, Sims *et al.* 2005, Bichat, Sims *et al.* 1999).

Matrix-assisted laser/desorption ionisation-mass spectrometry imaging (MALDI-MSI) is an emerging technique within plant biology (Kaspar, Peukert *et al.* 2011). In the past MALDI-MSI has been used to illustrate the distribution of various plant metabolites (Lee, Perdian *et al.* 2012, Burrell, Earnshaw *et al.* 2007, Li, Shrestha *et al.* 2008), including carbohydrates (Robinson, Warburton *et al.* 2007), oligosaccharides (Wang, Sporns *et al.* 1999), proteins (Grassl, Taylor *et al.* 2011, Schwartz, Reyzer *et al.* 2003), lipids (Vrkoslav, Muck *et al.* 2010, Horn, Korte *et al.* 2012), peptides (Kondo, Sawa *et al.* 2006), pesticides (Anderson, Carolan *et al.* 2009) and various agrochemicals (Mullen, Clench *et al.* 2005) within plant tissue. Until now the use of this technique to study nutrient cycles within plants has not been described. The work reported here aimed to demonstrate that mass spectrometry imaging is a valuable tool in the tracking of the distribution of ^{15}N labelled compounds and can be used to show uptake of species from dead organisms by living ones.

6.2 Materials and Methods

6.2.1 Materials

Alpha-cyano-4-hydroxycinnamic acid (CHCA), choline chloride, 99%, 4-aminobutyric acid, 99+%, methanol, acetonitrile, trifluoroacetic acid (TFA) (AR Grade), were purchased from Fisher Scientific (Loughborough, UK). Calcium chloride, calcium sulphate, magnesium sulphate, potassium phosphate and a trace element mix were all purchased from Hortifeeds (Lincoln, UK). 2, 5-dihydroxybenzoic acid (DHB), potassium nitrate- ^{15}N 98 atom % ^{15}N (^{15}N - KNO_3), potassium nitrate ReagentPlus® $\geq 99.0\%$ were purchased from Sigma-Aldrich (Gillingham, UK).

6.2.2 Cultivation

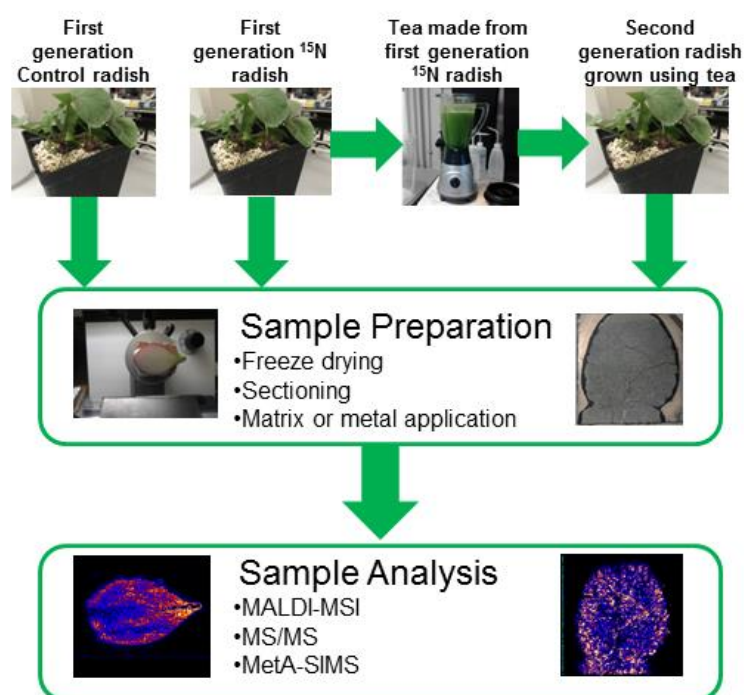


Figure 6.2-1: Experimental workflow used in this study.

Two groups of radish seeds (*Raphanus sativus*) were sown separately in a mix of perlite and vermiculite (4:3) in an artificially controlled environment. Initially, the environment was maintained at a temperature of 21°C, with an average humidity of 80%, under 24hr fluorescent (120W) light. Once germination had occurred, the light cycle was altered to 18 hours of light and the intensity increased (600W), with an average humidity of 65%. The control group utilized a nutrient system containing standard KNO₃ and the first generation ¹⁵N group replaced all of the KNO₃ with ¹⁵N-KNO₃ (98% labelled) as the only source of nitrogen. The pH of the solution was maintained at 6.0 and a conductivity (CF) of 12. Irrigation of the plants occurred once every 24 hours for 9 minutes. Plants were cropped, homogenised and left to ferment in ultra-pure water (18.2 MΩcm) obtained from a Purelab ultra water purification system (Elga, Ransbach-Baumbach, Germany) for two weeks to create a "tea". The "tea" was used as the only source of nitrogen for a second hydroponics experiment (second generation ¹⁵N group) where radishes were again grown in an artificially controlled environment. After five weeks of growth the radish plants were harvested. Samples of leaves, bulbs, and stems from each group (control, first generation ¹⁵N and second generation ¹⁵N) were cryosectioned and sections imaged by positive ion MALDI and SIMS imaging (Figure 6.2-1).

6.2.3 Sample preparation

The radishes were harvested and the bulbs separated from the roots and leaves and snap frozen in liquid nitrogen. The frozen radish bulbs were sectioned at a temperature of -20°C using a Leica Cryostat (Leica, Wetzlar, Germany) to obtain 12 μm sections, which were then thaw mounted onto glass slides and indium tin oxide (ITO) coated glass slides (4-8 Ω resistance, Delta Technologies, Stillwater, MN, USA). Leaves were prepared by placing fresh samples between tissue paper and pressing between two glass

slides. The slides were taped together and placed into a freeze drier at -36°C until they reached a constant mass, taking approximately ten days. The dried leaves were carefully removed from between the tissue paper and mounted onto either aluminium target plates or glass slides using double sided carbon tape to adhere the sample.

6.2.4 Matrix assisted laser desorption/ionisation mass spectrometry matrix deposition

Samples for MALDI were coated with a 5mg/ml solution of CHCA in 70:30 methanol: water with 0.2% TFA using the SuncollectTM automated pneumatic sprayer (Sunchrom GmbH, Friedrichsdorf, Germany) in a series of 10 layers. The initial seeding layer was performed at 2 μl /minute and subsequent layers were performed at 3 μl /minute. Some samples were coated with a 20 mg/ml solution of DHB in 50:50 acetonitrile: water with 0.2% TFA using the SuncollectTM automated pneumatic sprayer in a series of 30 layers. The initial seeding layer was performed at 10 μl /minute then stepped up to 20 μl /minute and subsequent layers were performed at 30 μl /minute.

6.2.5 Secondary ion mass spectrometry (SIMS) sample gold coating

Meta-SIMS imaging of the radish was performed by the FOM Institute AMOLF, Science Park 104, 1098 XG Amsterdam, The Netherlands. Prior to analysis the radish bulb sections were gold coated using a Quorum Technologies SC 7640 sputter coater (New Haven, USA) equipped with a FT7607 quartz crystal microbalance stage and FT690 film thickness monitor to deposit a 1 nm thick gold layer.

6.3 Instrumentation

6.3.1 Applied Biosystems Q-Star Pulsar I

Initial mass spectrometric analyses were performed using an Applied Biosystems API Q-Star Pulsar i hybrid quadrupole time-of-flight (QTOF) instrument (Concord, Ontario, Canada) fitted with an orthogonal MALDI ion source and a 1 kHz Nd:YAG solid-state laser. Images were acquired at a spatial resolution of 150 μ m x 150 μ m in “raster image” mode (Trim, Djidja *et al.* 2010), using ‘oMALDI Server 5.1’ software supplied by MDS Sciex (Concord, Ontario, Canada) and generated using the freely available Biomap 3.7.5.5 software (Novartis, Basel, Switzerland). Mass spectra were processed either in Analyst MDS Sciex (Concord, Ontario, Canada) or using the open source multifunctional mass spectrometry software mMass (Strohalm, Kavan *et al.* 2010).

MALDI-MS spectra were obtained in positive ion mode in the mass range between m/z 50 and 1000. Declustering potential 2 was set at 15 arbitrary units and the focus potential at 10 arbitrary units, with an accumulation time of 0.999 sec. Average spectra were acquired over a 0.5 cm² region on the leaves. The MALDI-MS/MS spectrum of the unknown precursor ions at m/z 104.1.1 and 105.1.1 was obtained using argon as the collision gas; the declustering potential 2 was set at 15 and the focusing potential at 20, and the collision energy and the collision gas pressure were set at 20 and 5 arbitrary units, respectively.

6.3.2 Waters Synapt G2 HDMS

Further MALDI data were acquired using a Waters MALDI SYNAPT™ G2 HDMS mass spectrometer (Waters Corporation, Manchester, UK) to acquire mass spectra and images. Prior to MALDI-MSI analysis the samples were optically scanned using a flatbed scanner to produce a digital image for future reference, this image was then imported into the

MALDI imaging pattern creator software (Waters Corporation) to define the region to be imaged. The instrument was calibrated prior to analysis using a standard mixture of polyethylene glycol. The instrument was operated in V-mode and positive ion mode, all data was acquired in the mass range m/z 100 to 500. The data was then converted using MALDI imaging converter software (Waters Corporation) and visualised using the BioMap 3.7.5.5 software (Novartis, Basel, Switzerland).

6.3.3 Metallization secondary ion mass spectrometry (MetA-SIMS) imaging

MetA-SIMS imaging of the radish was performed by the FOM Institute AMOLF, Science Park 104, 1098 XG Amsterdam, The Netherlands. SIMS data was acquired using a Physical Electronics TRIFT II TOF-SIMS (Physical Electronics, USA) equipped with an Au liquid metal gun tuned for 22keV Au⁺ primary ions. Images were acquired in mosaic mode using 64 tiles that each measure 125 μm square and contains 256 x 256 pixels. The total area scanned was 1 x 1 mm area with 60 seconds/tile resulting in a total of 4194304 spectra.

6.4 Data processing

Refer to Chapter 2, Section 2.6.1 for the software and procedure for data processing and image production.

Many people were involved in this study, with the design of the cultivation methodology, sample preparation and analysis performed by myself. Cultivation was performed at Aquaculture limited and Edinburgh zoo. All of the work performed to produce the SIMS data was performed by Bryn Flinders and his team at FOM Institute AMOLF, Science Park 104, 1098 XG Amsterdam, The Netherlands.

6.5 Results and discussion

Previous work has demonstrated that plants quickly metabolise nitrogen into amino acids after assimilation via the roots (Scott 2008). Initially glutamine and glutamate were investigated, as these are the primary amino acids formed from nitrogen uptake. Other amino acids were also investigated with particular attention to arginine (m/z 175) as previous work using MALDI-MSI had demonstrated its distribution within plants (Burrell, Earnshaw *et al.* 2007). The focus on these particular amino acids was intended to demonstrate the incorporation of nitrogen from the now dead radish plants into protein synthesis for the new living plants. However, unambiguous identification of these amino acids proved difficult owing to the complex overlapping isotope peaks present in this region of the positive ion mass spectrum.

Nevertheless, the B-complex vitamin choline, ($C_5H_{14}NO$), m/z 104.1, was found to have incorporated the labelled ^{15}N , producing an ion at m/z 105.1. These data are presented as Figure 6.5-1 and Figure 6.5-2. Further identification of these peaks as arising from choline is supported by the MALDI MS/MS data presented in Figure 6.5-3. Figure 6.5-3 confirms the identification of the m/z 104.1 and m/z 105.1 ions as choline and ^{15}N labelled choline respectively, clearly showing the appropriate product ions. The spectrum produced matched that generated data by the Scripps Centre for Metabolomics. Also, the product ions that contain nitrogen from the ^{15}N radish bulb and leaves have all increased in mass-to-charge by one, Figure 6.5-3b, which further confirms the identification.

The main distribution of the choline within the bulbs was found to be near to the skin, but not actually within the skin. It was also widely distributed through the bulb (Figure 6.5-1). This is supported by the distribution of pelargonidin (m/z 271). This is a natural food colouring found in radish skin, when overlaid with the choline, it can be clearly seen that these species exist in two distinct and separate areas (Figure 6.5-3).

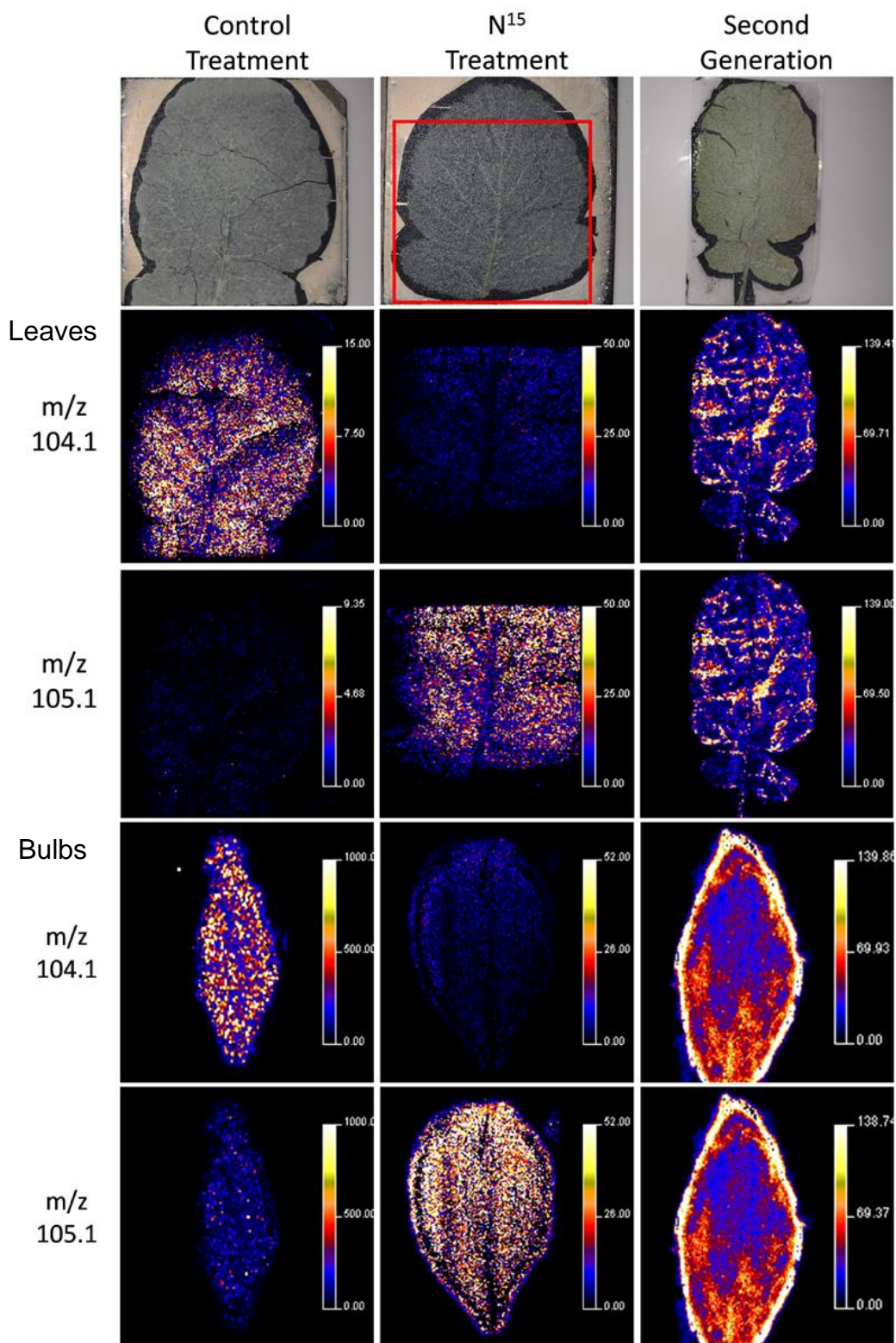


Figure 6.5-1: MALDI-MSI images showing the distribution of choline at m/z 104.1 and 105.1 with the leaf and the bulb of the radish (normalized against the TIC).

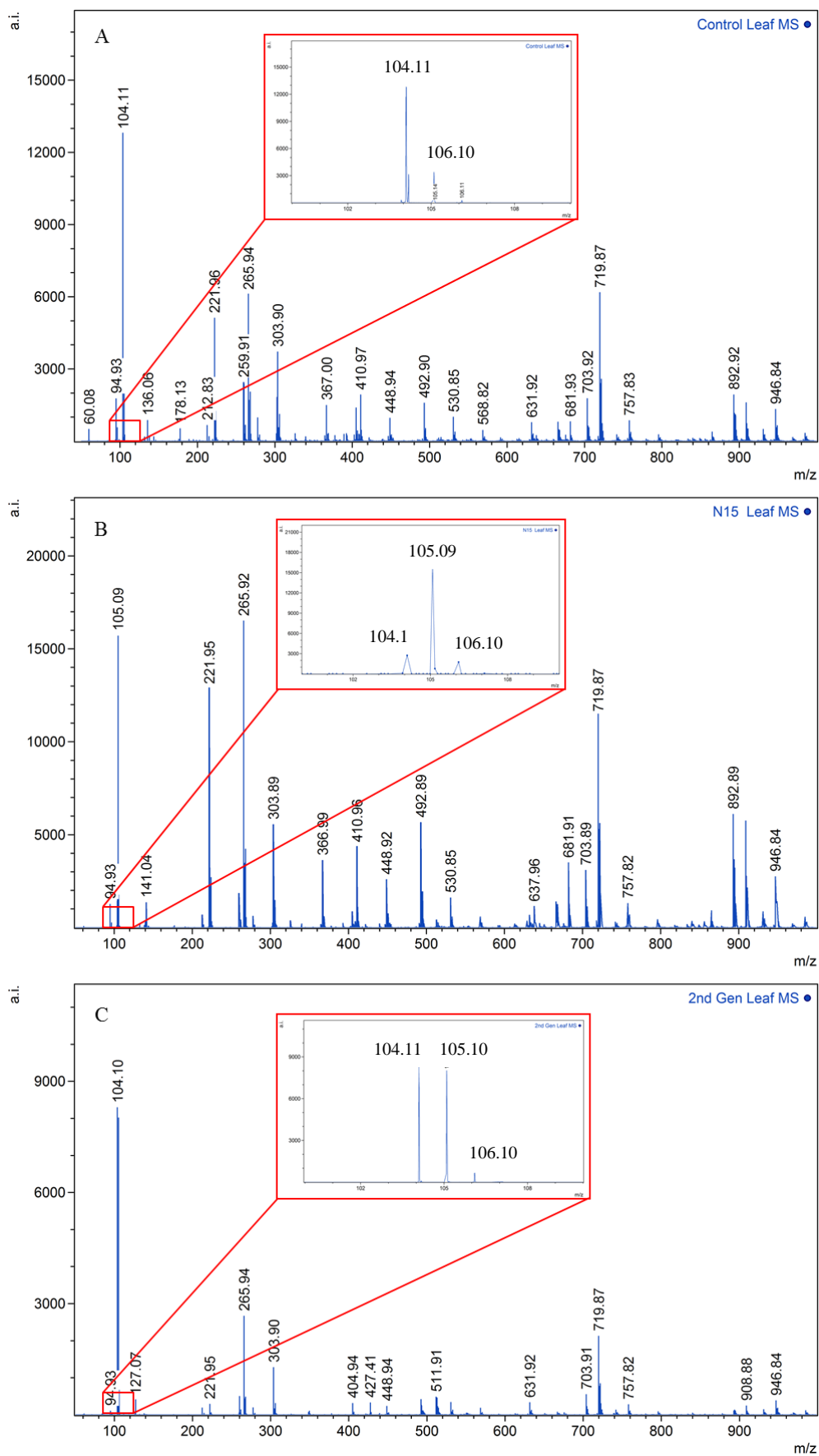


Figure 6.5-2: MALDI-MS spectra obtained from the leaves of the a) control, b) ^{15}N radish and c) second generation ^{15}N plant.

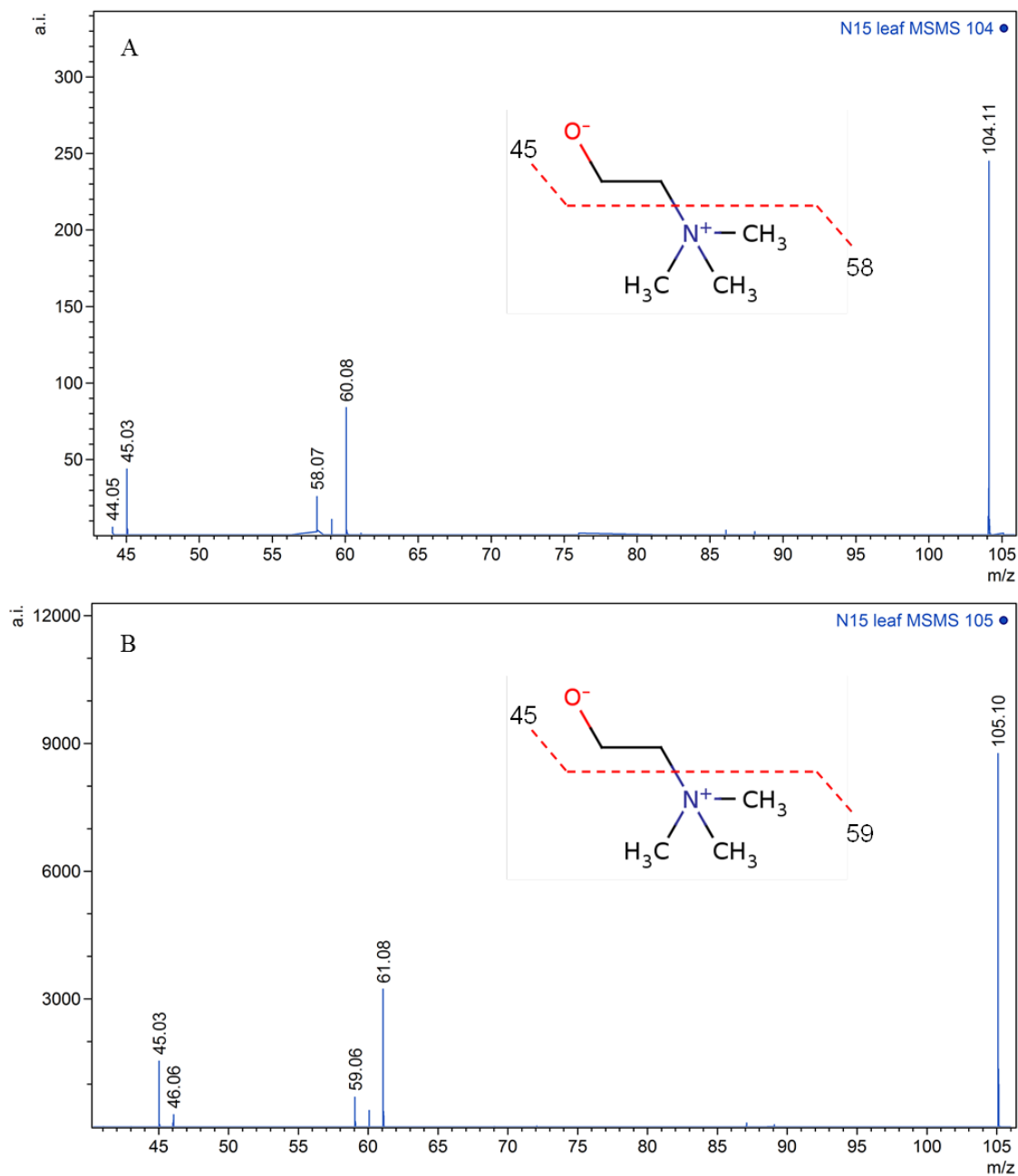


Figure 6.5-3: MALDI-MS/MS spectrum of a) m/z 104.1 and b) m/z 105.1 and the fragments taken from the N15 leaf.

The MALDI-MS images in Figure 6.5-1 show the full extent of the distribution of the labelled and the unlabelled choline. The MALDI-MS spectra of the three leaves in Figure 6.5-2, also reveal the difference in the intensity of the labelled (m/z 105.1) and unlabelled (m/z 104.1) choline. Figure 6.5-2a shows a higher intensity of the unlabelled choline (m/z 104.1), whereas Figure 6.5-2b shows a higher intensity of labelled choline (m/z 105.1), confirming that the ^{15}N was metabolised by the plant and incorporated into its structure. Figure 6.5-2c demonstrates that the ^{15}N was then passed from the first generation to the second-generation radish that was grown with plant material that had been fed exclusively ^{15}N nitrogen. The even intensity and distribution of labelled and unlabelled choline can be clearly seen in Figure 6.5-1 and Figure 6.5-2c.

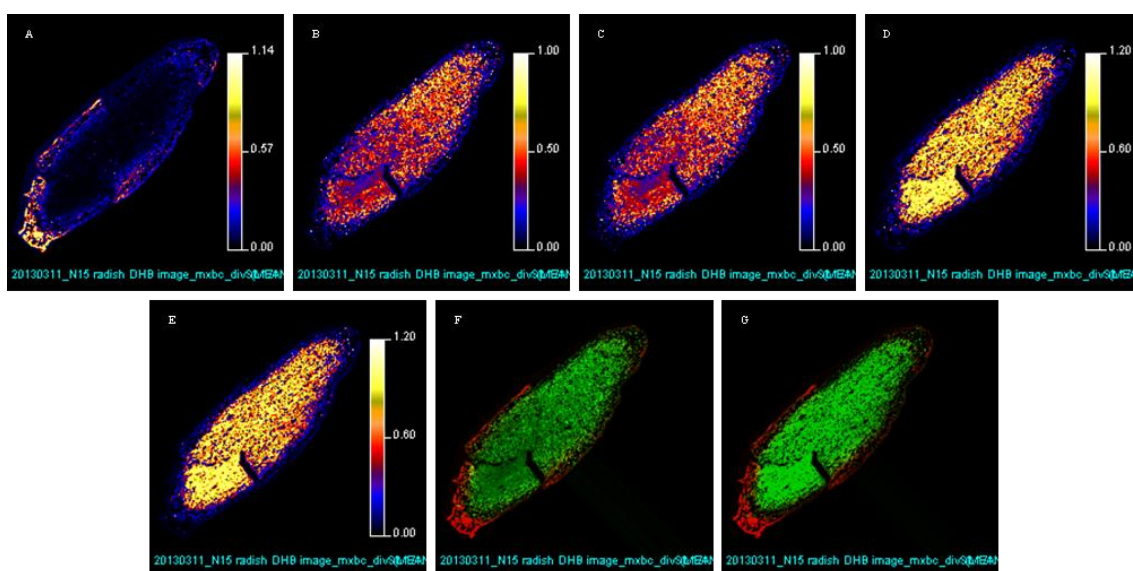


Figure 6.5-4: MALDI-MSI images showing the distribution of a) a species identified as anthocyanidin pelargonidin at m/z 271, b) choline at m/z 104.1, c) ^{15}N labelled choline at m/z 105.1, d) phosphocholine at m/z 184, e) ^{15}N labelled phosphocholine at m/z 185, f) ^{15}N labelled choline at m/z 105.1 overlaid onto the unknown species at 271 and g) ^{15}N labelled phosphocholine at m/z 185 overlaid onto pelargonidin species at m/z 271.

The MALDI-MS images displayed in Figure 6.5-4 show the distribution of labelled and unlabelled species in the second-generation radish bulb section, following normalization against the total ion current (TIC). The species at m/z 271 (Figure 6.5-4a) appears to be exclusively localized within the skin of the radish tissue section. This has been tentatively identified as anthocyanidin pelargonidin which is the natural food colour in the radish skin (Wu, Prior 2005). In order to confirm this assignment, MS/MS was performed and the resulting spectrum (Figure 6.5-5) matched that of the reference MS/MS data independently generated by the Scripps Centre for Metabolomics.

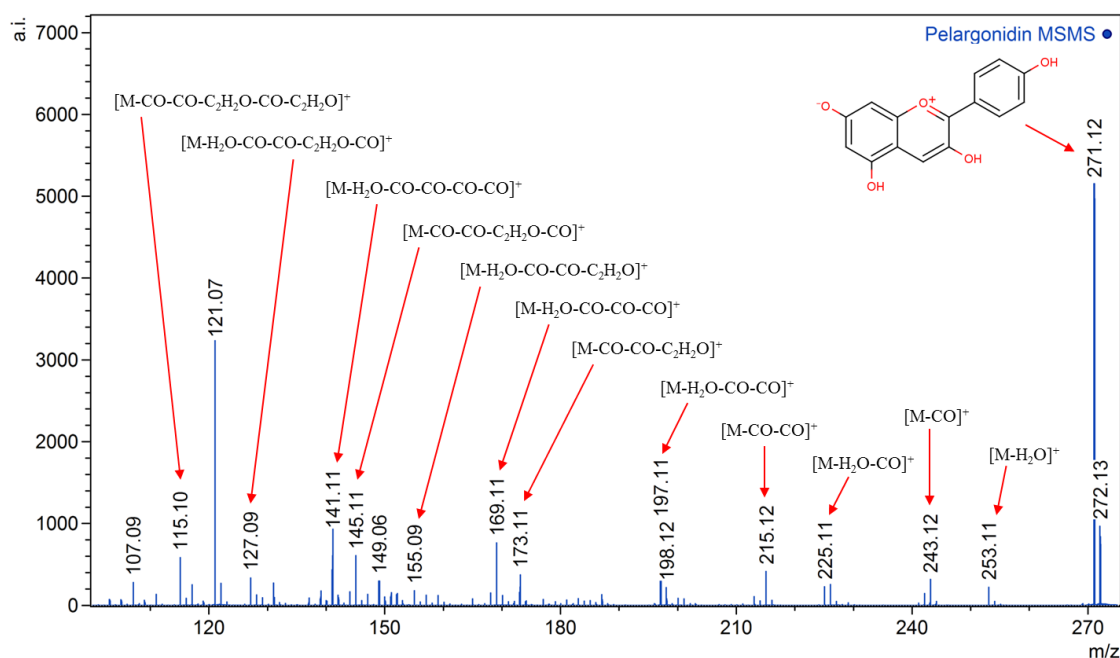


Figure 6.5-5: MALDI-MS/MS spectrum of Pelargonidin and fragments.

The distributions of the unlabelled and labelled choline at m/z 104.1 and m/z 105.1 (Figure 6.5-3b and Figure 6.5-3c respectively) are predominantly in the centre of the radish tissue. This is also observed with unlabelled and labelled phosphocholine at m/z 184 and m/z 185 (Figure 6.5-3d and Figure 6.5-3e respectively). The distributions of labelled choline and phosphocholine at m/z 105.1 and m/z 185 were overlaid with the distribution of pelargonidin at m/z 271, which is shown in Figure 6.5-4f and Figure 6.5-4g. These images

demonstrate that there is a clear distinction between the two regions and that the labelled species are only present in the centre of the radish.

The MALDI-MS spectrum (Figure 6.5-2c) shows that approximately 50% of the material from the first-generation radishes has successfully been transferred and assimilated into the formation of the second-generation radishes. This is also visually reflected in the MALDI-MS images shown in Figure 6.5-1 and Figure 6.5-4, which shows the same distribution with equal intensity for the labelled and unlabelled choline and phosphocholine.

The metal assisted-secondary ion mass spectrometry (MetA-SIMS) images produced by FOM Institute AMOLF (Science Park 104, 1098 XG Amsterdam, The Netherlands), of the control radish bulb section are displayed in Figure 6.5-6. The optical image (Figure 6.5-6a) shows a magnified view of the centre portion of the radish, which looks like that of the first-generation radish. The TIC image is shown in Figure 6.5-6b. The MetA-SIMS images of the control radish show the distribution of unlabelled choline at m/z 104.1 (Figure 6.5-6c) and the isotope of this peak at m/z 105.1 (Figure 6.5-6d). The mass spectrum (Figure 6.5-6e) shows a strong peak at m/z 104.1 which has been tentatively assigned to the unlabelled choline. This is expected to be the abundant form as this radish was grown exclusively with an unlabelled compound. The isotopic ratio (m/z 104.1/ m/z 105.1) for the control radish is 2.5322.

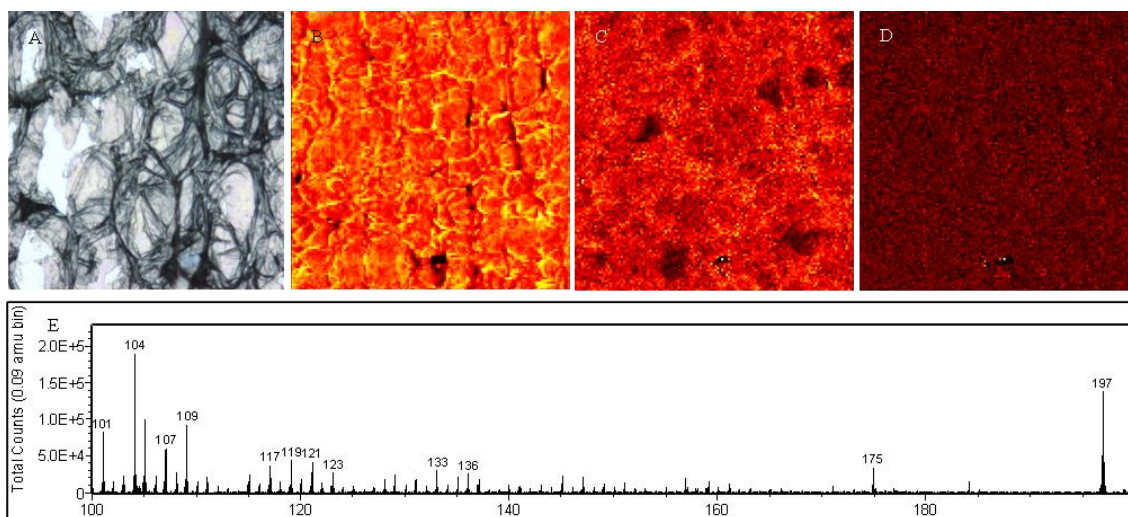


Figure 6.5-6: a) Optical image of the control radish bulb section and MetA-SIMS images showing b) the total ion current, the distribution of c) choline at m/z 104.1 and d) ¹³C isotope of choline at m/z 105, and e) MetA-SIMS spectrum obtained from the radish bulb.

The MetA-SIMS images displayed in Figure 6.5-7 shows the distribution of labelled and unlabelled choline in the first-generation radish bulb section. The optical image (a) shows a magnified view of the centre portion of the radish, the TIC image is shown in Figure 6.5-7b. The MetA-SIMS images of unlabelled choline at m/z 104.1 and ¹⁵N labelled choline at m/z 105.1 (Figure 6.5-7c and Figure 6.5-7d respectively) show both species are widely distributed in the string like network observed in the optical image. The related spectrum (Figure 6.5-7e) shows a strong peak at m/z 105.1 which could be ¹⁵N labelled choline, which is expected as this radish was grown exclusively with a ¹⁵N labelled compound. The isotopic ratio for the first-generation radish was calculated from the SIMS data to be 0.1963.

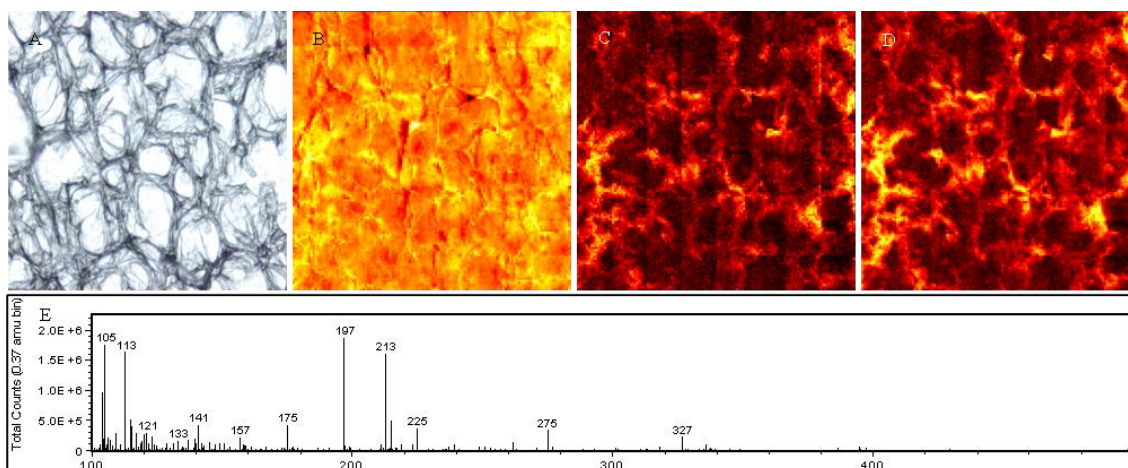


Figure 6.5-7: a) Optical image of the first-generation radish bulb section and MetA-SIMS images show (b) the total ion current, the distribution of (c) choline at 104.1 and (d) ¹⁵N-labelled choline at *m/z* 105.1, and (e) MetA-SIMS spectrum obtained from the radish bulb.

The MetA-SIMS images of the second-generation radish bulb section displayed in Figure 6.5-8 shows the distribution of labelled and unlabelled choline. The optical image (Figure 6.5-8a) shows a magnified view of the centre portion of the radish. The TIC image is shown in Figure 6.5-8b. The MetA-SIMS images of unlabelled choline at *m/z* 104.1 (Figure 6.5-8d) and ¹⁵N labelled choline at *m/z* 105.1 (Figure 6.5-8c) show both species are evenly distributed through the imaged area. The related spectrum (Figure 6.5-8e) again shows a peak at *m/z* 105.1 which could be ¹⁵N labelled choline, however neither the images nor the spectrum reflect the same pattern previously observed in the MALDI-MS data of the second-generation radish. The isotopic ratio calculated for the second-generation radish is 0.4689. This variation could possibly be due to the analysis of a very small portion of a large sample. The amount of detail that is achieved using MetA-SIMS also shows the local uptake of the ¹⁵N label and its incorporation into choline. In comparison to the MALDI-MS image (Figure 6.5-4) which shows the global distribution of labelled and unlabelled choline throughout the whole radish bulb section.

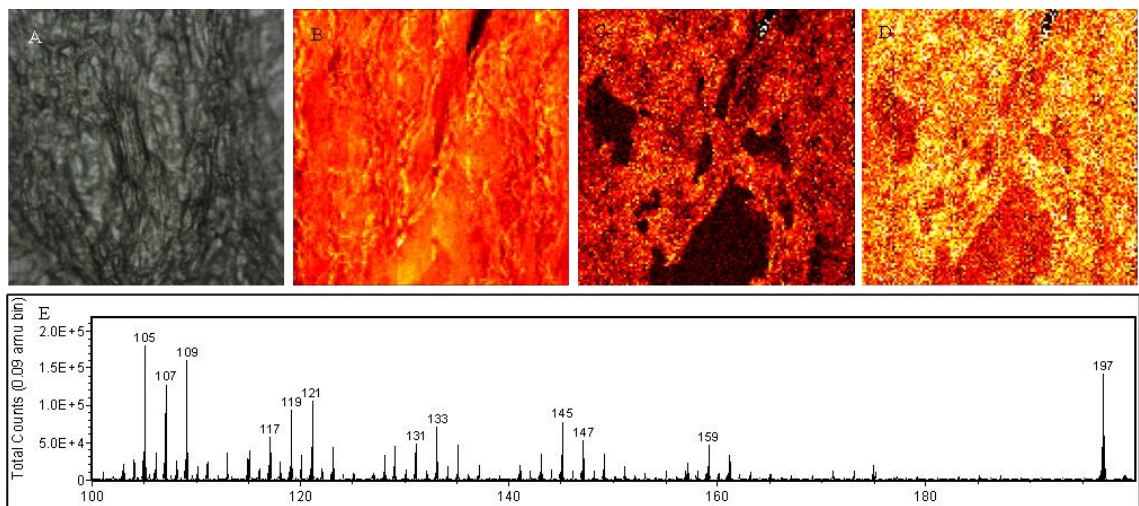


Figure 6.5-8: a) Optical image of the second-generation radish bulb section and MetA-SIMS images show (b) the total ion current, the distribution of (c) choline at 104.1 and (d) ¹⁵N-labelled choline at m/z 105.1, and (e) MetA-SIMS spectrum obtained from the radish bulb.

Previous studies using isotopes such as ¹⁴C, ¹⁵N and ³¹P have demonstrated the cycle of key nutrients in plants (Dawson, Mambelli *et al.* 2002, Marsh, Sims *et al.* 2005, Bichat, Sims *et al.* 1999, Engelsberger, Erban *et al.* 2006, Fiedler, Proksch 1972, Heltai, Jozsa 1995). Techniques such as inductively coupled plasma-mass spectrometry (ICP-MS) (Lechene, Luyten *et al.* 2007, Mihaylova, Lyubomirova *et al.* 2013), GC-MS (Engelsberger, Erban *et al.* 2006), ICP-OES (Fiedler, Proksch 1972), MIP-OES (Heltai, Jozsa 1995), NMR (Knicker, Lüdemann 1995) and LC-MS/MS (Engelsberger, Erban *et al.* 2006) are commonly utilized in the study of nutrient cycles and have all been used to demonstrate the nitrogen cycle. However, all of these techniques only gave a general distribution of the nitrogen within the tissue. All of these methods require the tissue to be destroyed either by digestion or extraction method in order to analyse. Imaging techniques have been used to study plants extensively, including laser ablation-inductively coupled plasma-mass spectrometry (LA-ICP-MS) (Lee, Perdian *et al.* 2012, Lombi, Scheckel *et al.* 2011, Wu, Zoriy *et al.* 2009, Wu, Becker 2012), X-ray absorption spectroscopy (XAS) (Lombi, Scheckel and Kempson 2011, Wu and Becker 2012), X-ray fluorescence (XRF) (Lombi, Scheckel and Kempson 2011, Wu and Becker 2012), SIMS

(Lechene *et al.* 2007, Lee *et al.* 2012, Wu and Becker 2012, Lombi, Scheckel and Kempson 2011) and MALDI-MS (Kaspar *et al.* 2011, Lee *et al.* 2012, Burrell, Earnshaw and Clench 2007, Li, Shrestha and Vertes 2008, Grassl, Taylor and Millar 2011, Vrkoslav *et al.* 2010, Horn *et al.* 2012), however, the data presented here is the first use of mass spectrometry to demonstrate unambiguously that atoms and molecules move from dead plant material into new living material.

This is also the first demonstration of the use of MALDI-MS and SIMS imaging to show the distribution, translocation and metabolism of nitrogen in plants. MALDI-MS imaging of plant material is a relatively new technique, with only a small number of researchers performing it. Compounds such as nicosulfuron (Anderson *et al.* 2009) and other agrochemical compounds (Mullen *et al.* 2005) have previously been monitored using this technique, but no demonstration of the cycle of this compound was performed. Other naturally occurring compounds in plants to be monitored and mapped using MALDI-MS imaging include amino acids (Kaspar *et al.* 2011, Burrell, Earnshaw and Clench 2007, Gogichaeva and Alterman 2012, Gogichaeva, Williams and Alterman 2007), oligosaccharides (Wang, Sporns and Low 1999), carbohydrates (Robinson *et al.* 2007), proteins (Grassl, Taylor and Millar 2011), peptides (Kondo *et al.* 2006), lipids (Vrkoslav *et al.* 2010, Horn *et al.* 2012) and other plant metabolites (Lee *et al.* 2012, Burrell, Earnshaw and Clench 2007, Li, Shrestha and Vertes 2008). The technique has also been proven to be useful in the monitoring of metabolites of nitrogen fixing bacteria known as rhizobia (Ye *et al.* 2013). MS imaging of stable isotope labelled compounds will, therefore, clearly be a useful tool in the future for monitoring the distribution of other species within plants, since this technique could be used to monitor the uptake and distribution of herbicides, pesticides and plant growth regulators (PGR) not only within the primary plant to which they were applied but, also, in the second-generation plants. It

could also be used to monitor bioremediation and show if plants have been grown on contaminated land. It also has the potential to help optimize plant nutrition, nutrient delivery and schedules. Previous work performed by Bateman and Kelly (Bateman and Kelly 2007, Bateman, Kelly and Jickells 2005) employing a PDZ Europa ANCA-GSL elemental analyser interfaced to a PDZ Europa 20-20 isotope ratio mass spectrometer for the analysis of fertilizers, could be utilized in further research to confirm that the nitrates taken up by the second generation plant were either from inorganic nitrates released from the first generation plants or organic nitrogen released into the tea.

6.6 Conclusion

The data presented here have demonstrated that atoms and molecules move from dead plant material into new living material. It has also been shown that MALDI-MS and TOF-SIMS imaging are useful tools for monitoring the distribution of compounds within plants and that the use of stable isotope labelled compounds in MS imaging experiments can yield useful information about uptake and fatality in metabolomic based experiments.

Mass spectrometry imaging has been used to demonstrate the uptake of labelled nitrogen species from composted radish leaves into growing radish plants. The "cycle of life" has been successfully demonstrated.

6.7 References

ANDERSON, D.M.G., CAROLAN, V.A., CROSLAND, S., SHARPLES, K.R. and CLENCH, M.R., 2009. Examination of the distribution of nicosulfuron in sunflower plants by matrix-assisted laser desorption/ionisation mass spectrometry imaging. *Rapid Communications in Mass Spectrometry*, **23**(9), pp. 1321-1327.

BATEMAN, A.S., KELLY, S.D. and JICKELLS, T.D., 2005. Nitrogen isotope relationships between crops and fertilizer: Implications for using nitrogen isotope analysis as an indicator of agricultural regime. *Journal of Agricultural and Food Chemistry*, **53**(14), pp. 5760-5765.

BATEMAN, A.S. and KELLY, S.D., 2007. Fertilizer nitrogen isotope signatures. *Isotopes in Environmental and Health Studies*, **43**(3), pp. 237-247.

BBC, Four., 2011-last update, AfterLife: The Strange Science of decay. Available: <http://www.bbc.co.uk/programmes/b012w66t2014>].

BERGLUND, M. and WIESER, M.E., 2011. Isotopic compositions of the elements 2009 (IUPAC Technical Report). *Pure and Applied Chemistry*, **83**(2), pp. 397-410.

BICHAT, F., SIMS, G.K. and MULVANEY, R.L., 1999. Microbial utilization of heterocyclic nitrogen from atrazine. *Soil Science Society of America Journal*, **63**(1), pp. 100-110.

BURRELL, M.M., EARNSHAW, C.J. and CLENCH, M.R., 2007. Imaging Matrix Assisted Laser Desorption Ionization Mass Spectrometry: a technique to map plant metabolites within tissues at high spatial resolution. *Journal of Experimental Botany*, **58**(4), pp. 757-763.

DAWSON, T.E., MAMBELLI, S., PLAMBOECK, A.H., TEMPLER, P.H. and TU, K.P., 2002. Stable isotopes in plant ecology. *Annual Review of Ecology and Systematics*, **33**, pp. 507-559.

ENGELSBERGER, W.R., ERBAN, A., KOPKA, J. and SCHULZE, W.X., 2006. Metabolic labeling of plant cell cultures with (KNO₃)-N-15 as a tool for quantitative analysis of proteins and metabolites. *Plant Methods*, **2**, pp. 14.

FIEDLER, R. and PROKSCH, G., 1972. Emission Spectrometry for Routine Analysis of Nitrogen-15 in Agriculture. *Plant and Soil*, **36**(2), pp. 371-&.

GOGICHAEVA, N.V. and ALTERMAN, M.A., 2012. Amino acid analysis by means of MALDI TOF mass spectrometry or MALDI TOF/TOF tandem mass spectrometry. *Methods in Molecular Biology (Clifton, N.J.)*, **828**, pp. 121-35.

GOGICHAEVA, N.V., WILLIAMS, T. and ALTERMAN, M.A., 2007. MALDI TOF/TOF tandem mass spectrometry as a new tool for amino acid analysis. *Journal of the American Society for Mass Spectrometry*, **18**(2), pp. 279-284.

- GRASSL, J., TAYLOR, N.L. and MILLAR, A.H., 2011. Matrix-assisted laser desorption/ionisation mass spectrometry imaging and its development for plant protein imaging. *Plant Methods*, **7**, pp. 21.
- GRIGNON, N., HALPERN, S., JEUSSET, J., BRIANCON, C. and FRAGU, P., 1997. Localization of chemical elements and isotopes in the leaf of soybean (*Glycine max*) by secondary ion mass spectrometry microscopy: Critical choice of sample preparation procedure. *Journal of Microscopy-Oxford*, **186**, pp. 51-66.
- HELTAI, G. and JOZSA, T., 1995. N-15-Tracer Technique with the Mip-Oes Detection of Stable N-Isotopes for Soil Ecological-Studies. *Microchemical Journal*, **51**(1-2), pp. 245-255.
- HORN, P.J., KORTE, A.R., NEOGI, P.B., LOVE, E., FUCHS, J., STRUPAT, K., BORISJUK, L., SHULAEV, V., LEE, Y. and CHAPMAN, K.D., 2012. Spatial Mapping of Lipids at Cellular Resolution in Embryos of Cotton. *Plant Cell*, **24**(2), pp. 622-636.
- KASPAR, S., PEUKERT, M., SVATOS, A., MATROS, A. and MOCK, H., 2011. MALDI-imaging mass spectrometry - An emerging technique in plant biology. *Proteomics*, **11**(9), pp. 1840-1850.
- KEENEY, D.R. and HATFIELD, J.L., 2008. Chapter 1 - The Nitrogen Cycle, Historical Perspective, and Current and Potential Future Concerns. In: R.F. FOLLETT and J.L. HATFIELD, eds, *Nitrogen in the Environment: Sources, Problems and Management*. USA: Elsevier Science, pp. 3-16.
- KNICKER, H. and LÜDEMANN, H.-., 1995. N-15 and C-13 CPMAS and solution NMR studies of N-15 enriched plant material during 600 days of microbial degradation. *Organic Geochemistry*, **23**(4), pp. 329-341.
- KONDO, T., SAWA, S., KINOSHITA, A., MIZUNO, S., KAKIMOTO, T., FUKUDA, H. and SAKAGAMI, Y., 2006. A plant peptide encoded by CLV3 identified by in situ MALDI-TOF MS analysis. *Science*, **313**(5788), pp. 845-848.
- LECHENE, C.P., LUYTEN, Y., MCMAHON, G. and DISTEL, D.L., 2007. Quantitative imaging of nitrogen fixation by individual bacteria within animal cells (vol 317, pg 1563, 2007). *Science*, **318**(5850), pp. 570-570.
- LEE, Y.J., PERDIAN, D.C., SONG, Z., YEUNG, E.S. and NIKOLAU, B.J., 2012. Use of mass spectrometry for imaging metabolites in plants. *The Plant Journal*, **70**(1), pp. 81-95.
- LI, Y., SHRESTHA, B. and VERTES, A., 2008. Atmospheric pressure infrared MALDI imaging mass spectrometry for plant metabolomics. *Analytical Chemistry*, **80**(2), pp. 407-420.
- LOMBI, E., SCHECKEL, K.G. and KEMPSON, I.M., 2011. In situ analysis of metal(loid)s in plants: State of the art and artefacts. *Environmental and Experimental Botany*, **72**(1), pp. 3-17.

MARSH, K.L., SIMS, G.K. and MULVANEY, R.L., 2005. Availability of urea to autotrophic ammonia-oxidizing bacteria as related to the fate of C-14- and N-15-labeled urea added to soil. *Biology and Fertility of Soils*, **42**(2), pp. 137-145.

MIHAYLOVA, V., LYUBOMIROVA, V. and DJINGOVA, R., 2013. Optimization of sample preparation and ICP-MS analysis for determination of 60 elements for characterization of the plant ionome. *International Journal of Environmental Analytical Chemistry*, **93**(13), pp. 1441-1456.

MULLEN, A.K., CLENCH, M.R., CROSLAND, S. and SHARPLES, K.R., 2005. Determination of agrochemical compounds in soya plants by imaging matrix-assisted laser desorption/ionisation mass spectrometry. *Rapid Communications in Mass Spectrometry*, **19**(18), pp. 2507-2516.

PETER SCOTT, 2008. *Physiology and Behaviour of Plants*. UK: John Wiley & Sons, Ltd.

ROBINSON, S., WARBURTON, K., SEYMOUR, M., CLENCH, M. and THOMAS-OATES, J., 2007. Localization of water-soluble carbohydrates in wheat stems using imaging matrix-assisted laser desorption ionization mass spectrometry. *New Phytologist*, **173**(2), pp. 438-444.

SCHWARTZ, S.A., REYZER, M.L. and CAPRIOLI, R.M., 2003. Direct tissue analysis using matrix-assisted laser desorption/ionization mass spectrometry: practical aspects of sample preparation. *Journal of Mass Spectrometry*, **38**(7), pp. 699-708.

SCOTT, P., 2008. *Physiology and Behaviour of Plants*. Chichester, UK: John Wiley & Sons Ltd.

SEAMAN, C., FLINDERS, B., EIJKEL, G., HEEREN, R.M.A., BRICKLEBANK, N. and CLENCH, M.R., 2014. "Afterlife Experiment": Use of MALDI-MS and SIMS Imaging for the Study of the Nitrogen Cycle within Plants. *Analytical Chemistry*, **86**(20), pp. 10071-10077.

STROHALM, M., KAVAN, D., NOVAK, P., VOLNY, M. and HAVLICEK, V., 2010. mMass 3: A Cross-Platform Software Environment for Precise Analysis of Mass Spectrometric Data. *Analytical Chemistry*, **82**(11), pp. 4648-4651.

TRIM, P.J., DJIDJA, M., ATKINSON, S.J., OAKES, K., COLE, L.M., ANDERSON, D.M.G., HART, P.J., FRANCESE, S. and CLENCH, M.R., 2010. Introduction of a 20 kHz Nd:YVO₄ laser into a hybrid quadrupole time-of-flight mass spectrometer for MALDI-MS imaging. *Analytical and Bioanalytical Chemistry*, **397**(8), pp. 3409-3419.

VRKOSLAV, V., MUCK, A., CVACKA, J. and SVATOS, A., 2010. MALDI Imaging of Neutral Cuticular Lipids in Insects and Plants. *Journal of the American Society for Mass Spectrometry*, **21**(2), pp. 220-231.

WANG, J., SPORNS, P. and LOW, N.H., 1999. Analysis of food oligosaccharides using MALDI-MS: Quantification of fructooligosaccharides. *Journal of Agricultural and Food Chemistry*, **47**(4), pp. 1549-1557.

WU, B. and BECKER, J.S., 2012. Imaging techniques for elements and element species in plant science. *Metallomics*, **4**(5), pp. 403-416.

WU, B., ZORIY, M., CHEN, Y. and BECKER, J.S., 2009. Imaging of nutrient elements in the leaves of *Elsholtzia splendens* by laser ablation inductively coupled plasma mass spectrometry (LA-ICP-MS). *Talanta*, **78**(1), pp. 132-137.

WU, X.L. and PRIOR, R.L., 2005. Identification and characterization of anthocyanins by high-performance liquid chromatography-electrospray ionization-tandem mass spectrometry in common foods in the United States: Vegetables, nuts, and grains. *Journal of Agricultural and Food Chemistry*, **53**(8), pp. 3101-3113.

YE, H., GEMPERLINE, E., VENKATESHWARAN, M., CHEN, R., DELAUX, P., HOWES-PODOLL, M., ANE, J. and LI, L., 2013. MALDI mass spectrometry-assisted molecular imaging of metabolites during nitrogen fixation in the *Medicago truncatula*-*Sinorhizobium meliloti* symbiosis. *The Plant Journal : for Cell and Molecular Biology*, **75**(1), pp. 130-145.

Chapter 7

7. Conclusion and suggestions for future work

With an ever-increasing population, one of the most significant global issues we face is sustainable food production that meets the nutritional needs of the entire population. As resources such as fertile soil and clean water become more limited, there will be an increasing need to improve the efficient use of these resources. Furthermore, if we are to tackle world hunger and malnutrition, a greater understanding of plant nutrition, assimilation of nutrients and elemental movement is required. Within the work presented in this thesis, a number of analytical techniques have been utilized and developed to help improve our understanding of plant nutrition.

The aim of Chapter 3, started off as the development of a precipitate free, single component commercially viable hydroponic nutrient. The work performed on the formulation of liquid nutrients in Chapter 3 demonstrated that the bioavailability of particular elements, such as calcium, sulphur and phosphorus are affected by factors including pH, total ion concentrations, speciation, complexation and precipitation reactions, that occur within a hydroponic nutrient solution. This, in turn, can affect the nutrition of the plant, leading to deficiencies and reduction in yield. Further work on the identification of the ion species will help in the development of strategies for the prevention of complexation and precipitation reactions. For example, chelating agents such as polyphosphates, EDTA complexes and related species, could be incorporated to prevent such reactions taking place.

The use of a seed coating to supply nutrition to the plant before sowing is becoming more popular. In Chapter 4, the aim was to assess if seed coat application had an effect on the production of haulage for livestock production. It was demonstrated that with increasing concentrations of seed coat, there is an increased zinc content within both the pre-germinated seed and the leaf material, proving that the nutritional content of the barley is increased without the addition of more fertilizer. This work also demonstrated

the use of LA-ICP-MS in studying the distribution of zinc and other elements within seeds and leaf material. In the past accurate quantification using LA-ICP-MS has been very difficult, with scientists such as Pozebon and Becker leading in this field. One of the most difficult challenges is producing homogeneous reference material to produce extrapolated calibration curves with software such as Iolite, with the aid of an internal standard. The work presented within Chapter 4, demonstrates effective methodology for the production of reference material for quantitative LA-ICP-MS imaging of plant material. It also validates the use of LA-ICP-MS as a quantitative method to support more destructive methods such as liquid ICP-MS or ICP-OES.

In Chapter 5 we aimed to evaluate the application of sodium selenate to the seedlings of the Se hyper-accumulator broccoli, via a sprinkler system. As expected it was found to increase the selenium content of the plant material, but also increased the seleno-amino acid concentration, such as Se-methionine. Over time this exponentially increased. Optimisation of the concentration and species of selenium is required in the future, to help produce biofortified broccoli which has the most health benefits to humans.

The recycling of elements such as nitrogen by plants has been well documented, however the monitoring of its distribution within a plant is less so. The aim of Chapter 6 was to validate the recycling of elements from living plants, through decaying plants and then into the new growth of plants. Chapter 6 demonstrates that nitrogen is recycled through decaying plants. This has been proven by the imaging of radish which has been fed with a compost tea made from radish which has been dosed with the isotope ^{15}N whilst growing. This further confirms that the nitrogen cycle is real.

It has been demonstrated within this work that mass spectroscopy imaging techniques such as MALDI-MS and LA-ICP-MS are valuable tools within plant science for the

tracking of the movement and distribution of elements and compounds within plants.

The quantitative methods developed will in the future allow for more accurate development of fertilizers and a better understanding of the metabolism and transportation of elements within plants. These techniques could be used to develop 3D imaging of plant material and the use of stable isotopes to track the movement and distribution.

All of the techniques used in the work presented in this thesis, have allowed a variety of elements to be tracked within plants, seeds and through the transfer from one organism to another as part of the recycling process of element. These imaging techniques offer a not only sensitive method but fantastic visual representation.

Appendices

1. Published work

- SEAMAN, C. and BRICKLEBANK, N., 2011. Soil-free farming. *Chemistry & industry*, (6), pp. 19-21.
- SEAMAN, C., FLINDERS, B., EIJKEL, G., HEEREN, R.M.A., BRICKLEBANK, N. and CLENCH, M.R., 2014. "Afterlife Experiment": Use of MALDI-MS and SIMS Imaging for the Study of the Nitrogen Cycle within Plants. *Analytical Chemistry*, **86**(20), pp. 10071-10077.
- COLE, L.M. (Ed), 2017. *Imaging Mass Spectrometry: Methods and Protocols, Methods in Molecular Biology*. **1618**, pp.125-135.

2. Conferences Attended

- BioResources Young Researchers 2010 – University of Reading, UK, 22nd June 2010. Poster presented.
- Biofortified and Functional Foods: A Healthy Future? – SCI HQ, London, UK, 19th May 2011. Poster presented.
- SCI members Forum 2011 – SCI HQ, Belgrave Sq., London UK. 29th November 2011, - Won 1st Prize for Poster presentation. – Included.
- BioResources Young Researchers 2011 – University of Reading, UK, 8th July 2011. Poster presented.
- More Crop per Drop – Raising water use efficiency – SCI HQ, London. Poster presented. Poster presented and helped to organise this event.
- SCI members Forum 2012 – SCI HQ, Belgrave Sq., London UK. 29th November 2012. Poster presented
- Scanning the Agricultural Horizon to 2050 – Jealott's Hill International Research Centre, Bracknell, Berkshire. UK. 30th November 2010 – Poster presented.
- SCI Young Researchers in Agrisciences 2013: Crop Production, Protection, Utilisation. University of Reading, UK - 2 July 2013 – Oral Presentation.

- SCI members Forum 2013 – SCI HQ, Belgrave Sq., London UK. 29th November 2013. Poster presented Won 2nd Prize for Poster presentation. – Included
- SIG Mass Spectrometry Imaging Symposium MALDI and Beyond. Sheffield Hallam university, UK - 9th of July 2014 - Poster presented.
- BMRC Faculty Day - Sheffield Hallam university, UK - 12th of July 2010 - Poster presented.
- BMRC Faculty Day - Sheffield Hallam university, UK - 2nd of July 2011 - Poster presented.

3. Additional work

- STEM ambassador for Sheffield Hallam university.
- Committee member ECSSC and BioResources with the Society Chemical Industry (SCI), helping to organise events.
- Biosciences YES – Yorkshire and Humber 2010 competition.
- Played a key role in the design and running of one of the experiments for the BBC Four educational program “Afterlife: The strange science of Decay” with Edinburg Zoo. (<http://www.bbc.co.uk/programmes/b012w66t>).
- Becoming involved with the Wellcome Trust’s educational project, “The Crunch”, demonstrates my ability to present and communicate effectively with a wide audience and hopefully inspire more of the next generation to choose science as a career. (<https://www.youtube.com/watch?v=DHjB4mxmwe>)

